Investigating the Impact of Molecular Structure Near Infra-Red Sensitive Dyes on Photoconversion for Cobalt Electrolyte Based Dye-Sensitized Solar Cells

Dissertation for the Doctor of Philosophy

Anusha Pradhan

Student Id-16899001

Under the Supervision of

Professor Shyam Sudhir Pandey

Graduate School of Life Science and System Engineering

Kyushu Institute of Technology

Wakamatsu Campus, Fukuoka, Japan

Dedicated to

My Parents and Teachers

ACKNOWLEDGEMENTS

First of all, I am very indebted to my supervisor *Professor Shyam Sudhir Pandey* for believing in me and taking me under his esteemed supervision for the doctoral programme. He has always been inquisitive about my research in all means. His seamless effort in nurturing me even in a minute work of mine is something, which deserves unfathomable gratitude from the core of my heart. Beside as a dedicated guide, he has always come forward as a moral supporter, which has made my stay in Japan more comfortable.

I am also very grateful to *Professor Shuzi Hayase and Professor Tingli Ma* for providing the excellently equipped laboratory facilities, which has helped me to learn more and getting quick results for my research. His vast area of research has always attracted my attention in getting inspired for the welfare of the society.

I am also very thankful to *Kyushu Institute of Technology* for providing the platform for my research and helping me in managing the necessary criteria for my graduation. In this context, I would like to thank *Masako Hayasi San* for taking good care of us and also in managing events for the universal friendship, which has helped me in making many international friends. I am grateful *to FAIS and Yukiko Shiraishi San* for managing many cultural events, which has helped me to learn more about cultures of Japan and other countries. Her jovial nature has helped me in maintaining a good bond. I am highly grateful to *Rotary Yoneyama Foundation* for providing the financial aid for my stay in Japan. I am thankful to *Wakamatsu Chuo Rotary Club* and my councillor *Hiroyuki Yamamoto Sensei* for introducing me to the Japanese society. The club has provided me with a new family whom I truly love and admire. The members there have always been supportive.

I am also thankful to *Dr Gaurav Kapil*, who has helped me a lot in my research work. I am also very grateful to *Dr Maryala Sai Kiran* for introducing me to KIT and his help in research. I am thankful to the entire lab members *of Pandey and Hayase Lab* for aiding me with both research and friendly environment. I am also very grateful to my father *Mr Dilip Pradhan*, mother *Mrs Radha Pradhan, uncle Bed Dhakal* and brothers *Rishi Pradhan* and *Gyanendra Pradhan* and the entire family for their unwavering love and moral support. I am also thankful *to Nilima Mam* for her motherly love and guidance.

Last but not the least, I owe my research to my beloved *Bhagawan Sri Satya Sai* who has always showered His blessings upon me as a friend, philosopher and guide.

ABSTRACT

Dye sensitized solar cell (DSSC) falls under one of the splendid solar cells, which have amicably attracted mammoth research. The superlative of it amongst the other solar cells is its inspiration from natural photosynthesis, transparency and vivid colors imparting beauty and attraction. In addition, the cost of fabrication is expected to be relatively low compared to commercial solar cells owing to low cost raw materials and processes not demanding for use of high energy. Research in past two decades have demonstrated not only nearly quantitative photon harvesting in visible region but also the photoconversion efficiency (PCE) 12-14 %. This poses acute need for the design and synthesis of novel NIR dyes to have more photon flux harvested leading to further enhancement in the photoconversion efficiency (PCE). Beside the panchromatic photon harvesting for high current density (Jsc), there is also need for maximizing the open circuit voltage (Voc), which demands for use of electrolytes with deeper redox potential.

The **1st chapter** introduces the need of huge energy demand by the growing population and hence the necessity of the next generation solar cells. Keeping this mind, a brief discussion of the third generation solar cells like organic solar cells, DSSCs and perovskite solar cells has been done with emphasis on DSSCs. Importance of various dye sensitizers and redox electrolytes employed for DSSC justifying the need for squaraine dyes as NIR sensitizer and cobalt redox electrolyte.

2nd chapter deals with details about necessary chemicals and reagent for synthesis of sensitizers and their intermediates, basic instrumentation and various characterization techniques used for the entire research work carried out during doctoral course.

3rd chapter focusses on estimation of minimum energy barrier for dye regeneration using NIR sensitive squaraine dyes as sensitizers and most commonly used I^-/I_3^- redox electrolytes redox electrolytes. It was found that the alkyl chain plays a crucial role in controlling the energetics. It has been demonstrated that it is possible to have dye regeneration with a minimum energy barrier of 0.12 eV.

In the **4th chapter**, optimization of DSSCs fabrication parameters was done using one of the model NIR sensitive squaraine dye (SQ-75) and $Co(bpy)^{2+/3+}$ redox electrolyte was conducted. $TiCl_4$ surface treatment was found to control the overall PCE and especially it was more effective when treatment was done on both of the FTO glass substrate and mesoporous TiO_2 layer. At the same time, only 6 μm thick mesoporous TiO_2 was found to be optimum considering the high molar extinction coefficient of the dye and bulky nature of the redox electrolyte. Dye aggregation owing

to planarity of dye molecule demanded optimization of coadsorber for dye aggregation prevention and 20 times of its use with respect to the dye was found to be optimum for the best device performance.

DSSCs using NIR dyes in combination of cobalt electrolyte needs strict surface passivation for both of conducting substrate as well as mesoporous TiO_2 layer. Utilization of optimized surface passivation discussed in the previous chapter, dye structure level optimization was attempted in the **5th chapter**. This chapter utilizes longer alkyl chain bearing NIR dyes to provide additional surface passivation needed for cobalt electrolyte based DSSCs. Newly designed squaraine dye with two long and branched alkyl chains (SQ-110) was found to perform well as NIR sensitizer providing best PCE amongst newly designed dyes.

Considering the narrow wavelength and intense light absorption by newly designed squaraine dyes, efforts was directed for wide wavelength photon harvesting utilizing a dye cocktail of one of the best NIR dye (SQ-110) with cobalt electrolyte compatible visible sensitizer (D-35) in the **6th chapter**. In the present dye-cocktail, DSSCs consisted of different ratios of the constituent dyes, mutual control of dye aggregation, complementary photon harvesting and FRET between two dyes are found to be responsible for synergistically enhanced photon harvesting in the wide wavelength region. It has been demonstrated that a compact TiO_2 on FTO and a bilayer TiO_2/MgO surface passivation was necessary for getting the optimum DSSC performance with optimum dye cocktail of D-35 and SQ-110 in (4:1).

Finally, last and **7th chapter** summarizes the general conclusion of the whole thesis along with the outlooks and future prospects of the present work.

TABLE OF CONTENTS

CHAPTER ONE. Introduction

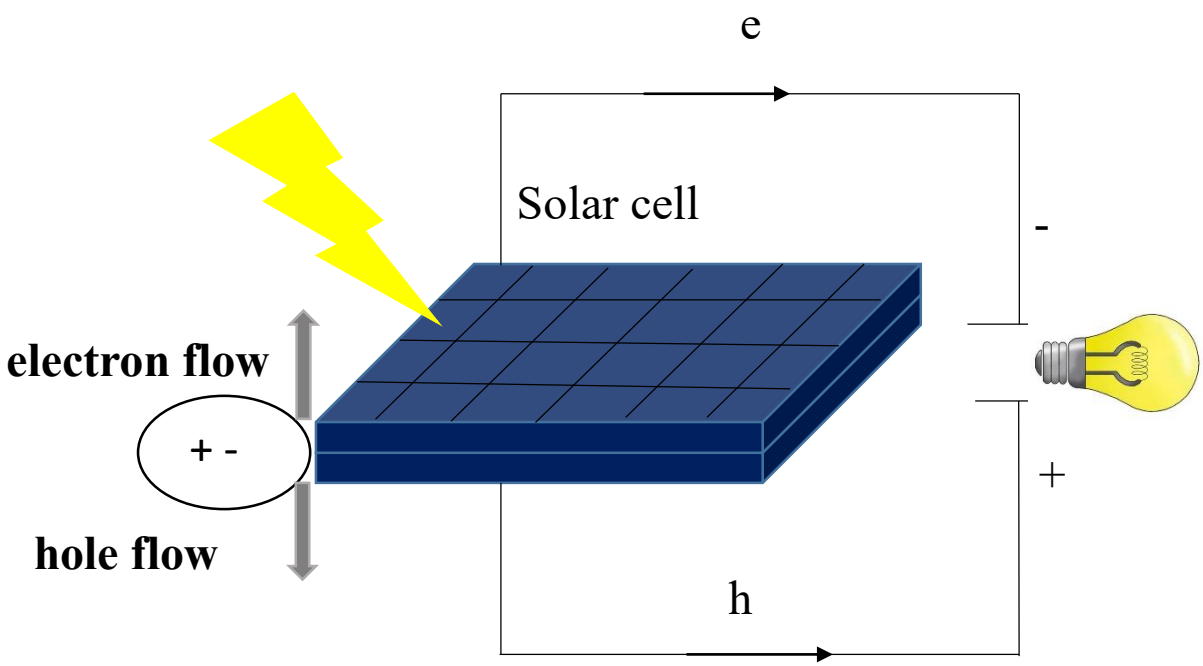

INTRODUCTION

The industrial revolution sometime 20 decades ago has paved the way for demand over clean, affordable and reliable energy to improve the extending world`s economy. At the blossoming of the industrial revolution, the native population was approximated as 7 million which is now approximated to enhance to 9 billion by 2050, and approx 10 billion by 2100 demanding more energy production and output [1]. It is obvious that, there will be a calculable growing energy demand as per human`s comfort and soon the world will face an acute shortage to meet the demand of certain fossil fuels like petroleum and coal, resulting in increased fossil fuel costs as formation of it requires billions and trillions of years [2]. Also the dangers and most scary hazard include the major global warming resulting in the incremental rise in temperature from the emitted hazardous gases CO_2, SO_2 etc. from fossil fuel. Moreover the fatal health issues associated with pollution due to daily huge use of fossil fuel triggered work to find an alternative clean and renewable source. The outstanding renewable energy systems include photovoltaics (PVs) (or solar cells), hydroelectric, ocean, solar thermal which embraces electric and thermal energy, wind, and geothermal [3].

Among the renewable sources of energy, solar energy stands as the most versatile and the superlative potential energy source in the present scenario with no hazardous emission of CO_2 unlike from fossil fuel combustion. In addition, the solar radiations striking the earth′s surface spread from 0.06 kW/m^2 at higher latitudes and 0.25 kW/m_2 at lower latitudes. Detailed study says that the lump sum ice-free land around the globe is around 13,000 MHa and from this energy, theoretical power output from the solar source is about 21,840 TW. In particular, solar PV meets a large prospective in green and technical solutions to the acute energy demands [4]. A.E. Becquerel is remembered for observing the photovoltaic effect in the year 1939 which bloomed to the development of the recent solar cells, a substitute for the traditional fossil fuels. Estimation of more than 1000 tonnes of CO_2 emission is being cut down for a single gigawatt—hour of electricity generated by photovoltaics. The pilot of photovoltaic devices using organic which is cheaper, inorganic and the hybrid of both have attracted a mammoth research. Though inorganic materials have been very assuring in the development of photovoltaics, organic materials are also showing great hope due to its low cost of processing [5]. The first silicon based solar cells was reported by Ohl in 1941 whose efficiency was less than 1%. Now, the recent revision of the internationally

accepted efficiency of crystalline silicon solar cell which belongs to the first generation of the solar cell is 25 % [6].

Thin film solar cells, a cheaper substitute to the first generation solar cells such as CIGS, CdTe and amorphous-Silicon are the classic examples of the second generation solar cells. In 1953, Hahn et al was the first to report the bandgap of 1.04 eV CIS material with. CIGS with 15% module efficiency is expected to be $0.34/W for a production capacity of 1000 MW/yr. In the present scenario, about 92% of the solar panels in the world is contributed from Si, followed with 5% from CdTe, 2 % from CIGS and less than 1% from amorphous silicon. However, Si solar cell durability and reliability for long run of around 20 years is unparalled with any other solar cell technology still [7]. Recently more research is focused on the third generation solar cell which will discussed on the next topic.

Solar Photovoltaics (PV) outstands in new power generating capacity in 2017 which has an enormous growth in China, with more solar PV installed globally than the net contribution from the pollution causing fossil fuels and nuclear power combined. The total PV (silicon, CIGS, CdTe) installations amounted to 415 GWp with a power generation at the end of 2017 wherein 32% is solely taken up by China. Also the PV power generation was estimated to be 443 TWh where the price for PV rooftop system is approximated to 1400 €/kWp. Now the PV tender price is 4.33 € / kWh as of February 2018. In 2017 about 38.4 TWh electrical energy generation by PV in Germany terminated the emission of 19 Mio CO_2 [8]. As lifetime of a silicon solar cell is 20 years. A total module area : $A_{sc} = P / (\eta_{sc} \cdot \Phi_{exp}) = 10^8$ m² could suffise for 1 GW. Thus by the year of 2050 the expected energy demand is to meet 30TW, which requires an area of $3 \cdot 10^{12}$ m² of solar panels, which represents India's area. So for a large area, the cost of manufacture and installation would be very high as silicon technology demands high processing cost. As nature is always generous, the synthesis and manufacture of organic dyes and inorganic materials having good photon harvesting property has paved the way for new thin film based third generation photovoltaic technology [9]. More explanation will be discussed in the section 1.2.

20 years of research and development on the third-generation thin-film solar devices have paved the way for commercialization which is monitored by leading companies like Konarka and Plextronics in the organic photovoltaics (OPV) domain, and Dyesol, EPFL, G24i, Mitsubishi and Peccell on the dye-sensitized solar cells (DSSC) domain. Though DSSC and

OPV technologies lag far behind on the efficiency histogram when compared to conventional solar (~ 25 percent efficiency), however appealing properties of them are their low cost, substrate flexibility, color and ability to execute in either of faint or variable lighting scenario. DSSC will target larger area Building Integrated Photo Voltaic (BIPV) applications while OPV will have the potential in employment for lower power consumer apparatus [10].

1.1 Third generation solar cells

Third generation solar cells is basically dominated with p-n junction diodes and advanced thin film technologies. It employs organic dyes and inorganic compounds as the light absorber. They have attracted huge expertized research due to its handling cost and ease of fabrication. It can be classified into three categories: Dye sensitized solar cells, Copper Zinc Tin Sulfide, Organic solar cells, Perovskite solar cells and Quantum dot solar cells [11].

1.1.1 Dye-sensitized solar cells

Dye sensitized solar cell was first reported by Michael Graetzel and O`Regan in the year 1991. It represents a clean and bio-amicable form of renewable energy till date as its operation resembles that of the natural photosynthesis, a gift of God. The first DSSC employed n-type TiO_2 semiconductor with Ruthenium dye (N3) as the sensitizer and iodine electrolyte. Platinum was used as the counter electrode. The DSSCs differ from any other semiconductor as the function of light absorption and charge carrier entity is separate. The dye after photon absorption injects electron into the TiO_2. The dye is regenerated by the electrolyte which is then reduced by the counter electrode. The diode was successful with a photon conversion efficiency of 7.9% under simulated light and 12 % under simulated light [12]. At present, the three exemplary efficiencies of DSSCs are 12% [13] as reported by Yella et al, 13% as per reported by Mathew et al [14] and 14.7 % by Kakiage et al [15] based on various molecular and surface engineering. The working principle and engineering of DSSCs will be discussed in detail in the section 1.3.1

A number of researchers have reported the implication of titanium foil or stainless steel, tungsten and zinc as photoanode and lightweight poly(ethylene terephthalate) (ITO/PET) ITO/polyethylene naphthalate (ITO/PEN) as photocathode to furnish a lightweight flexible DSSCs. These cells have the advantage to be used in watches, laptops and cell phones. However the efficiency with flexible

DSSCs is lower than the conventional DSSCs [16]. The magnificence of DSSCs is also in its transparency. This has propelled it towards the invention of smart windows and for other BIPV modules with intelligent dual property of both as electricity generator and light shading with decoration purpose. The other feature of DSSC is based on the cylindrical DSSCs which stands in a unique platform of liberty of incident angle of sun light for photo excitation. Not only on the windows, they can also be installed on the roof tops as well as on the building walls to pay no need for the barren land for installation of it [17].

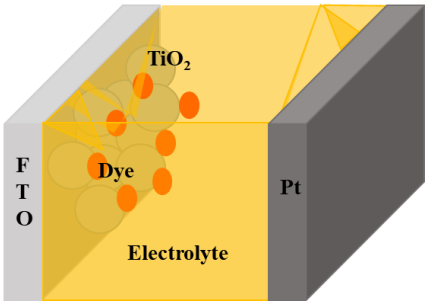

Figure 1. Constituents of a working DSSCs.

1.1.2 Organic solar cells

The high cost in the production of the inorganic solar cell had arisen interest in material scientists to design and synthesize organic molecules for photovoltaics. Organic solar cells can be divided into three categories-a) single layer organic solar cell b) Bilayer organic solar cell c) bulk heterojunction solar cell. Initially small organic molecules were implemented until the application of polymers into the organic solar cells which has now contributed to the evolution of brilliantly economical working cells [18]. The discovery of conducting polymers by Alan J. Heeger, Alan G. MacDiarmid and Hideki Shirakawa which also have made a new revolution in the field of organic solar cell have fetched them Nobel Prize. Bulk heterojunction solar cells come under polymer solar cell (PSC) where a polymer is mixed finely with other organic molecules which behave like a donor and acceptor materials with interpenetrating network to promote potent exciton dissociation. The first polymer based bulk heterojunction was reported by Heeger which employed poly(2-methoxy-5-(2'-ethyl-hexyloxy)-1,4-phenylene vinylene) MEH-PPV:C60 (fullerene) where fullerene is an electron acceptor and efficiency was below 1%.[19] Gradually from the enthusiastic contributions of scientists, many polymers like P3HT, PTB7, PTB, etc. and PCBM (fullerene

derivative [6,6]-phenyl-C61-butyric acid methyl ester) and interfacial engineering have pushed up the efficiency upto 15%. However, research is being carried out on non-fullerene materials to reduce the material cost and to increase the stability of the PSCs [20]. The basic working principle of DSSCs and PSC is almost similar except their macro attributes where DSSCs involves both inorganic and organic material whereas PSC is solely based on organic. Nevertheless the organic moiety is used for light harvesting in both the cases.

1.1.3 Perovskite solar cells

Perovskite solar cell, an inorganic-organic hybrid solar cell can be regarded as a modified form of solid

state DSSCs where the hole transporting material is a solid material unlike the classic DSSCs. The perovskite material $CH_3NH_3PbI_3$ was used a sensitizer by Miyasaka and group in 2009 for DSSCs with liquid electrolyte which had the then furnished an efficiency of 3.8 % [21]. This benchmark report has then evoked to the efficient perovskite solar cell which has now become the most efficient among the third generation solar cells. Then the first perovskite solar was reported by Nam Gyu Park and group with 6.5 % efficiency which opened up a new horizon for the efficiently perovskite solar cell of the generation [22]. As perovskite solar cell includes lead (Pb) as one of its major atom, major research has now been focused on substituting Pb with other metals as well as on its stabilization to make its way towards low cost commercialization. However, the perovskite $CH_3NH_3PbI_3$ have a broad absorption upto 800 nm which is good enough for far red photo harvest. Moreover scientists have discovered that the substitution of (lead) Pb with tin (Sn) not only increases the absorption upto 1060 nm but also increases the stability of the solar cells [23]. The device structure for a general perovskite solar cell is ITO/(electron transporting layer)TiO_2/perovskite $CH_3NH_3PbI_3$/ (hole transporting layer) Spiro compounds/Metal (Au). The beauty of perovskite solar cell is its low exciton binding energy which makes charge separation and collection easy unlike the organic solar cells. The working of perovskite solar cell starts with photon harvest by the perovskite material and exciton generation followed by charge separation. Then the electrons are transported to the electron transporting layer and holes to the respective hole collecting layer respectively. Then the electrons from the ITO reach the counter electrode thus generating current. However there still exists a vague understanding in the mechanism at the microscopic level [24]. Nevertheless within one decade, KRICT and NIST have been successful

in pushing the efficiency of perovskite solar cell upto 22.1% (as per NREL certification) which is comparable to that of the commercialized silicon solar cell with 25% efficiency [25]. Till now Oxford Photovoltaics is the leading company in the number of patents for perovskite solar cells. Oxford photovoltaics and Hunt energy enterprise outstands at material level, whereas Sekusui chemical, Fujifilm, Igchem and Chengdu new kelichem holds the highest position in the device level. At the academic level, Krict, Bohai university, EPFL, Tianjin university, Okinawa institute and CSIRO holds the top position in perovskite research area [26].

1.2 Dye sensitized solar cells

Dye sensitized solar cells resemble a multi junction p-n diode where there exist the individual role of the light harvester and charge collector which makes it more efficient than the single junction p-n diode. However there exist some obligatory conditions to be maintained to furnish a well working solar cells.

1.2.1 Working principle of dye sensitized solar cells

The main components of a typical DSSCs consist of a semiconductor, generally n-type TiO_2 which is coated on conducting substrate Fluorine doped Tin Oxide, FTO. The dye gets adsorbed via an ester linkage with the –OH group on the TiO_2 with the acid group on the dye. When the dye absorbs sunlight, with the required amount of energy, the electron in the Highest Occupied Energy level (HOMO) jumps to its Lowest occupied Energy Level (LUMO). That electron is then injected into the conduction band (CB) of the n type semiconductor. Thus when it comes to the energy level matching of the dye and the semiconductor, it is mandatory that the Lowest occupied Energy Level (LUMO) of the dye should be atleast 0.16 eV higher than the conduction band (CB) of the n type semiconductor to facilitate electron injection from the LUMO to the CB. When the electron has already been excited to the LUMO from the HOMO of the dye, there is a deficiency of electron in its HOMO. Thus to have the continuous run of the cycle (turn over number), the dye has to be regenerated by accepting electron. So for its regeneration, a redox couple (electrolyte) is generally employed which is termed as a hole transporting material in the case of solid state DSSCs. Also the redox couple has to be supplied with electrons which is fulfilled by a metal with a high work function which also receives electron via external load from the FTO. This way the cycle is complete. Again, the energy level matching has to be maintained in these cases as well, the redox

potential of the redox couple should be higher (against vacuum) that the HOMO of the dye for donating electron. The mode of movement of electrons is diffusion [27].

The efficiency of a solar cell is given by the equation:

$$Efficiency\ (\%) = \frac{Jsc\ X\ Voc\ X\ FF}{Pin} \quad \dots\dots\dots\dots\dots\dots\dots\dots\dots\dots\dots\dots \ (1)$$

Where, Jsc = short circuit current density, Voc = open circuit voltage, FF = fill factor and Pin = power input

Also, another elemental analysis on the peformance of the solar cell is measured in its terms of the Incident Photon Conversion efficiency (IPCE) which is given by-

$$IPCE = \frac{Jsc}{e\phi} \dots\dots\dots\dots\dots\dots\dots\dots\dots\dots\dots\dots\dots\dots\dots\dots\dots\dots\dots\dots\dots\dots\dots..(2)$$

$$e\ is\ the\ elementary\ charge$$

The current density (Jsc) depends on the nature of the dye and its ability to absorb photons and convert into electricity. A dye absorbing maximum photon flux, (Near Infrared Region) will be able to supply more current. As the open circuit voltage (Voc) is given by the difference in the fermi level of electrons in the TiO_2 and the redox potential of the electrolyte, an electrolyte with a deeper value of it will contribute to the more value of Voc. The fill factor (FF) is the ratio of the maximum power (Pmax) to the product of Jsc and Voc.

$$FF = \frac{Pmax}{Jsc\ X\ Voc} - - - - - - - - - - - - - - - (3)$$

Here Pmax is the product of the photocurrent and photovoltage where the power output is maximum. Equation (1), (2) and (3) are taken from a review `Dye Sensitized Solar Cell` by Anderson Hagfeldt [27].

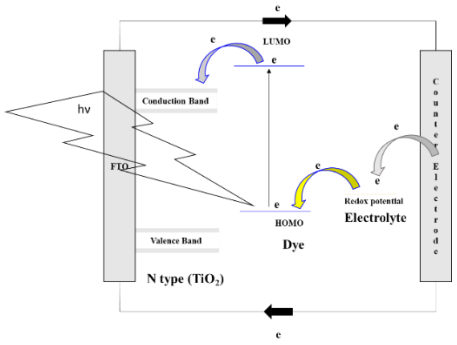

Figure 2. Electron flow pathway in a working DSSCs.

The arrows shown in the figure shows the forward electron injection which must dominate in order to bestow a good efficiency. However, it is never 100 % feasible. The excited electrons in the LUMO and the conduction band can be trasnsferred back (recombination) either to the HOMO of the dye or to the elelctrolyte which hampers the efficiency of the solar cell. As it is mentioned above that the Voc is given by the difference of the conduction band of TiO_2 and the redox potential of the electrolyte, however there will be some voltage loss on recombination. Thus it is very necessary to control recombination. On the other hand, FF can also be regarded as a measure of the internal resistance in forward charage transfer. The device affording less resistance diffusion will contribute to a better value of fill factor, hence better efficiency.

1.2.2 Function and necessity of dye structure as sensitizer

Dyes can be regarded as the vital tool, coined as the `Heart` by scientists for dye sensitized solar cell. The principle function of dyes is to absorb sunlight which gets converted into chemical energy in plants via photosynthesis and to electrical energy in DSSCs. However all dyes cannot work as a sensitizer in DSSCs. The primary requirement in dye is an anchoring group which could bind to the semiconductor via an ester linkage and supports electron injection from the LUMO of the dye to the semiconductor. Besides bearing a suitable and strongly binding anchoring group, the energy level (HOMO and LUMO) of the dye should have favourable energy as per required by DSSCs working principle as mentioned in 1.3.1. If the dye fails to meet these conditions, it cannot be employed as a sensitizer in DSSCs [28].

There lies only 27.7% of the photon flux at Air Mass 1.5 in the visible region which makes more photon flux in the Near Infrared region. (750-2500 nm) [29]. According to the theoretical

calculation, a dye absorbing till 800 nm wavelength will be able to give a maximum current density of 26 mA/cm^2 . Moreover, the Shockley Queisser limit gives a theoretical value of 33.7% efficiency at 1.34 eV of the semiconductor [30]. Thus to reach the limit, Near Infrared Dye (NIR) is of choice, provided the energy level condition is maintained as shown in figure 2. Besides absorbing in the NIR region, the dye should be stable to undergo many cycles of oxidation and reduction i.e with more turn over numbers of atleast 10^8 to give a DSSCs working lifetime of 20 years [31]. The choice of dye depends on the type of semiconductor employed i.e n type or the p type ones respectively.

As the excited electrons in the LUMO of the dye and the conduction band of the TiO_2 have the feasibility to bounce back to the HOMO of the dye as well as to the electrolyte, dyes bearing longer alkyl group is generally found to work well which is much required when the redox couple employed is a bulkier group and bears a positive charge, for example : cobalt redox shuttle. The main role of the long alkyl group is in blocking the back electron transfer [32-34].

1.2.2.1 Visible dyes

The wavelength from 390-700 nm of the solar spectrum upto which a normal human eye can visualise fall under the category of the visible light region. The colorful molecules (dyes) absorbing in this region generally appear to be either red, orange or yellow corresponding to the band gap (difference HOMO and LUMO) between 2.00-3.26 eV which also corresponds to the photon energy in the visible region. The visible dyes can be divided into two categories: a) with metal at the central core and b) purely organic.

a) with metal at the central core : The charge transfer in these type of dye with metal at the centre is basically via metal to ligand charge transfer (MLCT). The excitation for MLCT generally occurs in the visible region of the electromagnetic spectrum which is responsible for a distinct color of the metal complex. Various metal complexes such of ruthenium, copper, nickel, platinum, iridium and iron etc. have been reported as sensitizers among which the ruthenium based is used widely investigated. Many ruthenium dyes bears a 4,4`-dicarboxy-2,2`-bipyridine or 4,4`,4``-tricarboxy-2,2`,2``-terpyridine ligand. This ligand contains carboxylic moieties as anchoring groups. However, metal based dyes do not show a sharp absorbance and hence do not bear a good molar extinction coefficient. N3, a Ruthenium dye absorbing

around 525 nm was first implemented as a sensitizer for DSSCs by Michael Graetzel in 1991[12]. This dye was able to furnish a photocurrent density of 12 mA/cm^2. Thereafter, a number of metal based visible dyes with the modification in the ligand structure were reported for instance-N3, Z907, N749 (Black dye) etc [27]. Z907 varies with N719 only in the alkyl group of the ligands where the former bears a longer alkyl group and the latter bears none demonstrating the need of longer alkyl group for cobalt electrolyte. The black dye bears a molar extinction coefficient of 7X10^3 mol^{-1}cm^{-1} at around 600 nm bearing molar extinction coefficient of about 200 X10^3 mol^{-1} cm^{-1} at around 800 nm. Still it is able to harvest photons efficiently with an appreciable current density 21 mA/cm^2 where the theoretical value is limited to 33 mA/cm^2 [35].

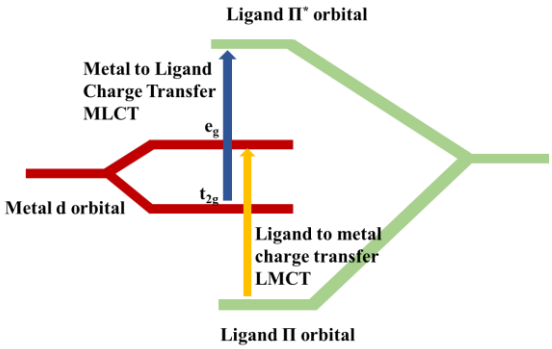

Figure 3. Metal to ligand charge transfer mechanism in case of metal complex.

Chlorophyll, the main pigment for photosynthesis with Mg metal at the centre has also been used as a sensitizer in DSSC but it did not stand upto its role as in photosynthesis [36]. Besides the application of visible dyes in DSSCs, they find wide application in photography, imaging etc.

b) purely organic (metal free): The advantage of purely organic dye lies in its ease of synthesis and fine tuning of its band gap which provides the scope for Near Infrared Dye design. In comparison to the metal based sensitizer, the metal free dye bears a higher molar extinction coefficient than the metal based. The higher molar extinctinction coefficient of it is contributed to the Π- Π* charge delocalization. The basic feature of organic dye is the Donor-Π-Acceptor (D-Π-A) and Donor-Acceptor-Π-Acceptor (D-A-Π-A) framework generally having a planar structure. For the dye with δ and σ as the dye density and absorption cross sectional area respectively, the light harvesting efficiency (LHE) is given as

$$LHE = 1\text{-}10^{-\delta\sigma(\lambda)} \ldots\ldots\ldots\ldots\ldots\ldots\ldots\ldots(4)$$

Thus for a lower molar extinction coefficient bearing dye, more thicker mesoporous TiO_2 is required. So in this case, metal free dyes have gained attention which surpass the application of thicker TiO_2 and gives appreciable perfomance with the thinner one and consequently builds a stone for transparent DSSCs. These class of dyes have the main Π framework as donor-pi-acceptor where the donor is basically a triarylamine and the acceptor is an acid group.

Many natural organic dyes from plants and fruits like, anthocyanin, flavonoid, carotenoid, etc have also been used as sensitizer in DSSCs with the hope of fabricating devices easily and efficiently. However, their role was not so appreciable as that in the case of photosynthesis [37]. The synthesized dyes performing very well in DSSCs till date are basically visible dyes. As the main framework of organic dyes is comprised of Π electrons, they are more prone to dye aggregation: H aggregation and J aggregation which is more visible in case of far red or NIR dye as well. The commercial dyes namely, D35, TASTCA, MK2, Y123 etc are well example of visible dyes giving good performance in DSSCs.

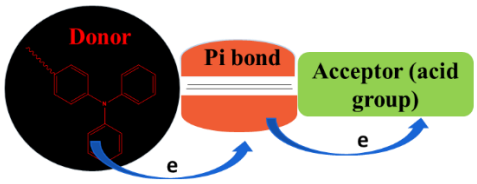

Figure 4. General structure of metal free organic dye with donor pi acceptor structure.

1.2.2.2 NIR dyes:

The low energy electromagnetic radiation ranging from 700 to 2500 nm belongs to the Near Infrared Region which is generally invisible to a normal human eye and transparent to human tissue. As, this ray would furnish more current density. According to Shockley Queisser limit, a maximum efficiency of 33.7% could be attained at 1.34 eV energy which correponds to the wavelength value of 925 nm. Thus dyes absorbing in this region would be able to reach the limit if proper working condition is maintained. Beside its application in DSSCs, NIR dyes find huge application in bioimaging, biosensing [38-40] etc. For DSSCs, efforts have been put in to design NIR dyes to utilise the photon flux of that region and to generate maximum current out of it.

However, energy level matching is the first and foremost criteria for a working DSSCs as shown in figure 2 which limits the further decrease in band gap than required for dye regeneration (in HOMO) and injection from its LUMO. Till date there is only a handful number of NIR dyes as sensitizer in DSSCs among which squaraine, porphyrin and cyanine find their application.

i) **Squaraine dyes** These class of dyes bear a central square core hence the name squaraine.The unique feature of squaraine dyes is its sharp absorbance ($\varepsilon \sim 10^5$) between (600-700) nm [41-43]. These dyes have two electron donating group (generally indoline moiety because of its excellent electron donating power) on the either side of the central core with a brilliant blue color. Detailed structure-property relation will be discussed in the next section.

ii) **Porphyrin Dyes** Porphyrin dye is a class of metal organic dye with the push pull electron system and good stability. The beauty of these class of dyes lies in the the dual absorbance in the visible and far red region. The absorbance in the visible region is defined in terms of its soret band (400-500 nm) and another in the far red region as the Q band (500-700 nm). For DSSC application, zinc porphyrin dyes have gained more attention due to its virtue by stability and excellent performance. The zinc metal porphyrin dye YD2-O-C8 as reported by Yella et al performs well enough as it harvest photons across the visible region and touches the NIR region with a current density of almost 18 mA/cm^2 with its corresponding efficiency of 12% [13]. The dye YD2 has also the same molecular skeleton like YD-O-C8. The other Zn porphyrin dye is based on the donor Π bridge acceptor design namely SM315 and SM371. These green dyes have the structural modification of YD-O-C8 by the introduction of benzothiadiazole group and results in the photon harvest across the visible region upto 800 nm. The dye SM315 furnishes high current density of $18mA/cm^2$ with an efficiency of 13% [14].

iii) **Others** Dyenamo blue, a structurally modified form of D35 has been reported with the motive to shift its absorbance in the NIR region which was only successful in absorbing in the far red region of 571 nm [44]. The dye Y123 bears a good Π conjugation, but still it is able to harvest photons till 600 nm, the maxima being concentrated around 550 nm [45]. Till date, only squaraine dyes stand as the sole example for NIR absorption offset around 750 nm with a sharp absorption.

1.2.3 Electrolytes in dye sensitized solar cells

The perfomance of DSSCs is entirely dependent on the three parameters : current density (Jsc), open circuit voltage (Voc) and the fill factor (FF) which as a whole is dependent on the the electrolyte and its interaction in the interfaces. Apart from the dye`s photon harvest and injection efficiency, the Jsc is also significantly governed by the degree of dye regeneration for which the electrolyte plays a major role. As the Voc is governed by the difference of the fermi level of the electron on the TiO_2 and the redox potential of the electrolyte, a good choice of electrolyte with a deeper redox potential will result in more Voc. The FF is controlled by the diffusion of charge and the interfacial resistances. Thus a better choice electrolyte is must to furnish a well working DSSCs. The electrolyte employed in the first DSSCs was the iodine electrolyte. However, due to its corrosive nature and light harvesting propensity, many electrolytes as a substitute to it have been reported. The redox shuttle for DSSCs should have the following feature:

a) Redox potential of the redox couple should be higher than that of the HOMO of the dye maintaining minimum energy barrier for dye regeneration.
b) Fast redox reaction between acceptor and donor in the couple
c) It should not compete with the dye in the photon absorption (iodine electrolyte absorbs some part of the visible light)
d) It should facilitate effective charge diffusion and less recombination and have good interfacial contact with the TiO_2 and as well as the counter electrode [46].

The best efficiency for the DSSCs till date has been attained with liquid electrolyte, generally with Co^{+2}/Co^{+3} and I^-/I_3^- redox mediator .The charge movement in liquid electrolyte is basically due to ions diffusion whereas it is due to electron and hole hopping in case of solid state DSSCs and liquid electrolytes have easy flow of ions than the solid transporter. The working efficiency of electrolyte is generally governed by its conductivity and diffusivity which is given by:

$$\sigma = \Sigma \mu_i \eta_i q_i \quad \text{..... (5)}$$

where σ, μ_i, n_i, and q_i stands for conductivity, mobility, carrier concentration, and charge of the ionic specimen, respectively [47].

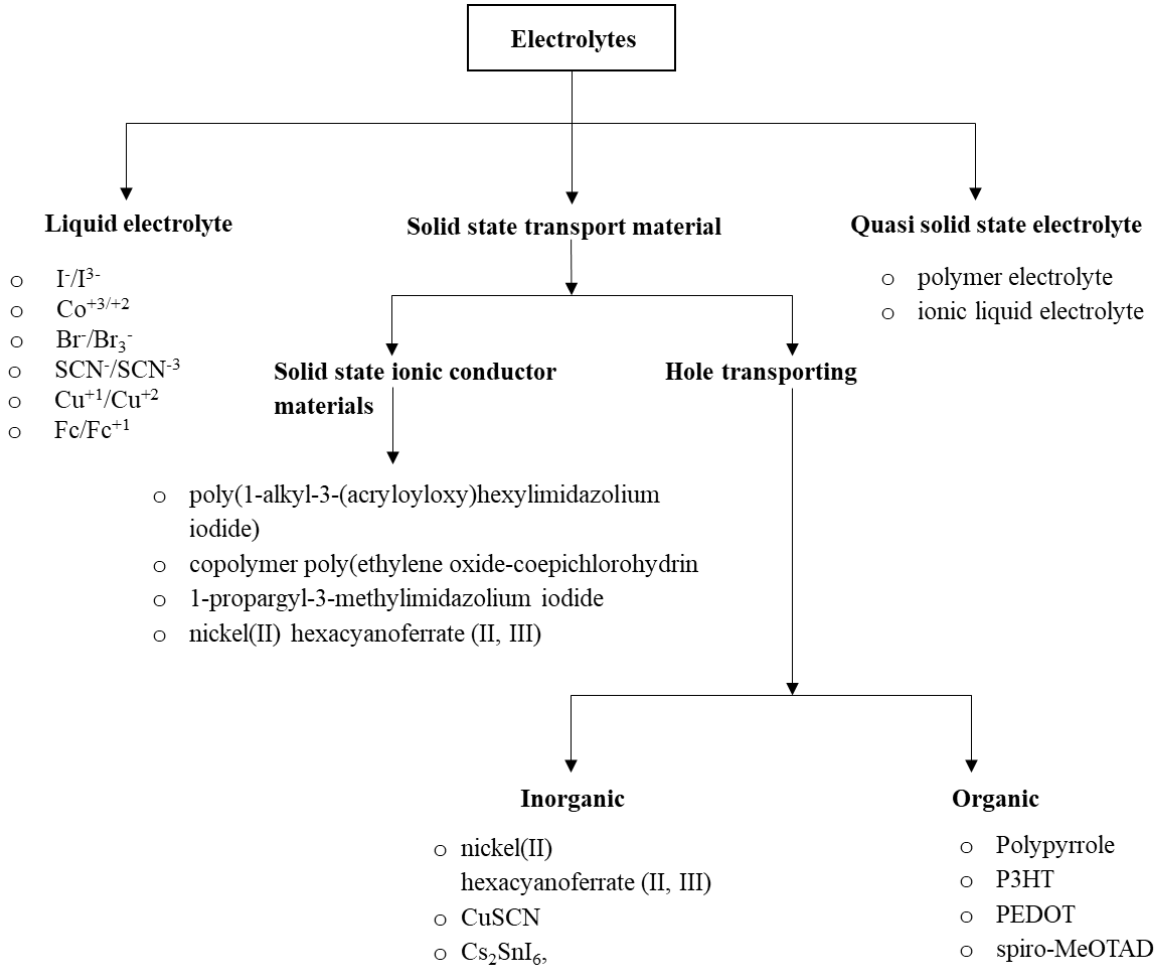

As mentioned above, that the better Voc is given by a deeper redox potential bearing electrolyte, bromine (Br^-/Br_3^-) electrolyte till date has been successful in giving the highest record Voc of 1.4 V with silyl as the anchoring group whereas DSSCs with iodine redox electrolyte has less than 0.9 eV [48]. Recently a very good Voc of 1.09 V and FF of 78% with Y123 dye has been achieved with Cu^+/Cu^{+2} redox mediator without the application of spacer between the photoanode and the photocathode to minimize the resistance for electron diffusion. The device based on this redox shuttle was also able to function even better when the solvent was completely evaporated (i.e the solid state DSSCs), which has given rise to the so called "Zombie cell" [49].

Quasi solid state electrolyte has been developed to rule out the disadvantage offered by the liquid electrolyte in solvent evaporation. It can be divided into a) polymer electrolyte and b) ionic liquid electrolyte. The polymers poly(ethylene oxide) (PEO or PEG), poly(acrylonitrile) (PAN), poly(vinyl pyrrolidinone) (PVP), polystyrene (PS), poly(vinyl chloride) (PVC), poly(vinylidene

ester) (PVE), poly(vinylidene fluoride) (PVDF), poly(methyl methacrylate) (PMMA), PEG and bifunctional [poly(ethylene glycol) etc. have been employed for hole transport in quasi solid state electrolyte. A quasi-solid ionic liquid electrolyte has high conductivity (~10^{-3} Scm^{-1}) which makes it a better source for hole transport. The ionic liquid electrolyte containing iodine and N-methylbenzimidazole (NMBI) in 1-methyl-3-propylimidazolium iodide (MPII) achieved an efficiency of 5.3%. DMII/EMImI/EMImB $(CN)_4/I_2$/NBB/GNCS contributed to QS-DSSC with C103 dye, yielding a record efficiency of 8.5% [46].

In case of solid state hole transporting, the material should possess a high hole mobility for effective regeneration of the dye. The solid state material generally employed are either conducting polymers or inorganic p type semiconductor. Polymers like polypyrole, polyaniline, poly(3,4-ethylenedioxythiophene) (PEDOT) etc. have found application as a solid hole transporting. Spiro compound MeOTAD as a hole transporting material has been able to furnish an efficiency of 7.2% for DSSCs [50]. P type semiconductor like Cs_2SnI_6 (perovskite structure) has been the substitute for expensive spiro compound though it has reached the efficiency of 3.4 % making rooms for commercialization [51].

1.2.3.1 Cobalt complex redox system

The widely used redox mediator for DSSCs is the cobalt redox shuttle other than that of the iodine based. Cobalt complex with ligands including terpyridine, bipyridine, and phenanthroline etc. have been explored as a redox shuttle. The main aim of employing organic ligand based redox shuttle is the flexibility in tuning the redox potential of the mediator. The cobalt complex like $[Co(terpy)_2]^{n+}$, $[Co(en)_3]^{n+}$, $[Co(en)3]^{n+}$ have their redox potential higher than that of the iodine, hence theoretically they will bestow with less Voc. So by modifying the ligand, the redox potential can be lowered. The complex like $[Co(dmbip)_2]^{n+}$, $[Co(bpy)_3]^{n+}$ have their redox potential lower than that of the iodine redox shuttle (0.45 E Vs NHE), the deepest being $[Co(bpy\text{-}pz)_3]^{n+}$ (0.86 E) [52].Thus these complexes will furnish more Voc which is directly linked with the performance of the DSSCs. The other advantage of the cobalt electrolyte is its zero absorbance in the visible region, therefore the photons will be absorbed by the dyes and dyes alone. However, the major drawback in case of the cobalt electrolyte is in mass transport due to bulky size as compared to that of the iodine which results in slow diffusion and more prone to recombination. Moreover the cobalt bears positive charge which creates more rooms for recombination.

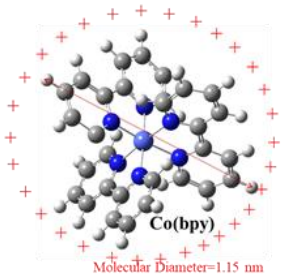

Figure 5. Molecular structure of $[Co(bpy)_3]^{+2/+3}$ complex.

The mode of electron transfer between the redox shuttle in cobalt complex is the one step outer sphere electron transfer mechanism which involves no intermediate step of bond formation unlike the iodine redox mediator.

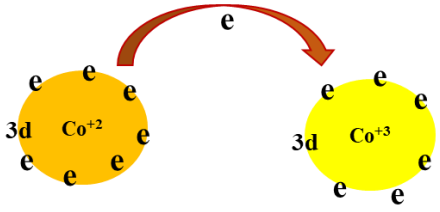

Figure 6. Outer sphere electron transfer in cobalt complex

According to the Marcus-Gerischer model, diffusion of the reactants, the driving force for the reaction to occur, the necessary reorganization energy, and the suitable electronic coupling determine the electron transfer rates. Cobalt complexes are known to have relatively slow electron transfer kinetics on account of the large internal reorganization energy when going from d^7 (high spin) to d^6 (low spin) which is required for redox shuttle in electrolyte [53].

The widely employed redox shuttle is cobalt bipyridyl (0.57 V) due to its relatively deeper redox potential and optimum size compared to the other cobalt complex like $[Co(dmbip)^{n+}]$ with bigger size. Bulkier ligands enhances the spatial separation between the interface and the cobalt centre and hence lower electronic coupling for charge transfer. It has also been found that electron lifetime in cobalt bipyridyl redox mediator is shorter than that of the iodine mediator.

$$Ln = \sqrt{\mathrm{D}}.\boldsymbol{\tau} \ldots\ldots\ldots\ldots\ldots\ldots\ldots\ldots\ldots\ldots\ldots\ldots (\mathbf{6})$$

Where, Ln, D and τ are Diffusion length, diffusion coefficient and lifetime of the electron respectively.

Thus to employ cobalt redox mediator, strict control on recombination has to be taken care of. Thus surface passivation with both metal oxide as well as dye is mandatory to minimize the voltage loss. Many metal oxide like MgO, Al_2O_3, NiO, Nb_2O_5 etc. have been found to be effective in blocking the back electron transfer [54]. All dyes are not suitable for cobalt electrolyte. Only the dyes bearing longer and branched alkyl groups work efficiently with cobalt electrolyte. The role of the long alkyl chain is to passivate the TiO_2 surface so that the electrons there are screened from reaching the cobalt complex [32,33,55]. Till date, the record efficiency of 14% has been achieved with co-sensitization of LEG 4 and ADEKA in conjunction with cobalt phenanthroline redox shuttle by Kakiage et al [56].

1.3 Squaraine dyes

The squaraine dye takes its name from its central moiety `squaric acid` which was first coined by Schmidt in 1980. The main framework of squaraine dyes consist of the central electron deficient four membered ring with electron donating groups on either side of it. Basically it is a class of polymethine Donor-Π-Acceptor (D-A-D) dye with resonance stabilization. The zwitterionic structure brings in a good dipole moment of the dye.

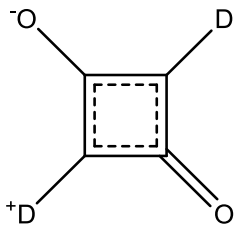

Figure 7. General structure of squaraine dye where D represents an electron donating group.

1.3.1 Background

The squaric acid was first reported by Sidney Cohen, John R. Lacher, and Joseph D. Park in the year 1959. The dibasic acid was prepared by the aqueous hydrolysis of 1,3,3,-triethoxy-2-chloro-4,4-difluorocyclobutene and also by both aqueous and acid hydrolysis of 1,2-diethoxy3,3,4,4-tetrafluorocyclobutene. The acid carbonyl group was further confirmed by the negative result to

the phenylhydrazine test [57]. The first squaraine (symmetric dye) was synthesized by Treibs in 1965 by reacting the squaric acid with pyrrole to give violet red dye [58]. Thereafter, a superfluity number of squaraine dyes with different donor groups came into existence.

1.3.2 Synthesis and properties

The squaraine dyes are generally prepared by the condensation of electron rich aromatic or heterocyclic compounds like N,N-dialkylanilines, benzothiazoles, phenols, azulenes, indole and pyrroles with squaric acid. Thus there exists a wide scope in tuning the properties of the respected dye. For synthesis of symmetric dye, two equivalent of electron donating moiety is condensed with one equivalent of squaric acid in toluene/butanol (1:1) system for about 18 hours. Whereas for the asymmetric dye, squaric acid is first converted into its mono ester form (squaric ester). Then an electron donating group is made to react with the squarate form to give a yellow colored half dye. Finally the half dye obtained is then condensed with another electron moiety for about 18 hours to give the bright blue dye [59].

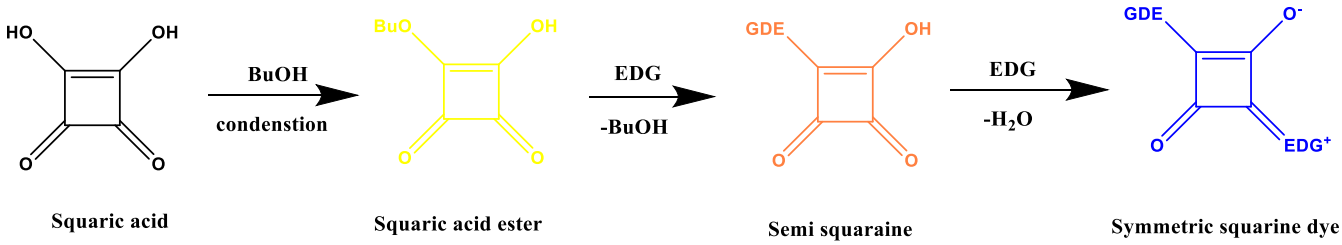

Figure 8. Shows the reaction scheme for squaraine dye synthesis.

Many oligomer and polymeric squaraine have also been synthesized for various application. It is synthesized by the condensation of squaric acid with more than one reaction center bearing electron-rich aromatic compounds leading to macromolecular analogues which even lowers the band gap to 1.1 eV [60,61]. In the squaraine framework, HOMO is concentrated in the central square moiety whereas the LUMO is delocalised on the electron donating moiety on either side of the central core. Squaraine is a planar molecule with pi (Π) electrons delocalization which is responsible for the bright blue to green color of it. The unique feature of squaraine dyes is its sharp absorbance in the far red region (650-700) nm with a high molar extinction coefficient of ~ 10^5 dm^3 mol^{-1} cm^{-1} which is attributed to the Π- Π* electron transfer. The band gap of the squaraine dye can be lowered by increases the electron donating property of the donor and increasing the

effective conjugation of the Π electrons. Also, squaraines generally exhibit a small stokes shifft (15-20) nm which shows its conformational rigidity. Due to its rigid and planar structure, the squaraine dyes are more prone to aggregation. They exhibit both H aggregation and J aggregation.

Aggregation: When planar molecules undergo self assembly owing to strong Vanderwaal reaction, it

results in aggregation. When the aggregate is due to face to face to overlapping, it results in H aggregation. Squaraine dye often tends to exhibit H aggregation due to its planar structure. H aggregate leads to the blue shift or hypsochromic shift in the lower wavelength region. The head to tail overlap of squaraine dye results in the formation of J aggregate. The J aggregate absorbs in the higher wavelength region compared to that of the monomer (bathochromic shift) [62].

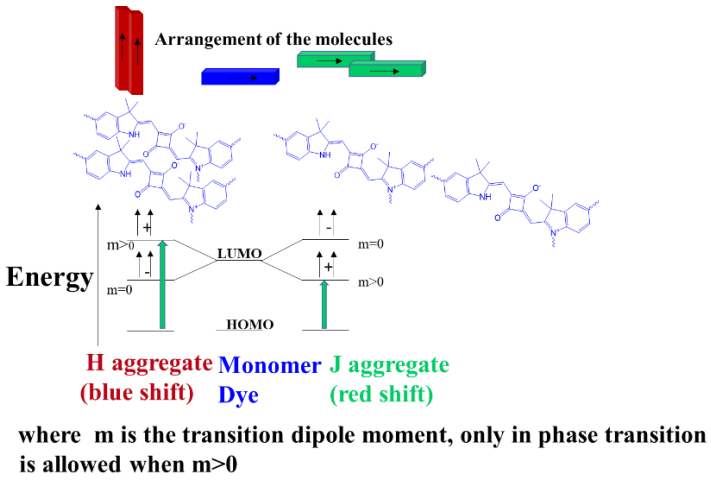

Figure 9. Energy diagram for monomer dye and its H aggregate and J aggregates.

One of the interesting properties of the squaraine dye is its two photon absorption (TPA). The squaraines with more Π extention with a good separation between the terminal electron donating group and the central core (with large TPA cross section) is found to exhibit this second order process. These dyes have a large TPA cross section as well as a two photon absorbtion wavelength of 1 μm [63].

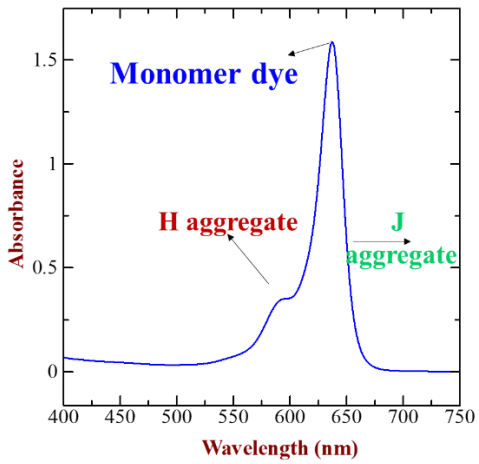

Figure 10. Electronic absorption spectrum a squaraine dye in ethanol solution.

1.3.3 Applications

i) **DSSCs**: Because of its sharp absorption in the far red region with high molar extinction coefficient of ~ 10^5 dm^3 mol^{-1} cm^{-1} , squaraine dyes open up a new hope for NIR photon harvest. The metal free, cost effective dye have been widely employed as sensitizer in both n-type and p-type DSSCs. Its high molar extinction coefficient has also favoured solid state DSSCs. Moreover, it finds application in both smart window as well as tandem solar cell for panchromatic photon harvest [41,43,64,65].

ii) **Organic Light emitting diode (OLED) and transistor :** Ambipolar light-emitting Organic Field Effect Transistors for emitting light in the NIR region. Also, organic-based devices emitting (OLED) in the near-infrared (NIR) is beneficial for utilization in broad-band optical telecommunication and sensors [66,67,68].

iii) **Biosensor and metal ion detector :** The far red absorbing squaraine dyes find application in biosensing very well as the biological entities are transparent to the NIR light. The high fluorescence yield of squaraine dyes employs it as implanted fluorescence biosensors as well as fluorescent protein label. It also finds application in selective detection of metals ion like Mg^{+2}, Hg^{+2}, Pb^{+2}, Na^{+}[69,70,71,72].

iv) **Photodynamic therapy :** Squaraines are used as sensitizer to inactive the living tumor cells by penetrating deep into the tissues in photodynamic therapy. It also finds applications in singlet oxygen generation [73].

1.4 Motivation of the research

Considering all acute needs of the renewable energy in the near future and also the depletion of the existing fossil fule, low cost and clean DSSCs has to be paid more attention with the aim for its commercialization. However, the efficiency and stability of the DSSCs till date is still a matter of concern and the two decades focussed research have only been able to result in the efficiency of 14% which is far beyond its theoretical limit. Thus the motive of my research is to fabricate DSSCs with good efficiency and to work on its stability.

1.4.1 Aim and challenges

My aim for the doctoral thesis is to design and synthesize near infrared dyes (NIR) with narrow and intense light absorption as sensitizer for DSSC for large wide wavelength photon harvesting in combination with potentail visible light harvesting dyes. On doing so, we can get a higher current density and the theory says that a value of 36 mA/cm^2 could be attained, when the photon harvesting inculdes from the visible to the NIR region. Fortunately the design and synthesis of visible dyes as sensitizer is easier and there are abundant reports on the visible dyes but we can only get a handful of reports for NIR dyes. The design of visible dye is feasible as sensitizer as it bears a large enough band gap and meets the energy barrier demand for electron injection and dye regeneration. On the other hand, the synthesis of NIR dyes requires obligatory caution as they bear a smaller band gap but has to maintain the necessary driving force conditions. Therefore, the design of NIR dyes as sensitizers for DSSCs is a challenging task. So this arouse an immense curiosity in me to work for the design of NIR dyes. Apart from the difficulty in the synthesis of the NIR dyes, the employment of a deeper redox potential bearing redox shuttle in conjunction with it further adds upto the task of in the scale of difficulty. Though the application of deeper redox potential bearing redox shuttle is fruitful in terms of enhancing the open circuit voltage (Voc), it however may resemble a lesser driving force for dye regeneration when a narrow band gap dye is employed. Nevertheless, I put up with my aim of designing NIR dyes for cobalt bipyridyl redox shuttle with the redox potential value of around -5.0 eV against vaccum.

I was successful in designing blue squaraine dyes with maximum absorbance around (640-660) nm. Therefore, they stand as the representative of far red dye. So to extend the absorption in the longer wavelength, I tried to introduce more conjugation in the main dye framework and was

successful in extending the absorption with the wavelength offset around 750 nm. The synthesis of NIR dyes as sensitizer required acute concern for energetics, when cobalt bipyridyl complex with a deeper redox potential was used. Theoretical calculations was done prior to synthesis in order to have the estimation of the driving force. However, the major drawback in DSSCs is the sacrifice of current density for the sake of high Voc and vice versa. So the band gap of the dye cannot be decreased beyond a certain limit when deeper potential redox shuttle is employed. Keeping all these in hand, I aimed at designing NIR dyes for DSSCs with cobalt electrolyte in conjunction. I synthesized NIR dyes compatible with cobalt electrolyte to increase both the current density as well as the Voc. In addition, handling cobalt electrolyte is not an easy task. It is more prone to Voc loss as a result of recombination. Thus many mandatory criteria in terms of both of the surface passivation and fine tuning of dye molecular structure must be amicably taken in to consideration.

References

1. Chu, S.; Majumdar, A., Opportunities and Challenges for a Sustainable Energy Future. *Nature* **2012**, *488*, 294.
2. https://www.nj.gov/dep/dsr/trends/pdfs/energy.pdf
3. Turner, J. A., A Realizable Renewable Energy Future. *Science* **1999**, *285*, 687-689.
4. Kumar Sahu, B., A Study on Global Solar Pv Energy Developments and Policies with Special Focus on the Top Ten Solar Pv Power Producing Countries. *Renewable and Sustainable Energy Reviews* **2015**, *43*, 621-634.
5. Wesley Jeevadason, A.; Kalidasa Murugavel, K.; Neelakantan, M. A., Review on Schiff Bases and Their Metal Complexes as Organic Photovoltaic Materials. *Renewable and Sustainable Energy Reviews* **2014**, *36*, 220-227.
6. Green, M. A., The Path to 25% Silicon Solar Cell Efficiency: History of Silicon Cell Evolution. *Progress in Photovoltaics: Research and Applications* **2009**, *17*, 183-189.
7. Ramanujam, J.; Singh, U. P., Copper Indium Gallium Selenide Based Solar Cells – a Review. *Energy & Environmental Science* **2017**, *10*, 1306-1319.
8. Honrubia, A.H.; Requena, G.P., Influence of Solar Technology in the Economic Performance of PV power plants in Europe. A comprehensive analysis. *Renewable and Sustainable Energy reviews* 2018, 448-501.
9. http://www.solarcell.science/2017/07/01/history-emerging-pv/
10. http://researchrepository.murdoch.edu.au/id/eprint/2081/1/Tominaga_2009.pdf
11. https://en.wikipedia.org/wiki/Third-generation_photovoltaic_cell
12. O'Regan, B.; Grätzel, M., A Low-Cost, High-Efficiency Solar Cell Based on Dye-Sensitized Colloidal Tio2 Films. *Nature* **1991**, *353*, 737.

13. Yella, A.; Lee, H.-W.; Tsao, H. N.; Yi, C.; Chandiran, A. K.; Nazeeruddin, M. K.; Diau, E. W.-G.; Yeh, C.-Y.; Zakeeruddin, S. M.; Grätzel, M., Porphyrin-Sensitized Solar Cells with Cobalt (Ii/Iii)–Based Redox Electrolyte Exceed 12 Percent Efficiency. *Science* **2011**, *334*, 629-634.
14. Mathew, S.; Yella, A.; Gao, P.; Humphry-Baker, R.; Curchod, B. F. E.; Ashari-Astani, N.; Tavernelli, I.; Rothlisberger, U.; Nazeeruddin, M. K.; Grätzel, M., Dye-Sensitized Solar Cells with 13% Efficiency Achieved through the Molecular Engineering of Porphyrin Sensitizers. *Nature Chemistry* **2014**, *6*, 242.
15. Kakiage, K.; Kyomen, T.; Hanaya, M., Improvement in Photovoltaic Performance of Dye-Sensitized Solar Cells by Cosensitization with an Organometal Halide Perovskite. *Chemistry Letters* **2013**, *42*, 1520-1521.
16. Ito, S.; Ha, N.-L. C.; Rothenberger, G.; Liska, P.; Comte, P.; Zakeeruddin, S. M.; Péchy, P.; Nazeeruddin, M. K.; Grätzel, M., High-Efficiency (7.2%) Flexible Dye-Sensitized Solar Cells with Ti-Metal Substrate for Nanocrystalline-Tio2 Photoanode. *Chemical Communications* **2006**, 4004-4006.
17. Attoye, D.; Tabet Aoul, K.; Hassan, A., A Review on Building Integrated Photovoltaic Façade Customization Potentials. *Sustainability* **2017**, *9*, 2287.
18. Hoppe, H.; Sariciftci, N. S., Organic Solar Cells: An Overview. *Journal of Materials Research* **2011**, *19*, 1924-1945.
19. Yu, G.; Gao, J.; Hummelen, J. C.; Wudl, F.; Heeger, A. J., Polymer Photovoltaic Cells: Enhanced Efficiencies Via a Network of Internal Donor-Acceptor Heterojunctions. *Science* **1995**, *270*, 1789-1791.
20. Lu, L.; Zheng, T.; Wu, Q.; Schneider, A. M.; Zhao, D.; Yu, L., Recent Advances in Bulk Heterojunction Polymer Solar Cells. *Chemical Reviews* **2015**, *115*, 12666-12731.
21. Kojima, A.; Teshima, K.; Shirai, Y.; Miyasaka, T., Organometal Halide Perovskites as Visible-Light Sensitizers for Photovoltaic Cells. *Journal of the American Chemical Society* **2009**, *131*, 6050-6051.
22. Im, J.-H.; Lee, C.-R.; Lee, J.-W.; Park, S.-W.; Park, N.-G., 6.5% Efficient Perovskite Quantum-Dot-Sensitized Solar Cell. *Nanoscale* **2011**, *3*, 4088-4093.
23. Ogomi, Y., et al., Ch3nh3snxpb(1–X)I3 Perovskite Solar Cells Covering up to 1060 Nm. *The Journal of Physical Chemistry Letters* **2014**, *5*, 1004-1011.
24. Zhou, D.; Zhou, T.; Tian, Y.; Zhu, X.; Tu, Y., Perovskite-Based Solar Cells: Materials, Methods, and Future Perspectives. *Journal of Nanomaterials* **2018**, *2018*, 15.
25. https://www.nrel.gov/pv/perovskite-solar-cells.html
26. https://solarmagazine.com/uk-company-patents-perovskite-solar-cell-technologies/
27. Hagfeldt, A.; Boschloo, G.; Sun, L.; Kloo, L.; Pettersson, H., Dye-Sensitized Solar Cells. *Chemical Reviews* **2010**, *110*, 6595-6663.
28. Mishra, A.; Fischer, M. K. R.; Bäuerle, P., Metal-Free Organic Dyes for Dye-Sensitized Solar Cells: From Structure: Property Relationships to Design Rules. *Angewandte Chemie International Edition* **2009**, *48*, 2474-2499.
29. https://www.nrel.gov/pv/perovskite-solar-cells.html
30. Rühle, S., Tabulated Values of the Shockley–Queisser Limit for Single Junction Solar Cells. *Solar Energy* **2016**, *130*, 139-147.
31. Wang, P.; Wenger, B.; Humphry-Baker, R.; Moser, J.-E.; Teuscher, J.; Kantlehner, W.; Mezger, J.; Stoyanov, E. V.; Zakeeruddin, S. M.; Grätzel, M., Charge Separation and

Efficient Light Energy Conversion in Sensitized Mesoscopic Solar Cells Based on Binary Ionic Liquids. *Journal of the American Chemical Society* **2005**, *127*, 6850-6856.
32. Kroeze, J. E.; Hirata, N.; Koops, S.; Nazeeruddin, M. K.; Schmidt-Mende, L.; Grätzel, M.; Durrant, J. R., Alkyl Chain Barriers for Kinetic Optimization in Dye-Sensitized Solar Cells. *Journal of the American Chemical Society* **2006**, *128*, 16376-16383.
33. Chai, Q.; Li, W.; Wu, Y.; Pei, K.; Liu, J.; Geng, Z.; Tian, H.; Zhu, W., Effect of a Long Alkyl Group on Cyclopentadithiophene as a Conjugated Bridge for D–a−Π–a Organic Sensitizers: Ipce, Electron Diffusion Length, and Charge Recombination. *ACS Applied Materials & Interfaces* **2014**, *6*, 14621-14630.
34. Feldt, S. M.; Wang, G.; Boschloo, G.; Hagfeldt, A., Effects of Driving Forces for Recombination and Regeneration on the Photovoltaic Performance of Dye-Sensitized Solar Cells Using Cobalt Polypyridine Redox Couples. *The Journal of Physical Chemistry C* **2011**, *115*, 21500-21507.
35. Robertson, N., Optimizing Dyes for Dye-Sensitized Solar Cells. *Angewandte Chemie International Edition* **2006**, *45*, 2338-2345.
36. Hao, S.; Wu, J.; Huang, Y.; Lin, J., Natural Dyes as Photosensitizers for Dye-Sensitized Solar Cell. *Solar Energy* **2006**, *80*, 209-214.
37. Ludin, N. A.; Al-Alwani Mahmoud, A. M.; Bakar Mohamad, A.; Kadhum, A. A. H.; Sopian, K.; Abdul Karim, N. S., Review on the Development of Natural Dye Photosensitizer for Dye-Sensitized Solar Cells. *Renewable and Sustainable Energy Reviews* **2014**, *31*, 386-396.
38. Guo, Z.; Park, S.; Yoon, J.; Shin, I., Recent Progress in the Development of near-Infrared Fluorescent Probes for Bioimaging Applications. *Chemical Society Reviews* **2014**, *43*, 16-29.
39. Kaur, M.; Choi, D. H., Diketopyrrolopyrrole: Brilliant Red Pigment Dye-Based Fluorescent Probes and Their Applications. *Chemical Society Reviews* **2015**, *44*, 58-77.
40. Luo, S.; Zhang, E.; Su, Y.; Cheng, T.; Shi, C., A Review of Nir Dyes in Cancer Targeting and Imaging. *Biomaterials* **2011**, *32*, 7127-7138.
41. Pradhan, A.; Morimoto, T.; Saikiran, M.; Kapil, G.; Hayase, S.; Pandey, S. S., Investigation of the Minimum Driving Force for Dye Regeneration Utilizing Model Squaraine Dyes for Dye-Sensitized Solar Cells. *Journal of Materials Chemistry A* **2017**, *5*, 22672-22682.
42. Saikiran, M.; Sato, D.; Pandey, S. S.; Ohta, T.; Hayase, S.; Kato, T., Photophysical Characterization and Bsa Interaction of the Direct Ring Carboxy Functionalized Unsymmetrical Nir Cyanine Dyes. *Dyes and Pigments* **2017**, *140*, 6-13.
43. Islam, A.; Akhtaruzzaman, M.; Chowdhury, T. H.; Qin, C.; Han, L.; Bedja, I. M.; Stalder, R.; Schanze, K. S.; Reynolds, J. R., Enhanced Photovoltaic Performances of Dye-Sensitized Solar Cells by Co-Sensitization of Benzothiadiazole and Squaraine-Based Dyes. *ACS Applied Materials & Interfaces* **2016**, *8*, 4616-4623.
44. Hao, Y., et al., Novel Blue Organic Dye for Dye-Sensitized Solar Cells Achieving High Efficiency in Cobalt-Based Electrolytes and by Co-Sensitization. *ACS Applied Materials & Interfaces* **2016**, *8*, 32797-32804.
45. Tsao , H. N.; Yi , C.; Moehl, T.; Yum, J.-H.; Zakeeruddin, S. M.; Nazeeruddin, M. K.; Grätzel, M., Cyclopentadithiophene Bridged Donor–Acceptor Dyes Achieve High Power Conversion Efficiencies in Dye-Sensitized Solar Cells Based on the Tris-Cobalt Bipyridine Redox Couple. *ChemSusChem* **2011**, *4*, 591-594.
46. Wu, J.; Lan, Z.; Lin, J.; Huang, M.; Huang, Y.; Fan, L.; Luo, G., Electrolytes in Dye-Sensitized Solar Cells. *Chemical Reviews* **2015**, *115*, 2136-2173.

47. Ratner, M. A.; Shriver, D. F., Ion Transport in Solvent-Free Polymers. *Chemical Reviews* **1988**, *88*, 109-124.
48. Kakiage, K.; Osada, H.; Aoyama, Y.; Yano, T.; Oya, K.; Iwamoto, S.; Fujisawa, J.-i.; Hanaya, M., Achievement of over 1.4 V Photovoltage in a Dye-Sensitized Solar Cell by the Application of a Silyl-Anchor Coumarin Dye. *Scientific Reports* **2016**, *6*, 35888.
49. Cao, Y.; Liu, Y.; Zakeeruddin, S. M.; Hagfeldt, A.; Grätzel, M., Direct Contact of Selective Charge Extraction Layers Enables High-Efficiency Molecular Photovoltaics. *Joule* **2018**, *2*, 1108-1117.
50. Burschka, J.; Dualeh, A.; Kessler, F.; Baranoff, E.; Cevey-Ha, N.-L.; Yi, C.; Nazeeruddin, M. K.; Grätzel, M., Tris(2-(1h-Pyrazol-1-Yl)Pyridine)Cobalt(Iii) as P-Type Dopant for Organic Semiconductors and Its Application in Highly Efficient Solid-State Dye-Sensitized Solar Cells. *Journal of the American Chemical Society* **2011**, *133*, 18042-18045.
51. Kaltzoglou, A.; Perganti, D.; Antoniadou, M.; Kontos, A. G.; Falaras, P., Stress Tests on Dye-Sensitized Solar Cells with the Cs2sni6 Defect Perovskite as Hole-Transporting Material. *Energy Procedia* **2016**, *102*, 49-55.
52. Pashaei, B.; Shahroosvand, H.; Abbasi, P., Transition Metal Complex Redox Shuttles for Dye-Sensitized Solar Cells. *RSC Advances* **2015**, *5*, 94814-94848.
53. Feldt, S. M.; Gibson, E. A.; Gabrielsson, E.; Sun, L.; Boschloo, G.; Hagfeldt, A., Design of Organic Dyes and Cobalt Polypyridine Redox Mediators for High-Efficiency Dye-Sensitized Solar Cells. *Journal of the American Chemical Society* **2010**, *132*, 16714-16724.
54. Kay, A.; Grätzel, M., Dye-Sensitized Core−Shell Nanocrystals: Improved Efficiency of Mesoporous Tin Oxide Electrodes Coated with a Thin Layer of an Insulating Oxide. *Chemistry of Materials* **2002**, *14*, 2930-2935.
55. Mosconi, E.; Yum, J.-H.; Kessler, F.; Gómez García, C. J.; Zuccaccia, C.; Cinti, A.; Nazeeruddin, M. K.; Grätzel, M.; De Angelis, F., Cobalt Electrolyte/Dye Interactions in Dye-Sensitized Solar Cells: A Combined Computational and Experimental Study. *Journal of the American Chemical Society* **2012**, *134*, 19438-19453.
56. Kakiage, K.; Aoyama, Y.; Yano, T.; Oya, K.; Fujisawa, J.-i.; Hanaya, M., Highly-Efficient Dye-Sensitized Solar Cells with Collaborative Sensitization by Silyl-Anchor and Carboxy-Anchor Dyes. *Chemical Communications* **2015**, *51*, 15894-15897.
57. Cohen, S.; Lacher, J. R.; Park, J. D., Diketocyclobutenediol. *Journal of the American Chemical Society* **1959**, *81*, 3480-3480.
58. Treibs, A.; Jacob, K., Cyclotrimethine Dyes Derived from Squaric Acid. *Angewandte Chemie International Edition in English* **1965**, *4*, 694-694.
59. Völker, S. Synthesis, Spectroscopic and Electrochemical Properties of Squaraine Polymers **2014**.
60. Chenthamarakshan, C. R.; Ajayaghosh, A., Synthesis and Properties of Water-Soluble Squaraine Oligomers Containing Pendant Propanesulfonate Moieties. *Chemistry of Materials* **1998**, *10*, 1657-1663.
61. Völker, Sebastian F., Shinobu Uemura, Moritz Limpinsel, Markus Mingebach, Carsten Deibel, Vladimir Dyakonov, and Christoph Lambert., Polymeric squaraine dyes as electron donors in bulk heterojunction solar cells. *Macromolecular Chemistry and Physics* **2010**, 211, 1098-1108.
62. Chen, G.; Sasabe, H.; Sasaki, Y.; Katagiri, H.; Wang, X.-F.; Sano, T.; Hong, Z.; Yang, Y.; Kido, J., A Series of Squaraine Dyes: Effects of Side Chain and the Number of Hydroxyl Groups on Material Properties and Photovoltaic Performance. *Chemistry of Materials* **2014**, *26*, 1356-1364.

63. Sreejith, S.; Carol, P.; Chithra, P.; Ajayaghosh, A., Squaraine Dyes: A Mine of Molecular Materials. *Journal of Materials Chemistry* **2008**, *18*, 264-274.
64. Park, J., et al., Panchromatic Symmetrical Squaraines: A Step Forward in the Molecular Engineering of Low Cost Blue-Greenish Sensitizers for Dye-Sensitized Solar Cells. *Physical Chemistry Chemical Physics* **2014**, *16*, 24173-24177.
65. Chang, C.-H.; Chen, Y.-C.; Hsu, C.-Y.; Chou, H.-H.; Lin, J. T., Squaraine-Arylamine Sensitizers for Highly Efficient P-Type Dye-Sensitized Solar Cells. *Organic Letters* **2012**, *14*, 4726-4729.
66. Stender, B.; Völker, S. F.; Lambert, C.; Pflaum, J., Optoelectronic Processes in Squaraine Dye-Doped Oleds for Emission in the near-Infrared. *Advanced Materials* **2013**, *25*, 2943-2947.
67. Dou, L.; Liu, Y.; Hong, Z.; Li, G.; Yang, Y., Low-Bandgap near-Ir Conjugated Polymers/Molecules for Organic Electronics. *Chemical Reviews* **2015**, *115*, 12633-12665.
68. Smits, E. C. P.; Setayesh, S.; Anthopoulos, T. D.; Buechel, M.; Nijssen, W.; Coehoorn, R.; Blom, P. W. M.; de Boer, B.; de Leeuw, D. M., Near-Infrared Light-Emitting Ambipolar Organic Field-Effect Transistors. *Advanced Materials* **2007**, *19*, 734-738.
69. Thomas, J.; Sherman, D. B.; Amiss, T. J.; Andaluz, S. A.; Pitner, J. B., Synthesis and Biosensor Performance of a near-Ir Thiol-Reactive Fluorophore Based on Benzothiazolium Squaraine. *Bioconjugate Chemistry* **2007**, *18*, 1841-1846.
70. Hu, L.; Yan, Z.; Xu, H., Advances in Synthesis and Application of near-Infrared Absorbing Squaraine Dyes. *RSC Advances* **2013**, *3*, 7667-7676.
71. Oswald, B.; Patsenker, L.; Duschl, J.; Szmacinski, H.; Wolfbeis, O. S.; Terpetschnig, E., Synthesis, Spectral Properties, and Detection Limits of Reactive Squaraine Dyes, a New Class of Diode Laser Compatible Fluorescent Protein Labels. *Bioconjugate Chemistry* **1999**, *10*, 925-931.
72. Chen, C.; Wang, R.; Guo, L.; Fu, N.; Dong, H.; Yuan, Y., A Squaraine-Based Colorimetric and "Turn on" Fluorescent Sensor for Selective Detection of Hg2+ in an Aqueous Medium. *Organic Letters* **2011**, *13*, 1162-1165.
73. Ramaiah, D.; Joy, A.; Chandrasekhar, N.; Eldho, N. V.; Das, S.; George, M. V., Halogenated Squaraine Dyes as Potential Photochemotherapeutic Agents. Synthesis and Study of Photophysical Properties and Quantum Efficiencies of Singlet Oxygen Generation*. *Photochemistry and Photobiology* **1997**, *65*, 783-790.

CHAPTER TWO: Experimental: (Instrumentation and Characterization)

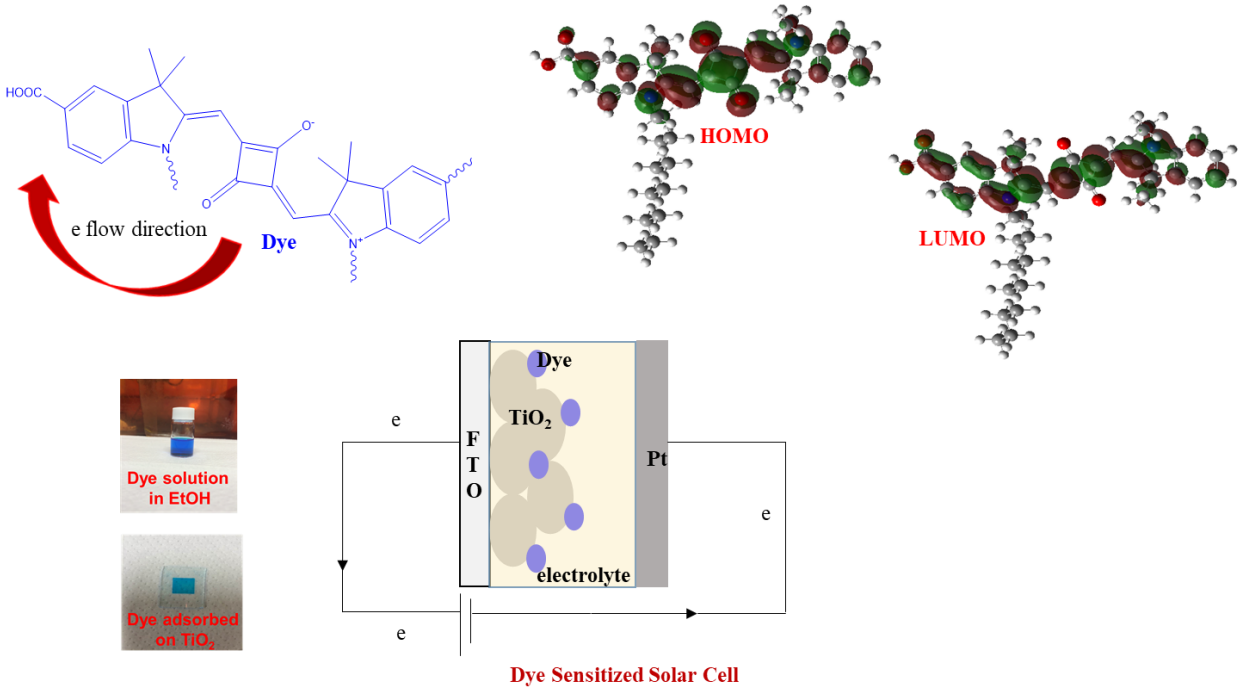

CHAPTER TWO: Experimental: (Instrumentation and Characterization)

2.1 Synthesis and Characterization of Dyes

Electrons are the entity that is involved in any chemical reaction or bond formation. In a molecule, the atoms are bonded either by covalent bond (sigma bond or pi bond) or ionic bond. However, non-covalent like Vander Waal interaction, London forces and hydrogen bonding also play an influential role in governing the energy of the system. Before practically synthesizing dyes, the molecular structure of the dye was subjected to computational calculation to get an idea of the quantum states of the electron system from quantum mechanics and its equation.

2.1.1 Theoretical MO calculations

It was found that the atomic particle, electron has a dual nature i.e it behaves like a particle as well as a wave. The particle nature is proven by its mass and charge while it also exhibits diffraction pattern like a wave. Therefore wave functions could explain the nature of the electrons and Schrodinger was the first person to write down about the wave functions and its equations known as `Schrodinger`s wave equation for particle in 1D`. This equation describes the changes in wave function as a function of time and spatial position due to quantum effects.

The Hartee fock method: The Hartee Fock method finds solutions to the Schrodinger wave equation. It determines the wave function and energy for many electron system in static state and is also known as the Self consistent Field Method (SCF). Basically it starts with a computed field iteration for the system and demands the same assumed field (self consistent) due to charge distribution after the computation is finished, though it is not valid always. Firstly, the Schrodinger equation for Z/2 one-particle dynamic in the potential zone contributed by the nucleus and the other electrons is solved with an electron charge density iteration to obtain the Z electron wavefunctions. Then from the potential for individual wavefunction contributed from both the nucleus and other electrons, the Z/2 Schrodinger equations again is solved again. Fock then modified this Hartree's method by the introduction of antisymmetry requirements as required by fermions as well as the Pauli`exclusion principle (*Slater determinant*) [1].

$$\epsilon_i \Psi_i(r) = \left(-\frac{1}{2}\nabla^2 + v_{ion}(r)\right)\Psi_i(r) + \sum_j \int dx' \frac{|\Psi_j r'|^2}{|r-r'|}\Psi_i(r) - \sum_j \delta\sigma_i\sigma_j \int dx' \frac{\Psi_j{}^*\Psi_i(r')}{|r-r'|}\Psi_j(r) \ldots\ldots (1)$$

The first term represents the kinetic energy and electron-ion potential. The second term represents the "Hartree" term, which bears the electrostatic potential from the charge distribution of N electrons. The third term known as the "exchange" term,is implied only on electrons with the twin spin and is taken from the Slater determinant form of the wavefunction respectively.

Density Functional Theory (DFT): Koch and Holthausen first introduced the density functional theory. In this theory, they eliminated the many-body electronic wavefunction (in Hartee Fock method). They considered that the electronic density is the more prime quantity as density depends only on the three variables. This theory is based on the principle that the electron distribution the energy is dependent on the electron density, and this functional is a minimum for the ground-state density. The recent DFT as approximated by Kohn–Sham considers non interacting system yielding the same electron density. This is the major drawback of the DFT as the precise functional operator for exchange and correlation are not recognized excluding the free electron gas atom. Moreover DFT is limited to only the ground state. Therefore, a modified version of DFT, Time Dependent (TDDFT) calculation determines the transition energy which is more reliable rather than excited state`s total energy [2]. The time dependent Kohn–Sham equation is given by

$$\left[-\frac{\mathbf{1}}{\mathbf{2}}\boldsymbol{\nabla}^{\mathbf{2}} + \boldsymbol{v_{eff}}(\boldsymbol{r},\boldsymbol{t})\right]\boldsymbol{\Psi}(\boldsymbol{r},\boldsymbol{t}) = \boldsymbol{i}\frac{\boldsymbol{\partial}}{\boldsymbol{\partial t}}\boldsymbol{\Psi}(\boldsymbol{r},\boldsymbol{t}) \ldots\ldots(\mathbf{2})$$

$$\boldsymbol{v_{eff}}(\boldsymbol{r},\boldsymbol{t}) = \boldsymbol{v}(\boldsymbol{t}) + \boldsymbol{v_{SCF}}(\boldsymbol{r},\boldsymbol{t}) \ldots\ldots\ldots\ldots\ldots\ldots\ldots\ldots(\mathbf{3})$$

$\boldsymbol{v_{eff}}(\boldsymbol{r},\boldsymbol{t})$ and $\boldsymbol{\Psi}(\boldsymbol{r},\boldsymbol{t})$ are the potential and orbitals of an independent particle system where $\boldsymbol{\Psi}(\boldsymbol{r},\boldsymbol{t})$ yield the same charge density like in the interating system. $\boldsymbol{v}(\boldsymbol{t})$ and $\boldsymbol{v_{SCF}}(\boldsymbol{r},\boldsymbol{t})$ are the applied field and the SCF field.

To run the calculation, Gaussian software package is used. The approximation like Linear Spin Density Approximation (LSDA), Local Density Approximation (LDA) and basis set B3LYP, 6311G etc are basically used. We have used LSDA approximation and B3LYP basis set for our computation. LSDA uses the Slater exchange functional and the correlation functional for the DFT calculation.A basis set is a set of functions which constitutes the electronic wave functions in the DFT whose function is to partially convert the differential equations into the algebraic form so that the computer could read and calculation could be done. The "basis set" in quantum chemistry, presents the set of nonorthogonal one-particle functions. This function represents atomic orbitals

needed to construct molecular orbitals. The Pople basis sets 6-311G(3df) comprises of three d and one f orbitals and is a split valence triple zeta basis. A triple zeta basis employs three basis functions for each atomic orbital (AO) and a split-valence basis uses only one basis function for each inner AO, and a larger basis for the valence AO's [3]. The LSDA is more accurate in terms of determination of HOMO. Beside this, the program also gives the approximation of the UV spectra, IR, NMR etc.

The computation was carried out using a G09 software package and the struture was input using the Gauss view software. After that the input program was submitted for quantum calculation using TDDFT. LSDA and the 6311G basis set was used for the calculation. The calculation was carried out in the singlet state with default spin and with no solvation effect using 1000 MB of the CPU memory. The calculation took about 6 hours to complete. The values of the HOMO, LUMO, oscillator strength (equal to the value of the molar extinction coefficient) and kinetic energy of the system was obtained in the log file. Similarly, the electron density in the HOMO and LUMO could be visualized in the log file, gauss view. The UV-vis absorbance spectra could be visualized in its check file which was near to its experimental spectra.

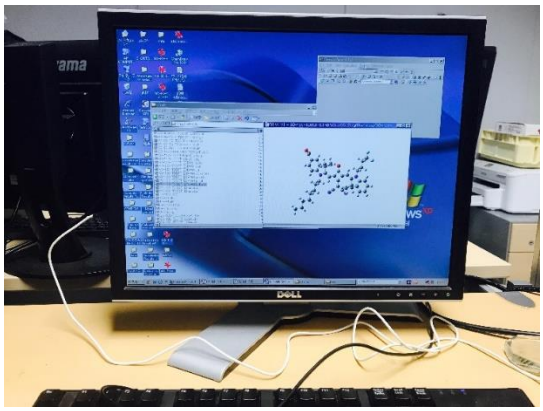

Figure 1. Gaussian calculation set up used for theoretical MO calculations.

2.1.2 High performance liquid chromatography

High Performance Liquid Chrromatography (HPLC) is a major tool for compound detection and separation (collection in case of preparative HPLC) in synthetic chemistry. It basically works on the principle of the affinity of the sample molecule with the stationary phase. The stationary phase is generally a silica particles (< 5 µm) in a stainless steel at high pressure [4]. The HPLC apparatus

comprises of a) pump b) sample injector c) column (column oven is not mandatory) d) detector e) Photodiode array detector (PDA). Initially the baseline program is run to eradicate any noise in which the the HPLC grade solvent will be flowing through the column. Then a diluted sample (5 µL) is injected through the pump under almost constant pressure. The sample then reaches the column where the separation takes place. Different compounds will be retained for different time in the column known as the retaintion time (R_t) according to its affinity with the stationary phase. The eluted samples are then detected by the software in the form of peaks with respect to time. The use of the Photodiode detector (PDA) makes it useful to obtain the UV spectrum of each of the compounds in sample [5]. We have run the command for about 20 mins to identify our intermediates and dyes using different gradients of methanol in water. As basically our samples comprised of the indole moiety, we run the 254 nm.

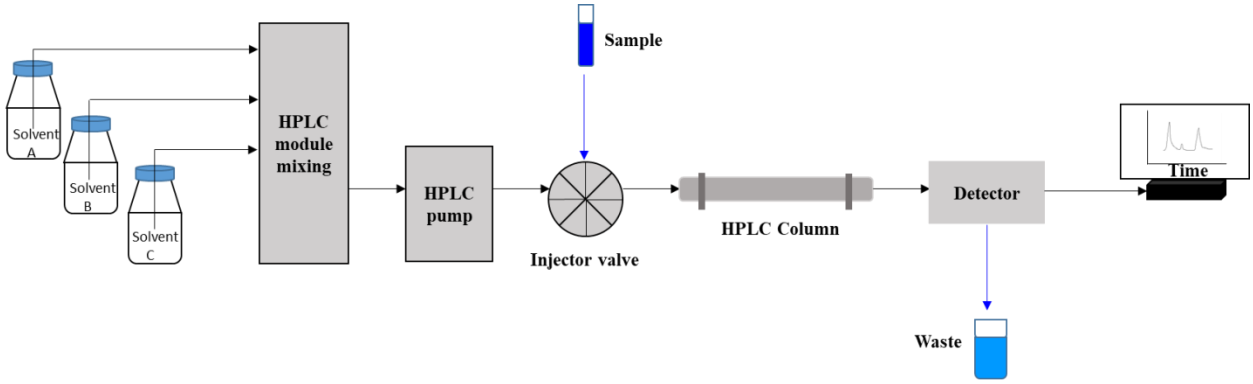

Figure 2. Outline of the working process of HPLC.

The separation of the peaks determines to what degree the resolution was successful. The resolution value R_s should be not less than 1.5 to have an efficient separation. Value of R_s is determined by the width (W) and the retention time (T) of the peak as shown below [6].

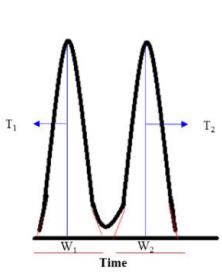

Figure 3. HPLC trace on the monitor with time dependent peaks.

$$R_S = \frac{(T_{R2}-T_{R1})}{(w_{b1}+w_{b1})/2} = \frac{2(T_{R2}-T_{R1})}{(w_{b1}+w_{b1})} \quad \text{(4)}$$

The above equation depicts that the resolution depends upon the width of the peak and time. Therfore longer column should favour appropriate separation.

2.1.3 Electronic Absorption Spectroscopy

Electronic Absorption spectroscopy is so called because it measures the electron`s jump from lower energy lying atomic orbital to higher energy atomic orbital on absorbing the photon. The absorption of the radiation (generally UV-vis, Near Infrared), is measured with respect to wavelength. In case of metal complex, the transition is from d-d orbitals or Ligand to Metal or Metal to Ligand and Π- Π^* in case of organic compound [7]. Depending on the band gap of it, the molecule absorbs the photon of the same energy and gets excited. The ability of a molecule how efficiently it can absorb the radiation is determined in terms of its molar extinction coefficient and the absorbance is given by :

$$A = \log I_0/I \quad \text{(5)}$$

where I_0 and I are the incident and transmitted light intensity repectively.

$$A = \varepsilon cl \quad \text{(6)}$$

$$\text{Or,} \quad \varepsilon = A/cl$$

where, A, ε, c and l are absorbance, molar extinction coefficient, concentration and length of the cell respectively.

The schematic diagram below shows the working principle of UV-vis spectrometer. The Deutarium light source is for lower wavelength ranging from 160 nm to lesser than 370 nm and the tungsten source is from 370 nm to 2500 nm. We have used 5 µM of the sample solution in cubet as well as on solid state on TiO_2 coated on glass. JASCO model V550 was used for the elctronic absorption spectroscopy.

Figure 4. UV-Vis spectrometer used for measuring the electronic spectra of the compounds discussed in the thesis.

2.1.4 Fluorescence Spectroscopy

Fluorescence is the property of the excited molecule to relax into its ground state with the loss of its vibrational energy as a result of collision. When the molecule relaxes, it emits the photon giving fluorescence [8]. Fluorescence spectroscopy can be regarded as the reverse of the electronic absorbance spectroscopy as it measures the decay of the excited state. For measuring the fluorescence of a molecule, initially the molecule is excited around its highest absorption wavelength. The excitation and relaxation of the molecule could be studied with the help of Jablonski diagram. If the excited molecule relaxes to its own singlet state from where it has been excited, it is known as fluorescence and if it relaxes to its triplet state, it is known as phosphorescence.

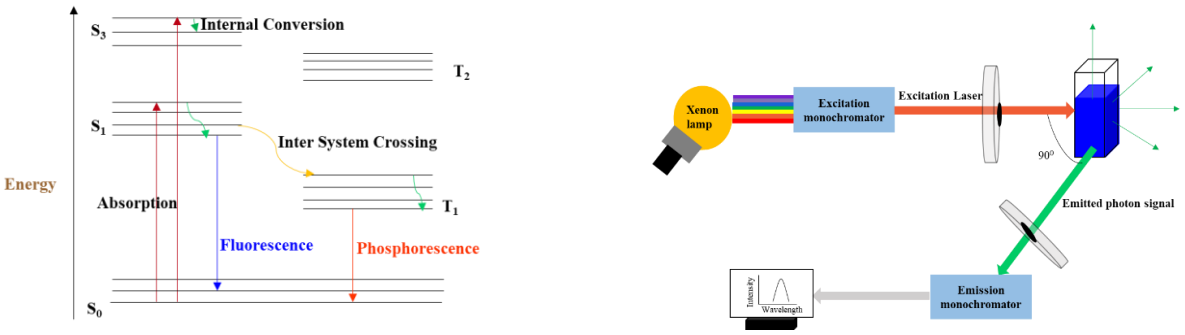

a) b)

Figure 5. a) Jablonski diagram for electronic transition. b) Ray diagram for fluorescence spectroscopy.

Figure 6. Fluorescence spectrometer in the lab.

The internal conversion (IC) generally results in vibrational relaxation with non-radiative decay whereas the fluorescence and phosphorescence results in a radiative decay. Xe lamp has a continuous emission spectrum in between (300-800) nm. The emitted light is placed at 90^0 with respect to the excited light to avoid interference of the transmitted excited light. In our experiment, we used the same solution that was used for the UV-vis measurement. The intersection point at the respective wavelength of the UV spectra and that of its fluorescence gives the idea of the band gap of the molecule (E_{0-0}) [9].

Time Resolved Fluorescence Spectroscopy

It as a technique which measures the time interval between the excitation of the sample (absorption of a photon by a molecule) by a laser and arrival of the emitted photon (fluorescence) by a detector. Generally the fluorescence spectrum is measured as a function of time. The intensity of the fluorescence is proportional to the number of the excited electrons. The fluorescence intensity will decrease with the lapse of time as shown by the equation

$$I_t = I_0\, e(-k_f\, t) \ldots\ldots\ldots\ldots\ldots\ldots\ldots\ldots\ldots\ldots\ldots \quad (7)$$

Where I_t, I_0, k_f, are the fluorescence intensity at time t, initial fluorescence intensity, fluorescence decay rate respectively. The fluorescence lifetime $\boldsymbol{\tau}=1/\,k_f$.

For my experiment, we have used the *Time Correlated single Photon Counting* for time resolved fluorescence spectroscopy. As the electrons will remain in the excited state for some time and after time interval Δt, it decays to ground state by emitting photon. If the value of Δt is measured multiple times by exciting the molecule with a large number of laser pulses, the obtained time

values will be distributed accordingly depending on the probability of the radiation at the specified time. This principle is implemented in time-correlated single photon counting (TCSPC). The principle of TCSPC is based on the "start", dispensed by the laser pulse (sapphire laser) and a defined "stop" signal, perceived by single-photon sensitive detectors. The time delay is repeated many times to portray the statistics of fluorophores emission. This delay time is sorted into a fluorescence decay histogram that plots the occurrence of emission over time after the excitation pulse [11]. The TCSPC was performed in both the solution as well as solid state. Quantarus Tau Model C-11370, Hamamatsu Photonics, Japan was employed for the lifetime measurement.

Figure 7. Fluorescence lifetime measuring apparatus used for my experiment.

2.1.5 Nuclear Magnetic Resonance Spectroscopy (NMR)

Every nuclei has certain amount of charge and a spin (1/2) which gives a certain magnetic moment to it. When the nuclei is exposed to external magnetic field, the degenerate energy is split into different energy level ($\Delta E=h\nu$) which is known as Zeeman Effect [12]. The energy transfer takes place at a certain frequency and when the spin relaxes, it does so by emitting the same frequency which is utilized in obtaining the NMR spectrum. Some important NMR active nuclei is the one with an odd spin like ^{1}H, ^{13}C, ^{15}N, ^{19}F, ^{31}P etc. However, the widely used is the one with the most abundant element ^{1}H. NMR is an important tool in identifying the structure of the molecule, functional groups and the position of the respected atoms in it. Generally the NMR data is taken employing tetramethylsilane (TMS) as the reference as it has all equivalent protons. The chemical shift (δ) of the nuclei is measured in terms of parts per million (ppm) with respect to the zero value of the reference [13]. The samples are dissolved in the deuterated solvent like $CDCl_3$, d-6 DMSO,

D_2O to avoid the signals from the solvent. JEOL, 500 MHz NMR spectrometer was used for the experiment.

2.1.5.1 ^{1}H-NMR

It is the NMR study of the ^{1}H nuclei in a molecule to determine the number of the hydrogen atoms and to some extent the functional groups (Infrared spectroscopy is used for detecting the functional group). The value of chemical shift (δ) for H-NMR ranges from -4 to 14 ppm. Expected is the single peak for a single proton, however a peak undergoes splitting due to its chemical environment due to spin –spin coupling. The value of the coupling constant `J` is given in Hertz and the splitting pattern is given by Pascal`s triangle. For the first order coupling (when the J for all the protons is same), the number of peaks obtained is (n+1) for `n` number of neighbors [14]. For n=0, it is a singlet peak (s), n=1, doublet (d), n=2, triplet (t) and so on. Whereas for non-first order coupling (when the J for all the protons is not same), the signal obtained will be multiplet. The non-equivalent proton undergoes splitting by one another which in turn is splitted by the another proton, thus giving doublet of doublet (dd) peaks [15].

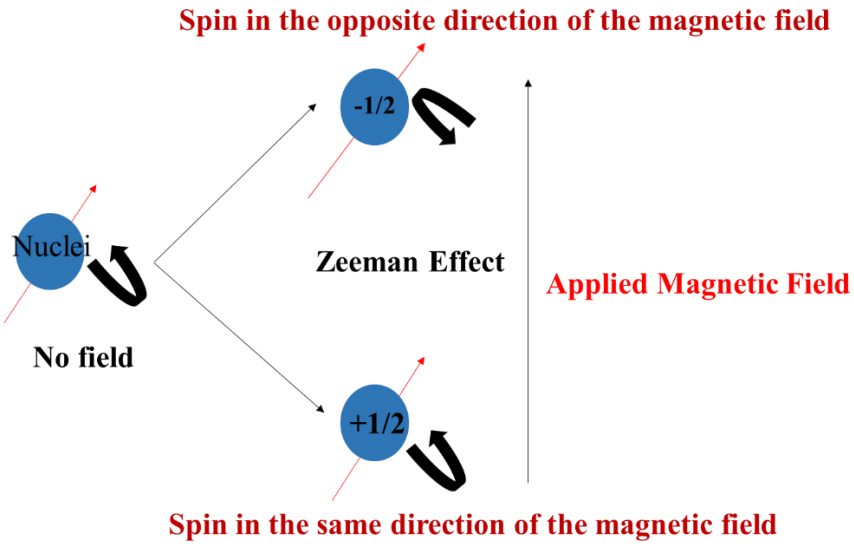

Figure 8. Spin splitting of the atomic nucleus in the presence of the magnetic field which results in the appearance of the peaks in the NMR analysis.

2.1.5.2 ^{13}C-NMR

It is analogous to H-NMR but in determining the carbon atoms. The ^{13}C NMR does not detect ^{12}C as it has a net zero spin but only the ^{13}C isotope with net non-zero spin. The ^{13}C- NMR is less sensitive than the H-NMR as it is less abundant and constitutes only 1.1% of the natural abundance. The value of chemical shift (δ) for ^{13}C-NMR ranges from 20 to 220 ppm. Moreover, it requires a large number of scans (around thousands) and more amount of the sample (~15 mg) dissolved in the required solvent. In ^{13}C-NMR, unlike the H-NMR, there is no splitting of the peaks due to the neighbouring carbon due to the scarcity of the ^{13}C isotope. Hence each peak corresponds to each carbon atom.

The NMR samples were prepared by dissolving 15 mg of the sample in the respected deuterated solvent in a closed tube. ^{1}H NMR and ^{13}C-NMR spectrum were recorded by JEOL JNM-A500 Nuclear Magnetic Resonance Spectrometer operated at 500 MHz and 125 MHz respectively. Rarely, small peaks seems to appear at the shoulder of ^{1}H NMR which is due to coupling of the ^{1}H proton with the ^{13}C and not the proton-proton coupling. These peaks known as carbon satellites [16] are not taken into consideration.

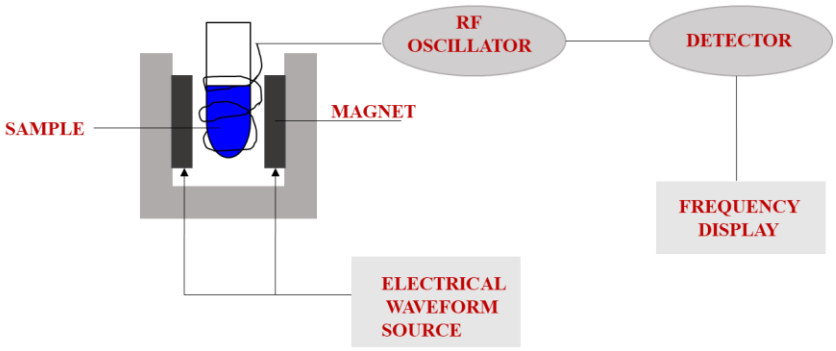

Figure 9. NMR spectroscopy scheme and the required components.

2.1.7 Mass Spectroscopy

Mass spectroscopy measures the mass of the defined compound subjected to it. At first the sample is ionized due to bombardment. And the ionized species then migrate according to the law of mass, (the smaller mass species moves faster than the heavy ones. They also undergo deflection in the

course of its path. The detector then detects the ions in its mass/charge ratio. Finally the spectra is obtained in the form of sharp peak. There are various techniques for measuring the mass of the sample basically by MALDI for small molecules and Fast Atom Bombardment (FAB) mass for complex molecules.

2.1.7.1 MALDI TOF

Matrix Assisted Laser Desorption Ionization Time of Flight employs a matrix for the measurement of mass. Initially, the sample whose mass has to be measured is mixed uniformly with an optimum matrix. The matrix should not chemically interact with the sample neither it should undergo decomposition. The most commonly used matrix are 3,5-dimethoxy-hydroxycinnamic acid (sinapinic acid), α-cyano-4-hydroxycinnamic acid (α-CHCA, alpha-cyano or alpha-matrix) and 2,5-dihydroxybenzoic acid (DHB) [17]. The mixture is then shone with UV laser which then absorbs the ultraviolet light and converts into heat energy. With that heat energy, both the matrix and the sample gets evaporated. The ionized species then moves under applied electric field through the same potential. Consequently ions with larger mass move slowly and those with smaller mass moves faster and will be detected by the detector first [18]. Hence each species has its own drift velocity and drift time. As the ions with different masses move at different speed and thus the time of its motion varies, this phenomena is known as `Time of Flight` .

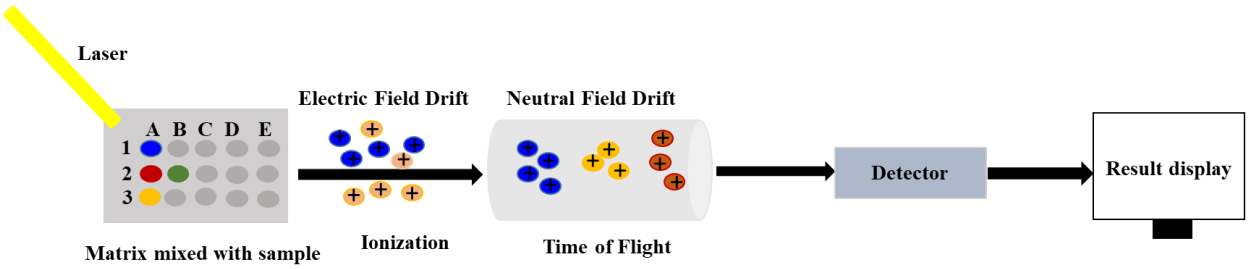

Figure 10. MALDI-TOF analysis scheme of the samples mixed with matrix.

For my experiment, the samples dissolved in ethanol were mixed finely with α CHCA matrix. The mixture was then drop casted on the MALDI TOF plate which was then allowed for drying. Once it was dried, the plate was inserted into the MALDI TOF instrument. And the program was run and detected to get the respective mass data of the sample.

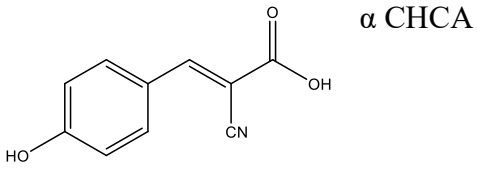

α CHCA

Figure 11. Molecular structure of the matrix.

2.1.7.1 FAB mass spectroscopy

In this spectroscopy, fast Atom Bombardment (FAB) process is used for the ionization of the sample. Generally, energetically high atomic beam of noble gases like Argon or Xenon are the sources for ionization unlike the laser in MALDI TOF mass spectroscopy. FAB mass spectroscopy utilizes liquid matrix (generally glycerol) to gives the ion of the sample. The main advantage of employing the matrix is that the maximum energy of the beam is absorbed by the matrix inhibiting the damage of the sample as well as controlling its aggregation [19]. Once the sample is mixed with the matrix (substrate) on the sample holder stainless steel, it is subjected to the high energy (around 10keV) atomic beam. Once the beam reaches the substrate, the collision of between them results in the ionization and produces +ve (A^+) and –ve (A^-) ions of them. The ions then reach the analyzer and are detected by the detector in terms of m/z ratio. Trifluoroacetic acid (TFA) is generally added to give $[A+H]^+$. If the sample contains some salts, the peak appears for $[A+Na]^+$.

For the FAB mass measurement of our sample, we had used the 2,2 Dithiodiethanol as the matrix.

2.1.8 Cyclic Voltammetry

Voltammetry is the electroanalytical study of the behavior of an analyte of its current as a function of potential. In cyclic voltammetry, the potential of the working electrode gradients with time. Once the highest potential is reached, it again slopes down in the opposite direction to reach the initial potential, hence the name cyclic. The rate of voltage change with respect to time is known as the scan rate generally denoted by V/s. For a cyclic voltammetry set up, working electrode, reference electrode and a counter electrode are needed to be dipped in the analyte solution containing a supporting electrolyte.

Working electrode: The oxidation or the reduction of the analyte takes at the interface of this electrode. Inert metals like platinum, gold, silver and glassy carbon etc. are used as working electrode.

Reference electrode: This electrode maintains almost a constant potential and hence can be taken as a reference for the potential of the other working and the counter electrode. The most commonly used reference electrode is the Ag/AgCl/KCl, standard Calomel electrode (Hg/HgCl/KCl), Standard Hydrogen Electrode (SHE) etc.

Counter electrode: The primary function of this electrode is to serve as the source or sink of electrons to complete the circuit depending on the reaction taking place at the working electrode. It is to say that if oxidation takes place at the working electrode, its reverse reaction will occur and vice versa. The area of the counter electrode is taken larger than the working electrode so that the kinetics of electron (reaching or leaving) at the counter electrode is not limited at the counter electrode level. Generally, platinum, gold, silver etc. are used as the counter electrode.

Supporting electrolyte: Supporting electrolyte is generally an ionic salt with a high conductivity, added along with the analyte in the electrolytic solution. The main function of it is to increase the conductivity of the analyte as well as to eliminate the so the called IR drop which may result in the shift of the peaks which is very crucial as it determines the HOMO-LUMO level in our case.

To conduct the cyclic voltammetry of the analyte (dyes in this case), it was dissolved in dimethyl formamide (DMF) with tetrabutyl ammoniumhexafluorophosphate (0.1M) as the supporting electrolyte. The CV was carried at a scan rate of 20mV/s. High concentration of the supporting electrolyte was used as the conductivity of the dye involved is lower. The first peak on the CV curve corresponds to its first oxidation state from where the value of the HOMO of the molecule is estimated. Its complementary peak corresponds to its LUMO value. Before conducting the CV of the dyes, the instrument was calibrated using ferrocene as the reference. An auto-polarization system HSV-100, Hakuto Denko, Japan was employed for the CV measurements.

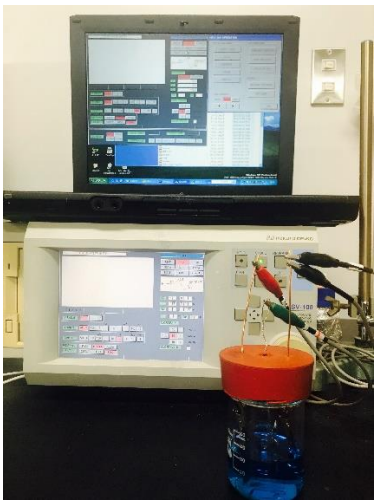

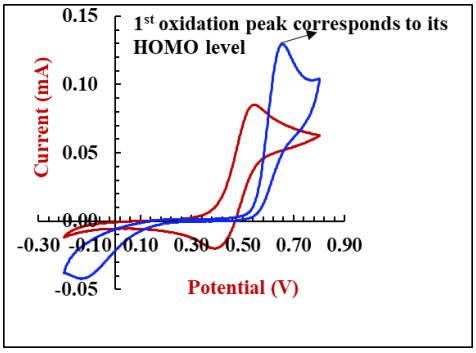

a) **b)**

Figure 12. CV measuring apparatus set up along with the electrochemical cell (a). CV plot of a squaraine dye along with ferrocene as the reference in DMF with a scan rate of 20 mV/s (b).

2.1.9 Photoelectron Yield Spectroscopy

It is a spectroscopic technique in determining the occupied electronic state of a material. In our case it was employed for determining the Highest Occupied Molecular Orbital of the molecule. The beauty of it lies in the fact that they be conducted either under vacuum or without it. The basic principle here involves the extraction of the electrons on irradiation with UV radiation crossing its threshold energy. The measurement is done in terms of the quantum yield as a function of the photon energy.

$$\phi(Y) = \frac{\text{emitted photoelectrons}}{\text{photons absorbed}} \text{.....(8)}$$

The yield of the emitted electrons is proportional to the energy of the incident photon (hν). At a certain point, the energy of the photon becomes stronger than the threshold energy (E_T) of the electrons so that the yield will have a sharp increase in its slope. Therefore from the threshold energy, one could determine the ionization energy. The ionization energy corresponds to the minimum amount of energy needed to extract an electron from its HOMO level towards the vacuum. Basically for the determination of threshold energy, the yield curve is fitted to a certain function. For organic molecules, the yield is given by the relation:

$$Y \alpha (h\nu - E_T)^{1/3} \quad \ldots\ldots\ldots\ldots\ldots\ldots\ldots\ldots\ldots\ldots(9)$$

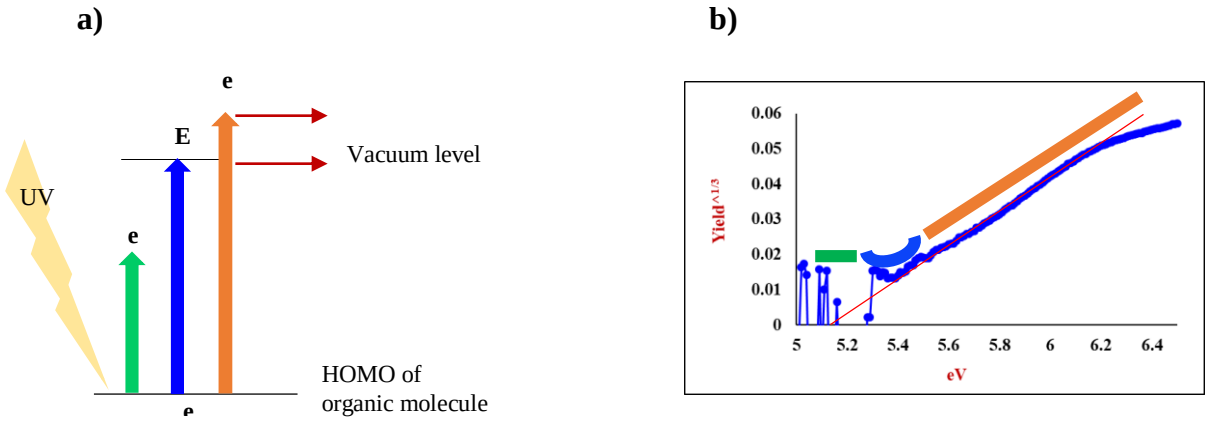

Figure 13. Working postulation of photoelectron yield spectroscopy for organic molecule. (a) Photoelectron Yield spectra of one of the dyes involved in the thesis (b)

To measure the PYS spectra, solid dye powder was spread on FTO and taped with a carbon tape. The edge of the allotted dye area was connected with aluminum foil to make the contact. The sample was then introduced to high pressure of about 10^3 Pascal with the UV source for electron extraction from the HOMO of the dye. The above figure (a) shows the operation of PYS. The blue arrow denotes the ionization energy which corresponds to the HOMO energy level. The value of HOMO is obtained by drawing a tangent on the curve (b) The intersection of the curve on the X axis gives the value of the HOMO level. Model Bunko Keiki, model KV-205 HK, Japan was used for PYS.

Figure 14. A snapshot of PYS instrument in the lab.

2.2 Fabrication of Dye sensitized Solar Cells (DSSCs)

DSSCs function is a p n junction diode. However it has more number of interfaces like the FTO/TiO_2 (dye), TiO_2 (dye)/electrolyte and electrolyte/counter electrode. The fabrication of DSSCs basically starts with the preparation of the photoanode and photocathode individually followed by its adherence with separation by the electrolyte layer.

2.2.1 Preparation of photoanodes

Firstly fluorine doped tin (FTO) oxide glass were cut into1 by 2 cm. The substrates were then subjected for washing in detergent, distilled water, acetone and isopropanol sequentially for 15 minutes each under sonication. The substrates were then rinsed with distilled water and dried with air gun. Then they were subjected to ozone plasma treatment to remove the organic dirt from the surface of the FTO for about 9 minutes. Thereafter, the substrates are dipped in 40 mM $TiCl_4$ in distilled water for 30 minutes at 70^0. The samples are rinsed in distilled water and then subjected to ramp heating at 450^0 for 30 minutes in a furnace. The samples are taken out at room temperature and coated with the commercial TiO_2 paste (D/SP and 30 NRD) to give the required thickness of the mesoporous TiO_2. The coating of the TiO_2 was done with the screen printing technique. For this a metal mask of 5X5 mm area was used where the substrate was placed beneath it. The beauty of the screen printing lies in its fine tuning of the thickness required with the adjustment in the z direction. It has the variation in all x,y,z as well as the angle θ. The deviation of the angle beyond zero degree results in a non-uniform thickness which could be adjusted with the help of a label. By varying the z variable, the thickness of the TiO_2 could be adjusted. Once coated, the samples are subjected to heating at 450^0. The substrates are again subjected to final $TiCl_4$ treatment followed by heating to give a compact TiO_2 layer. The substrates are taken out at 100^0 and dipped in the dye solution and left at room temperature for the adsorption of dye onto the TiO_2 nanoparticle. After complete dye adsorption, the substrates are taken out and then rinsed in the respective solvent to remove the physically adsorbed dye molecules. Hence the working electrode is ready.

2.2.2 Preparation of photocathodes

Generally in a working cell, the cathode is an electrode where reduction occurs. As DSSCs is also an electrochemical cell, it comprises of the photocathode (counter electrode) (photocathode

because the reaction is initiated by the light source) where the reduction takes place. Moreover, DSSCs has a diode nature, the flow of electron direction if from the cathode towards to the anode in the forward bias. In my experiment, we had used Platinum as the counter electrode and it was prepared by sputtering and spin coating respectively.

2.2.2.1 Sputtering

Sputtering is a technique of depositing a thin film of target onto the substrate due to vapor phase deposition. To meet the criteria for sputtering process, a very high energy using either DC voltage known as direct current sputtering or AC voltage known as RF sputtering is applied. Highly energized electrons from the cathode collide with the noble gas atom in the sputtering chamber. This electrons then extract electrons from the gas atom making it positively charged and hence highly energetic. The gaseous ions thus obtained gain momentum on collision with each other. If the collision frequency is so large enough than the threshold displacement energy of the target, the target atom will be dislocated from its lattice site which gets sputtered on the substrates. The secondary electrons emitted from the target is responsible for the plasma which could be seen in the sputtering machine on sputtering which confirms the process being executed. The free electrons may also combine with the gas ion to form the neutral gas atom.

For the counter electrode preparation, platinum was sputtered on the FTO. Before platinum being sputtered, a thin layer of titania was sputtered to maintain a proper contact.

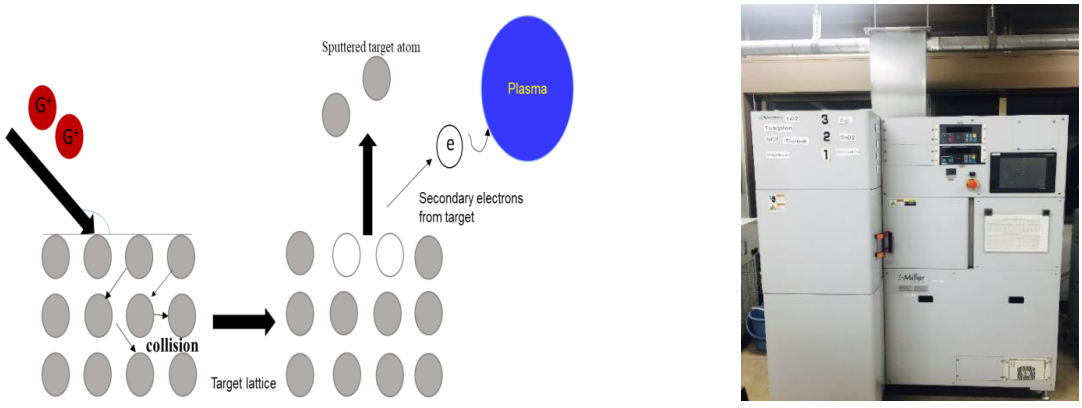

(a) **(b)**

Figure 15. Mechanism of target sputter by the incident highly energetic ions (a) and sputtering machine in the lab (b).

2.2.2.2 Spin Coating

Cleaned 1 X 2 cm FTO substrates were subjected to spin coating with hexachloroplatinic acid as the precursor. 1 mM solution of the hexachloroplatinic acid was prepared in 2-propanol. 50 µL of the solution was drop casted on the FTOs placed under vacuum on the spin coater. It was then allowed to stand for 30 seconds for proper spreading on the FTO. It was then spun for 400 rpm for 5 seconds and then 1400 rpm for 10 seconds. Then the substrates were subjected to thermal pyrolysis at 450^0 for the resulting deposition of Pt in few nm range. The resultant counter electrode is transparent which also paves the way for transparent DSSCs.

a)  b) 

Figure 16. Spin coater (a) and muffle furnace (b).

2.3 Measurement and Characterizations

2.3.1 Photovoltaic measurement

2.3.1.1 Current-Voltage characteristics

The ability of a solar cell how efficiently it is able to generate electricity from the absorbed photons is governed by the three important parameters namely: Short circuit current density (Jsc), open circuit voltage (Voc) and the fill factor (FF) and it is given by the equation:

$$\eta = \frac{Jsc\ X\ Voc\ X\ FF}{Pin} \ldots\ldots\ldots\ldots\ldots\ldots (10)$$

where *Pin* is the intensity of the incident light. Besides the above mentioned parameters, the efficiency of the solar cell also depends on the external factors like temperature, irradiation

intensity, angle of the incidence of the sun`s ray. In the context, angle of the incidence of the sun`s ray has been cautiously taken care of and has a defined value as a standard. The standard value of solar spectrum for solar cell measurement is given by air mass (AM) 1.5 G. The standard AM 1.5 spectrum designate an angle of incident sun ray of 48.2˚ with an intensity of 100 mW/cm^2

$$AM = \frac{1}{cos\phi} \ldots\ldots\ldots\ldots\ldots\ldots \quad (11)$$

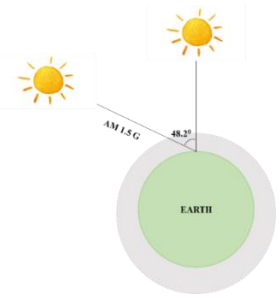

Figure 17. Portray of AM 1.5 G

The current voltage curve of the DSSCs were characterized with the CEP-2000 Bunko Keiki Co. Ltd, Japan Solar simulator provisioned with a xenon lamp (Bunko Keiki BSO-X150LC) employing a light source of a simulated solar intensity of 100 mW/cm^2 .

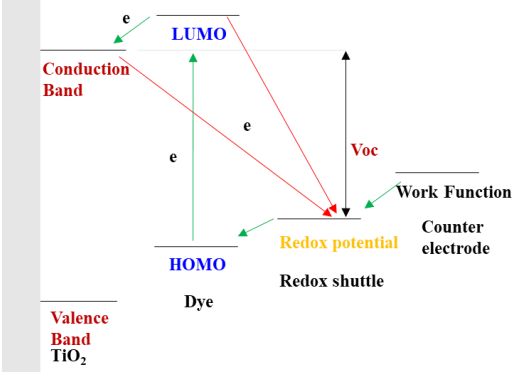

Figure 18. Mechanism of a working DSSCs.

Short Circuit Current Density (Jsc): The short circuit current is the maximum current obtained from a working solar cell. This is the current when the device is short circuit i.e when the voltage is zero. The primary dependency of short circuit current is the photon harvesting efficiency of the

dye. It is also depends on the charge injection and collection efficiency. In fact, the value of Jsc is obtained from the integration of the Incident Photon to Current Conversion Efficiency (IPCE) and is given by:

$$Jsc = \int q\, F(E)\, IPCE(E) dE \quad \ldots\ldots\ldots\ldots\ldots\ldots\ldots\ldots\ldots\ldots \quad (12)$$

Where q is the electronic charge, F(E) is the incident photon flux density. Therefore it is well understood that the higher the photon flux density, higher the current density.

Dark current: The dark current refers to the current flow in the absence of light. In dark condition, the instead of current flow in the forward direction, the electrons in the conduction band of the TiO_2 recombine with the HOMO of the dye to the electrolyte. Hence the extent of recombination could be estimated from the dark current. The basic cell equation in dark is given by:

$$I_{dark} = I_0 \left[exp\ (qV/nkT) - 1\right] \ldots\ldots\ldots\ldots\ldots\ldots\ldots\ldots\ldots\ldots (13)$$

Where I_{dark} is the dark current, V is the charge and voltage across the diode, I_0 is the saturation dark current, q and k are the electronic charge constant and Boltzmann constant respectively. T and *n* are the temperature in kelvin and ideality of the diode respectively.

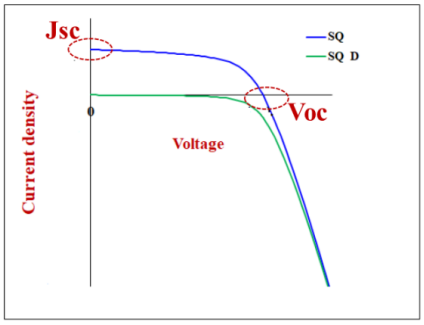

Figure 19. Current-voltage plot under 1 sun illumination and in dark.

Open Circuit Voltage (Voc): It is the maximum voltage output obtained in a cell. In fact it is the voltage output when the system is in short circuit condition i.e. when there is no net current flow and in case of solar cell, it is given by the difference of the fermi level of the conduction band of TiO_2 and the redox potential of the electrolyte. Thus the internal quantum efficiency in such case is zero. In electrochemical system, the open circuit voltage is given by the equation [21].

$$Voc = \frac{kT}{e} ln \frac{I}{ncb\ k} \ldots\ldots\ldots\ldots\ldots\ldots\ldots\ldots (14)$$

Where *k, is* the Boltzmann constant, T stands for temperature and *e* is the charge respectively. Similarly *I*, *ncb* and *k* are the photocurrent injected to the TiO_2 from the exited dye, photoelectron density of the conductive band and *k* is the reaction rate constant for the reverse electron transfer from the conduction band of the TiO_2 to the electrolyte.

Fill Factor (FF): Fill factor in a solar cell is defined by the ratio of the maximum power output to the product of the current density and open circuit voltage. It is generally a measure of the resistance of the charge flow in the device. The fill factor is given by:

$$FF = \frac{Pmax}{Jsc\ X\ Voc} \ldots\ldots\ldots\ldots\ldots\ldots\ldots\ldots (15)$$

The maximum power (Pmax) is represented by the product of the maximum current density and the maximum voltage of the solar cell. Its values range from 0 to 1. Higher the value of FF, lesser the resistance in the system. The FF is greatly influenced also by the shunt resistance and series resistance and increasing the shunt resistance and decreasing the series resistance result in higher FF.

Efficiency of the solar cell: The efficiency of the solar cell is given by the equation:

$$\eta = \frac{\text{Jsc X Voc X FF}}{\text{Pin}} \ldots\ldots\ldots\ldots\ldots\ldots\ldots\ldots (16)$$

where Pin is the input power, generally taken as 100 mW/cm^2 .

2.3.1.2 Photocurrent action spectrum

Incident photon conversion efficiency (IPCE) is a measure of how much absorbed photon is converted into electricity, hence it is also better represented as external quantum efficiency. The value of IPCE depends on the current flow i.e photon harvest, charge injection and collection. It has the maximum limit of value 1 when there is 100% conversion efficiency. The equation which describes the IPCE is given as follows [22]:

$$\text{IPCE}(\lambda) = \text{LHE}(\lambda) \times \Phi_{\text{inj}} \times \eta_{\text{c}} = \text{LHE}(\lambda) \times \text{APCE} \ldots..(17)$$

Where LHE, Φ_{inj} and η_c are light harvesting efficiency, injection efficiency and collection efficiency respectively. The LHE is the portion of absorbed photons at the wavelength where the dye absorbs which can be given by the Beer's law :

$$LHE = 1 - 10^{-\varepsilon(\lambda)L_n C} \quad \text{.....(18)}$$

where $\varepsilon(\lambda)$ is the molar extinction coefficient, C is concentration (which is determined by the effective photoanode roughness) of the dye respectively and L_n is the shorter of the diffusion length of the electrons.

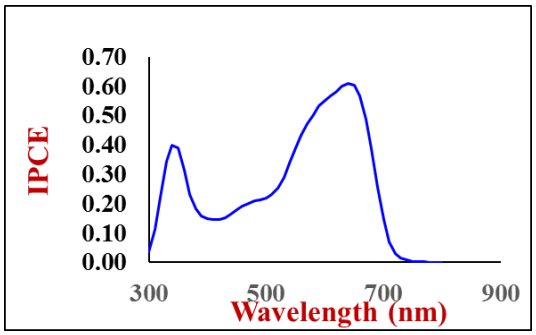

Figure 20. Incident photon current efficiency (action spectrum) of a squaraine dye.

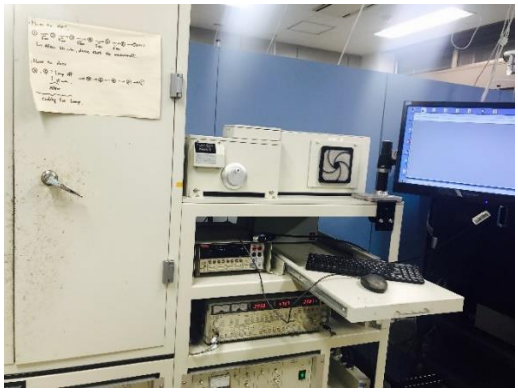

Figure 21. Solar simulator equipped with xenon lamp with intensity of 100 mW/cm^2.

2.3.2 Electrochemical impedance Spectroscopy

Electrochemical Impedance Spectroscopy is an important aid for the dielectric and transport properties of materials. In solar cells, it has found a wide application in terms of measuring the resistances across the interfaces [22-24]. The "father" of impedance spectroscopy Oliver Heaviside, defined the terms of "impedance", by the equation below where V(S), I(S) and S stand for the Laplace transforms of the voltage and the current, and Laplace frequency [25]:

$$Z(s) = \frac{\mathrm{V(S)}}{\mathrm{I\ (S)}} \ldots\ldots\ldots\ldots\ldots\ldots\ldots\ldots\ldots\ldots\ldots\ldots\ldots\ldots (19)$$

Later the Laplace frequency S was substituted by `jω` where j and ω are the complex number and frequency respectively. The EIS spectra therefore defines the current and voltage loss as a result of recombination. Generally the EIS plot is represented in two ways: a) the plot of Z`` (imaginary) in the coordinate and Z` (real) in the abscissa. This plot is known as the Nyquist plot. b) the plot of the log Z versus log ω known as the Bode plane. In a solar cell, the Nyquist plot generally comprises of three semicircles.

Figure 21. shows the Nyquist plot of a DSSC. The length from the origin to the beginning of the first semicircle denotes the series resistance. The first semicircle correlate to the resistance at the counter electrode interface, the second semicircle denotes the resistance across the TiO_2/Dye/electrolyte interface and the third semicircle denotes the diffusion resistance. Electrochemical impedance spectroscopy (EIS) measurements were carried out using a frequency response analyzer (Solartron Analytical, 1255B) It is connected to a potentiostat Solartron Analytical, 1287. A modest 10 mV AC perturbation was applied in the frequency range from 5 × 10−3 to 105 Hz.

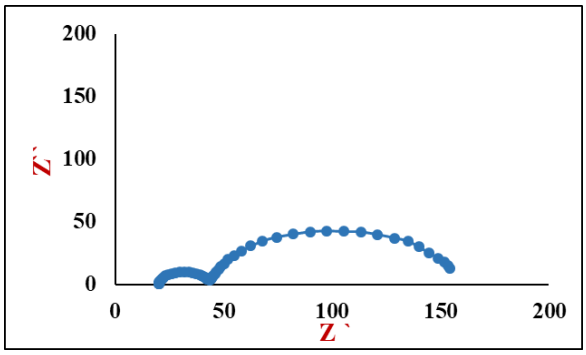

Figure 21. Nyquist plot of the DSSCs with squaraine dye as the sensitizer.

References

1. https://www2.ph.ed.ac.uk/~gja/qp/qp10.pdf
2. Photosynthesis Research December 2009, Volume 102, Issue 2–3, pp 443–453
3. http://vergil.chemistry.gatech.edu/courses/chem6485/pdf/basis-sets.pdf
4. https://www.quora.com/What-is-the-principle-of-HPLC
5. Snyder, L. R.; Kirkland, J. J.; Glajch, J. L., *Practical Hplc Method Development*; John Wiley & Sons, 2012.

6. https://www.chromacademy.com/lms/sco2/Theory_Of_HPLC_Chromatographic_Parameters.pdf
7. Chi, Y.; Chou, P.-T., Transition-Metal Phosphors with Cyclometalating Ligands: Fundamentals and Applications. *Chemical Society Reviews* **2010**, *39*, 638-655.
8. Lakowicz, Jr, Principles of Fluorescence Spectroscopy. Springer US, New York: 2006, 353-382.
9. El-Shafei, A.; Hussain, M.; Islam, A.; Han, L., Structure–Property Relationship of Hetero-Aromatic-Electron-Donor Antennas of Polypyridyl Ru (Ii) Complexes for High Efficiency Dye-Sensitized Solar Cells. *Progress in Photovoltaics: Research and Applications* **2014**, *22*, 958-969.
10. http://www.mit.edu/~tokmakof/5.38_Mod11_2009.pdf
11. http://web.vu.lt/ff/m.vengris/images/TR_spectroscopy02.pdf
12. Vaara, J.; Manninen, P.; Lantto, P., Perturbational and Ecp Calculation of Relativistic Effects in Nmr Shielding and Spin–Spin Coupling. *Calculation of NMR and EPR Parameters: Theory and Applications* **2004**, 209-226.
13. Diehl, B., Principles in Nmr Spectroscopy. In *Nmr Spectroscopy in Pharmaceutical Analysis*, Elsevier: 2008; pp 1-41.
14. Haruo Hayao, Pascal's Triangle, Non-Adjacent Numbers, and D-Dimensional Atomic Orbitals. *Hyper space* **1999**, *8*, 48-57.
15. http://www.chem.ucla.edu/~harding/notes/notes_14C_nmr02.pdf
16. Bax, A.; Freeman, R.; Frenkiel, T.; Levitt, M., Assignment of Carbon-13 Nmr Spectra Via Double-Quantum Coherence. *Journal of Magnetic Resonance (1969)* **1981**, *43*, 478-483.
17. Korfmacher, W. A., *Using Mass Spectrometry for Drug Metabolism Studies*; CRC Press, 2009.
18. Guilhaus, M., Special Feature: Tutorial. Principles and Instrumentation in Time-of-Flight Mass Spectrometry. Physical and Instrumental Concepts. *Journal of mass spectrometry* **1995**, *30*, 1519-1532.
19. Dass, C., *Fundamentals of Contemporary Mass Spectrometry*; John Wiley & Sons, 2007; Vol. 16
20. Ishii, H.; Kinjo, H.; Sato, T.; Machida, S.-i.; Nakayama, Y., Photoelectron Yield Spectroscopy for Organic Materials and Interfaces. In *Electronic Processes in Organic Electronics*, Springer: 2015; pp 131-155.
21. Lv, Z.; Yu, J.; Wu, H.; Shang, J.; Wang, D.; Hou, S.; Fu, Y.; Wu, K.; Zou, D., Highly Efficient and Completely Flexible Fiber-Shaped Dye-Sensitized Solar Cell Based on Tio 2 Nanotube Array. *Nanoscale* **2012**, *4*, 1248-1253.

CHAPTER THREE. Investigation of minimum driving force for the dye regeneration utilizing model squaraine dyes for dye-sensitized solar cells

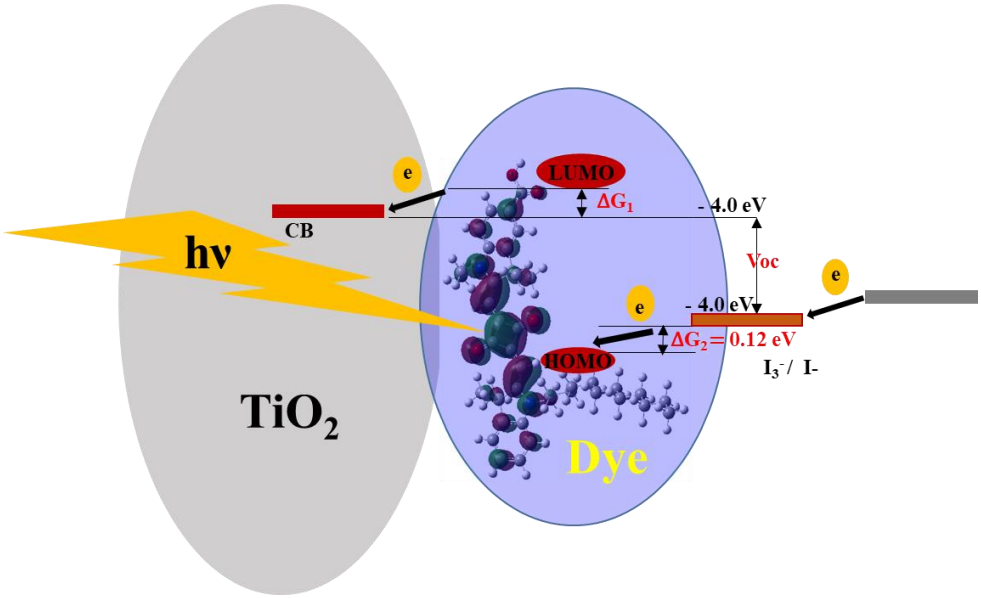

Anusha Pradhan, Takuya. Morimoto, Sai Kiran Maryala, Gaurav Kapil, Shuzi Hayase and Shyam Sudhir Pandey, ***Journal of Materials Chemistry A***, 2017, **5**, 22672-22682

3.1 Introduction

Growing human population and their demands for daily energy usage have increased the rapid and quick utilization of fossil fuels like coal, petroleum etc. as major energy resources. The daily use of them in the high technical, worldwide has both led to the fast reduction of highly prized non-renewable source of energy which takes billions of years for formation but also has enormously contributed to the emission of greenhouse gas like CO_2, SO_2 etc. which have led to global warming [1]. Even half a degree increment in the earth`s temperature shall enhance the greenhouse effect and cause danger to the mother nature. However limitation of global warming to 1.5^0 C could be achieved if the usage of the fossil fuel is ruled out [2]. Therefore an alternative renewable source of energy has to cope up in order the control the misfortune of global warming. One form of renewable energy i.e solar energy, clean and vastly available is found to be promising to meet this demand [3]. The application of solar cells is intelligently an important approach to belt this unending attainable light energy into directly utilizable electricity for daily use. Dye-sensitized solar cells (DSSCs) have cropped in as one of the standing candidates amongst next-generation solar cells which is basically due to its ease of fabrication, availability of cheap raw materials and solar energy harvesting in green manner. Implementation of solar cells have been effective in converting the solar energy into electrical energy. Not only on function, solar cell is expected to be cheap and eco-friendly as to make its way towards commercialization. To meet this demand as well as in its flexibility and light weight, dye Sensitized Solar Cells (DSSCs) have budded as one of the intended candidates among the next generation solar cell [4-5]. The attention of various researchers on it has been able to surpass an efficiency of 12% comparable to that of the amorphous silicon solar cells which gives a ray of hope for its commercialization. The achievement of good efficiency has been obtained from efficient new wide band gap semiconductor, dye design, electrolyte, counter electrode etc. as DSSCs is a multiple interface device and requires optimization in all parts [6-12].

Among the components of DSSCs, sensitizing dyes control a crucial role in exhibiting the overall external PCE since its primary function is to trap the photons from sunlight which is the initiation of the operation in DSSCs. Advantageously, dyes with the photon harvest only in the 400 nm to 750 nm visible wavelength region from has been able to reach an appreciable efficiency of 12% [13-15]. Therefore it arises an enthusiasm that how the implication of the Near Infrared Dyes (NIR)

would positively affect the current density in DSSCs as the maximum photon flux falls in the NIR region, and the dye would be able to harvest more photons. However all NIR dyes cannot be employed as the sensitizers, therefore logical design is the need of the hour. Also, these dyes could be used in combination with the visible dye as to result in the improvement in the external photon conversion efficiency (PCE). These two variety of dyes can be used as sensitizers for manufacturing hybrid or tandem DSSC device architectures [15-18]. However, the dyes reported till date have been able to harvest photons in the far red region around 650 nm and the aim of the design of NIR dye is still yet to be attained [19-21].

Beside its prospective in the extensive wavelength photon harvesting, the sensitizers must bear a facile energetic barrier with the electron accepting wide band gap semiconductor and redox shuttle in order to have an electron injection and dye regeneration, consecutively. In this context, synthesis and development of efficient NIR dyes is rather more provocative as they bear comparatively smaller band gap (Eg) between its HOMO and LUMO. This small Eg of NIR sensitizers require strict control on their energetics for their efficient operational energy barrier and thus a judicious molecular design is highly demanded. Therefore to proceed with the NIR dye design, minimum possible energy barrier for dye injection and regeneration should be investigated to promote unidirectional flow of electron. Such a vivid idea about this energy barrier offsets shall trigger the design of novel NIR sensitizers with maximum possible photon harvest wavelength window for a unique set of mesoporous wide band gap semiconductor and the redox shuttle. Study on a set of squaraine dyes, demonstrated that energetics could be controlled by 0.1 eV simply by varying the alkyl chain length substituents maintaining the main Π-conjugated framework intact [22]. Also, it has also been reported by us that the facile electron injection from the lowest unoccupied molecular orbital (LUMO) of the photo excited dye, (squaraine in this case) to the conduction band of the TiO_2 is also possible only with a least energy barrier of 0.16 eV [23]. This gives us the reliance for the synthesis of NIR dyes.

Nowadays, before the in hand synthesis of the dyes, state-of-art theoretical calculations employing the Gaussian program package have found its wide utilization in the prediction of the energetics of the dyes to promote the design and development of novel sensitizers [24]. The energy of dye molecules in the ground and excited states could be estimated theoretically of which is much required for the DSSCs as energetics control the operation of it. Not only the energetics, the

electronic absorption spectra could also be obtained which gives the idea of the dye`s absorption limit which is highly desired in order to ignite the development of applicable sensitizers. It has been studied by us that a logical choice of basis set under the time-dependent density functional theory (TD-DFT) approximation minimises error between the theoretical and experimentally values of the energy and electronic absorption maximum (λ_{max}) [25]. This present work explains the estimation of the least possible energy barrier for electron donation by the electrolyte to the electron deficient dye. In this case, iodine-based (I^-/I_3^-) redox electrolyte was used as the redox shuttle in conjunction with some few unsymmetrical infrared sensitive squaraine dyes with the molecular structure as shown in the Fig. 1. The knowledge of both the energy barrier in electron injection as per reported before and the one in the dye regeneration in this work would synergistically improvise the blooming of novel NIR sensitizers. Beside the theoretical computation of the dye structure as shown in the Fig. 1, they were synthesized, confirmed the synthesis from mass and NMR spectroscopy, and characterized as to compare the theoretical results with the ones obtained from experiment. And finally their Photophysical performance was studied. Computed and experimentally obtained outputs on energy of molecules in both the ground and excited states, the energy band gap and λ_{max} for these molecules were then co-related from the optimum molecular structure with the least driving force for effective dye regeneration with good performance.

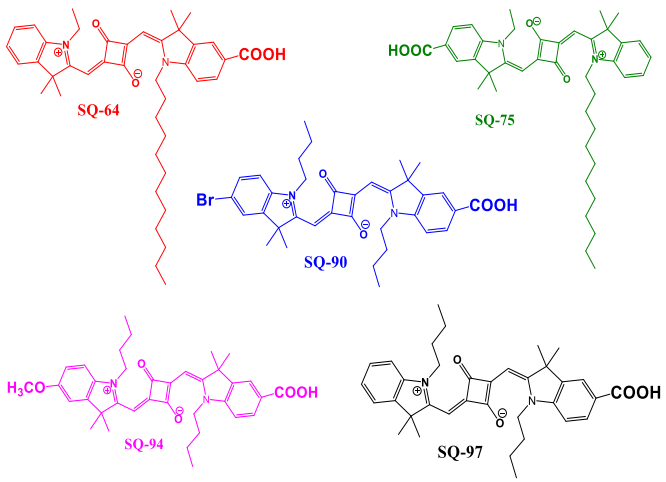

Figure 1. Molecular structure of unsymmetrical squaraine dyes used for present investigation.

3.2 Experimental

3.2.1 Synthesis of squaraine dyes

Indole with direct ring bearing carboxy functionalized as the anchoring group and its derivative *2,3,3-trimethyl-3H-indole-5-carboxylic acid* (1) was synthesized adopting the method as per reported by Pham et al [26]. Comprehensive synthesis and characterization of the dye intermediates (2) and (3) have been already published by us elsewhere [23]. The unsymmetrical squaraine dye SQ-64 along with its intermediates has been synthesized as per our earlier publication [27]. Semi-squaraine dye intermediates (4, 5, 6 and 7) were synthesized and characterized as per our earlier publications [28]. The scheme as shown in Fig. 2. Portrays the unsymmetrical squaraine dyes SQ-75, SQ-90, SQ-94 and SQ-97 along with their corresponding intermediate indolium iodide salts were synthesized as per the scheme is shown in Fig. 2.

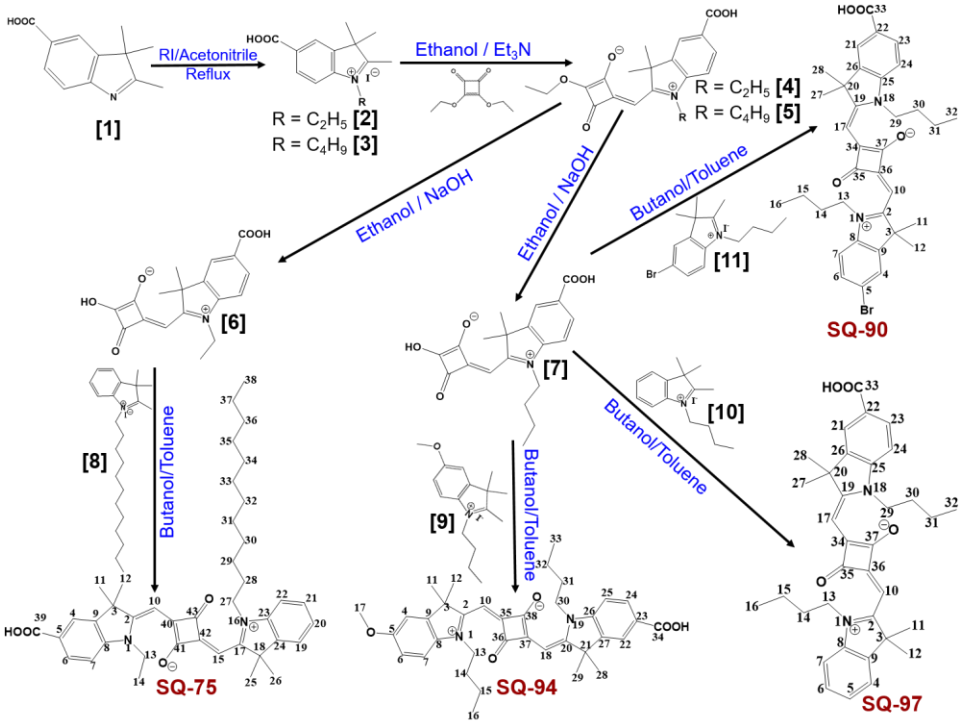

Figure 2. Synthetic route for direct –COOH functionalized unsymmetrical squaraine dyes.

2.2.1 Synthesis of intermediate 2,3,3-trimethyl-1-dodecyl-3H-indolium iodide [8]

1 equivalent of 2,3,3 trimethyl-3H-Indole, 3.18 g (20mmol) of and 3 equivalent 15 mL of 1-Iodo-dodecene (60 mmol) were dissolved a round bottom flask containing 40 mL acetonitrile and then

refluxed for 48 hours [29].The completion of the reaction was monitored by TLC where the alkylated compound exhibited a visible pink color within few seconds. After the complete removal of the solvent, excess diethyl ether was added for precipitation. The obtained precipitate was filtered and washed 3 times successively with ether. The residue was dried under vacuum to afford the titled compound in 8.13 g (18 mmol) (90%) yield. HR-MS (measured m/z: 328.3013; calculated m/z: 328.2999).

2.2.2 Synthesis of intermediate 5-Methoxy-2,3,3-trimethyl-1-Butyl-3H-indolium iodide [9]

(5 mmol) of 5-Methoxy-2,3,3-trimethyl-3H-indole (1.0 g) and 10 mmol of 1.4 mL of 1-Iodobutane were dissolved in 25 mL of acetonitrile and reaction mixture was refluxed for 36 hours [30]. After the completion of the reaction as monitored by HPLC and TLC, the solvent was evaporated and the obtained viscous crude product was subjected to flash column (silica gel) using chloroform-methanol as an eluting system. The purification resulted in the 1.2 g (3.21 mmol) of the desired compound in a purple viscous liquid with 64 % yield. MALDI-TOF mass (measured m/z: 248.0 [M+2]+; calculated m/z: 246.19) confirms the synthesis of this intermediate.

2.2.3 Synthesis of intermediate 2,3,3-trimethyl-1-Butyl-3H-indolium iodide [10]

1 equivalent of 2,3,3-trimethyl indole and 3 equivalent of 1-Iodobutane were dissolved in dehydrated acetonitrile and the reaction mixture was subjected to reflux for 24 hours [31]. After the completion of the reaction as monitored by TLC, the solvent was evaporated and the resulted crude was washed thoroughly with ample diethyl ether to afford brown solid in 95% yield. HPLC purity: 98%. The m/z : 216.2 confirms the successful synthesis of this intermediate.

2.2.4 Synthesis of 5-Bromo-2,3,3-trimethyl-1-Butyl-3H-indolium iodide [11]

5-Bromo-2,3,3-Trimethyl-Indole was synthesized following the fischer indole synthesis protocol first before it was subjected to quaternization. A mixture of 8.0 g, (35.7 mmol) of 4-bromophenyl hydrazine hydrochloride, 9.6 mL, (89 mmol) of 3-Methyl-2-Butanone and Ethanol (60 mL) were taken in 200 mL round bottom flask. It was refluxed for 2 hours under the same inert condition. After the completion of the condensation, ethanol was evaporated over vacuum and 100 mL of glacial acetic acid was added. This resulting mixture was then again heated at 120^{o}C for 12 hours the same inert condition [32]. Acetic acid was then removed at reduced pressure by the rotary

evaporator and the crude was subjected to flash silica gel column using chloroform-methanol (98:2) as the eluting solvent system which resulted the desired product of 5-Bromo-2,3,3-Trimethyl-Indole in 77 % yield (6.5 gm, 27.4 mmol). Purity as confirmed >98 % by HPLC. HR FAB-mass (measured m/z: 238.0 [M]+ ; calculated m/z: 238.1).

1 equivalent (1.8 g, 0.75 mmol) of 5-Bromo-2,3,3-trimethyl-3H-indole and 3 equivalent (2.6 mL, 2.25 mmol) of 1-Iodobutane were dissolved in 40 mL of acetonitrile as the reaction solvent and refluxed for 24 hours. After the completion of the reaction, the solvent was completely evaporated. The obtained crude was washed with ample amount of diethyl ether to remove the excess iodobutane. It was then subjected to silica gel flash column with chloroform-methanol eluting system. 2.85 gm (6.75 mmol) of the desired brown powder was obtained in 90 % yield having >98 % purity as confirmed by HPLC. FAB-mass (measured m/z: 295.0 [M]+ ; calculated m/z: 295.2).

2.2.5 Synthesis of squaraine dye SQ-75

220 mg (0.5 mmol) of 2,3,3-trimethyl-1-dodecyl-3H-indolium iodide (8) and semi-squaraine dye intermediate (6) (164 mg, 0.5 mmol) were taken in a round bottom flask fitted with condenser, followed by the addition of the 30 ml of dehydrated benzene-butanol (1:1 v/v) to it. The reaction mixture was refluxed using Dean-Stark trap. After the complete consumption of the reactant as monitored by TLC in 12 hours, the solvent was evaporated over vacuum and the crude was subjected to purification by the silica-gel flash column chromatography using chloroform-methanol as the eluting system. 230 mg (0.3 mmol) of the titled compound was obtained as a bright blue solid in 72% yield with 99% HPLC purity. ESI- TOF mass (Calculated - 636.87 and observed – 637.39 $[M+1]^+$). ^{1}H NMR (500 MHz, d6-DMSO): d/ppm = 8.12 (d, H-19), 8.06 (dd, H-20), 7.41 (dd, H-4), 7.35 (dd, H-6), 7.21 (d, H-22), 7.05 (dd, H-21), 6.98 (dd, H-7), 6.10 (s, H-15), 6.02 (s, H-10), 4.07 (t, 2H, H-27), 4.03 (q, 2H, H-13), 1.94 (s, 6H, H-11 & H-12), 1.83 (s, 6H, H-25 & H-26), 1.25 (t, 3H, H-14), 0.87 (t, 3H, H-38). ^{13}C NMR (125.75 MHz, $CDCl_3$) : δ/ppm =182.3 (C-27+ 29), 171.2 (C-28), 167.7 (C 25), 167.5 (C-25), 142.4 (C-32), 141.9 (C-2), 130.7 (C-8), 128.6 (C-38), 125.5 (C-39), 124.9 (C-9), 123.5 (C-6), 122.8 (C-36), 111.2 (C-5), 109.9 (C-35), 87.4 (C-10), 87.0 (C-30), 49.7 (C-33), 48.3 (C-3), 43.3 (C-13), 40.5 (C-14), 31.7 (C-42), 29.4 (C-20), 29.3 (C-21), 29.1 (C-22), 27.1 (C-15), 26.8 (C-11+12), 26.6 (C-40+41), 26.5 (C-16), 22.5 (C-23) 14.4 (C-24), 12.3 (C-43).

2.2.6 Synthesis of squaraine dye SQ-90

210 mg (0.5 mmol) of *5-Bromo-1-butyl-2,3,3-trimethyl-3H-indolium iodide* (**11**) and 178 mg (0.5 mmol) of semi-squaraine dye intermediate (**7**) were taken in a round bottom flask fitted with condenser dissolved in 30 mL of dehydrated benzene-butanol (1:1 v/v) mixture. The reaction mixture was refluxed using a Dean-Stark trap for 18 hours. Then the solvent was evaporated and the obtained crude was purified by silica-gel flash column using chloroform-methanol as the eluting solvent. 215 mg of the titled compound was obtained as blue solid in 68 % yield with HPLC purity of >98 %. ESI-TOF mass (Calculated – 631.6 and observed – 632.2 $[M+2]^+$) and ^{1}H NMR (500 MHz, DMSO-d6): d/ppm = 8.0 (dd, H-7), 7.94 (dd, H-21), 7.82 (dd, H-23), 7.54 (dd, H-4), 7.38 (dd, H-6), 7.34 (dd, H-24), 5.85 (s, H-10), 5.83 (s, H-17), 4.09 (t, 2H, H-13), 4.07 (t, 2H, H-29), 0.94 (t, 6H, H-16 & H-32). ^{13}C NMR (125.75 MHz, DMSO-d_6) : δ/ppm = 181.5 (C-35+37), 180.9 (C-36), 178.9 (C-34), 170.3 (C-2), 168.9 (C-19), 167.5 (C-33), 146.6 (C-25), 144.5 (C-9), 141.8 (C-8), 131.2 (C-26), 130.7 (C-23), 126.0 (C-6), 125.8 (C-22), 123.5 (C-5), 116.8 (C-21), 113.0 (C-4), 110.2 (C-7+24), 87.6 (C-17), 87.4 (C-10), 60.8 (C-3), 49.6 (C-20), 48.6 (C-29), 43.6 (C-13), 43.3 (C-30), 35.1 (C-14), 29.1 (C-27+28), 29.1 (C-11+12), 27.05 (C-31), 26.6 (C-15), 20.1 (C-32), 20.0 (C-16). The mass data and the NMR data confirms the successful synthesis of the unsymmetrical squaraine dye **SQ-90**.

2.2.7 Synthesis of squaraine dye SQ-94

In a round bottom flask fitted with condenser 187 mg (0.5 mmol) of *1-butyl-5-methoxy-2,3,3-trimethyl-3H-indolium iodide* (**9**) and 178 mg (0.5 mmol) of semi-squaraine dye intermediate **(7**) were dissolved in 30 mL of dehydrated benzene-butanol (1:1 v/v) mixture. The reaction mixture was refluxed using Dean-Stark trap overnight. After the completion of the reaction, the solvent was evaporated and crude product was purified by silica-gel flash column chromatography using chloroform-methanol as an eluting solvent. 230 mg of the titled compound was obtained as a blue solid in 79 % yield. ESI-TOF mass (Calculated – 582.74 and observed – 583.31 $[M+1]^+$) and ^{1}H NMR (500 MHz, DMSO-d6): d/ppm = 7.94 (dd, H-22), 7.90 (dd, H-7), 7.39 (dd, H-24), 7.27 (dd, H-4), 7.24 (dd, H-6), 6.96 (dd, H-25), 5.86 (s, H-10), 5.74 (s, H-18), 4.16 (t, 2H, H-13), 3.98 (t, 2H, H-30), 3.32 (s, 3H, H-17), 0.94 (t, 6H, H-16 & H-33. ^{13}C NMR (125.75 MHz, DMSO-d_6): δ/ppm =181.8 (C-38+36), 174.4 (C-37), 171.8 (C-35), 167.6 (C-34), 166.1 (C-2), 158.2 (C-20), 146.9 (C-26), 144.2 (C-9), 141.4 (C-8), 135.7 (C-27), 130.7 (C-24), 124.9 (C-6), 123.4 (C-23),

113.7 8C-5), 112.5 (C-22), 109.4 (C-4), 82.7 (C-7), 82.7 (C-25), 87.3 (C-18), 87.1 (C-10), 74.0 (C-21), 56.2 (C-3), 50.2 (C-30), 47.9 (C-13), 47.3 (C-31), 43.9 (C-14), 31.9 (C-17), 29.4 (C-28+29), 28.4 (C-11+12), 28.4 (C-32), 27.3 (C-15), 20.1 (C-33), 20.0 (C-16),) confirms the successful synthesis of the unsymmetrical squaraine dye **SQ-94.**

2.2.8 Synthesis of squaraine dye SQ-97

In a 100 mL round bottom flask fitted with condenser 174 mg (0.5 mmol) of *1-butyl-2,3,3-trimethyl-3H-indolium iodide* (10) and 178 mg (0.5 mmol) of semi-squaraine dye intermediate (7) were dissolved in 30 mL of dehydrated benzene-butanol (1:1 v/v) mixture. The reaction mixture was subjected to azeotrope reflux using Dean-Stark trap for overnight. After the completion of the reaction, the solvent was evaporated and the crude product was purified by silica-gel flash column chromatography using chloroform-methanol as an eluting solvent. 220 mg of the titled compound was obtained as a blue solid in 79 % yield. ESI-TOF mass (Calculated – 552.71 and observed – 553.30 $[M+1]^+$) and ^{1}H NMR (500 MHz, DMSO-d6): d/ppm = 7.97 (dd, H-24), 7.93 (dd, H-21), 7.57 (dd, H-23), 7.42 (d, H-7), 7.39 (dd, H-5), 7.33 (dd, H-6), 7.23 (d, H-4), 5.89 (s, H-17), 5.80 (s, H-10), 4.15 (t, 2H, H-29), 4.04 (t, 2H, H-13), 0.93 (t, 6H, H-16 & H-32). ^{13}C NMR (125.75 MHz, DMSO-d_6) : δ/ppm = 182.1 (C-35+37), 171.6 8C-36), 1673.8 (C-34), 167.5 (C-33), 161.0 (C-2), 146.7 (C-19), 142.4 (C-25), 142.3 (C-9), 137.4 (C-8), 131.2 (C-26), 130.7 (C-23), 128.5 (C-6), 127.9 (C-22), 125.4 (C-5), 124.9 (C-21), 123.5 (C-4), 123.3 (C-7), 122.8 (C-24), 105.6 8C-17), 105.2 (C-10), 79.6 (C-3), 76.9 (C-20), 49.7 (C-29), 43.6 (C-13), 43.2 (C-30), 30.2 (C-14), 29.3 (C-27+29), 29.0 (C-11+12), 27.2 (C-319, 26.7 (C-15), 20.2 (C-32), 20.1 (C-16), confirms the synthesis of the unsymmetrical squaraine dye **SQ-97.**

3.2.2 Cyclic Voltammetry

The Highest Occupied Molecular Orbital (HOMO) was estimated from the oxidation peak potential in Cyclic Voltametry (CV) curve. The estimation of HOMO from this method is more reliable as it involves the electrolyte interface like the DSSCs where solvation effect could also be encountered which is the real model for DSSCs. First, the CV of ferrocene was done to be taken as a reference. Then the CV of sensitizing dyes was conducted sequentially to obtain the curve as shown in the figure 3. in the similar electrochemical measurement. Ferrocene (Fc) has been classically used as a reference material owing to its sharp redox reaction and the visibility of

distinct peak [34]. The HOMO energy level of the dyes was measured from the shift in the dyes' oxidation potential with respect to ferrocene. Though there are various reports on the absolute potential of Fc^{+}/Fc redox couple in literature, however, its value of -5.01 eV reported by Su and Girault has been taken into account [35]. The approval of this value has also been theoretically verified by Namazian et al in his outstanding logical calculation as well [36]. The HOMO values of the dyes estimated by CV exhibit the same trends as given by the theoretically calculated values. To conduct the CV, the respective dyes (0.2mM) were dissolved in dimethyl formamide (DMF) with tetrabutylammonium hexafluorophosphate (0.1M) as the supporting electrolyte. The scan rate was maintained as 20 mV/s.

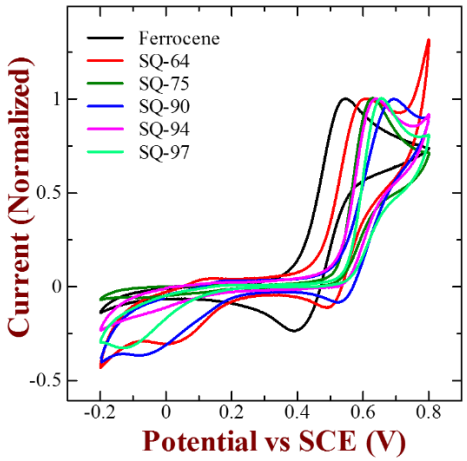

Figure 3. CV of ferrocene as reference and the sensitizing dyes along in DMF solution. Peak values of current for respective dyes are normalized in order to clearly visualize the shift of oxidation potential of dyes with respect to ferrocene.

3.2.3 Photoelectron Yield Spectroscopy

The photoelectron yield spectroscopy of the dyes in solid state was conducted in high vacuum (10^3 Pascal). The dye was grinded properly and spread on the assigned area of the FTO with carbon tapes that the laser light source could fall on it. The sample was then placed on the sample holder and subjected to the process under high vacuum. The obtained data was then fitted on the curve with the yield ($Y^{1/3}$) on the coordinate and the energy (eV) on the abscissa.

3.2.4 Time resolved Photoluminescence

Fluorescence lifetime was measured using the time dependent frequency domain. The dye solution in the cuvette was placed inside the fluorescence lifetime measurement system (Quantarus Tau

Model C-11370, Hamamatsu Photonics, Japan). The sample was then excited with the laser light source around the excitation wavelength of the dye. The lifetime was then measured from the fluorescence decay around 680 nm.

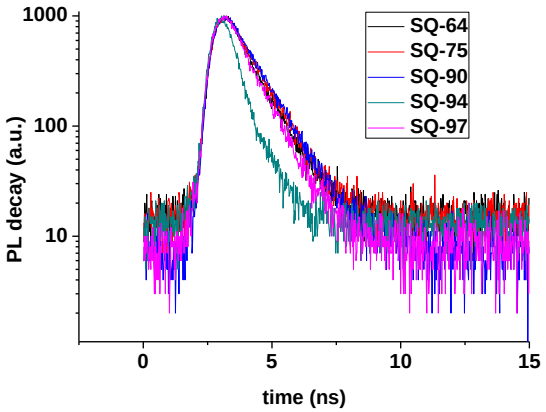

Figure 4. Shows the fluorescence lifetime decay curve of the sensitizing dyes.

3.3 Results and Discussion

3.3.1 Theoretical Molecular Orbital Calculations

Theoretical Quantum computations employing density functional theory (DFT) for the deeper knowledge about energetics, electronic absorption spectra etc. has been tremendously used to predict the electronic distribution and development of new sensitizers for DSSC [37]. The prospect of DFT for theoretical quantum chemical calculation is its consideration of correlation of electron and lone pair like ab-initio method at the minimum cost for computation which is observed alike in the Hartree- Fock method. Gaussian program package implementing time-dependent extension (TD-DFT) provides trusty results for electronic absorption spectrum using standard correlation functional [38]. Theoretical structural minimum energy optimization, under the Gaussian G09 program, of the squaraine dyes under study were computed using DFT, 6-311G basis set and linear spin density approximation (LSDA) functional. The condition of the default convergence was sustained for all of the theoretical calculations in the process of the geometry optimizations. It has been reported by us that the implication of LSDA functional under DFT justifies more trust worthy results for the prediction of both the HOMO energy level and also the λ_{max} as related to other

functional operation under Gaussian program for squaraine dyes[39]. Structural optimization in the HOMO and LUMO electron density distribution of the dyes considered in this chapter is shown in the Figure 6a.

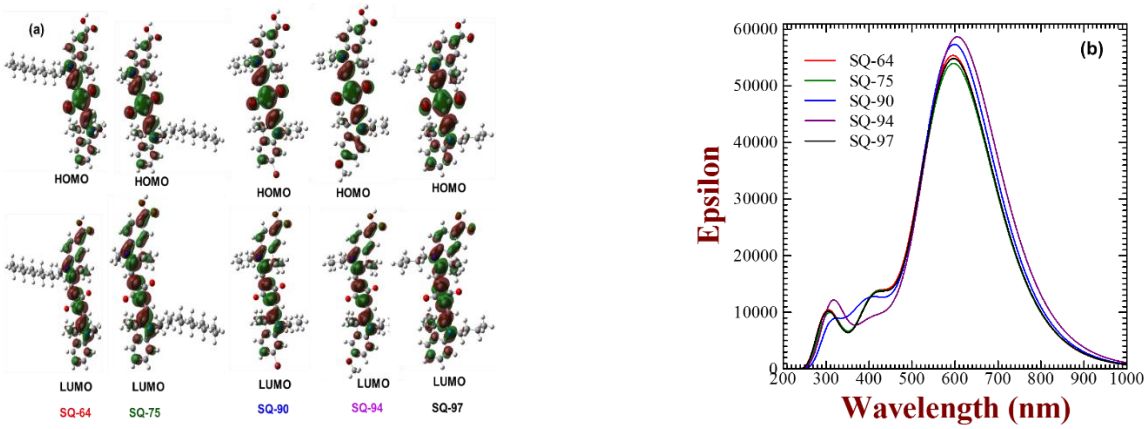

Figure 5. Calculated HOMO and LUMO orbital diagrams after structural optimization (a) computed electronic absorption spectra in isolated gaseous state for unsymmetrical squaraine dyes (b) using LSDA functional under TD-DFT and 6-311G basis set.

The above figure vividly portrays that the electron density of the HOMO the dyes is basically allocated in the central square moiety while the electron density distribution for the corresponding LUMOs is more concentrated in the electron donating –COOH functional group. The good separation in the electron density between the HOMO and LUMO is practically needed to afford a better functioning dye due to the facile charge transfer. Simultaneously, it is also visible that the surplus electron density is present in the LUMO of the anchoring group. This excellently ensures the better electronic coupling through the ester linkage between the photoexcited dye molecules and 3d-orbital of the mesoporous TiO_2 leading to the facile adsorption of dye molecules. The good adsorption promotes facile interfacial injection of electrons from the excited state (LUMO) of the dye molecule into the conduction band of the n type semiconductor. It has been exemplified that TD-DFT provides more accurate and reliance on the estimation for the electronically exciting sensitizers used for DSSCs. This precision of the results depends on the mutual choice of the functional and basis set generally used for the calculations which may vary from the kind of molecule subjected to computation [38,39]. The simulated electronic absorption spectra for the unsymmetrical squaraine dyes accomplished using LSDA functional and 6-311G basis set under TD-DFT is exhibited in figure 4b. It can be studied that the calculated electronic absorption spectra

showcase prominent and secure absorption between 500-700 nm. This is due to the Π– Π* electronic transition as discussed previously. It can also be observed that the theoretical spectral shape shows close resemblance with that of the respective experimental results as in its solution state demonstrated in figure 8 in the next section (Photophysical Characterization). It can also be observed that the computed values of λmax tabulated in table 1 are a bit lesser as compared to its respective experimentally measured values in solution. The reason for this is because the theoretical computation has been carried out for a single molecule in its gaseous state where the contribution from the intermolecular interactions are pretty well negligible as compared to the solution state where the molecules are closer enough for interaction. Also in the theoretical calculation, solvation effect has been ruled out which is prominent in the experimental measurement. Fortunately, the dyes SQ-90 and SQ-94 exhibit a visible 4-8 nm red-shifted λmax as compared to other dyes discussed here coinciding the trend as shown by them in the experimental measurement. In a lump sum, in the recent scenario TD-DFT promises a precise and reliable predictions that the functional and basis set selected for TD-D FT calculations are justifiable.

3.3.2 Photophysical Characterizations

The basic beauty of squaraine dyes is in its sharp optical absorption in the infrared (550-700 nm) wavelength region on account for the intramolecular π-π* electron transition. They also exhibit the fluorescence emission extending up to the higher IR-region [40]. Electronic absorption of the unsymmetrical squaraine dye along with its fluorescence emission spectra study of the studied here are shown in Figure 6. The results thus obtained based on the photophysical characterizations have been summarized in Table 1. A perusal of the Figure 6. clearly demonstrates that all dyes exhibit substantial light absorption between 550 nm-700 nm which is an indication of main absorption in the infrared region of the white light spectrum. Also the high molar extinction coefficient (ε) of the squaraine dyes with the values between 1.8-3.5X10^5 $dm^3mol^{-1}cm^{-1}$ adorns the application of it to thin semiconductor based DSSCs. The spectrum also consists of a clear vibronic shoulder between 550-600 nm which is due to the formation of H aggregate which will be discussed in detail later. Amongst the dyes considered in this work, SQ-94 seems to exhibit an observable bathochromic shift in its optical absorption maxima spectrum (λmax) which naturally red shifts its optical absorption edge. The main reason for this fruitful bathochromic shift could be due to its

virtue of the presence of electron donating methoxy group at the 5th position of indole ring opposite to the indole ring bearing –COOH group. The presence of electron donating and accepting groups in the opposite poles would have promoted a facile unidirectional electron transfer which would have red shifted the absorption spectrum.

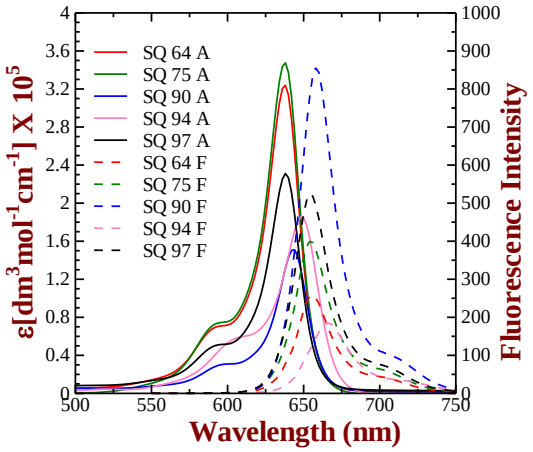

Figure 6. The solid lines denote the electronic absorption and the dotted lines denote the fluorescence emission spectra of the concerned squaraine dyes in ethanol solution.

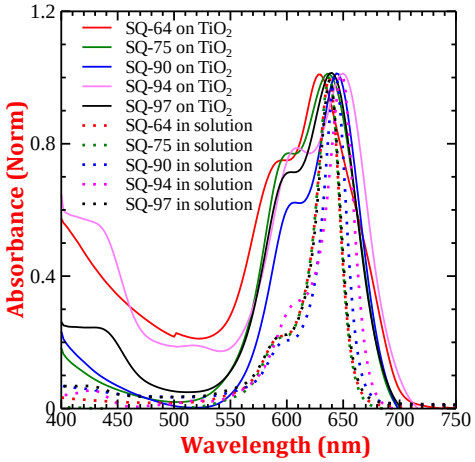

Figure 7. The solid lines denote the normalized electronic absorption spectra in solid state of the dyes and the dotted lines denotes that of in the solution state.

The observed Stokes shift between (16-18 nm) in all of the new squaraine dyes under study is very low compared to the other dyes which indicates the conformational rigidity of it. Therefore, less Stokes shift means the conformal rigidity of the dyes maintaining the almost same configuration of the dye molecules in both of its ground state and the excited states [41]. Therefore this could

support many turnover number and frequency. The spectra of the electronic absorption of the dyes in its solid state i.e on a transparent film of mesoporous TiO_2 was also taken to study the real nature of the dye in its operation in the working DSSCs. They were normalized with their corresponding spectra in ethanolic solution to study the nature of it as depicted in the Figure 7. A study of those spectral features vividly validates that an enhancement in the full width at half-maximum (FWHM) is observed upon adsorption of dyes onto the mesoporous TiO_2 surface as compared to that of their respective spectrum in the ethanolic solution.The observed spectral broadening is due to the molecular aggregation in the condensed state and the interaction of the anchoring carboxylic acid group of the dyes with the TiO2 surface due to the formation of ester linkage [41]. Concurrently, a small vibronic shoulder in the 550-600 nm perceived for dyes in solution, seems to be enchantly pronounced after adsorption onto the TiO_2. Due to the intact molecules in the solid state, the enhancement in the vibronic shoulder is exemplified. It has been shown that in squaraine dyes, the blue shifted hump is due to the dye aggregate formation which is illustrated when the dye co-adsorber like chenodeoxycholic acid (CDCA) is added to the dye solution [42].

It is noteworthy to observe here that the solid-state broadening (the blue shifted hump) is more enhanced towards lower wavelength region designating the presence of H-aggregates. Moreover the unsymmetrical squaraine dyes SQ-64 and SQ-94 prominently showcase the relatively enhanced absorption and vivid visible absorption peak in the visible wavelength regions of 400 nm-500 nm which could be associated with the enhanced Π- Π stacking leading to H-aggregate formation. Kim et al have clearly evidenced the formation of hypsochromic shifted (H-aggregates) in squaraine dyes as adsorbed on the SnO_2 semiconductor surface [43]. The diminished fluorescence intensity is an indication of H-aggregate formation by these dyes (Fig. 7) in solution pointing the H-aggregate assisted fluorescence quenching. A report by Xu et al has also clearly implied that H-aggregated squaraine dyes are almost non-fluorescent and there was significant fluorescence when they were interacted with bovine serum albumin (BSA) [44].

Table 1. Experimental data for the photophysical characterization of the unsymmetrical squaraine dyes in Ethanol solution.

Dye	Abs_{max} (nm)[a]	Em_{max} (nm)[b]	ε ($dm^3mol^{-1}cm^{-1}$)	E_{o-o} (eV)[c]	E_{opt} (eV)[d]	Stokes shift (nm)[e]	FWHM (nm)[f]	τ(ns)[g]
SQ 64	638 (597)	656	$3.23x\ 10^5$	1.90	704 nm (1.76)	18	100	0.948 ± 0.004
SQ 75	638 (597)	654	$3.47\ x\ 10^5$	1.91	698 nm (1.77)	16	82	1.044 ± 0.005
SQ 90	644 (600)	660	$1.50\ x\ 10^5$	1.92	698 nm (1.77)	16	78	1.153 ± 0.006
SQ 94	648 (606)	666	$1.80\ x\ 10^5$	1.87	710 nm (1.75)	18	93	0.434 ± 0.076
SQ 97	639 (597)	656	$2.30\ x\ 10^5$	1.92	698 nm (1.77)	17	83	0.9043± 0.004

Electronic absorption[a] and fluorescence emission[b] maximum of dyes in the ethanol solution. Values of absorption maximum shown in parenthesis are obtained from the simulation absorption spectra using TD-DFT. Transition energy[c] was calculated from the wavelength of an intersection of absorption and emission spectrum of corresponding dyes in ethanol. Optical absorption edge (E_{opt})[d] was estimated from the onset wavelength of solid state electronic absorption spectrum of respective dyes adsorbed on thin mesoporous TiO_2. Stokes shift[e] was estimated from the separation between the absorption maximum and emission maximum. The full width at half maximum (FWHM)[f] was calculated from the electronic absorption of dyes adsorbed on TiO_2. Average fluorescence lifetime τ[g] for the dyes was calculated from transient fluorescence spectrum using time-correlated single photon counting measurements.

3.3.3 Energy Band Diagram

The energetics of the various components in the DSSCs play a significant role in determining the functioning it. The energy level should be optimum in order to facilitate the flow of electrons which is the source of current. Also the Voc as determined by the difference in the fermi level of the electrons on the TiO_2 and the redox potential of the electrolyte has so much to say in the kinetics

of DSSCS. The basic trigger for the working DSSCs is the excitation of the electrons from the HOMO of the dye to the LUMO of it. When the sunlight (incident photons), fall on the dye molecule covalently adsorbed onto the surface of TiO_2, the electron in the HOMO gets excited from the normal ground state to its excited state due to the intramolecular π-π* electronic transition. The incongruity in the energy levels of the two interfacial materials in contact is the main reason for driving force for electron transfer [45]. Hence, sensitizers having energy level higher than the TiO_2 conduction band (CB) is required for efficient electron injection. Thus they are available to electron injection after photoexcitation as which is impossible otherwise. After the excitation of the dye, the dye bears a positive charge which has to be nullified for another cycle of excitation. In other words, dye molecule attains the oxidized state which needs to be reduced by electron transfer from redox couple (I^-/I_3^- in our case). This process is well known as dye regeneration [46]. The energy difference should be such that the redox potential of the electrolyte should be higher than that of the HOMO of the dye. Therefore, the CB of TiO_2 and LUMO of the dye, HOMO of the dye molecules and redox potential of the redox couple should bear a certain energetic cascade for efficient electron injection and dye regeneration. Implication of the combined theoretical and experimental approaches, it has been demonstrated by us that it is feasible to inject electrons from the excited dye molecules (LUMO) to the CB of TiO_2 with least possible energy cascade as low as 0.15 eV[38]. In this recent work, unsymmetrical squaraine dyes have been reasonably synthesized to acquire the minimum possible energy barrier for regeneration of the excited dye molecules by redox shuttle using traditional used I^-/I_3^- redox couple at their interface. In a typical DSSC, molecular structure of the dye and its HOMO energy level play the crucial role in regeneration efficiency which is mandatory for more turnover number. The energy band diagram for all of the concerned dyes and the TiO_2 and I^-/I_3^- is shown in the Fig. 8.

Energy band diagram was compiled by considering the redox potential of I_3^-/I^- redox couple to be 0.44 V vs. NHE or -4.90 eV with respect to the vacuum level [47]. Whereas, CB energy level for TiO2 was taken to be -4.0 eV as given in the reference reported by Li et al [48]. Fortunately, the energy level of dye molecules in this work showcase the favourable energetics with respect to the CB of TiO_2 and redox energy level of I_3^-/I^- redox couple which ensures the thermodynamic feasibility of electron injection and dye regeneration. From the figure 8. it can be noticed that the values of the HOMO energy level of dyes calculated using TD-DFT depicts a very good congruency with a minimal error range of 0.01-0.09 eV with their respective experimentally

obtained values by PYS as well as with CV. This further assures the authenticity of our theoretical computation of the energetics. Also it can be observed from the band diagram that the molecular structure of the dyes plays a significant role in controlling the energetics and their energy level. It is also well known that the electron withdrawing group pulls down the energetic of the molecule. The dyes SQ 90, 94 and 97 differ only in the 5th position group substitute opposite to that of the indole bearing –COOH group. The HOMO of SQ-97 lies at -5.09 eV and LUMO energy at -3.16 eV, Whereas SQ 90 with a Br group at the 5th results in a downward shift of the energetics due to the presence of electron withdrawing -Br attached to the Indole ring (Fig. 1). Whereas SQ 94 with an electron donating –OCH_3 group presents an upward shift in its energetic value. This clearly proves that the electron donating group shifts the energy level upward against vacuum. Squaraine dyes like SQ-75 and SQ-64 with long alkyl chain (due to the dye dipole from the longer alkyl) exhibited an upward shift in their energetics as compared to the dyes with short alkyl chains. For example in SQ 64 with the longer alkyl spanning its HOMO energy level very near to the redox potential of the I_3^-/I^- redox couple. In case of SQ 64, the HOMO level energy level maintains only a least energy difference of 0.11 eV with respect to the redox potential of the electrolyte. It has also been shown by us that the increase in alkyl chain length is results in the upward shift in the energy level of squaraine dyes which explaining the possibility of minute tuning of the energy with the alkyl chain length [49].

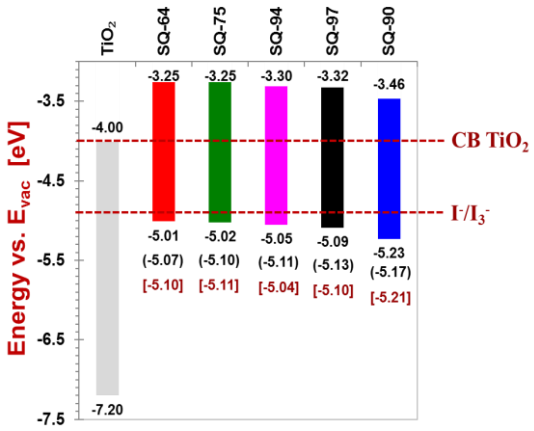

Figure 8. Depicts the energy band diagram for the concerned sensitizing dyes. Values of the HOMO energy level shown in () are experimental values by CV while that shown in [] are theoretically calculated values using TD-DFT and the values without parenthesis is the experimental value obtained from PYS.

3.3.4 Photovoltaic properties

The dyes discussed above were employed as sensitizers for fabricating DSSCs. It was already observed that there is good energy matching for the electron injection and dye regeneration. In other words, proper energy level congruency between the unsymmetrical squaraine with that to the CB of TiO_2 and redox potential level of iodine redox electrolyte portrayed as in the Fig. 8 emboldened us to study their photovoltaic characteristics. The electron injection energy barrier of 0.16 eV was already investigated by us which also motivated us to scrutinize to find the least driving force necessary for the dye regeneration [38]. Fig. 9 (a) portrays the photocurrent density-voltage (*J*-V) curve for the DSSCs based squaraine sensitizers obtained and the basic photovoltaic parameters of the DSSCs from these dyes as derived from the J-V curves are tabulated in table-2 under global AM 1.5G simulated solar illumination. It can be clearly observed from this figure and table that among the DSSCs fabricated, the dye SQ-75 as sensitizer resulted in the superlative photoconversion efficiency (PCE) of 4.25% with a short circuit current density (Jsc) of 10.92 mA/cm^2, open circuit voltage (Voc) of 0.57 V, and fill factor (FF) of 0.67. Amongst the dyes used, this dye SQ-75 exhibited superlative highest Jsc and of Voc leading to the best overall PCE. Efficient electron injection and dye generation could be the reason for the highest Jsc. As Jsc could be obtained from the integration of the incident photon conversion efficiency [50], there is a spectral matching of the curves in trend as per the confirmation by the measurement of photocurrent action spectra as shown in the Fig. 9 (b).

In the photocurrent action spectrum, the dye SQ-75 bears the highest incident photon to current conversion efficiency (IPCE) of about (~56%) mainly in the infrared wavelength which peaks around 640 nm and could be due to the attaining of the highest Jsc in the J-V characteristic amongst the dyes employed as a sensitizer in this task. A study of Fig. 9 (b) and table 2 explains that the J-V current is higher than that obtained from the integrated IPCE for all of sensitizers employed for DSSC fabrication. In real, there are multi reports and explanations with similar findings. The valid reason for this abnormality could be the lower illumination intensity of the monochromatic light source during the photocurrent action measurement. The other explanations could be the recombination processes which includes the trap states and the of recombination accompanied by the space-charge effects [51, 52]. A report by Zimmerman et al have verified that about 20 % mismatch from one sun illumination between the Jsc obtained and that from the integrated value

of IPCE curve stands for the valid correlation [53]. Here, the difference is more than 20 % for the DSSCs based on SQ-94 and SQ-97, which could be obviously due to comparatively prominent charge recombination as indicated by hampered Voc.

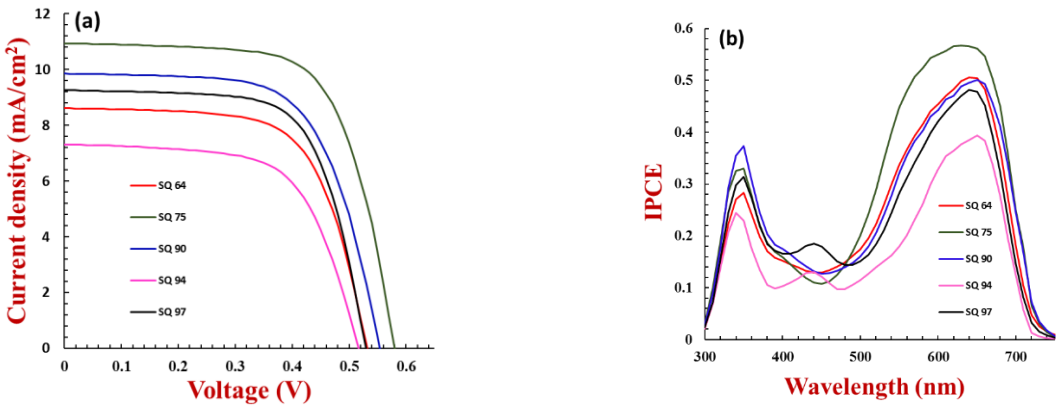

Figure 9. Current-voltage plot of the DSSCs with the different squaraine sensitizer (a). Incident photon conversion spectra against wavelength (b).

Organic dyes with planar molecular structure are more prone to aggregate formation of dye. These dye blue-shifted H-aggregates generally burden and inhibit the electron injection relative to their monomeric dye counterparts [54-56]. This obstructs the electron injection due to dye aggregation leading to enhanced charge recombination or back electron transfer ultimately leading to the deteriorated Voc and PCE. Inoue et al clearly studied and explained that symmetrical squaraine dyes with H-aggregates showcased both poor Jsc and poor Voc. Consequently, it lead to the deterioration of the DSSC performance [57]. It has been discussed in section 3.1 that squaraine dyes with H-aggregation enhanced light absorption in lower wavelength (400-500 nm) region. But the dye SQ-75 is devoid of this H-aggregation even when they are in the close vicinity even in the solid-state (Fig. 7). Therefore, this supports that the least aggregated of SQ-75 dye molecules could be due to the obtained highest Voc. Also the fluorescence lifetime of about (1.044 ± 0.005 ns) in table 1support the reason for higher Voc.

The isomer dye of SQ 75, dye SQ-64 bear the almost similar energy level but performs less well with PCE of 3.08% (reduced Jsc and Voc). This could be explained due to excess charge recombination as shown by the decrease in fluorescence lifetime (0.9478 ± 0.00423 ns). This enhancement in recombination could be due to the deteriorated electron injection into TiO_2 promoted by H-aggregate formation. It is necessary to point here that SQ-97 and SQ-94 both

exhibit exaggerated dye aggregation as supported by solid-state electronic absorption spectral in the Fig. 6. A study of table 2 and Fig. 9 (a) vividly indicate that DSSCs based on dyes SQ-97 and SQ-94 perform poorly with the efficiency of 3.3 % and 2.4 %, respectively. The hampered PCE due to lower Voc could be due to the availability of enhanced light absorption Fig. 6 and vivid peak in the action spectra (Fig. 9 b) in the lower wavelength region (400-500 nm). This explanation is also previously reported by the application of symmetrical squaraine dyes with smaller and longer alkyl group for DSSC fabrication. It was found that the shorter alkyl chain length (ethyl) dye gives relatively lower Jsc, Voc and clear peak in 400-500 nm region (associated with dye aggregation) along with diminished external quantum yield than from the dyes with its long alkyl chain (octyl) substituted counterparts [57]. The femtosecond transient absorption studies of both the dyes with shorter and longer alkyl chain have explained that the dye with short alkyl chain show a less electron injection efficiency of 75 % in comparison to that of its long alkyl chain (90 %) counterparts [58-59].

Table 2. Shows the photovoltaic parameters with unsymmetrical squaraine dyes as sensitizers for the DSSCs under simulated solar irradiation of 1.5 AM (1 sun).

Sensitizing dyes	**Jsc (mA/cm^2)**	**Voc (V)**	**FF**	**Efficiency (%)**
SQ 64	8.70	0.54	0.64	3.08
SQ 75	10.92	0.57	0.67	4.25
SQ 90	9.84	0.55	0.64	3.52
SQ 94	7.30	0.51	0.63	2.4
SQ 97	9.25	0.53	0.67	3.3

Simultaneously, the relative less lifetime for dyes SQ-97 and SQ-94 in ethanolic solution with measured values of 0.904 ± 0.004 ns and 0.434 ± 0.076 ns, respectively, proves the comparative pronounced charge recombination which is responsible for lower Voc. The HOMO energy level of the dyes could be controlled by the logical dye design. It is well attained that the unsymmetrical squaraine dye SQ-75 had photon harvesting only in the infrared region but showed the highest PCE and also had the small energy difference of 0.12 eV only when iodine redox shuttle. In

comparison to other potential sensitizers reported employed in DSSC with Voc > 0.7, the squaraine dyes as sensitizers in this report have showcased relatively lower Voc (0.5-0.6 V). It could be the indication of the excessive charge recombination and comparatively poor charge injection followed by dye regeneration. The another possibility of lesser value of Voc in these dyes could be due to the building of positive dipoles at TiO_2/dye interface which could lead to upward shift in the potential of the surface and also the negative shift of TiO_2 conduction band edge which was also reported before by us which was based on scanning Kelvin probe microscopic study [60]. Also, with varying energetics amongst the dyes used in this work, SQ-75 has shown both of the highest Jsc as well as of Voc even with a small driving force 0.12 eV only for dye regeneration. Thus it can be concluded that only 0.12 eV for dye regeneration was good enough along with the least minimum energy barrier of only 0.16 eV [38] for injection was sufficient to design NIR dyes with a band gap of only 1.18 eV for efficient DSSCs. Therefore, newly designed sensitizers with good logical and structural modification could be focused more for the utilization of them as sensitizers for efficient DSSCs with mesoporous TiO_2 as dye adsorbing semiconductor and I_3^-/I^- redox shuttle as the electrolyte which could be able to harvest photon up to 1050 nm

3.4 Conclusions

Finally it can be concluded that the infrared sensitive unsymmetrical squaraine dyes were logically designed using both combined theoretical and successfully synthesized with experimental approaches in order to find the least driving force for dye regeneration. It has been successfully shown that the only slight variation in the alkyl chain length as substituents while maintaining the main pi-molecular framework constant as seen in (SQ-64 and SQ-75) led to an observable differences in their photovoltaic performances. The isomer dyes SQ-64 and SQ-75 differ in the alkyl chain position. The dye SQ 75 has the alkyl chain in the opposite indole moiety to that of the –COOH group whereas it is the just the opposite in case of SQ 64. In case of SQ 75, the adsorption is easier as compared to that of SQ 64. The long alkyl group just in the vicinity of the anchoring group would somehow would hinder the adsorption. Also it can be explained in terms of their differential aggregation behavior. It has been beautifully shown that the application of LSDA functional and 6311G basis set under DFT predicts the energetics and electronic absorption spectrum of squaraine dyes under investigation very well to almost its accurate experimental value. To the best of our knowledge, there was only an error of 0.01-0.09 eV in the HOMO value between

the corresponding experimentally measured values by PYS and that obtained from the theoretical. Hence it validates the reliability of our theoretical prediction of the energetics. The dye SQ 75 with the minimum energy barrier of only 0.12 eV acquired the highest photon harvesting efficiency. Therefore, the champion dye SQ-75 paves the pathway for the possibility of the dye regeneration with a least energy barrier of 0.12 eV in conjunction to the most commonly employed I^-/I_3^- redox electrolytes with a good efficiency even when harvesting photon in the NIR region. Thus the research of executing the minimum energy barrier of 0.12 eV for dye regeneration in this work and combining the already found minimum energy barrier required for electron injection published by us before gives us the direction and hope for the design of novel dyes, which could make a new history for photon harvest ability upto 1050 nm so as required for NIR photon harvest with the respective NIR dyes. Hence this work is fruitful in terms of novelty.

References

1. Lund, H.; Mathiesen, B. V., Energy System Analysis of 100% Renewable Energy Systems—the Case of Denmark in Years 2030 and 2050. *Energy* **2009**, *34*, 524-531.
2. https://climateanalytics.org/blog/2016/we-can-limit-global-warming-to-1-5c-if-we-do-these-things-in-the-next-ten-years/
3. Omer, A. M., Environmental and Socio-Economic Aspects of Possible Development in Renewable Energy Use. *Journal of Agricultural Extension and Rural Development* **2010**, *2*, 001-021.
4. Gong, J.; Liang, J.; Sumathy, K., Review on Dye-Sensitized Solar Cells (Dsscs): Fundamental Concepts and Novel Materials. *Renewable and Sustainable Energy Reviews* **2012**, *16*, 5848-5860.
5. Jung, H. S.; Lee, J.-K., Dye Sensitized Solar Cells for Economically Viable Photovoltaic Systems. *The journal of physical chemistry letters* **2013**, *4*, 1682-1693.
6. Nattestad, A.; Mozer, A. J.; Fischer, M. K.; Cheng, Y.-B.; Mishra, A.; Bäuerle, P.; Bach, U., Highly Efficient Photocathodes for Dye-Sensitized Tandem Solar Cells. *Nature materials* **2010**, *9*, 31.
7. Odobel, F.; Pellegrin, Y., Recent Advances in the Sensitization of Wide-Band-Gap Nanostructured P-Type Semiconductors. Photovoltaic and Photocatalytic Applications. *The Journal of Physical Chemistry Letters* **2013**, *4*, 2551-2564.
8. Mishra, A.; Fischer, M. K.; Bäuerle, P., Metal‐Free Organic Dyes for Dye‐Sensitized Solar Cells: From Structure: Property Relationships to Design Rules. *Angewandte Chemie International Edition* **2009**, *48*, 2474-2499.
9. Yum, J.-H.; Baranoff, E.; Kessler, F.; Moehl, T.; Ahmad, S.; Bessho, T.; Marchioro, A.; Ghadiri, E.; Moser, J.-E.; Yi, C., A Cobalt Complex Redox Shuttle for Dye-Sensitized Solar Cells with High Open-Circuit Potentials. *Nature communications* **2012**, *3*, 631.

10. Yum, J.-H.; Baranoff, E.; Kessler, F.; Moehl, T.; Ahmad, S.; Bessho, T.; Marchioro, A.; Ghadiri, E.; Moser, J.-E.; Yi, C., A Cobalt Complex Redox Shuttle for Dye-Sensitized Solar Cells with High Open-Circuit Potentials. *Nature communications* **2012**, *3*, 631.
11. Shi, Z.; Deng, K.; Li, L., Pt-Free and Efficient Counter Electrode with Nanostructured Coni 2 S 4 for Dye-Sensitized Solar Cells. *Scientific reports* **2015**, *5*, 9317.
12. Hagfeldt, A.; Boschloo, G.; Sun, L.; Kloo, L.; Pettersson, H., Dye-Sensitized Solar Cells. *Chemical reviews* **2010**, *110*, 6595-6663.
13. Nazeeruddin, M. K.; De Angelis, F.; Fantacci, S.; Selloni, A.; Viscardi, G.; Liska, P.; Ito, S.; Takeru, B.; Grätzel, M., Combined Experimental and Dft-Tddft Computational Study of Photoelectrochemical Cell Ruthenium Sensitizers. *Journal of the American Chemical Society* **2005**, *127*, 16835-16847.
14. Grätzel, M., Recent Advances in Sensitized Mesoscopic Solar Cells. *Accounts of chemical research* **2009**, *42*, 1788-1798.
15. Islam, A.; Akhtaruzzaman, M.; Chowdhury, T. H.; Qin, C.; Han, L.; Bedja, I. M.; Stalder, R.; Schanze, K. S.; Reynolds, J. R., Enhanced Photovoltaic Performances of Dye-Sensitized Solar Cells by Co-Sensitization of Benzothiadiazole and Squaraine-Based Dyes. *ACS applied materials & interfaces* **2016**, *8*, 4616-4623.
16. Ogomi, Y.; Pandey, S. S.; Kimura, S.; Hayase, S., Probing Mechanism of Dye Double Layer Formation from Dye-Cocktail Solution for Dye-Sensitized Solar Cells. *Thin Solid Films* **2010**, *519*, 1087-1092.
17. Kimura, M.; Nomoto, H.; Masaki, N.; Mori, S., Dye Molecules for Simple Co‐Sensitization Process: Fabrication of Mixed‐Dye‐Sensitized Solar Cells. *Angewandte Chemie* **2012**, *124*, 4447-4450.
18. Chae, S. Y.; Park, S. J.; Joo, O.-S.; Jun, Y.; Min, B. K.; Hwang, Y. J., Highly Stable Tandem Solar Cell Monolithically Integrating Dye-Sensitized and Cigs Solar Cells. *Scientific reports* **2016**, *6*, 30868.
19. Burke, A.; Schmidt-Mende, L.; Ito, S.; Grätzel, M., A Novel Blue Dye for near-Ir 'Dye-Sensitised'solar Cell Applications. *Chemical Communications* **2007**, 234-236.
20. Hamann, T. W.; Jensen, R. A.; Martinson, A. B.; Van Ryswyk, H.; Hupp, J. T., Advancing Beyond Current Generation Dye-Sensitized Solar Cells. *Energy & Environmental Science* **2008**, *1*, 66-78.
21. Mishra, A.; Fischer, M. K.; Bäuerle, P., Metal‐Free Organic Dyes for Dye‐Sensitized Solar Cells: From Structure: Property Relationships to Design Rules. *Angewandte Chemie International Edition* **2009**, *48*, 2474-2499.
22. Pandey, S. S.; Inoue, T.; Fujikawa, N.; Yamaguchi, Y.; Hayase, S., Substituent Effect in Direct Ring Functionalized Squaraine Dyes on near Infra-Red Sensitization of Nanocrystalline Tio2 for Molecular Photovoltaics. *Journal of Photochemistry and Photobiology A: Chemistry* **2010**, *214*, 269-275.
23. Pandey, S. S.; Inoue, T.; Fujikawa, N.; Yamaguchi, Y.; Hayase, S., Alkyl and Fluoro-Alkyl Substituted Squaraine Dyes: A Prospective Approach Towards Development of Novel Nir Sensitizers. *Thin Solid Films* **2010**, *519*, 1066-1071.
24. Kim, S.; Lee, J. K.; Kang, S. O.; Ko, J.; Yum, J.-H.; Fantacci, S.; De Angelis, F.; Di Censo, D.; Nazeeruddin, M. K.; Grätzel, M., Molecular Engineering of Organic Sensitizers for Solar Cell Applications. *Journal of the American Chemical Society* **2006**, *128*, 16701-16707.

25. Matsuzawa, N. N.; Ishitani, A.; Dixon, D. A.; Uda, T., Time-Dependent Density Functional Theory Calculations of Photoabsorption Spectra in the Vacuum Ultraviolet Region. *The Journal of Physical Chemistry A* **2001**, *105*, 4953-4962.
26. Pham, W.; Lai, W.-F.; Weissleder, R.; Tung, C.-H., High Efficiency Synthesis of a Bioconjugatable near-Infrared Fluorochrome. *Bioconjugate chemistry* **2003**, *14*, 1048-1051.
27. Pandey, S. S.; Watanabe, R.; Fujikawa, N.; Ogomi, Y.; Yamaguchi, Y.; Hayase, S. In *Fine Tuning the Structure of Unsymmetrical Squaraine Dyes Towards the Development of Efficient Dye-Sensitized Solar Cells*, SPIE Solar Energy + Technology, SPIE: 2011; p 10.
28. Morimoto, T.; Fujikawa, N.; Ogomi, Y.; Pandey, S. S.; Ma, T.; Hayase, S., Design of Far-Red Sensitizing Squaraine Dyes Aiming Towards the Fine Tuning of Dye Molecular Structure. *Journal of nanoscience and nanotechnology* **2016**, *16*, 3282-3288.
29. Matsui, M.; Yamamoto, T.; Kubota, Y.; Funabiki, K., Survey, Fluorescence Spectra, and Solubility of Liquid Cyanine Dyes. *New Journal of Chemistry* **2016**, *40*, 10187-10196.
30. Li, H.; Pang, M.; Wu, B.; Meng, J., Synthesis, Crystal Structure and Photochromism of a Novel Spiro [Indoline–Naphthaline] Oxazine Derivative. *Journal of Molecular Structure* **2015**, *1087*, 73-79.
31. Saikiran, M.; Sato, D.; Pandey, S. S.; Ohta, T.; Hayase, S.; Kato, T., Photophysical Characterization and Bsa Interaction of the Direct Ring Carboxy Functionalized Unsymmetrical Nir Cyanine Dyes. *Dyes and Pigments* **2017**, *140*, 6-13.
32. Levitz, A.; Ladani, S. T.; Hamelberg, D.; Henary, M., Synthesis and Effect of Heterocycle Modification on the Spectroscopic Properties of a Series of Unsymmetrical Trimethine Cyanine Dyes. *Dyes and Pigments* **2014**, *105*, 238-249.
33. Ogomi, Y.; Kato, T.; Hayase, S., Dye Sensitized Solar Cells Consisting of Ionic Liquid and Solidification. *Journal of Photopolymer Science and Technology* **2006**, *19*, 403-408.
34. Gagne, R. R.; Koval, C. A.; Lisensky, G. C., Ferrocene as an Internal Standard for Electrochemical Measurements. *Inorganic Chemistry* **1980**, *19*, 2854-2855.
35. Su, B.; Girault, H. H., Absolute Standard Redox Potential of Monolayer-Protected Gold Nanoclusters. *The Journal of Physical Chemistry B* **2005**, *109*, 11427-11431.
36. Namazian, M.; Lin, C. Y.; Coote, M. L., Benchmark Calculations of Absolute Reduction Potential of Ferricinium/Ferrocene Couple in Nonaqueous Solutions. *Journal of Chemical Theory and Computation* **2010**, *6*, 2721-2725.
37. Pastore, M.; Fantacci, S.; De Angelis, F., Modeling Excited States and Alignment of Energy Levels in Dye-Sensitized Solar Cells: Successes, Failures, and Challenges. *The Journal of Physical Chemistry C* **2013**, *117*, 3685-3700.
38. Pandey, S. S.; Morimoto, T.; Fujikawa, N.; Hayase, S., Combined Theoretical and Experimental Approaches for Development of Squaraine Dyes with Small Energy Barrier for Electron Injection. *Solar Energy Materials and Solar Cells* **2017**, *159*, 625-632.
39. Sánchez-de-Armas, R.; San Miguel, M. Á.; Oviedo, J.; Sanz, J. F., Coumarin Derivatives for Dye Sensitized Solar Cells: A Td-Dft Study. *Physical Chemistry Chemical Physics* **2012**, *14*, 225-233.
40. Sreejith, S.; Carol, P.; Chithra, P.; Ajayaghosh, A., Squaraine Dyes: A Mine of Molecular Materials. *Journal of Materials Chemistry* **2008**, *18*, 264-274.
41. Yum, J.-H.; Walter, P.; Huber, S.; Rentsch, D.; Geiger, T.; Nüesch, F.; De Angelis, F.; Grätzel, M.; Nazeeruddin, M. K., Efficient Far Red Sensitization of Nanocrystalline Tio2

Films by an Unsymmetrical Squaraine Dye. *Journal of the American Chemical Society* **2007**, *129*, 10320-10321.
42. Yum, J. H.; Moon, S. J.; Humphry-Baker, R.; Walter, P.; Geiger, T.; Nüesch, F.; Grätzel, M.; Nazeeruddin, M. d. K., Effect of Coadsorbent on the Photovoltaic Performance of Squaraine Sensitized Nanocrystalline Solar Cells. *Nanotechnology* **2008**, *19*, 424005.
43. Kim, Y. S.; Liang, K.; Law, K. Y.; Whitten, D. G., An Investigation of Photocurrent Generation by Squaraine Aggregates in Monolayer-Modified Tin Oxide (Sno2) Electrodes. *The Journal of Physical Chemistry* **1994**, *98*, 984-988.
44. Xu, Y.; Li, Z.; Malkovskiy, A.; Sun, S.; Pang, Y., Aggregation Control of Squaraines and Their Use as near-Infrared Fluorescent Sensors for Protein. *The Journal of Physical Chemistry B* **2010**, *114*, 8574-8580.
45. Cahen, D.; Hodes, G.; Grätzel, M.; Guillemoles, J. F.; Riess, I., Nature of Photovoltaic Action in Dye-Sensitized Solar Cells. *The Journal of Physical Chemistry B* **2000**, *104*, 2053-2059.
46. Boschloo, G.; Hagfeldt, A., Characteristics of the Iodide/Triiodide Redox Mediator in Dye-Sensitized Solar Cells. *Accounts of Chemical Research* **2009**, *42*, 1819-1826.
47. Ogomi, Y.; Kato, T.; Hayase, S., Dye Sensitized Solar Cells Consisting of Ionic Liquid and Solidification. *Journal of Photopolymer Science and Technology* **2006**, *19*, 403-408.
48. Li, Z.-X.; Xie, Y.-L.; Xu, H.; Wang, T.-M.; Xu, Z.-G.; Zhang, H.-L., Expanding the Photoresponse Range of Tio2 Nanotube Arrays by Cds/Cdse/Zns Quantum Dots Co-Modification. *Journal of Photochemistry and Photobiology A: Chemistry* **2011**, *224*, 25-30.
49. Pandey, S. S.; Inoue, T.; Fujikawa, N.; Yamaguchi, Y.; Hayase, S., Substituent Effect in Direct Ring Functionalized Squaraine Dyes on near Infra-Red Sensitization of Nanocrystalline Tio2 for Molecular Photovoltaics. *Journal of Photochemistry and Photobiology A: Chemistry* **2010**, *214*, 269-275.
50. Cheng, M.; Yang, X.; Li, J.; Zhang, F.; Sun, L., Co-Sensitization of Organic Dyes for Efficient Dye-Sensitized Solar Cells. *ChemSusChem* **2013**, *6*, 70-77.
51. Krüger, J.; Plass, R.; Grätzel, M.; Cameron, P. J.; Peter, L. M., Charge Transport and Back Reaction in Solid-State Dye-Sensitized Solar Cells: A Study Using Intensity-Modulated Photovoltage and Photocurrent Spectroscopy. *The Journal of Physical Chemistry B* **2003**, *107*, 7536-7539.
52. Christians, J. A.; Manser, J. S.; Kamat, P. V., Best Practices in Perovskite Solar Cell Efficiency Measurements. Avoiding the Error of Making Bad Cells Look Good. *The Journal of Physical Chemistry Letters* **2015**, *6*, 852-857.
53. Zimmermann, E.; Ehrenreich, P.; Pfadler, T.; Dorman, J. A.; Weickert, J.; Schmidt-Mende, L., Erroneous Efficiency Reports Harm Organic Solar Cell Research. *Nature Photonics* **2014**, *8*, 669.
54. Khazraji, A. C.; Hotchandani, S.; Das, S.; Kamat, P. V., Controlling Dye (Merocyanine-540) Aggregation on Nanostructured Tio2 Films. An Organized Assembly Approach for Enhancing the Efficiency of Photosensitization. *The Journal of Physical Chemistry B* **1999**, *103*, 4693-4700.

CHAPTER FOUR: Parametric Optimization of DSSCs Using Far red Sensitizing Dye with Cobalt Electrolyte

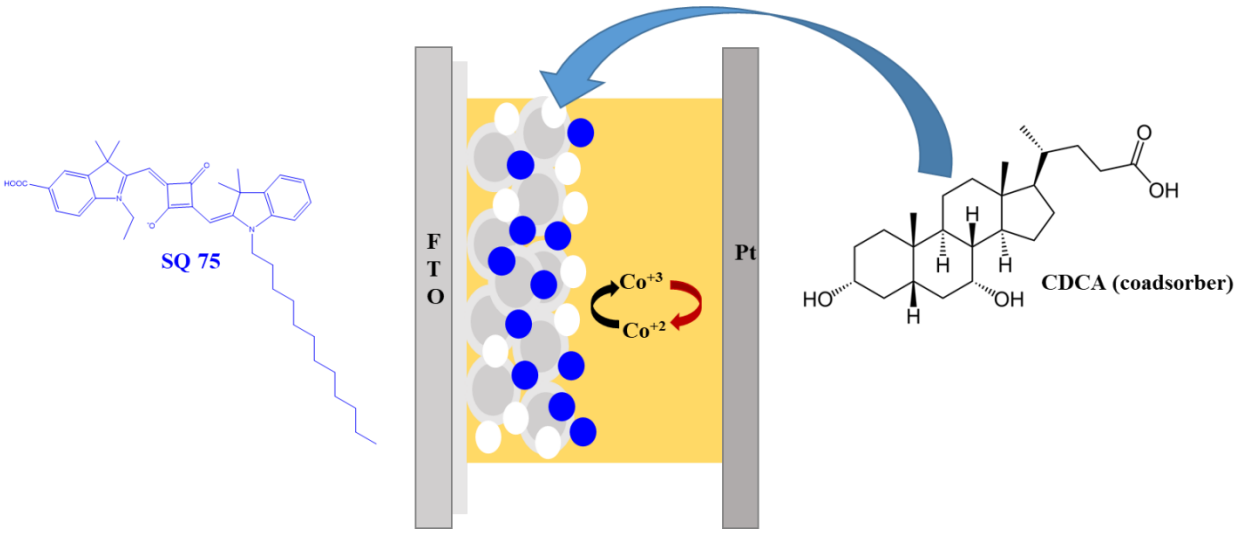

Anusha Pradhan, Maryala Saikiran, Gaurav Kapil, Shyam Sudhir Pandey and Shuzi Hayase, *Journal of Physics: Conference Series*, Volume 924 pages 01200.

4.1 Introduction

Dye-sensitized solar cells (DSSCs) have been emerged as one of the potential candidates amongst next generation solar cells owing to their low production cost, ease of fabrication and widely tunable optical properties [1]. The beauty of DSSC is in its clean nature and efficient charge separation like in photosynthesis. Hence the working principle of it can be considered as artificial photosynthesis [2]. DSSC is basically a photoelectrochemical cell which is typically comprised of a sensitizing dye adsorbed to the surface of wide band gap semiconductor like TiO_2 as a photoanode, Platinum (Pt) coated conducting substrate as a photocathode and an electrolyte system containing redox couple [3-5]. However many alternate semiconductor like SnO_2, ZnO, Nb_2O_5etc have been employed as well as efforts have been made to replace the costly Pt with other system like carbon bare, graphene, polymers [6-8]. The dyes which are heart of this kind of solar cells plays a crucial role in photon harvesting since they actually absorb the sun light and controls the overall obtainable photoconversion efficiency (PCE) and have shown nearly quantitative photon harvesting in the visible wavelength region [9-11]. In order to enhance the PCE even higher, there has been a continuous research in developing the sensitizing dyes having photon harvesting in the far-red to near infra-red (NIR) wavelength region, a various dyes including dyes from squaraine family have attempted to extend the light absorption as well as photon harvesting in the red to NIR spectral region [12-19]. In order to probe for the achievement of NIR photo harvest, many nonmetallic dyes have been designed as sensitizers [20]. Recent past has witnessed that DSSCs have successfully achieved a PCE of 11.9% with iodine (I_3^-/ I^-) based electrolytes [21] even having efficient photon harvesting mainly in the visible region of the solar spectrum only. However, disadvantages such as potential loss, corrosion and competitive light absorption by iodine based redox electrolyte itself have limited the efficiency of DSSCs compelled the search for alternate redox electrolytes to circumvent these issues. In this context, new alternative redox mediators such as based on cobalt complexes redox shuttles have been successfully employed to achieve higher open circuit voltage (Voc) as well as high PCE [22-26]. However, involving cobalt complex as redox electrolyte demands optimal surface as it is more prone to recombination owing to its bulky size and slow ionic diffusion. Many other redox electrolyte have also been the substitute for the trend iodine based electrolyte [27]. Interestingly, a theoretical PCE reaching 20% with an assumption of minimal potential loss and better fill factor, can be attained by combining NIR and visible dye. Unfortunately there are no reports regarding fabrication of DSSCs employing NIR

dyes and cobalt complex based redox shuttles to the best of our knowledge. Therefore, we feel that squaraine dyes having sharp and intense light absorption mainly in the far-red to NIR region as a representative model of NIR dyes with Cobalt complex based electrolyte is an important and interesting area of research to be focused on and exploring it could be a milestone for the future highly efficient DSSCs.

Squaraine dyes exhibit narrow full width at half maximum and very high molar extinction coefficients and tunable light absorption from visible to IR wavelength region. They show strong dye aggregation behavior due to their relatively planar molecular structure and extended π–conjugation [14]. Many reports on squaraine dyes could be obtained as a role model sensitizer for DSSCs with iodine electrolyte. However there exists any handful reports of it with the cobalt electrolyte [28]. Therefore, we have accepted these challenges and tried to improvise the efficiency of DSSCs based on squaraine dyes specially utilizing cobalt complex based redox electrolyte. A well-known dye deaggregating agent chenodeoxycholic acid (CDCA) was co-adsorbed on the nanoporous TiO_2 surface along with the dye molecules to prevent dye aggregation [29]. In this work, we have employed an unsymmetrical squaraine dye (SQ-75) as a representative of NIR dye with $Co(bpy)^{2+/3+}$ redox electrolyte to optimize Device fabrication parameters such as thickness of mesoporous TiO_2 layer, and surface treatment with $TiCl_4$ affects the performance of DSSCs [30-36], hence, similar kinds of experiments have also been carried out in current study on this novel dye-electrolyte combination in order to optimize the performance.

4.2 Experimental

Synthesis and Fabrication

The sensitizer employed in the present study unsymmetrical squaraine dye SQ-75 was synthesized following the methodology as per our earlier publications [13,25]. The basic advantage of unsymmetrical squaraine dyes over the symmetrical is the unidirectional of the charge unlike that of the symmetrical dyes [37]. After the synthesis and purification by silica-gel column chromatography, structure of SQ-75 was confirmed by ^1H nuclear magnetic resonance and fast ion bombardment-mass spectrometry. Electronic absorption spectra of the sensitizing squaraine dye (SQ-75) in ethanol solution as well as the dye adsorbed on thin films of the mesoporous TiO_2 was measured with a UV-visible-NIR spectrophotometer (JASCO, V670). DSSC fabrication was started with the cleaning of fluorine doped tin oxide (FTO) glasses by detergent solution, distilled

water, acetone, isopropanol and acetone for 10 minutes each. After this, the photoanodes were prepared by screen-printing mesoporous DS/P and 30 NRD TiO_2 pastes (Solaronix) on FTO followed by baking at 500^0C for 30 min. This coating procedure was done one or several times to obtain TiO_2 thickness in the range of 2 to 18 μm especially for the thickness optimization of mesoporous TiO_2 layer. Some of the samples were pre and post-treated to freshly prepared TiO_2 films with aqueous $TiCl_4$ solution. This TiO_2 surface treatment was conducted by dipping the substrates dipped in the 40 mM aqueous $TiCl_4$ solution at 800C for 30 min under continuous magnetic stirring at 500 rpm followed by the sintering at 5000C for 30 minutes. Different photoanodes such as TiO_2 only (untreated samples), bottom TiCl4 (pre-treated samples) on FTO, top $TiCl_4$ (post-treated samples) on mesoporous TiO_2 and top/bottom $TiCl_4$ (pre and post-treated samples) were prepared for the current study. All of the samples were dipped in 0.2 mM dye solution in ethanol containing a fixed amount of CDCA varying from 2 mM to 30 mM for 4 hours at room temperature. For optimization of TiO2 thickness and concentration of CDCA top/bottom $TiCl_4$ based photoanodes were taken. Counter electrode was prepared by FTO glass sputtered with 240 nm Ti followed 40 nm Pt and DSSC was assembled using this counter electrode with the photoanode and a 25 μm thick Himilan film (Mitsu-Dupont) spacer which melts at 110^0C by pressing the two parts for 20-30 seconds. Electrolyte was then injected and cell was finally sealed using UV resin to avoid any solvent leakage. The electrolyte was composed of 0.22 mM $Co(bpy)_3(PF6)_2$, 0.033 mM $Co(bpy)_3(PF6)_3$, 0.2 M tertiary butyl pyridine and 0.1 M $LiClO_4$ in Acetonitrile for all of the devices. Chemical structure of the unsymmetrical squaraine dye (SQ-75) and bipyridyl ligand bearing cobalt complex based redox electrolyte used in this work have been shown in the Fig.1

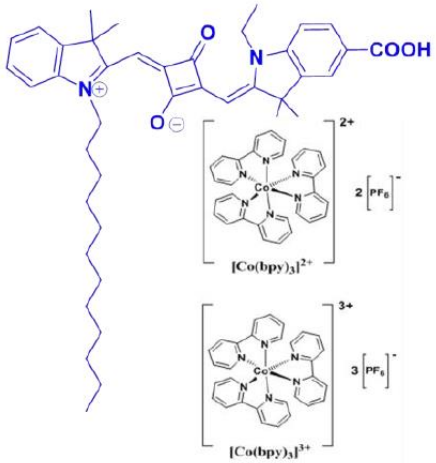

Figure 1. Shows the molecular structure of the sensitizer SQ-75 and cobalt complex based redox electrolyte for optimization in the present study.

Measurement: The thickness of the mesoporous TiO_2 was measured with a surface profilometer. Photovoltaic (PV) performances of the devices were measured with a solar simulator (CEP-2000, Bunko-Keiki, Japan) equipped with a xenon lamp (XLS-150A). The intensity of light irradiation was adjusted to AM 1.5 (100 mW/cm^2) using a spectroradiometer (LS-100, Eiko Seiki, Japan). The exposure power was also corrected with a standard amorphous Si photo detector (BS-520 S/N 007, Bunko-Keiki, Japan), which has similar light sensitivity to the DSSCs. Irradiation area of 0.2025 cm^2 was precisely controlled by a black metal mask for all of the samples during the measurement of photovoltaic characteristics. Incident photon to current conversion efficiency (IPCE) as a function of wavelength for the devices prepared were also measured with a constant photon flux of 1 x 10^{16} photon per cm^2 at each wavelength in the direct current mode using the action spectrum measurement system connected to the solar simulator.

4.3 Results and Discussion

4.3.1 Dye Design and Electronic Absorption Spectra

The dyes in general plays a basic trigger in the working of DSSCs along with the electrolyte. Thus its molecular structure play a crucial role to control the performance DSSCs especially using cobalt based redox electrolytes where dyes in general possess multiple and long alkyl chains [21, 26, 38]. And working with cobalt electrolyte demands surface passivation from dye level as well as with blocking layers. It was demonstrated that the long alkyl groups behaves like a barrier for back electron transfer (recombination) [39]. This importance of alkyl chain for the sensitizers of DSSCs based on cobalt complex based electrolyte was further experimentally verified by the fact ruthenium based dye N-719 which works very well with iodine based electrolyte exhibit very poor performance with cobalt electrolyte. At the same time its long alkyl chain substituted analogue Z-907 works very well with cobalt based electrolytes [40]. Also, the long alkyl chains of the dyes lead to effective surface passivation of the mesoporous TiO_2 surface and suppress the charge recombination by preventing obvious electrostatic attractive interaction between the positively charged cobalt complex ions with the negatively charged TiO_2 surface [41]. Therefore keeping all these mandatory requirements in mind we logically selected the unsymmetrical squaraine dye SQ-75 having very long dodecyl substituent at the opposite end of the dye from the –COOH

functionalized indole ring as anchoring site. This not only supports the facile dye anchoring but also effectively passivates the negatively charged TiO_2 as required for working with cobalt electrolyte.

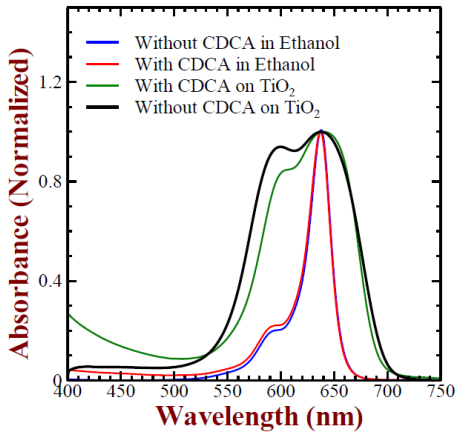

Figure 2. Electronic absorption spectra of SQ 75 ethanol solution and thin film adsorbed on mesoporous TiO_2 (3 µm).

Along with the advantage of the planarity of squaraine dyes in effective charge delocalization, the planarity also somehow contributes to the formation of dye aggregation. The H aggregation is not advantageous for the efficient electron injection and thus resulting in a hampered PCE. To circumvent this, Chenodeoxycholic acid (CDCA) been most widely used in combination with dye as coadsorber to prevent the dye aggregation [42, 43]. Electronic absorption spectra of the SQ-75 in ethanol solution in the presence as well as well as in the absence of CDCA along with the solid-state thin film adsorbed on TiO_2 are shown in Fig. 2. Electronic absorption spectrum of SQ-75 in ethanol solution (5 mM with 4 mM CDCA) exhibits a very sharp absorption peak having absorption maximum (λmax) at 638 nm with very high molar extinction coefficient of 3.18 x 10^5 $dm^3.mol^{-1}.cm^{-1}$ along with vibronic shoulder at 592 nm. This is a typical characteristic of squaraine dyes and this sharp electronic absorption peak is associated with the π-π* electronic transition [5, 13]. Interestingly in the absence of CDCA as well, there is neither any shift in the spectral shape nor position of the λmax which indicates that in the solution state at this concentration (5 µM), there is no dye aggregation and dye exists in the monomeric form. Upon adsorption on the mesoporous TiO_2, not only there is a visible spectral broadening as compared to that observed in solution but also there is an enhancement in the intensity of the vibronic shoulder. The blue shifted vibronic shoulder corresponds to the H aggregation. This spectral broadening is attributed to the

interaction between TiO_2 and dye molecules in the condensed state as reported previously [36]. The small difference in the intensity of the vibronic shoulder in the presence as well as in the absence of CDCA on TiO_2 suggests that long alkyl chain present in the dye are also involved in the suppression of dye aggregation in the condensed state.

4.3.2. Impact of $TiCl_4$ Treatment on Photovoltaic Property

DSSCs have been fabricated in the device configuration of FTO/TiO_2/dye/Electrolyte/Pt with different interfaces between its all components and they are expected to work optimally for good device performances. Amongst these, FTO/TiO_2/dye interfaces play an important role in deciding the overall PCE [44-45]. Open circuit voltage (Voc) for a device varies inversely to the recombination rates at these interfaces, which in turn affects the short current density (Jsc) and fill factor (FF) also [32]. Control of this charge recombination by surface passivation using compact and conformal TiO_2 layer has been well documented. This surface passivation especially for DSSCs based on cobalt complex based electrolytes is more crucial owing to their relatively bulky nature as compared to iodine redox electrolyte counterparts and their relatively slow diffusion imparts more chances for the charge recombination [23]. Apart from passivation, the compact TiO_2 layer has been reported to play various roles such as to increase the TiO_2 surface area, to enhance electron transport, to promote light scattering and dye anchoring, which finally results in better device performance [30]. The compact TiO_2 layer possesses a dense structure which minimizes the FTO contact with the electrolyte and proves beneficial to the performance improvement of the DSSCs. Also the surface area is increased which helps in more dye loading [46]. In this work, attempts have been made to investigate the role of this compact layer on overall device performance and to demonstrate that which one plays the predominant role. In order to predict this effect more explicitly, other factors such as thickness of mesoporous TiO_2 layer (6-7μm), dye (SQ-75), dye/CDCA ratio (1/50) and electrolyte $Co(bpy)^{2+/3+}$ were maintained constant.

Figure 3(a) shows the current-voltage (I-V) characteristics of fabricated DSSCs under simulated solar condition of 1.5 AM with different surface treatment conditions. The short circuit current density (Jsc), open circuit voltage (Voc), fill factor (FF) and the overall PCE (η) have been summarized in the Table 1. All of the DSSCs with $TiCl_4$ treatment exhibited better device performance as compared to that of untreated one due to reduced charge recombination. It can be

clearly seen from this figure that surface treatment on mesoporous TiO2 (top $TiCl_4$) has more pronounced effect than that on the FTO (bottom $TiCl_4$) which is concluded due to the rise in current density of 2.08 mA/cm^2 to 3.48 mA/cm^2 and hence the PCE of 0.57% to 0.81%. This increase in current density is well supported by the increased IPCE of 30% to 45 % between the wavelengths from 600-700 nm as shown in Fig 3(b). The beneficial effect of the $TiCl_4$ treatment is best presented by Jsc = 4.31 mA/cm2, Voc = 0.56 V, FF = 0.56 and η = 1.34%, when surface treatment was conducted on both of the FTO as well as mesoporous TiO_2 (top/bottom $TiCl_4$). IPCE shown in Fig. 3(b) also confirms the far-red photon harvesting by the sensitizer and maxima of the observed IPCE is in accordance with the Jsc measured in the I-V characteristics.

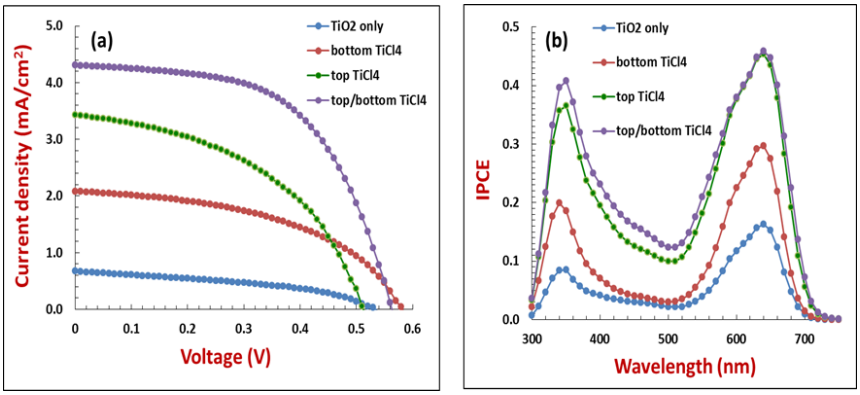

Figure 3. Photovoltaic characteristics of DSSCs under simulated solar irradiation (a) and photocurrent action spectra (b) after monochromatic incident light for DSSCs with different types of $TiCl_4$ surface treatments

Table 1. Photovoltaic data of the surface passivation by compact TiO_2.

Treatment conditions	**Jsc (mA/cm^2)**	**Voc (V)**	**FF**	**Efficiency (%)**
No surface treatment	0.67	0.53	0.41	0.14
Treatment only on FTO	2.08	0.58	0.47	0.57
Treatment only onTiO_2	3.43	0.51	0.46	0.81
Treatment on both TiO_2 and FTO both	4.31	0.56	0.56	1.34

4.3.3 Influence of the TiO_2 thickness

Optimizing the thickness of light absorbing layer is an important issue to be solved as it affects the solar cell performance mainly the current density. Neither very thin nor very thick TiO_2 is actually required which depends on the nature of the dye chosen [47]. It can be easily understood that if the thickness of absorber layer is less, in that case most of the light transmits without proper absorption. Therefore, a minimum optimized thickness is must for proper device functioning. This minimum thickness of the absorber layer will be less if the absorption coefficient of the absorbing material dyes is high. This also contribute for a better performing solid state DSSCs [48]. Squaraine dyes with a high molar extinction coefficient generally requires not very thick mesoporous TiO_2 as it is capable of harvesting photon excellently. However, there is limitation on the maximum thickness of absorbing layer also, as with the increase in thickness after certain limit the chances of recombination increase because photoexcited electrons has to travel a long distance compared to their diffusion length [49]. This diffusion length varies for different dye and electrolyte systems used in DSSCs and need to be optimized for obtaining the better device functioning. In case of DSSCs, the absorbing layer thickness totally depends on mesoporous TiO_2 layer which acts as a scaffold for the dye monolayer. Hence, we can control and confirm the optimized thickness for better results by varying the thickness of mesoporous TiO_2 thickness.

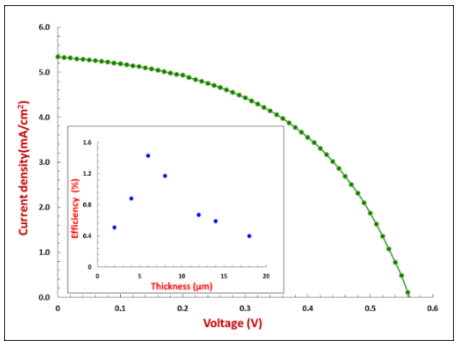

Figure 4. Photovoltaic characteristic of DSSC with TiO_2 layer thickness of 6 µm under simulated Under solar irradiation. Inset shows the thickness dependence of PCE.

In the present work, DSSCs were fabricated by varying the thickness of mesoporous TiO_2 layer in top/bottom $TiCl_4$ treated photoanodes keeping other variables such as dye concentration, electrolyte, CDCA concentration constant. Table 2 summarizes photovoltaic parameters obtained from I-V characteristics of the DSSCs. A perusal of table 2 corroborates the increase in thickness of the mesoporous TiO_2 layer from 2 µm to 4 µm there is increase in Jsc and PCE from 2.4 mA/cm2

to 3.38 mA/cm^2 and 0.51% to 0.88%, respectively, due to enhanced photon harvesting. With further increase in the thickness of the mesoporous TiO2 up to 6 μm, it was noticed that devices achieved their best Jsc of 5.33 mA/cm2 and PCE of 1.43% whose photovoltaic characteristic is shown in the Fig. 4. When the thickness was increased more than 6 μm to 8 μm, there was a sharp decrease in the PCE as a function of thickness as shown in the inset of the Fig. 4. For Ruthenium complex based dyes (N-719) it has been demonstrated that 15 μm thick TiO_2 layer was optimum for achieving the best efficiency [34]. Therefore, we conclude that in our case, for the DSSC using sensitizing dye SQ-75 having a high molar extinction coefficient nearly 10 times as compared to typical ruthenium based sensitizers, a relatively thinner TiO2 (6 μm) is capable of sufficient photons harvesting.

Table 2. Photovoltaic characteristics of DSSC with varying thickness of mesoporous TiO_2.

Thickness	**2μm**	**4μm**	**6μm**	**8μm**	**12μm**	**14μm**	**18μm**
Jsc (mA/cm^2)	2.4	3.37	5.33	3.75	2.59	2.1	1.62
Voc (V)	0.56	0.55	0.56	0.56	0.55	0.55	0.52
FF	0.37	0.47	0.48	0.55	0.47	0.50	0.48
Efficiency (%)	0.51	0.88	1.43	1.17	0.67	0.59	0.40

4.3.4 Effect of Chenodeoxycholic acid in the dye solution

Squaraine dyes are completely organic dye. Due to its planar structure and extended π conjugation, they are prone to dye aggregate formation facilitated by the π-π stacking which leads to the hampered charge injection. Thus to prevent these dye aggregates, an adequate amount of CDCA has been most commonly used functions which not only functions as coadsorber but also suppresses the dye aggregation [29]. However, efficient sensitization is observed from both the monomeric and aggregated forms of the unsymmetrical squaraines. Aggregation of symmetrical dyes on the TiO_2 photoelectrode results in significant decrease in their sensitization efficiency [50]. As CDCA plays the role of coadsorber without actually participating in photon harvesting, hence optimization for its adequate amount is necessary for the optimum device performance. For the optimization, top/bottom $TiCl_4$ based photoanode was implemented along with the same

mesoporous TiO_2 thickness (6 μm), dye concentration and electrolyte. Figure 5 presents the plot of change in PCE for the DSSCs fabricated by changing the concentration of CDCA. Device containing 4 mM of CDCA in dye solution exhibited an improved PCE of 1.57% compared to the device without any CDCA (1.3%). Further increase in the CDCA concentration with respect to the dye resulted in to decrease of the PCE. This behavior could be understood considering the fact that presence of excess amount of CDCA inhibits the dye molecules present on the mesoporous TiO2 surface due to competitive adsorption and hampers the effective absorption of the incident photons. It is also interesting to note that SQ-75 dye structure is less prone to dye aggregation as devices without CDCA also showed the comparatively good PCE of 1.3% to that of the devices with CDCA as shown in Table 3.

Table 3. Photovoltaic parameters for DSSCs with varying concentration of CDCA with SQ-75.

CDCA conc. (mM)	**0**	**2**	**4**	**10**	**15**	**20**	**30**
Jsc(mA/cm^2)	4.30	4.56	5.67	4.31	4.14	2.55	1.17
Voc	0.55	0.55	0.56	0.56	0.56	0.55	0.53
FF	0.55	0.51	0.49	0.56	0.48	0.49	0.35
Efficiency (%)	1.3	1.28	1.57	1.34	1.12	0.73	0.21

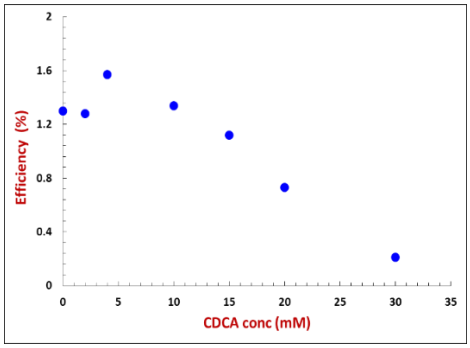

Figure 5. Effect of coadsorber CDCA concentration on the PCE of DSSCs based on SQ-75 and $Co(bpy)^{2+/3+}$ redox electrolyte.

It can be seen that the optimum CDCA concentration of 4 mM has a better Voc than its respective counterparts. Also, the CDCA coadsorbed onto the TiO2 surface would have induced an upward band edge shift of TiO_2. Moreover, the high surface coverage by CDCA also inhibited the recombination process, which resulted in a longer electron lifetime. The longer lifetime of the cell

with CDCA could have resulted in a higher photovoltage for the cells [51]. The lower efficiency for high concentration of CDCA could be due to due to less dye coverage of the squaraine.

4.4 Conclusions

In summary, optimization of DSSCs fabricated using a model unsymmetrical squaraine dye SQ-75 and $Co(bpy)^{2+/3+}$ redox electrolyte was conducted. The main objective was to optimize different device fabrication parameters amicably in order to achieve the optimum PCE. $TiCl_4$ surface treatment was found to control the overall PCE and especially it was more effective when treatment was done on both of the FTO glass substrate and mesoporous TiO_2 layer leading to the best PCE of 1.34 %. The surface passivation with $TiCl_4$ is mandatory in order to work with cobalt electrolyte. Surface passivation on both FTO and TiO_2 was needed to in order to achieve a better efficiency. It was also found that mesoporous TiO_2 thickness variation also affects the device performance and thickness of 6 μm was best suited for DSSCs based on this dye-electrolyte system as SQ has a high molar extinction coefficient and does not require thicker mesoporous TiO_2 layer. Finally, the PCE of SQ-75 dye based DSSCs seem to be less affected by the dye aggregation owing to its special molecular design as confirmed by photovoltaic measurements as well as electronic absorption spectral investigations. And 4mM of the CDCA concentration was found to be optimum in order to prevent aggregation without hampering photon harvest.

References

1. Grätzel, M., Recent Advances in Sensitized Mesoscopic Solar Cells. *Accounts of chemical research* **2009**, *42*, 1788-1798.
2. McConnell, I.; Li, G.; Brudvig, G. W., Energy Conversion in Natural and Artificial Photosynthesis. *Chemistry & biology* **2010**, *17*, 434-447.
3. Kakiage, K.; Aoyama, Y.; Yano, T.; Otsuka, T.; Kyomen, T.; Unno, M.; Hanaya, M., An Achievement of over 12 Percent Efficiency in an Organic Dye-Sensitized Solar Cell. *Chemical Communications* **2014**, *50*, 6379-6381.
4. Wang, M.; Grätzel, C.; Zakeeruddin, S. M.; Grätzel, M., Recent Developments in Redox Electrolytes for Dye-Sensitized Solar Cells. *Energy & Environmental Science* **2012**, *5*, 9394-9405.
5. Morimoto, T.; Fujikawa, N.; Ogomi, Y.; Pandey, S. S.; Hayase, S. In *Parametric Optimization of Experimental Conditions for Dye-Sensitized Solar Cells Based on Far-Red Sensitive Squaraine Dye*, Journal of Physics: Conference Series, IOP Publishing: 2016; p 012002.

6. Park, N. G.; Kim, K., Transparent Solar Cells Based on Dye-Sensitized Nanocrystalline Semiconductors. *physica status solidi (a)* **2008**, *205*, 1895-1904.
7. Hong, W.; Xu, Y.; Lu, G.; Li, C.; Shi, G., Transparent Graphene/Pedot–Pss Composite Films as Counter Electrodes of Dye-Sensitized Solar Cells. *Electrochemistry Communications* **2008**, *10*, 1555-1558.
8. Choi, H.; Kim, H.; Hwang, S.; Han, Y.; Jeon, M., Graphene Counter Electrodes for Dye-Sensitized Solar Cells Prepared by Electrophoretic Deposition. *Journal of Materials Chemistry* **2011**, *21*, 7548-7551.
9. Ito, S.; Murakami, T. N.; Comte, P.; Liska, P.; Grätzel, C.; Nazeeruddin, M. K.; Grätzel, M., Fabrication of Thin Film Dye Sensitized Solar Cells with Solar to Electric Power Conversion Efficiency over 10%. *Thin solid films* **2008**, *516*, 4613-4619.
10. Gao, F.; Wang, Y.; Shi, D.; Zhang, J.; Wang, M.; Jing, X.; Humphry-Baker, R.; Wang, P.; Zakeeruddin, S. M.; Grätzel, M., Enhance the Optical Absorptivity of Nanocrystalline Tio2 Film with High Molar Extinction Coefficient Ruthenium Sensitizers for High Performance Dye-Sensitized Solar Cells. *Journal of the American Chemical Society* **2008**, *130*, 10720-10728.
11. Barbe, C. J.; Arendse, F.; Comte, P.; Jirousek, M.; Lenzmann, F.; Shklover, V.; Grätzel, M., Nanocrystalline Titanium Oxide Electrodes for Photovoltaic Applications. *Journal of the American Ceramic Society* **1997**, *80*, 3157-3171.
12. Sreejith, S.; Carol, P.; Chithra, P.; Ajayaghosh, A., Squaraine Dyes: A Mine of Molecular Materials. *Journal of Materials Chemistry* **2008**, *18*, 264-274.
13. Pandey, S. S.; Inoue, T.; Fujikawa, N.; Yamaguchi, Y.; Hayase, S., Alkyl and Fluoro-Alkyl Substituted Squaraine Dyes: A Prospective Approach Towards Development of Novel Nir Sensitizers. *Thin Solid Films* **2010**, *519*, 1066-1071.
14. Morimoto, T.; Fujikawa, N.; Ogomi, Y.; Pandey, S. S.; Ma, T.; Hayase, S., Design of Far-Red Sensitizing Squaraine Dyes Aiming Towards the Fine Tuning of Dye Molecular Structure. *Journal of nanoscience and nanotechnology* **2016**, *16*, 3282-3288.
15. Chang, J.; Lee, C.-P.; Kumar, D.; Chen, P.-W.; Lin, L.-Y.; Thomas, K. J.; Ho, K.-C., Co-Sensitization Promoted Light Harvesting for Organic Dye-Sensitized Solar Cells Using Unsymmetrical Squaraine Dye and Novel Pyrenoimidazole-Based Dye. *Journal of Power Sources* **2013**, *240*, 779-785
16. Hara, K.; Tachibana, Y.; Ohga, Y.; Shinpo, A.; Suga, S.; Sayama, K.; Sugihara, H.; Arakawa, H., Dye-Sensitized Nanocrystalline Tio2 Solar Cells Based on Novel Coumarin Dyes. *Solar Energy materials and Solar cells* **2003**, *77*, 89-103.
17. Chang, C.-H.; Chen, Y.-C.; Hsu, C.-Y.; Chou, H.-H.; Lin, J. T., Squaraine-Arylamine Sensitizers for Highly Efficient P-Type Dye-Sensitized Solar Cells. *Organic letters* **2012**, *14*, 4726-4729.
18. Jradi, F. M.; Kang, X.; O'Neil, D.; Pajares, G.; Getmanenko, Y. A.; Szymanski, P.; Parker, T. C.; El-Sayed, M. A.; Marder, S. R., Near-Infrared Asymmetrical Squaraine Sensitizers for Highly Efficient Dye Sensitized Solar Cells: The Effect of Π-Bridges and Anchoring Groups on Solar Cell Performance. *Chemistry of Materials* **2015**, *27*, 2480-2487.
19. Jradi, F. M.; O'Neil, D.; Kang, X.; Wong, J.; Szymanski, P.; Parker, T. C.; Anderson, H. L.; El-Sayed, M. A.; Marder, S. R., A Step toward Efficient Panchromatic Multi-Chromophoric Sensitizers for Dye Sensitized Solar Cells. *Chemistry of Materials* **2015**, *27*, 6305-6313.

20. Lee, C.-P.; Lin, R. Y.-Y.; Lin, L.-Y.; Li, C.-T.; Chu, T.-C.; Sun, S.-S.; Lin, J. T.; Ho, K.-C., Recent Progress in Organic Sensitizers for Dye-Sensitized Solar Cells. *RSC Advances* **2015**, *5*, 23810-23825.
21. Mathew, S.; Yella, A.; Gao, P.; Humphry-Baker, R.; Curchod, B. F.; Ashari-Astani, N.; Tavernelli, I.; Rothlisberger, U.; Nazeeruddin, M. K.; Grätzel, M., Dye-Sensitized Solar Cells with 13% Efficiency Achieved through the Molecular Engineering of Porphyrin Sensitizers. *Nature chemistry* **2014**, *6*, 242.
22. Wu, J.; Lan, Z.; Lin, J.; Huang, M.; Huang, Y.; Fan, L.; Luo, G., Electrolytes in Dye-Sensitized Solar Cells. *Chemical reviews* **2015**, *115*, 2136-2173.
23. Zong, X.; Liang, M.; Fan, C.; Tang, K.; Li, G.; Sun, Z.; Xue, S., Design of Truxene-Based Organic Dyes for High-Efficiency Dye-Sensitized Solar Cells Employing Cobalt Redox Shuttle. *The Journal of Physical Chemistry C* **2012**, *116*, 11241-11250.
24. DeVries, M. J.; Pellin, M. J.; Hupp, J. T., Dye-Sensitized Solar Cells: Driving-Force Effects on Electron Recombination Dynamics with Cobalt-Based Shuttles. *Langmuir* **2010**, *26*, 9082-9087.
25. Marchena, M. J.; de Miguel, G.; Cohen, B.; Organero, J. A.; Pandey, S.; Hayase, S.; Douhal, A., Real-Time Photodynamics of Squaraine-Based Dye-Sensitized Solar Cells with Iodide and Cobalt Electrolytes. *The Journal of Physical Chemistry C* **2013**, *117*, 11906-11919.
26. Feldt, S. M.; Gibson, E. A.; Gabrielsson, E.; Sun, L.; Boschloo, G.; Hagfeldt, A., Design of Organic Dyes and Cobalt Polypyridine Redox Mediators for High-Efficiency Dye-Sensitized Solar Cells. *Journal of the American Chemical Society* **2010**, *132*, 16714-16724.
27. Cong, J.; Yang, X.; Kloo, L.; Sun, L., Iodine/Iodide-Free Redox Shuttles for Liquid Electrolyte-Based Dye-Sensitized Solar Cells. *Energy & Environmental Science* **2012**, *5*, 9180-9194.
28. Qin, C.; Wong, W. Y.; Han, L., Squaraine Dyes for Dye-Sensitized Solar Cells: Recent Advances and Future Challenges. *Chemistry–An Asian Journal* **2013**, *8*, 1706-1719.
29. Yum, J.; Moon, S.; Humphry-Baker, R.; Walter, P.; Geiger, T.; Nüesch, F.; Grätzel, M.; d K Nazeeruddin, M., Effect of Coadsorbent on the Photovoltaic Performance of Squaraine Sensitized Nanocrystalline Solar Cells. *Nanotechnology* **2008**, *19*, 424005.
30. Yoshida, Y.; Tokashiki, S.; Kubota, K.; Shiratuchi, R.; Yamaguchi, Y.; Kono, M.; Hayase, S., Increase in Photovoltaic Performances of Dye-Sensitized Solar Cells—Modification of Interface between Tio2 Nano-Porous Layers and F-Doped Sno2 Layers. *Solar Energy Materials and Solar Cells* **2008**, *92*, 646-650.
31. Sommeling, P.; O'regan, B.; Haswell, R.; Smit, H.; Bakker, N.; Smits, J.; Kroon, J.; Van Roosmalen, J., Influence of a Ticl4 Post-Treatment on Nanocrystalline Tio2 Films in Dye-Sensitized Solar Cells. *The Journal of Physical Chemistry B* **2006**, *110*, 19191-19197.
32. Park, N.-G.; Schlichthörl, G.; Van de Lagemaat, J.; Cheong, H.; Mascarenhas, A.; Frank, A., Dye-Sensitized Tio2 Solar Cells: Structural and Photoelectrochemical Characterization of Nanocrystalline Electrodes Formed from the Hydrolysis of Ticl4. *The Journal of Physical Chemistry B* **1999**, *103*, 3308-3314.
33. Long-Yue, Z.; Song-Yuan, D.; Kong-Jia, W.; Xu, P.; Cheng-Wu, S.; Li, G., Mechanism of Enhanced Performance of Dye-Sensitized Solar Cell Based Tio2 Films Treated by Titanium Tetrachloride. *Chinese Physics Letters* **2004**, *21*, 1835.

34. Kang, M.-G.; Ryu, K.-S.; Chang, S.-H.; Park, N.-G.; Hong, J.-S.; Kim, K.-J., Dependence of Tio 2 Film Thickness on Photocurrent-Voltage Characteristics of Dye-Sensitized Solar Cells. *Bulletin of the Korean Chemical Society* **2004**, *25*, 742-744.
35. Gregg, B. A.; Pichot, F.; Ferrere, S.; Fields, C. L., Interfacial Recombination Processes in Dye-Sensitized Solar Cells and Methods to Passivate the Interfaces. *The Journal of Physical Chemistry B* **2001**, *105*, 1422-1429.
36. Yum, J.-H.; Walter, P.; Huber, S.; Rentsch, D.; Geiger, T.; Nüesch, F.; De Angelis, F.; Grätzel, M.; Nazeeruddin, M. K., Efficient Far Red Sensitization of Nanocrystalline Tio2 Films by an Unsymmetrical Squaraine Dye. *Journal of the American Chemical Society* **2007**, *129*, 10320-10321.
37. Choi, H.; Kim, J.-J.; Song, K.; Ko, J.; Nazeeruddin, M. K.; Grätzel, M., Molecular Engineering of Panchromatic Unsymmetrical Squaraines for Dye-Sensitized Solar Cell Applications. *Journal of Materials Chemistry* **2010**, *20*, 3280-3286.
38. Ellis, H.; Eriksson, S. K.; Feldt, S. M.; Gabrielsson, E.; Lohse, P. W.; Lindblad, R.; Sun, L.; Rensmo, H. k.; Boschloo, G.; Hagfeldt, A., Linker Unit Modification of Triphenylamine-Based Organic Dyes for Efficient Cobalt Mediated Dye-Sensitized Solar Cells. *The Journal of Physical Chemistry C* **2013**, *117*, 21029-21036.
39. Yang, J.; Ganesan, P.; Teuscher, J. l.; Moehl, T.; Kim, Y. J.; Yi, C.; Comte, P.; Pei, K.; Holcombe, T. W.; Nazeeruddin, M. K., Influence of the Donor Size in D− Π–a Organic Dyes for Dye-Sensitized Solar Cells. *Journal of the American Chemical Society* **2014**, *136*, 5722-5730.
40. Liu, Y.; Jennings, J. R.; Huang, Y.; Wang, Q.; Zakeeruddin, S. M.; Grätzel, M., Cobalt Redox Mediators for Ruthenium-Based Dye-Sensitized Solar Cells: A Combined Impedance Spectroscopy and near-Ir Transmittance Study. *The Journal of Physical Chemistry C* **2011**, *115*, 18847-18855.
41. Kawano, M.; Nishiyama, T.; Ogomi, Y.; Pandey, S. S.; Ma, T.; Hayase, S., Relationship between Diffusion of Co 3+/Co 2+ Redox Species in Nanopores of Porous Titania Stained with Dye Molecules, Dye Molecular Structures, and Photovoltaic Performances. *RSC Advances* **2015**, *5*, 83725-83731.
42. Wang, Z.-S.; Cui, Y.; Dan-oh, Y.; Kasada, C.; Shinpo, A.; Hara, K., Thiophene-Functionalized Coumarin Dye for Efficient Dye-Sensitized Solar Cells: Electron Lifetime Improved by Coadsorption of Deoxycholic Acid. *The Journal of Physical Chemistry C* **2007**, *111*, 7224-7230.
43. Hu, L.; Yan, Z.; Xu, H., Advances in Synthesis and Application of near-Infrared Absorbing Squaraine Dyes. *Rsc Advances* **2013**, *3*, 7667-7676.
44. Yu, H.; Zhang, S.; Zhao, H.; Xue, B.; Liu, P.; Will, G., High-Performance Tio2 Photoanode with an Efficient Electron Transport Network for Dye-Sensitized Solar Cells. *The Journal of Physical Chemistry C* **2009**, *113*, 16277-16282.
45. Zheng, Y.; Klankowski, S.; Yang, Y.; Li, J., Preparation and Characterization of Tio2 Barrier Layers for Dye-Sensitized Solar Cells. *ACS applied materials & interfaces* **2014**, *6*, 10679-10686.
46. Yu, H.; Zhang, S.; Zhao, H.; Will, G.; Liu, P., An Efficient and Low-Cost Tio2 Compact Layer for Performance Improvement of Dye-Sensitized Solar Cells. *Electrochimica Acta* **2009**, *54*, 1319-1324.

47. Sedghi, A.; Miankushki, H. N., The Effect of Drying and Thickness of Tio2 Electrodes on the Photovoltaic Performance of Dye-Sensitized Solar Cells. *International Journal of Electrochemical Science* **2015**, *10*, 3354-3362.
48. Geiger, T.; Kuster, S.; Yum, J. H.; Moon, S. J.; Nazeeruddin, M. K.; Grätzel, M.; Nüesch, F., Molecular Design of Unsymmetrical Squaraine Dyes for High Efficiency Conversion of Low Energy Photons into Electrons Using Tio2 Nanocrystalline Films. *Advanced Functional Materials* **2009**, *19*, 2720-2727.
49. Barnes, P. R.; Anderson, A. Y.; Koops, S. E.; Durrant, J. R.; O'Regan, B. C., Electron Injection Efficiency and Diffusion Length in Dye-Sensitized Solar Cells Derived from Incident Photon Conversion Efficiency Measurements. *The Journal of Physical Chemistry C* **2008**, *113*, 1126-1136.
50. Alex, S.; Santhosh, U.; Das, S., Dye Sensitization of Nanocrystalline Tio2: Enhanced Efficiency of Unsymmetrical Versus Symmetrical Squaraine Dyes. *Journal of Photochemistry and Photobiology A: Chemistry* **2005**, *172*, 63-71.
51. Yum, J.; Moon, S.; Humphry-Baker, R.; Walter, P.; Geiger, T.; Nüesch, F.; Grätzel, M.; d K Nazeeruddin, M., Effect of Coadsorbent on the Photovoltaic Performance of Squaraine Sensitized Nanocrystalline Solar Cells. *Nanotechnology* **2008**, *19*, 424005.

CHAPTER FIVE: Development of Unsymmetrical Squaraine Dyes for DSSCs utilizing Cobalt Electrolyte

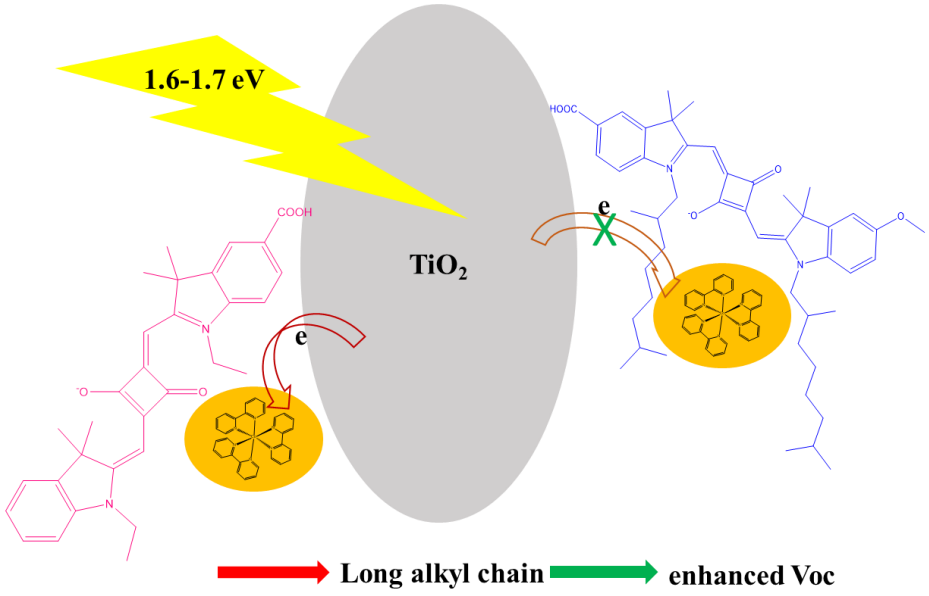

Anusha Pradhan, Maryala Sai Kiran, Gaurav Kapil, Shuzi Hayase, Shyam Sudhir Pandey.; *ACS Applied Energy Materials*, **2018**, *1* (9), pp 4545–4553

5.1 Introduction

The rise in the world's population and thus the strong need for energy and the continuous and inevitable depletion of fossil fuels urge an urgent need to discover alternative supplies of energy. The need for the hour is therefore, further research to explore alternative, safe and renewable energy sources. The photovoltaics, which works on the use of solar energy, have a bright future with no harmful side effects among the endless renewable energy technologies. In addition, solar energy supplies a thousand times higher energy than global requirement [1]. The green and affordable dye-sensitized solar cells (DSSCs) are in all ways one of the rising prospects for the next generation solar cells, whether in terms of fabricating ease, cheap raw materials, varied color and versatile applications. Following Reagan and Gratzel`s pioneering discovery in 1991, DSSC stood as one of the alternative hopes in paving the way for cost-effective and ecofriendly solar energy harvesting to the expensive silicon solar cells [2]. The DSSCs architecture consists of a photoanode, generally a TiO_2 semiconductor with a monolayer absorbed dye on the mesoporous TiO_2. The dyes primary function is to harvest the photons and generate photoexciton and trigger the current generation mechanism [3]. After photoexcitation, the dye donates an electron into the TiO_2 conductive band (CB) which then reaches the counter electrode through the external circuit. Sensitizing dyes therefore plays a vital role in the DSSC function as the genuine photon harvester and deserves to be regarded as the core of the DSSCs [4]. Once the dye is photoexcited, the ionic electrolyte must regenerate it to complete the circuit. The regeneration of injected electrons in TiO_2 must be faster than recombination. It consignes that the forward injection should be faster than the photoanode / electrolyte interface back electron transfer [5]. Therefore, electrolyte plays a crucial role as it is the dye and counter electrode interface and controls all the photovoltaic parameters [6]. In addition, the dye should also meet the criteria for good harvesting, injection and regeneration of photons [7, 8]. A good enough efficiency of (PCE) >12% has been reported using porphyrin dyes, even though the photon harvest is mainly in the solar spectrum`s visible wavelength region experiencing less photon flux [9, 10]. Therefore, as the NIR region bears more photon flux, there is a curiosity to achieve more current density if the dye is capable of harvesting photon in that region [11]. Thus, the study of the electronic absorption spectrum and the productive harvesting of photons by a large number of visible sensitizers shows the thirst for design and development of new sensitizers able to absorb in the near infrared (NIR) wavelength region for the further improvement in the PCE [12, 13, 14].

The electrolyte most widely used is based on the iodine redox shuttle, although many of them have been executed to replace them. There are basically two ways of recombining in the functioning of DSSCs that are the transfer of back-electron from TiO_2 particle to the oxidized dye or to the redox shuttle's oxidized form. If the regeneration has a faster time scale, a good redox shuttle can kinetically inhibit recombination with the oxidized dye. These plural kinetic parameter of quick dye regeneration and slow recombination make selecting effective redox shuttles very taxing. Thus, the reason for all DSSC research over the past 20 years had apparently relied on the I_3^-/I^- redox shuttle [15]. However, this class of electrolytes has demanded complex redox mechanism, intense color and abrasive to implement alternative redox shuttle [16]. One electron transfer redox shuttles of the metal organic CO(II)/CO(III) complexes have emerged as a good choice to meet this demand of their simpler mono-electron outer sphere transfer kinetics and easy dye regeneration process, minimizing the associated open-circuit voltage loss [17]. The cobalt electrolytes, however, bear positive surface charge which has an attraction with the negatively charged TiO_2, which in the case of iodine electrolyte is just the reverse. The application of cobalt electrolyte therefore, requires a strict passivation of the surface to reduce the transfer of back-electron [18, 19]. The mandatory need of surface passivation in case of cobalt electrolyte is the notice why majority of the sensitizers functioning well with iodine-based electrolyte showcase deteriorated photon harvesting when they are being used with cobalt electrolyte [17, 20]. The plural long alkyl chains as a group in the main dye backbone have been proven to function as a blocking layer for transferring of back-electron from the TiO_2 to the redox shuttle and to work well with the cobalt redox mediators [21, 22]. In addition to tuning the redox potential of cobalt-complex electrolytes by modifying the ligands, control of back-electron transfer from conductive oxide substrates to TiO_2 is required to attain high Voc. This is particularly relevant for cobalt-based electrolytes that exhibit relatively faster recombination kinetics with the electrons injected into the TiO_2 following the photoexcitation of the dye molecule which has been attributed to the one electron charge transfer as well as its slow ionic diffusions [23]. Therefore, the TiO_2 surface passivation plays a necessary role for cobalt electrolytes. The cobalt electrolyte-based DSSC requires more than 90 % full dye coverage, while the high coverage is not so influential for an iodine-based electrolyte [24]. The dyes have been reported as sensitizers in conjunction with cobalt electrolyte as the secondary requirement for cobalt electrolyte generally bear

multiple and long alkyl chain, but their photo harvest does not exceed 750 nm. This speaks for a huge demand for the design and development of NIR dyes compatible with cobalt redox mediators that maintain regeneration driving forces [25-28]. Actually, we have previously reported that DSSCs employing squaraine dyes as sensitizer in conjunction with both iodine/cobalt based redox electrolytes and it has been found that for the same dyes, which bore nice far-red photon harvesting and efficiency with I^-/I_3^- electrolyte resulted in a pity efficiency (0.2-0.3%) with cobalt electrolyte [29]. Since the cobalt-based redox electrolytes bear a comparatively lower level of redox energy of approximately 0.5 eV compared to traditional iodine-based electrolytes, acute caution must be taken to control the energetics of the novelty designed dyes as NIR dyes are less band gap. We have recently investigated the requirement for a minimum driving force of 0.12 eV for dye regeneration utilizing far-red absorbing squaraine dyes and redox electrolyte based on iodine [30].

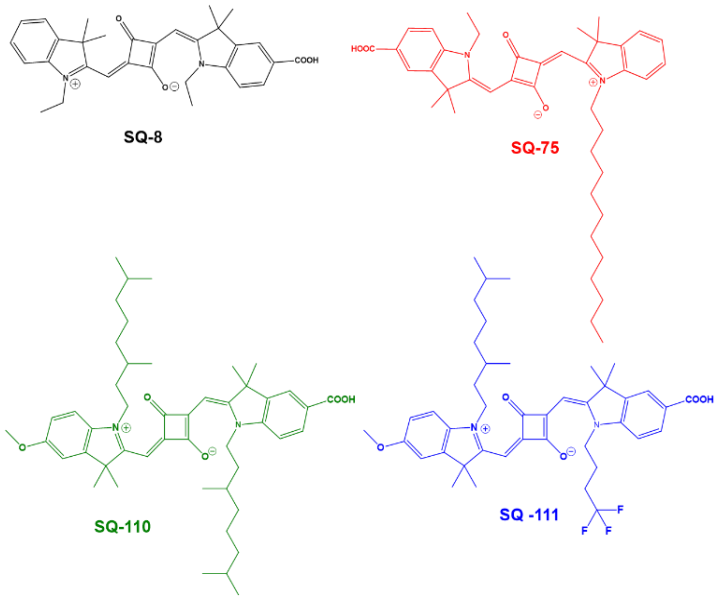

Figure 1. Molecular Structure of the unsymmetrical squaraine dyes utilized in the present work.

As the representative of the far red dye, this work focuses on the design of novel blue coloured dyes. They seem to have intense and sharp absorption of light along with the harvesting of photons mainly in the far-red region which is our main objective. In order to meet the cobalt-based redox shuttle, the requirement of long alkyl chains in the dye molecular structure was also achieved. The energetics condition of CB of TiO2, HOMO and LUMO of the dyes as well as the redox potential of the cobalt bipyridyl complex was maintained for a functioning DSSCs. Far-

red sensitive unsymmetrical squaraine dyes with molecular structure shown in the Fig. 1 were synthesized and subjected to their photophysical characterization along with application as sensitizer for DSSCs.

5.2 Experimental

Synthesis of the squaraine dyes

The dye intermediate 1,1,1-Trifluorobutyl-5-carboxy-2,3,3-trimethyl-indolium iodide (6) and unsymmetrical squaraine dyes SQ-8 and SQ-75 have been synthesized in accordance with our previous publications [31, 32]. Following Yuan et al report the intermediate 1 (5-methoxy-2,3,3-Trimethyl) was synthesized [33]. Branched alkyl chain (3,7-dimethyl-octyl) substituted intermediates (2, 3, 4, and 5) were synthesized adopting procedures reported by Stender and Volker et al [34, 35]. The overall synthetic scheme with their respective intermediates for the unsymmetrical squaraine dyes SQ-110 and SQ-111 is portrayed in Fig. 2.

2.2.1 Synthesis of 5-Methoxy-2,3,3-Trimethyl 3H –Indolium Iodide [1]

A round bottom flask containing 50 mmol of 4-methoxy phenyl hydrazine hydrochloride (8.6 g) in 80 mL of glacial acetic acid was added with 3-methyl-2-butanone (10.9 g, 125 mmol). The mixture was refluxed for 18 hours. Solvent was evaporated under reduced pressure and the chloroform was used to extract the concentrated compound. Chloroform was evaporated and the crude compound obtained was subjected to flash column chromatography in Ethyl acetate/ Hexane system (1:1) as the eluting solvent leading to a 94% yield of targeted compound as a brown viscous liquid. Synthesis of the titled compound was justified by the MALDI-TOF measurement (measured m/z: 248.0 $[M+2]^+$; calculated m/z: 246.19) confirms the synthesis of this intermediate.

2.2.2 Synthesis of 5-Methoxy-2,3,3-Trimethyl-1-Dimethyl-Octyl-Indolium Iodide [2] :

In a condenser-fitted round bottom flask, 3.6 g (18.4 mmol) of compound (1) and 1.5 equivalents (7.4 gm; 27.6 mmol) of 3,7-Dimethyl-1-Octyl-Iodide were dissolved in 50 mL nitromethane and refluxed for 48 hours. The solvent was completely evaporated after the completion of the reaction as confirmed by TLC and the compound was washed with ample diethyl ether to obtain the title product as an orange viscous liquid in 67% yield and >98 % purity of HPLC. [FAB-MS Calculated, 330.28 and measured, 331.57 $(M+1)^+$] confirms the successful synthesis of this intermediate.

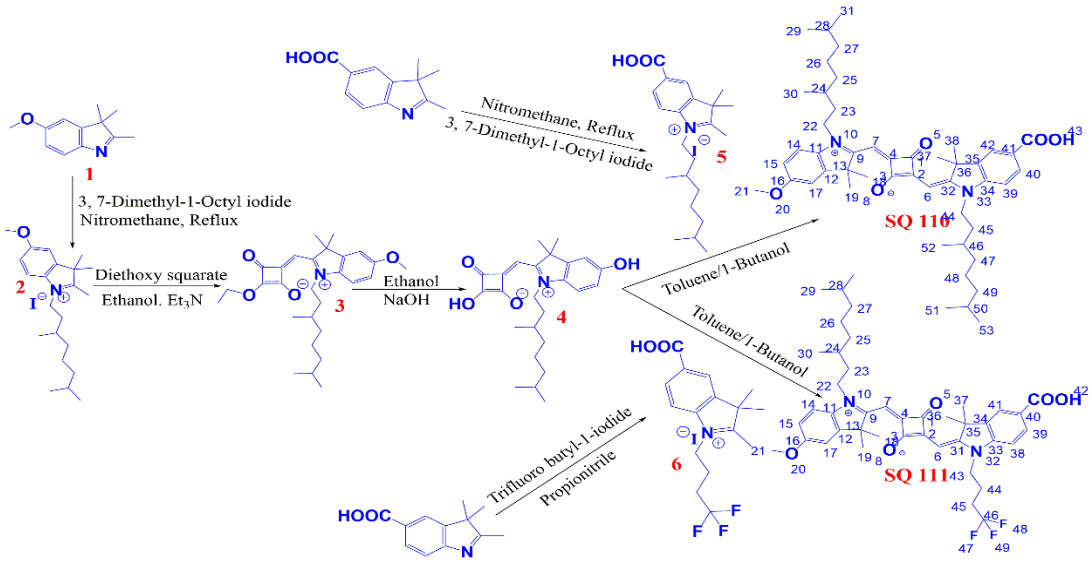

Figure 2. Scheme for the synthesis of unsymmetrical squaraine dyes SQ-110 and SQ-111.

2.2.3 Synthesis of 5-Methoxy-2,3,3-Trimethyl-N-Dimethyl-octyl-Semisquaraine ethyl-ester[3]and its hydrolyzed product [4]

In a round bottom flask fitted with condenser, 10 mmol of compound (2), 3 ml of 3,4-diethoxy-3-cyclobutene-1,2-dione (20 mmol) and 1ml of trimethylamine and ethanol (50 ml) were taken. Followed by progress monitoring with TLC, the reaction mixture was refluxed and quenched after 8 hours leading to a green solution. The reaction mixture was concentrated by rotary evaporator and crude product was purified using ethyl acetate/hexane as flash column chromatography eluting system with a 50 % yield as yellow solid titled compound (3). This semi-squaraine ester (3) was then subjected to hydrolysis using 40% NaOH in ethanol for 30 mins. The solvent was removed and HCl was added for neutralization. The compound was then extracted in ethyl acetate washing thoroughly with 10 % Na_2CO_3 aqueous solution. The extract was then concentrated to give orange solid. FAB-MS measured (426.40) and calculated (425.25) confirms the identity of synthesized product.

2.2.4 Synthesis of 5-Carboxy-2,3,3-Trimethyl-1-Dimethyl-Octyl-Indolium Iodide [5]

2.0 gm of 5-Carboxy-2,3,3-trimethyl indole (9.6 mmol) was taken in a round bottom flask fitted with a condenser. 13.8 mmol of 3,7-dimethyl-1-octyl iodide and 40 mL in anhydrous

acetonitrile were added and the reaction mixture was refluxed followed by monitoring of the reaction with TLC. Upon the completion of reaction in 48 hours, the solvent was evaporated under vacuum and ample diethyl ether was added for precipitation and followed by filtration. The pinkish solid compound was obtained in 60% yield. FAB-MS (345.72) is well in accordance with the calculated mass of 345.26.

2.2.5 SYNTHESIS OF SQUARAINE DYE SQ-110

In a round bottom flask fitted with condenser, 0.7 mmol (330 mg) of the intermediate (5) and hydrolysed semi-squaraine dye intermediate (4) were dissolved in 30 mL toluene/butanol (1:1). Reaction mixture was then refluxed for 18 hours followed by solvent removal with the aid of rotary evaporator. Crude dye was then subjected to flash column chromatography using $CHCl_3$/MeOH (9:1) as the eluting solvent giving titled dye SQ-110 as blue solid in 82% yield > 98 % purity as confirmed by HPLC. High resolution FAB-MS measured 751.5012 $[M+1]^+$ and calculated (750.4972) and 1H NMR (500 MHz, d6-DMSO): d/ppm = 7.95 (d, H-30), 7.92 (d, H-4), 7.34 (dd, H-6), 7.28 (d, H-27), 7.23 (dd, H-29), 6.95 (dd, H-7), 5.87 (s, H-10), 5.72 (s, H-23), 4.03 (t, 2H, H-13), 4.15 (t, 2H, H-35), 1.03 (s, 6H, H-11 & H-12), 1.13 (s, 6H, H-33 & H-34), 0.87 (m, 15H, H-20, H-21, H-22, H-42 & H-43) confirms the successful synthesis of this dye.

2.2.6 SYNTHESIS OF THE SQUARAINE DYE SQ-111

0.5 mmol (236 mg) of the intermediate (4) and hydrolysed semi-squaraine dye intermediate (6) were dissolved in 30 mL toluene/butanol (1:1) in a round bottom flask fitted with condenser. Reaction mixture was then refluxed for 18 hours allowing condensation. Upon the completion of reaction as confirmed by TLC, the solvent was removed under reduced pressure. The crude dye was then subjected to flash column chromatography using $CHCl_3$ / MeOH (9:1) as the eluting solvent. The isolated pure fraction was then concentrated to give a blue solid as titled dye in the 62% yield and >98 % purity. The measured HR-FAB-MS 721.3784 $[M+1]^+$ supported the synthesis of SQ 111 whose mass was obtained as 720.3790 theoretically. ^{1}H NMR (500 MHz, d6-DMSO): d/ppm = 7.93 (dd, H-24), 7.92 (d, H-4), 7.68 (d, H-6), 7.36 (d, H-21), 7.29 (d, H-23), 6.97 (dd, H-7), 5.88 (s, H-17), 5.76 (s, H-12), 4.18 (t, 2H, H-13), 4.07 (t, 2H, H-29), 1.71 (s, 6H, H-10 & H-11), 1.28 (s, 6H, H-

27 & H-28), 0.87 (m, 9H, H-32, H-37, H-38). FB-MS and NMR data verifies the identity of the synthesized final dye SQ 111.

2.2.7 Synthesis of cobalt bipyridyl complexes

The 2,2-bipyridyl 30 mmol (3 equivalent) was dissolved in 25 mL methanol and gently stirred until dissolution. 1 eq. of $CoCl_2$ (10 mmol) was added and the reaction mix was then subjected to reflux for 3 hours. Following this, 70% of the solvent was removed and aqueous solution of NH_4PF_6 (31 mmol, 3 equivalent) was added to the above reaction mixture which immediately resulted in a light yellow precipitate. The precipitate was filtered and washed thoroughly with ample methanol to give the $Co(bpy)_3(PF_6)_2$. For the synthesis of Co(III) complex, 2 mmol of this $Co(bpy)_3(PF_6)_2$ was dissolved in 20 mL acetonitrile followed by the addition of 3 mmol of $NOBF_4$ for its oxidation. This reaction mixture was stirred for 30 minutes at room temperature. Excess of aqueous NH_4PF_6 (6 mmol) was then added for precipitation followed filtration to get the $Co(bpy)_3(PF_6)_3$ as bright yellow solid.

2.2 MATERIALS AND METHODS

Characterization of Dyes

TLC (60G F_{25}) and high-performance liquid chromatography (HPLC) was used to monitor the progress of synthesis reactions. The HPLC was also used utilized to check the purity of the samples by taking into account the peak of the compound`s with respect to the peak of the other samples. To confirm the synthesis, MALDI-TOF or fast ion bombardment (FAB)-mass spectrometry in the positive ion-monitoring mode was then subjected to dye intermediates as well as the final dyes. Finally, by dissolving them in $CDCl_3$/DMSO-d_6 for the structural verification, the dyes were subjected to nuclear magnetic resonance (NMR) spectroscopy (JEOL, 500 MHz).

Electronic Absorption spectroscopy

Electronic absorption spectra of the sensitizers in solution (ethanol) as well as solid-state on thin transparent TiO_2 film of about 3µm was conducted with the aid of UV-Visible-NIR spectrometer

(JASCO model V550). The lambda onset on the solid state was utilized to calculate the energy band gap using the equation:

$$Eg = \frac{1240}{\lambda}$$

Energy level estimation

The photoelectron yield spectroscopy (Bunko Keiki, model KV-205 HK, Japan) and with cyclic voltametry techniques were used to determine the HOMO energy level of the sensitizers for DSSC.. The PYS was performed under 10^3 Pascal high pressure. The HOMO value was obtained from the intersection of the yield ($Y^{1/3}$) of the photoexcited electrons. The other way to determining the HOMO was through the curve of cyclic voltammetry (CV). The experiment was executed in an electrochemical three-electrode cell which comprised a Pt foil as counter electrode, Pt wire as working electrode and saturated calomel electrode (SCE) as the reference electrode. The concentration of the electrolyte comprised of 2 mM solution of respective squaraine dyes and ferrocene as the supporting electrolyte. It was run at a scan rate of 20 mV/s. An auto-polarization system (HSV-100, Hakuto Denko, Japan) was used for the CV measurements. The HOMO energy level from the CV plot was obtained by calculating the shift in dyes oxidation potential in reference to the oxidation potential of Fc+/Fc redox couple. LUMO energy level was subsequently calculated by adding the HOMO energy level of the respective dyes with their optical band gap (Eg).

Measurements of Device parameter

The current-voltage curve of the DSSCs was measured using a solar simulator (CEP-2000 Bunko Keiki Co. Ltd, Japan) equipped with a xenon lamp (Bunko Keiki BSO-X150LC) employing a simulated solar intensity of 100 mW/cm^2 as light source, where the light source was calibrated using a silicon diode. The working electrode area has been maintained precisely with a black metallic mask of area of 0.25 cm^2 that also prevents extra light scattering.

Electrochemical impedance spectroscopy (EIS)

EIS was performed on the various interfaces to study the resistances. A frequency response analyser (Solartron Analytical, 1255B), connected to a potentiostat (Solartron Analytical, 1287)

was used for the measurements. A small AC perturbation of 10 mV was applied at room temperature in the frequency range from 5 x 10^{-3} -10^{5} Hz.

Device Fabrication

An area of 2 × 1 cm^2 of FTO glass were subsequently washed with detergent, distilled water, acetone and isopropyl alcohol under sonication for 15 minutes each and by treating them with ozone plasma. Then using 40mM, the cleaned FTO was then subjected to $TiCl_4$ treatment. The substrates were submerged at 70^0C for 30 minutes in the solution, followed by sintering at 450^0C. After sintering, the FTO TiO2 paste (DS/P Solaronix with 10-20 nm particle size) were screen printed on glasses to afford the 7 μm of mesoporous TiO_2 thickness. They were then again contented to $TiCl_4$ treatment as described above. The substrates were taken out at 100^0 C and then dipped in an ethanol solution of 0.2 mM dye containing 4 mM CDCA. The counter electrode comprised of a sputtered platinum with 60 nm thickness. The two electrodes were affixed with 25 μm surlyn spacer at 110^0 C. The electrolyte was injected via the small aperture through the vacuum. The electrolyte comprised of 0.22M $[Co(bpy)_3(PF_6)_2]$, 0.033 M of $[Co(bpy)_3(PF_6)_3]$, 0.2 M of tert.-butyl-pyridine and 0.1 M $LiClO_4$ in acetonitrile.

5.3 Results and Discussion

5.3.1 Optical Characterization

The electronic absorption spectra of the new unsymmetrical squaraine dyes employed as sensitizers in this study was recorded both in the solution and on the solid-state as shown in the Fig. 3. Table 1 summarizes the parameters obtained from the electronic absorption spectral study. The spectra clearly shows the absorption from the respective dyes in the far red region. In addition, the attractive feature of them lies in their high molar extinction coefficient in the range of 10^5. The dyes discussed here exhibit high molar extinction coefficients (ε) ranging from 1.8-2.4 ×10^5 $dm^3mol^{-1}cm^{-1}$ in the wavelength region of 550 nm-700 nm. In this region the absorption is attributed with the π- π* charge transfer from their HOMO to LUMO on photoexciton [36]. A perusal of the Fig. 3(a) vividly demonstrates that SQ-110 showcase the supreme bathochromically shifted light absorption with maximum absorption (λ_{max}) at 649 nm with appreciable high ε of 2.4 ×10^5 dm^3 mol^{-1} cm^{-1} amongst all the unsymmetrical squaraine dyes concerned. The dyes SQ-110 and SQ-111 showcase an appreciable bathochromic shift. This bathochromic shift could be

consigned to the of electron donating methoxy (–OCH_3) in the 5th position of the indole ring opposite to that containing –COOH group. The electron donating moiety on one side and the accepting on the opposite end would have contributed to the push-pull electron system and hence red shifting the spectra [37]. Although SQ 110 and SQ 111 had a red shifted electronic spectra, they show a relatively pronounced vibronic shoulders around 600 nm. The blue shifted vibronic shoulder is primarily due to the H aggregate formation and is common in squaraine dyes and appears to control the aggregation due to steric hindrance in long alkyl groups [38]. However this is not the case here with the long alkyl groups. The high hydrogen bonding interconnection between the dyes facilitated by methoxy group would have resulted in aggregation of dye. The vibronic shoulder intensification could be attributed by the dye molecules for the formation of H-aggregates as previously reported [39].

Following their adsorption on mesoporous TiO_2 (Fig 3b), solid-state electronic absorption spectra of dyes were also recorded to get this observation more accurate. The dye was permitted to adsorb on to the 3 μm thick mesoporous TiO_2 for 30 minutes. Both the bathochromic shift in the λ_{max} as well as the relatively higher spectral broadening were showcased in solid state spectra. The reason for such observation could be elucidated on the formation of ester linkage of the dye`s –COOH group interaction with that of $TiO_2$`s –OH group [40]. The alternate π bonded molecule generally results in a planar structure and the induced extended π-conjugation in these dyes support the feasible to aggregation of dye. The H-aggregates of the dyes are less susceptible to electron injection with respective to the monomeric dye. Less injection of electrons therefore means diminished photon harvest and hence less PCE in solar cells [41]. Therefore, to circumvent this inefficiency, CDCA is generally employed to control the aggregation with the sensitizing dyes and thus play a crucial role for appreciable good photon harvesting in DSSCs [42-43].

Fig. 3b shows the normalized solid-state electronic absorption spectrum of the dyes on TiO_2. The spectra perusal shows a prominent a blue-shifted vibronic shoulder around 610 nm due to the formation of H-aggregates. This peak of aggregation is more pronounced in solid state as compared to that in solution which may due to the close proximity of the dye molecules in the solid state. The H-aggregation index could therefore be estimated from the ratio of absorbance of the H-aggregate band (around 610 nm) to the monomer band in solution (650) which defines the extent of H-aggregation, summarized in the table 1. It is worth mentioning here that no CDCA has been

added in recording solid-state electronic absorption spectrum of dyes to study the precise nature of the dye solely in solution and in the solid state.

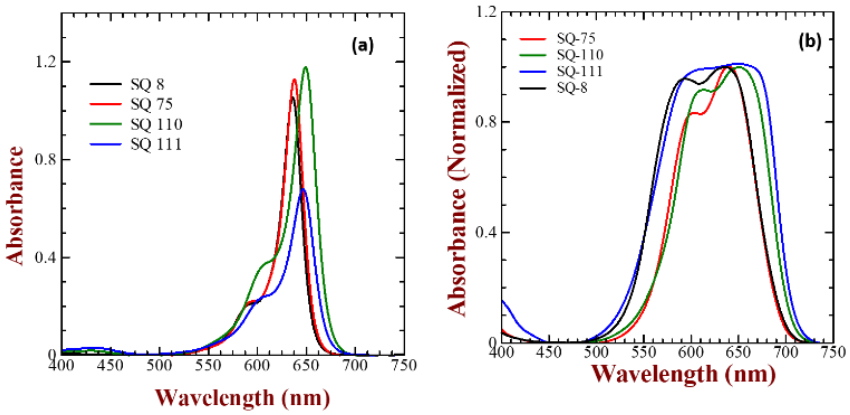

Figure 3. Electronic absorption spectra of the unsymmetrical squaraine dyes in ethanol (5µM) (a) and normalized absorption spectra in solid-state for the same dyes adsorbed on 3µm thick transparent TiO_2 (b).

Table 1. Optical and energetic parameters of the unsymmetrical squaraine dyes extracted from the photophysical investigations.

Dye	λmax solution	ϵ in solution ($dm^3 \cdot mol^{-1} \cdot cm^{-1}$)	λmax solid-state	Aggregation on TiO_2*	HOMO (eV)	LUMO (eV)
SQ-8	637 nm	2.08×10^5	638 nm	0.96	-5.15	-3.33
SQ-75	638 nm	2.24×10^5	640 nm	0.84	-5.05	-3.37
SQ-110	649 nm	2.34×10^5	652 nm	0.92	-5.10	-3.22
SQ-111	648 nm	1.75×10^5	652 nm	0.99	-5.20	-3.40

* Ratio between absorbance of the aggregate band (around 610 nm) and the monomer band at (650 nm) has been used to calculate the extent of aggregation.

Yum et al. reported that the degree of H-aggregates of squaraine dye in the solid state i.e on the mesoporous TiO_2 is inversely related to the added fraction of coadsorber, CDCA in dye solution, the major role of which is to prevent the aggregation of dye [44]. Fig. 3(b) and table 1 clearly explain the enhanced formation of H-aggregates both in the solid and solution state. This is due to the pronounced intermolecular interaction. The highest degree of aggregation is found for SQ-8 (0.96) which possess the shortest alkyl group among all.

SQ-75 has the minimum aggregation degree of 0.84 compared to that of SQ 8. However on the other hand, SQ 110 and SQ 111 exhibit higher extent of dye aggregation though have long alkyl chains in the main framework . This is due to the availability of direct ring substituted methoxy group and terminal fluorine substitution in the alkyl chains, which could be attributed to enhanced intermolecular hydrogen bonding.

5.3.2 Energy Band Diagram

The energy of the various DSSCs components plays a vital role in DSSC operation. In fact, the dye that lies between the semiconductor and the electrolyte has significat role to play in maintaining the energetics in both injection of electrons and as well as for its regeneration. A good dye should therefore maintain the minimum requirement of energetic cascade in correspondence to the wide band gap semiconductor which is TiO_2 here and redox electrolyte with a good anchoring group. Their HOMO energy should be below the energy level of electrolyte`s redox, while the energy of LUMO should be higher than TiO2`s CB for the dye regeneration and electron injection, respectively [45]. Photoelectron yield spectroscopy (PYS) in vacuum under high pressure of 10^{-3} Pascal was used for the approximation of the dye`s HOMO energy level. The band gap was obtained from the offset of the electronic spectra of solid-state absorption of the respective dyes depicted in the Fig. 3(b).

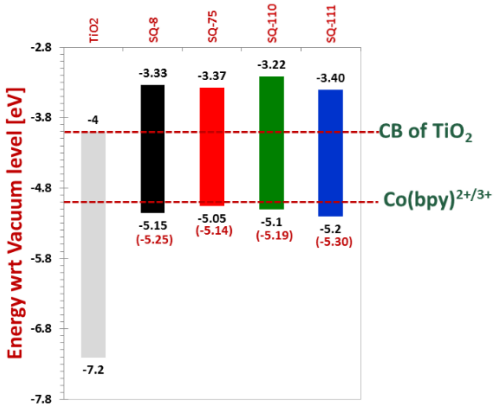

Figure 4. Energy band diagram showcasing energy level of squaraine dyes, cobalt complex electrolyte and wide band gap semiconductor (TiO_2). Values in the bracket are the HOMO energy of the dyes obtained from CV measurement.

And the LUMO value was obtained by adding the band gap of the dye to its HOMO value. Hence the energy band diagram was made taking their respective values along with the TiO_2 and cobalt redox shuttle is shown in the Fig. 4. Fig. 4 clearly depicts that all of the unsymmetrical squaraine

dyes maintain their LUMO energy higher than the CB of the TiO_2, which is embraced to be lower than the vacuum level by 4 eV [46]. This supports the picture that after the photoexcitation, the efficient electron injection from the excited dye molecules to the TiO_2 is maintained.

The figure above clearly conveys that SQ-110 bears the highest LUMO energy level amongst all the sensitizers employed, resulting in the highest driving force for the electron injection with an energy cascade of 0.67 eV with the semiconductor TiO_2. Among all the dyes concerned, SQ-110 and SQ-75 have longer alkyl chains. These alkyl groups as such have the electron donating tendency which contribute to the rise in the energy level in comparison to that of SQ-8 [31]. In case of SQ-110 the electron donating group ($–OCH_3$) at the 5^{th} position would also have shifted the HOMO energy level upwards, making it more suitable for electron injection into the semiconductor. However, the fundamental difference between SQ 110 and SQ-111 lies only in one N substitution, where the former dye carries the electron donating dimethyl octyl group while the latter bears trifluoro substituent as the electron withdrawing due to negative inductive effect. The result of the electron-withdrawing group (fluorine) in controlling the energetics is clearly demonstrated in the downward shift in both the HOMO and LUMO level of SQ-111 in comparison to that of SQ-110. This observation of energetics is also supported by findings of Mathew et al [47]. It is appealing that the SQ-75 bearing solely one long alkyl chain has its highest HOMO energy level of -5.05 eV amidst dyes used approaching the redox potential value -5.00 eV of the cobalt bipyridyl complex based electrolyte. It maintains only a minimum energy barrier of (0.05 eV) with the cobalt electrolyte but can still function properly in DSSCs which is the proof for dye regeneration.

The other way to determine the dye`s HOMO is through the CV technique. The CV of ferrocene (Fc) was also measured under the similar condition as the reference for the experiment. The CV of the dyes under study has been demonstrated in the Fig. 5. Ferrocene displays a sharp redox peak due to its mechanism of rapid oxidation and reduction. Therefore, as a reference material, it has been widely employed to calibrate the oxidation potential of new materials including dyes for DSSC.

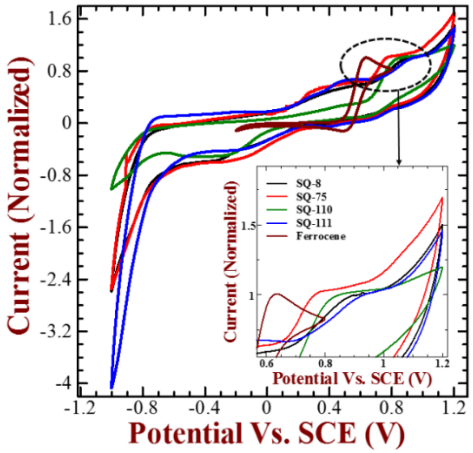

Figure 5. CV of the new squaraine dyes and also ferrocene as reference, in DMF solution. Normalization of the peak values of the current were done (zoomed oxidation potential region in the inset) to clearly visualize the shift of the oxidation potential of dyes in correspondence to ferrocene.

In this report, the dyes HOMO energy level was also assessed by approximating the shift in the dyes oxidation potential respect to that of the Fc^{+}/Fc redox couple. As a reference bar, oxidation potential of the Fc^{+}/Fc was taken as -5.01 eV vs. vacuum level considering the value taken from the report by Su and Girault. [48]. Although different values of ferrocene`s oxidation potential have been reported in literature, the above stated one proves to be more reliable, which is also supported by the theoretical benchmark calculations [49]. Beneficially, the calculated values of the HOMO of squaraine dyes obtained also incorporates the solvation effect as in the actual DSSC model. The values as shown in the bracket which is that obtained from CV in Fig. 4 reflects a similarity in the PYS curve. This confirms the definitive of the reported experimental values with the theoretical value. Simultaneously, the HOMO values obtained by CV are approximately 0.1 eV lower as comparison to that of PYS. This could be due to the solvation energy of the dyes associated with the in solution and stabilisation.

5.3.3 Photovoltaic Characterization

The structure of the dyes discussed in this work possessed a suitable energetics to be employed as sensitizer for DSSCs. The blue colour of them made it more appealing to DSSCs due to the far red photo harvest with high molar extinction coefficient. The dyes were used in conjunction with $Co(bpy)^{2+/3+}$ complex as the redox shuttle as a sensitizer which had a large band gap TiO_2 as

semiconductor. DSSCs were fabricated in the similar experimental conditions like described above in the experimental section. It included photoelectrode fabrication, dye/CDCA concentration and cobalt redox electrolyte by altering the sensitizers SQ-8, SQ-75, SQ-110 and SQ-111. The DSSCs photovoltaic plot thus made-up have been shown in the Fig. 6 together with their photovoltaic parameters presented in the table 2. The Fig. 6 communicates that SQ-110 with the two long alkyl groups showed an exceptional photoconversion efficiency (PCE) of 1.98 % with good photon harvest resulting in the best short-circuit current density (Jsc) of value o5.9 mA/cm2 and 0.57 V as open-circuit voltage (Voc) under solar irradiation of simulated 1-Sun.

In order to investigate the best performance by SQ 110, the explanation from its energetics stands well defended. SQ-110 has a better electron injection driving force that facilitates faster injection of electron onto the TiO_2 and reduce charge recombination. Another credit for par excellent performance could be attributed to the logical molecular structure of the dye. The two branched long alkyl dimethyloctyl chain functioned well as an effective charge recombination barrier thus minimizing voltage loss. In addition, electron injection with the high driving force for also supports for the better performance of the DSSCs with SQ 110 as sensitizer. The dye SQ 8 exhibited least performance with a PCE of 1.24 %. This could be credited to the presence of shortest alkyl group which is not sufficiently capable of inhibiting the transfer of back electron. As a result of recombination, the electrolyte which involves cobalt redox shuttle and mesoporous TiO_2 show more voltage loss. The electrons from the TiO_2 is likely to recombine with the oxidized species of cobalt. Thus requires the strict surface passivation. This surface passivation generally employs a thin layer of compact oxide. In the dye level, employment of dyes with long alkyl chains provide electron screening and hence induces beneficial effective surface passivation for the mesoporous TiO_2 [50-53]. Many reports indicate that the long alkyl chains bearing sensitizing dyes bearing are mandatory for cobalt-based redox shuttle DSSCs using which acts an insulator for the injected electrons of TiO2 from back electron transfer towards the positive ions $Co^{2+/3+}$ of the electrolyte [54].

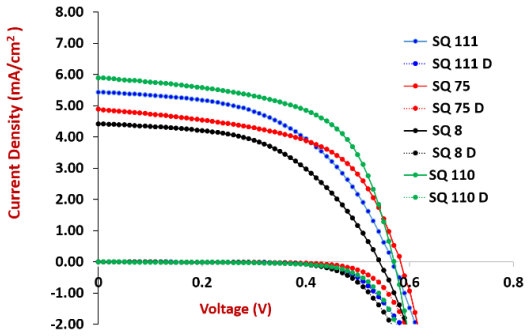

Figure 6. Photovoltaic spectra of DSSCs under irradiation of simulated 1-Sun fabricated. The IV data of different sensitizers with cobalt redox electrolyte is shown by different colored solid curve wheras the dotted lines denote the corresponding I-V dark characteristics for the respective devices.

In this context, we would like to point out that in our previous work we had tried to use cobalt redox electrolyte with SQ-8 as sensitizer for DSSC, but efficiency was pity low (0.2-0.3 %) [29]. Absence of passivating the FTO surface and mesoporous TiO_2 could have resulted in the deterioration of the PCE for SQ-8 which, in present scenario led astonishingly to the enlarged enhancement of the PCE by 1.23 % after surface passivation. At the same time, the lack of long alkyl chain in the dye molecular framework of SQ-8 is the reason for its comparatively hampered PCE compared to the other dyes discussed here. In DSSC research, the value of the driving force for electron injection and regeneration of dye has been well chronicled and there is a consent that they are promoted by higher driving force [55, 56]. Interestingly, although SQ-75 exhibits a lower LUMO and a higher HOMO than SQ 8, it shows a higher Jsc of 4.88 mA/cm2 and Voc of 0.58 V (table-2) which is better than the SQ 8. This clearly explains the screening availability of the long alkyl chain (dodecyl) on the back electron transfer, which is absent in case of SQ-8. The photovoltaic parameters obtained from the I-V curve for all the dyes portrays the worth of long alkyl chains for making them effective for cobalt electrolytes. Though SQ-111 exhibits deeper HOMO energy level than SQ 110, the DSSCs exhibited relatively diminished PCE (1.58 %) compared to SQ-110. Due to the large dye aggregation (H-aggregates, table-1), this could be due to the hampered electron injection leading to the increased recombination of charge and inefficient electron injection. It was also reported that dye aggregates showcase lower efficiency of forward thus resulting in the hampered Jsc (table-2) compared to monomeric dye molecules [57].

Table 2. Photovoltaic parameters extracted from photovoltaic characteristics for the DSSCs fabricated using different sensitizers and cobalt redox electrolyte

Dye	Jsc (mA/cm^2)	Voc (V)	FF	Efficiency (%)
SQ-8	4.43	0.54	0.52	1.24
SQ-75	4.88	0.58	0.56	1.58
SQ-110	5.90	0.57	0.59	1.98
SQ-111	5.44	0.56	0.51	1.58

In our case, we can clearly demonstrate that its molecular structure dominates the overall efficiency of the DSSCs rather than the dye energetics. Current-voltage (I-V) characteristics of the DSSCs under dark has been globally used for studying the related current leakage which is directly related to recombination. Dark I-V characteristics in the Fig. 5 indicates the high extent of charge recombination of DSSC-with short alkyl chain length (SQ-8) squaraine dyes with respect to to the devices fabricated from long alkyl chain- bearing SQ sensitizers.

The spectra of photocurrent action gives the idea of the current density and the wavelength to which the photon is being harvested. It has thus, found a wide application for independent affirmation of the visible photovoltaic characteristics as a whole and Jsc as such in solar cell research. Incident photon to electron conversion efficiency (IPCE) is plotted as a dependent function of incident photons wavelength . The Fig. 7 displays the photocurrent action spectra of DSSCs fabricated with different unsymmetrical squaraine dyes in conjunction with cobalt redox electrolyte.

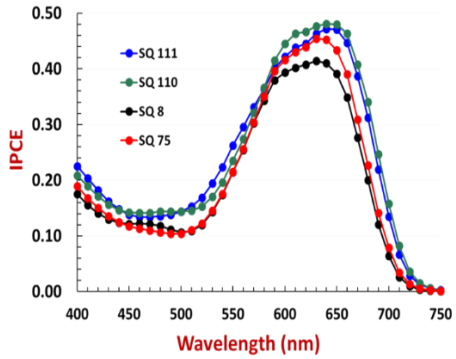

Figure 7. Photocurrent action spectra for DSSCs fabricated using different sensitizers and cobalt redox electrolyte after monochromatic illumination.

The spectral matching between the photocurrent action spectrum and solid-state electronic absorption spectrum (Fig. 3b) of the sensitizer ensures that the photocurrent is triggered from the excited dye molecule (LUMO) to the TiO_2`s CB after photoexcitation by the electron injection. Fig. 7 and table-2 shows that the IPCE peak for the respective sensitizers follows the similar trend of Jsc values, the higher IPCE means more photocurrent. The figure also says that the SQ-110 gives an IPCE of 48 % at 650 nm, the maximum in this case. On the other hand, SQ-8 exhibits only 41 % at 640 nm which explains the larger Jsc value for the DSSC fabricated with dye SQ-110. The presence of electronic donating methoxy group in the SQ-110 and SQ-111 sensitizers resulted in the bathochromically shifted edge of λ_{max} and optical absorption (Fig. 3b). This has an impact on DSSC performance which was also been represented pretty well in the DSSC photon harvesting nature. The dye with the minimum energy barrier of only 0.05 eV (Fig. 4) is worth appreciation for dye regeneration with $Co(bpy)^{2+/3+}$ electrolyte, as well as for good photon harvest in the far-red wavelength region. This gives the hope for the novel NIR photon harvesting sensitizing design and development.

5.3.4 Electrochemical Impedance Spectroscopy (EIS)

The DSSCs employing the four different squaraine dyes with varying alkyl chain length were fabricated and was its photovoltaic nature was described considering, energetics, dark I-V and action spectral behaviour in to account. Furthermore, electrochemical impedance spectroscopy was performed to measure the resistance afforded by the device. EIS has been measured by with the doing the forward bias the solar cells near to their Voc respectively in dark condition. The various resistances R1, R2 and R3 have been taken into account. The equivalent circuit model for DSSC was explained brilliantly in the literature, and it is possible to categorize various resistances in the fabricated DSSC fabricated as shown in the in the Fig. 8 [58,59]. R1 is the resistance afforded in the FTO/TiO_2 interface, R2 stands for the resistance of charge transfer at the counter electrode (platinum in this case) and R3 concerns the charge transfer resistance at TiO_2/Dye/electrolyte interface. In our case, R1 and R2 should have the same value for all the DSSC fabricated, as the device is fabricated with the same FTO glass and platinum as the counter electrode. From the fig.8, there is an appreciable difference in the value of R3 which actually controls the device performance

of the respective dyes as explained by Hoshikawa et al [57]. The highest R3 value for SQ-110 (324 ± 1.3 Ω), shows the highest resistance to recombination as compared to SQ-111(192.9± 0.7 Ω) followed by SQ-75(92.87± 0.34 Ω) and which is minimal for SQ 8. This explains the contribution of long alkyl chain of SQ-110 and the shorter alkyl group of SQ-75 and SQ-8 contributes poor passivation surface passivation of TiO_2 surface. The device performance stands well to support this, and vice versa. This vividly confirms that in the case of DSSC with SQ-8, it is the reason that the shortest alkyl chain length in SQ 8 results in the pronounced reduced value of R3 (21.01± 0.24 Ω) which is the cause for the diminished performance owing to the pity surface passivation.

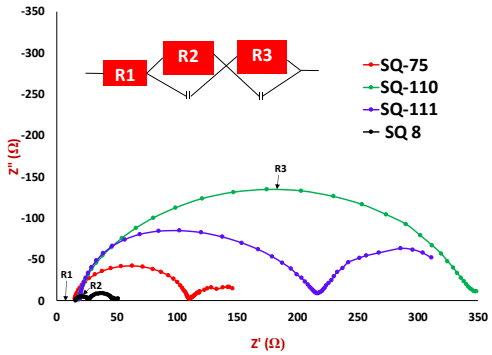

Figure 8. EIS measured under dark near to Voc in each case.

5.4 Conclusions

In conclusion, a number of infrared sensitive unsymmetrical squaraine dyes have been successfully designed and synthesized. It was followed by their photophysical characteristics and application in DSSC sensitizing with cobalt redox shuttle. This is the first report where NIR dye is used in conjunction with cobalt redox shuttle to the best of our knowledge. Logical molecular design maintaining all the necessary requirements such as driving force etc. led to the harvesting of photon mainly in the infrared wavelength region extending up to 750 nm. The blue coloured squaraine dyes used in this work have functioned brilliantly for sensitizingr DSSC utilizing cobalt complex based redox electrolyte with their structural variations. It was executed to acquire knowledge that the molecular structure of the dyes dominate its role in determining and controlling the govern performance of the DSSCs rather than the energetics. It has been well demonstrated that long alkyl chains prevent the direct contact of TiO2 and the cobalt ions of the electrolyte

and TiO2 surface in its passivation role that impedes the charge recombination resulting in minimum voltage loss. Beautifully, it has also been explained that DSSC based on one of the newly designed NIR sensitizer SQ-110 bearing two long bulky alkyl chains has been successful in achieving the appreciable PCE of about 2 % with photon harvesting when only in the NIR region extending up to 750 nm. This paves the new way and hopes for the further enhancement in the efficiency as well as the photon harvesting at longer wavelength.

References

1. Ladomenou, K.; Kitsopoulos, T.; Sharma, G.; Coutsolelos, A., The Importance of Various Anchoring Groups Attached on Porphyrins as Potential Dyes for Dssc Applications. *Rsc Advances* **2014**, *4*, 21379-21404.
2. O'regan, B.; Grätzel, M., A Low-Cost, High-Efficiency Solar Cell Based on Dye-Sensitized Colloidal Tio2 Films. *nature* **1991**, *353*, 737.
3. Shalini, S.; Balasundaraprabhu, R.; Kumar, T. S.; Prabavathy, N.; Senthilarasu, S.; Prasanna, S., Status and Outlook of Sensitizers/Dyes Used in Dye Sensitized Solar Cells (Dssc): A Review. *International Journal of Energy Research* **2016**, *40*, 1303-1320.
4. Grätzel, M., Conversion of Sunlight to Electric Power by Nanocrystalline Dye-Sensitized Solar Cells. *Journal of Photochemistry and Photobiology A: Chemistry* **2004**, *164*, 3-14.
5. Tachibana, Y.; Moser, J. E.; Grätzel, M.; Klug, D. R.; Durrant, J. R., Subpicosecond Interfacial Charge Separation in Dye-Sensitized Nanocrystalline Titanium Dioxide Films. *The Journal of Physical Chemistry* **1996**, *100*, 20056-20062.
6. Wu, J.; Lan, Z.; Lin, J.; Huang, M.; Huang, Y.; Fan, L.; Luo, G., Electrolytes in Dye-Sensitized Solar Cells. *Chemical reviews* **2015**, *115*, 2136-2173.
7. Salvatori, P.; Marotta, G.; Cinti, A.; Anselmi, C.; Mosconi, E.; De Angelis, F., Supramolecular Interactions of Chenodeoxycholic Acid Increase the Efficiency of Dye-Sensitized Solar Cells Based on a Cobalt Electrolyte. *The Journal of Physical Chemistry C* **2013**, *117*, 3874-3887.
8. Robertson, N., Optimizing Dyes for Dye-Sensitized Solar Cells. *Angewandte Chemie International Edition* **2006**, *45*, 2338-2345.
9. Yella, A.; Mai, C. L.; Zakeeruddin, S. M.; Chang, S. N.; Hsieh, C. H.; Yeh, C. Y.; Grätzel, M., Molecular Engineering of Push–Pull Porphyrin Dyes for Highly Efficient Dye-Sensitized Solar Cells: The Role of Benzene Spacers. *Angewandte Chemie International Edition* **2014**, *53*, 2973-2977.
10. Higashino, T.; Imahori, H., Porphyrins as Excellent Dyes for Dye-Sensitized Solar Cells: Recent Developments and Insights. *Dalton Transactions* **2015**, *44*, 448-463.
11. Burke, A.; Schmidt-Mende, L.; Ito, S.; Grätzel, M., A Novel Blue Dye for near-Ir 'Dye-Sensitised'solar Cell Applications. *Chemical Communications* **2007**, 234-236.
12. Pandey, S. S.; Watanabe, R.; Fujikawa, N.; Shivashimpi, G. M.; Ogomi, Y.; Yamaguchi, Y.; Hayase, S., Effect of Extended Π-Conjugation on Photovoltaic Performance of Dye

Sensitized Solar Cells Based on Unsymmetrical Squaraine Dyes. *Tetrahedron* **2013**, *69*, 2633-2639.
13. Hardin, B. E.; Snaith, H. J.; McGehee, M. D., The Renaissance of Dye-Sensitized Solar Cells. *Nature photonics* **2012**, *6*, 162.
14. Hamann, T. W.; Jensen, R. A.; Martinson, A. B.; Van Ryswyk, H.; Hupp, J. T., Advancing Beyond Current Generation Dye-Sensitized Solar Cells. *Energy & Environmental Science* **2008**, *1*, 66-78.
15. Hamann, T. W., The End of Iodide? Cobalt Complex Redox Shuttles in Dsscs. *Dalton Transactions* **2012**, *41*, 3111-3115.
16. Cheng, M.; Yang, X.; Li, S.; Wang, X.; Sun, L., Efficient Dye-Sensitized Solar Cells Based on an Iodine-Free Electrolyte Using L-Cysteine/L-Cystine as a Redox Couple. *Energy & Environmental Science* **2012**, *5*, 6290-6293.
17. Mosconi, E.; Yum, J.-H.; Kessler, F.; Gómez García, C. J.; Zuccaccia, C.; Cinti, A.; Nazeeruddin, M. K.; Grätzel, M.; De Angelis, F., Cobalt Electrolyte/Dye Interactions in Dye-Sensitized Solar Cells: A Combined Computational and Experimental Study. *Journal of the American Chemical Society* **2012**, *134*, 19438-19453.
18. Feldt, S. M.; Gibson, E. A.; Gabrielsson, E.; Sun, L.; Boschloo, G.; Hagfeldt, A., Design of Organic Dyes and Cobalt Polypyridine Redox Mediators for High-Efficiency Dye-Sensitized Solar Cells. *Journal of the American Chemical Society* **2010**, *132*, 16714-16724.
19. Molla, M. Z.; Kawano, M.; Baranwal, A. K.; Pandey, S. S.; Ogomi, Y.; Ma, T.; Hayase, S., Enhancing the Performance of Transparent Conductive Oxide-Less Back Contact Dye-Sensitized Solar Cells by Facile Diffusion of Cobalt Species through Tio 2 Nanopores. *RSC Advances* **2016**, *6*, 33353-33360.
20. DeVries, M. J.; Pellin, M. J.; Hupp, J. T., Dye-Sensitized Solar Cells: Driving-Force Effects on Electron Recombination Dynamics with Cobalt-Based Shuttles. *Langmuir* **2010**, *26*, 9082-9087.
21. Murakami, T. N.; Koumura, N.; Uchiyama, T.; Uemura, Y.; Obuchi, K.; Masaki, N.; Kimura, M.; Mori, S., Recombination Inhibitive Structure of Organic Dyes for Cobalt Complex Redox Electrolytes in Dye-Sensitised Solar Cells. *Journal of Materials Chemistry A* **2013**, *1*, 792-798.
22. Massin, J.; Ducasse, L.; Abbas, M.; Hirsch, L.; Toupance, T.; Olivier, C., Molecular Engineering of Carbazole-Fluorene Sensitizers for High Open-Circuit Voltage Dsscs: Synthesis and Performance Comparison with Iodine and Cobalt Electrolytes. *Dyes and Pigments* **2015**, *118*, 76-87.
23. Yang, J.; Ganesan, P.; Teuscher, J. l.; Moehl, T.; Kim, Y. J.; Yi, C.; Comte, P.; Pei, K.; Holcombe, T. W.; Nazeeruddin, M. K., Influence of the Donor Size in D− Π–a Organic Dyes for Dye-Sensitized Solar Cells. *Journal of the American Chemical Society* **2014**, *136*, 5722-5730.
24. Pazoki, M.; Lohse, P. W.; Taghavinia, N.; Hagfeldt, A.; Boschloo, G., The Effect of Dye Coverage on the Performance of Dye-Sensitized Solar Cells with a Cobalt-Based Electrolyte. *Physical Chemistry Chemical Physics* **2014**, *16*, 8503-8508.
25. Tsao, H. N.; Yi, C.; Moehl, T.; Yum, J. H.; Zakeeruddin, S. M.; Nazeeruddin, M. K.; Grätzel, M., Cyclopentadithiophene Bridged Donor–Acceptor Dyes Achieve High Power Conversion Efficiencies in Dye-Sensitized Solar Cells Based on the Tris-Cobalt Bipyridine Redox Couple. *ChemSusChem* **2011**, *4*, 591-594.

26. Hao, Y.; Saygili, Y.; Cong, J.; Eriksson, A.; Yang, W.; Zhang, J.; Polanski, E.; Nonomura, K.; Zakeeruddin, S. M.; Gratzel, M., Novel Blue Organic Dye for Dye-Sensitized Solar Cells Achieving High Efficiency in Cobalt-Based Electrolytes and by Co-Sensitization. *ACS applied materials & interfaces* **2016**, *8*, 32797-32804.
27. Yum, J.-H.; Holcombe, T. W.; Kim, Y.; Rakstys, K.; Moehl, T.; Teuscher, J.; Delcamp, J. H.; Nazeeruddin, M. K.; Grätzel, M., Blue-Coloured Highly Efficient Dye-Sensitized Solar Cells by Implementing the Diketopyrrolopyrrole Chromophore. *Scientific reports* **2013**, *3*, 2446.
28. Qin, C.; Peng, W.; Zhang, K.; Islam, A.; Han, L., A Novel Organic Sensitizer Combined with a Cobalt Complex Redox Shuttle for Dye-Sensitized Solar Cells. *Organic Letters* **2012**, *14*, 2532-2535.
29. Marchena, M. J.; de Miguel, G.; Cohen, B.; Organero, J. A.; Pandey, S.; Hayase, S.; Douhal, A., Real-Time Photodynamics of Squaraine-Based Dye-Sensitized Solar Cells with Iodide and Cobalt Electrolytes. *The Journal of Physical Chemistry C* **2013**, *117*, 11906-11919.
30. Pradhan, A.; Morimoto, T.; Saikiran, M.; Kapil, G.; Hayase, S.; Pandey, S. S., Investigation of the Minimum Driving Force for Dye Regeneration Utilizing Model Squaraine Dyes for Dye-Sensitized Solar Cells. *Journal of Materials Chemistry A* **2017**, *5*, 22672-22682.
31. Pandey, S. S.; Inoue, T.; Fujikawa, N.; Yamaguchi, Y.; Hayase, S., Substituent Effect in Direct Ring Functionalized Squaraine Dyes on near Infra-Red Sensitization of Nanocrystalline Tio2 for Molecular Photovoltaics. *Journal of Photochemistry and Photobiology A: Chemistry* **2010**, *214*, 269-275.
32. Pandey, S. S.; Inoue, T.; Fujikawa, N.; Yamaguchi, Y.; Hayase, S., Alkyl and Fluoro-Alkyl Substituted Squaraine Dyes: A Prospective Approach Towards Development of Novel Nir Sensitizers. *Thin Solid Films* **2010**, *519*, 1066-1071.
33. Yuan, L.; Lin, W.; Zhao, S.; Gao, W.; Chen, B.; He, L.; Zhu, S., A Unique Approach to Development of near-Infrared Fluorescent Sensors for in Vivo Imaging. *Journal of the American Chemical Society* **2012**, *134*, 13510-13523.
34. Stender, B.; Völker, S. F.; Lambert, C.; Pflaum, J., Optoelectronic Processes in Squaraine Dye-Doped Oleds for Emission in the near-Infrared. *Advanced materials* **2013**, *25*, 2943-2947.
35. Völker, S. F.; Dellermann, T.; Ceymann, H.; Holzapfel, M.; Lambert, C., Synthesis, Electrochemical, and Optical Properties of Low Band Gap Homo-and Copolymers Based on Squaraine Dyes. *Journal of Polymer Science Part A: Polymer Chemistry* **2014**, *52*, 890-911.
36. Yum, J.-H.; Walter, P.; Huber, S.; Rentsch, D.; Geiger, T.; Nüesch, F.; De Angelis, F.; Grätzel, M.; Nazeeruddin, M. K., Efficient Far Red Sensitization of Nanocrystalline Tio2 Films by an Unsymmetrical Squaraine Dye. *Journal of the American Chemical Society* **2007**, *129*, 10320-10321.
37. Orbelli Biroli, A.; Tessore, F.; Pizzotti, M.; Biaggi, C.; Ugo, R.; Caramori, S.; Aliprandi, A.; Bignozzi, C. A.; De Angelis, F.; Giorgi, G., A Multitechnique Physicochemical Investigation of Various Factors Controlling the Photoaction Spectra and of Some Aspects of the Electron Transfer for a Series of Push–Pull Zn (Ii) Porphyrins Acting as Dyes in Dsscs. *The Journal of Physical Chemistry C* **2011**, *115*, 23170-23182.
38. Koumura, N.; Wang, Z.-S.; Mori, S.; Miyashita, M.; Suzuki, E.; Hara, K., Alkyl-Functionalized Organic Dyes for Efficient Molecular Photovoltaics [J. Am. Chem. Soc.

2006, 128, 14256− 14257]. *Journal of the American Chemical Society* **2008**, *130*, 4202-4203.
39. Yum, J.; Moon, S.; Humphry-Baker, R.; Walter, P.; Geiger, T.; Nüesch, F.; Grätzel, M.; d K Nazeeruddin, M., Effect of Coadsorbent on the Photovoltaic Performance of Squaraine Sensitized Nanocrystalline Solar Cells. *Nanotechnology* **2008**, *19*, 424005.
40. Yum, J.-H.; Walter, P.; Huber, S.; Rentsch, D.; Geiger, T.; Nüesch, F.; De Angelis, F.; Grätzel, M.; Nazeeruddin, M. K., Efficient Far Red Sensitization of Nanocrystalline Tio2 Films by an Unsymmetrical Squaraine Dye. *Journal of the American Chemical Society* **2007**, *129*, 10320-10321.
41. Zhang, L.; Cole, J. M., Dye Aggregation in Dye-Sensitized Solar Cells. *Journal of Materials Chemistry A* **2017**, *5*, 19541-19559.
42. Pradhan, A.; Saikiran, M.; Kapil, G.; Pandey, S. S.; Hayase, S. In *Parametric Optimization of Dye-Sensitized Solar Cells Using Far Red Sensitizing Dye with Cobalt Electrolyte*, Journal of Physics: Conference Series, IOP Publishing: 2017; p 012001.
43. Kang, X.; Zhang, J.; O'Neil, D.; Rojas, A. J.; Chen, W.; Szymanski, P.; Marder, S. R.; El-Sayed, M. A., Effect of Molecular Structure Perturbations on the Performance of the D–a− Π–a Dye Sensitized Solar Cells. *Chemistry of Materials* **2014**, *26*, 4486-4493.
44. Yum, J.; Moon, S.; Humphry-Baker, R.; Walter, P.; Geiger, T.; Nüesch, F.; Grätzel, M.; d K Nazeeruddin, M., Effect of Coadsorbent on the Photovoltaic Performance of Squaraine Sensitized Nanocrystalline Solar Cells. *Nanotechnology* **2008**, *19*, 424005.
45. Ananthakumar, S.; Ramkumar, J.; Babu, S. M., Semiconductor Nanoparticles Sensitized Tio2 Nanotubes for High Efficiency Solar Cell Devices. *Renewable and Sustainable Energy Reviews* **2016**, *57*, 1307-1321.
46. Lenzmann, F.; Krueger, J.; Burnside, S.; Brooks, K.; Grätzel, M.; Gal, D.; Rühle, S.; Cahen, D., Surface Photovoltage Spectroscopy of Dye-Sensitized Solar Cells with Tio2, Nb2o5, and Srtio3 Nanocrystalline Photoanodes: Indication for Electron Injection from Higher Excited Dye States. *The Journal of Physical Chemistry B* **2001**, *105*, 6347-6352.
47. Mathew, S.; Iijima, H.; Toude, Y.; Umeyama, T.; Matano, Y.; Ito, S.; Tkachenko, N. V.; Lemmetyinen, H.; Imahori, H., Optical, Electrochemical, and Photovoltaic Effects of an Electron-Withdrawing Tetrafluorophenylene Bridge in a Push–Pull Porphyrin Sensitizer Used for Dye-Sensitized Solar Cells. *The Journal of Physical Chemistry C* **2011**, *115*, 14415-14424.
48. Su, B.; Girault, H. H., Absolute Standard Redox Potential of Monolayer-Protected Gold Nanoclusters. *The Journal of Physical Chemistry B* **2005**, *109*, 11427-11431.
49. Namazian, M.; Lin, C. Y.; Coote, M. L., Benchmark Calculations of Absolute Reduction Potential of Ferricinium/Ferrocene Couple in Nonaqueous Solutions. *Journal of chemical theory and computation* **2010**, *6*, 2721-2725.
50. Chai, Q.; Li, W.; Wu, Y.; Pei, K.; Liu, J.; Geng, Z.; Tian, H.; Zhu, W., Effect of a Long Alkyl Group on Cyclopentadithiophene as a Conjugated Bridge for D–a− Π–a Organic Sensitizers: Ipce, Electron Diffusion Length, and Charge Recombination. *ACS applied materials & interfaces* **2014**, *6*, 14621-14630.
51. DeVries, M. J.; Pellin, M. J.; Hupp, J. T., Dye-Sensitized Solar Cells: Driving-Force Effects on Electron Recombination Dynamics with Cobalt-Based Shuttles. *Langmuir* **2010**, *26*, 9082-9087.

52. Kay, A.; Grätzel, M., Dye-Sensitized Core− Shell Nanocrystals: Improved Efficiency of Mesoporous Tin Oxide Electrodes Coated with a Thin Layer of an Insulating Oxide. *Chemistry of Materials* **2002**, *14*, 2930-2935.
53. Cui, Y.; Wu, Y.; Lu, X.; Zhang, X.; Zhou, G.; Miapeh, F. B.; Zhu, W.; Wang, Z.-S., Incorporating Benzotriazole Moiety to Construct D–a− Π–a Organic Sensitizers for Solar Cells: Significant Enhancement of Open-Circuit Photovoltage with Long Alkyl Group. *Chemistry of Materials* **2011**, *23*, 4394-4401.
54. Qu, S.; Wu, W.; Hua, J.; Kong, C.; Long, Y.; Tian, H., New Diketopyrrolopyrrole (Dpp) Dyes for Efficient Dye-Sensitized Solar Cells. *The Journal of Physical Chemistry C* **2009**, *114*, 1343-1349.
55. Feldt, S. M.; Wang, G.; Boschloo, G.; Hagfeldt, A., Effects of Driving Forces for Recombination and Regeneration on the Photovoltaic Performance of Dye-Sensitized Solar Cells Using Cobalt Polypyridine Redox Couples. *The Journal of Physical Chemistry C* **2011**, *115*, 21500-21507.
56. Daeneke, T.; Mozer, A. J.; Uemura, Y.; Makuta, S.; Fekete, M.; Tachibana, Y.; Koumura, N.; Bach, U.; Spiccia, L., Dye Regeneration Kinetics in Dye-Sensitized Solar Cells. *Journal of the American Chemical Society* **2012**, *134*, 16925-16928.
57. Khazraji, A. C.; Hotchandani, S.; Das, S.; Kamat, P. V., Controlling Dye (Merocyanine-540) Aggregation on Nanostructured Tio2 Films. An Organized Assembly Approach for Enhancing the Efficiency of Photosensitization. *The Journal of Physical Chemistry B* **1999**, *103*, 4693-4700.
58. Hoshikawa, T.; Yamada, M.; Kikuchi, R.; Eguchi, K., Impedance Analysis of Internal Resistance Affecting the Photoelectrochemical Performance of Dye-Sensitized Solar Cells. *Journal of the Electrochemical Society* **2005**, *152*, E68-E73.
59. Kapil, G.; Ohara, J.; Ogomi, Y.; Pandey, S. S.; Ma, T.; Hayase, S., Fabrication and Characterization of Coil Type Transparent Conductive Oxide-Less Cylindrical Dye-Sensitized Solar Cells. *RSC Advances* **2014**, *4*, 22959-22963.

CHAPTER SIX: Wide Wavelength Photon Harvesting: Implication of dye cocktail and surface Passivation

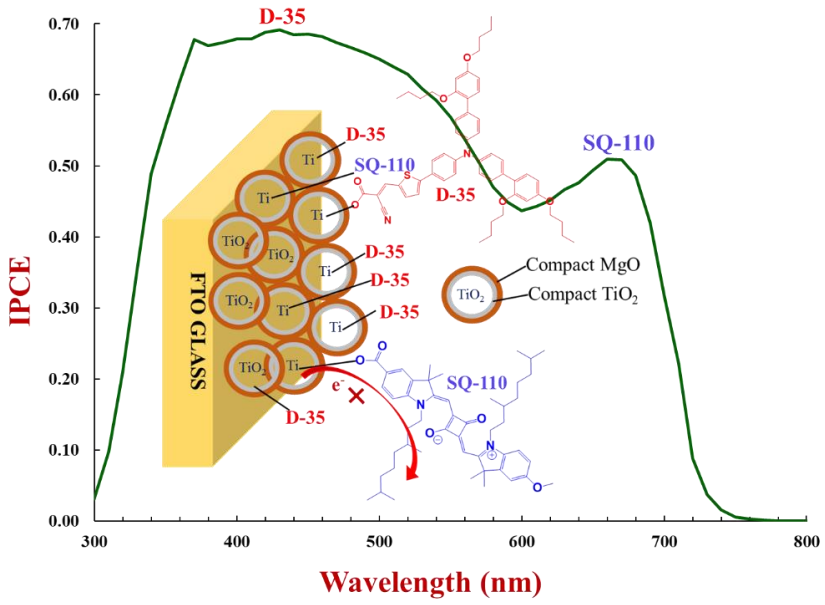

Anusha Pradhan, Sai Kiran Maryala, Gaurav Kapil, Shuzi Hayase and Shyam Sudhir Pandey, **Sol. Energy Mater Sol. Cells**. Volume 195, Pages 122-133

6.1 Introduction

Solar energy is one of the friendly energy sources to replace the traditional fossil fuel. Solar cells have therefore attracted enormous attentions to the pursuit for harnessing immense solar energy since it directly converts solar energy into most convenient electrical energy [1]. This led to the emergence of solar cells based on silicon, GaAs, CIGS, CdTe etc. that were already commercialized [2-4]. Moreover there is also high efficiency and extra stability in the $Cu(In,Ga)Se_2$ (CIGS) and CdTe. Due to their high tolerance to high-energy irradiation, which is even more superlative to conventional Si or GaAs solar cells these solar cell classes are suitable for space applications [5]. However, one of the bottlenecks for their large-scale implementation at common mass level remains a high cost of producing these solar cells. Research interest in next-generation solar cells Such as, thin film polymer solar cells, dye-sensitized solar cell (DSSCs) and recently entered perovskite solar cells have triggered a momentum [6], in which perovskite has achieved comparable efficiency with $Cu(In,Ga)Se_2$ (CIGS) and CdTe and silicon technology [7]. Therefore, DSSCs have emerged as one of the promising candidates in the world of acute need for the renewable energy owing to its environment friendly production, low cost of raw materials and ease of fabrication [8]. Since 1991, the report of novel nature as a mechanism with appreciable good photoconversion efficiency (PCE) over 7 %, the past two decades have attracted tremendous growth in research interests in DSSCs related to further enhancement in the PCE [9]. It is well known that the key elements for enhancing the Solar cell's PCE are the short-circuit current density (Jsc) and open-circuit voltage (Voc), where, Jsc is controlled by efficient and panchromatic photon harvesting, while Voc is administered by the judicious selection of mesoporous semiconductor and redox electrolyte. The amicable optimization results of the DSSC components like conducting substrates, mesoporous wideband semiconductors, sensitizing dyes and counter electrode materials directed in nearly quantitative photon harvesting in the visible wavelength region (400-700) with PCE exceeding 12% [10,11]. Sensitizing dyes are one of the key components of DSSC being light absorber and availability of good photon flux (>55 %) beyond the visible region is needed to be harvested in order to further enhance PCE [12]. This results in urgent attention to the design and development of efficient near infra-red (NIR) dyes and their incorporation with efficient visible sensitizers to boost the PCE through wide wavelength photon harvesting and accelerate DSSC marketing.

The primary sensitizer employed for DSSC was based on the Ruthenium complex with a good stability and brilliant PCE but however concerns arise in its cost and rareness of Ruthenium which suggested the emergence of metal free organic dyes [13]. Metal free organic dyes generally bear donor- π -bridge-acceptor (D-π-A) molecular frame allowing for the smooth π-π^* intramolecular charge transfer. This offers synthetic flexibility and versatility owing to a wide variation of D and A moieties and fine energy tuning [14]. In order to extend the optical absorption window in these dyes, electron acceptors like benzothiadiazole, benzotriazole, quinoxaline and diketopyrrolopyrrole etc. have been attempted in the D-A-π-A framework, but their very high aggregation tendency that resulted in PCE being impaired [15-18]. To achieve panchromatic photosensitization and result in a better performance, it has been widely used to blend two or more dyes (referred to as dye-cocktail) with the criteria of complementary light absorption leading to enhanced PCE [19-21]. Another most important component in DSSC is the electrolyte which controls the overall PCE by controlling the Voc where the value of it in DSSCs is given by the energy difference between the Fermi level of the wide band gap semiconductor and the redox energy level of the electrolyte. The first electrolyte used in DSSC was based on the iodine redox shuttles, but their corrosiveness, deep color and search for electrolytes with deeper redox potential focused the investigation on alternate redox electrolytes. Among the numerous electrolytes reported for DSSCs, redox electrolytes based on cobalt complexes have emerged as a strong candidate due to their relatively deeper redox potential leading enhanced PCE in particular through contribution from Voc [22]. Research on DSSCs utilizing cobalt-based electrolytes has perceived that compatibility, unlike iodine based redox electrolytes, is limited to selected sensitizers owing to their relatively bulky size causing slow ionic diffusion and increased recombination of charge. Iodine electrolytes with negative charges are repelled by TiO_2 nanoparticles with negative charges. On the other hand, the positively charged cobalt complex exhibits attractive interaction resulting to slow ion diffusion and enhanced recombination of charge [23]. Therefore, the TiO_2 surface must be passivated effectively either by long alkyl chains bearing dyes to hinder the approaching $Co^{3+/2+}$ to the uncovered TiO_2 surfaces along with post surface TiO_2 treatments before dye adsorption [24]. Therefore, in order to passivate the TiO_2 surface, various wide band gap metal oxides such as Al_2O_3, SiO_2, ZnO, MgO etc. were employed to form the compact metal oxide conformal layer in order to suppress the charge recombination due to transfer of back electrons [25-26].

The synthesis and characterization of a far-red sensitive Squaraine dye (SQ-110) described in the previous chapter is to be described in this chapter. This dye is a representative of NIR dyes with intense light absorption mainly in the solar spectrum of far-red region. Squaraine dye belongs to the D-A-D family and exists in the Zwitter-ionic [27]. This class of dye has the central squaric acid core as an electron acceptor and the logical utilization of various donor moieties enables the optical absorption window to be tuned from the visible the IR wavelength region [28]. The dye SQ-110 has been logically designed in this work with the primary necessity of introducing long alkyl chains to work effectively with the bulky and positively charged $Co^{3+/2+}$ ions [29]. As squaraine dyes only bear sharp and intense optical absorption in the far-red wavelength region, it used another complementary dye D-35 to make dye-cocktails to cover a wide wavelength region from visible to the far red [30]. Yan *et al* have also used D35 in cocktail with Dyenamo Blue in conjunction with Cobalt electrolyte in an interesting report. And it was observed that the PCE for dye cocktail (8.7%) was increased by 16 % compared with Dynamo Blue (7.3 %) [31].

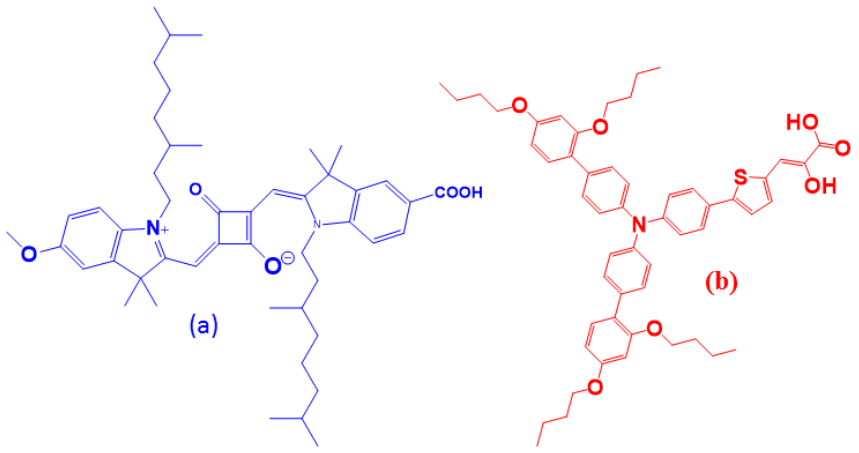

Figure 1. Molecular structure of a) far red SQ 110 dye and b) visible dye D35

More interestingly in this current work, there is a marked enhancement in the PCE from 3.6 % to 5.5 %, which was further improved to 7.2 % by compact metal oxide surface passivation. Implication of the compact layer of different types of metal oxides (single/multilayer) on both the conductive substrate and mesoporous TiO_2 have also been executed in order to probe their effect on the suppression on charge recombination and photovoltaic performance. Squaraine dyes are prone to the formation of dye aggregates that require an auxiliary coadsorber like chenodeoxycholic acid

(CDCA) to prevent the same and control the charge recombination. Beneficially, utilization of D-35 with SQ-110 in dye cocktail eliminated the use of the CDCA and hence serves as a dye co-adsorber, deaggregating agent and as well as light harvester in lower wavelength region for multiple roles. Molecular structure of sensitizing dyes used for present investigation has been shown in the Fig. 1.

6.2 Experimental

Synthesis

Unsymmetrical squaraine dye (SQ-110) along with their intermediates were synthesized as per the scheme shown in Fig. 2. The indole intermediate derivatives 5-Methoxy-2,3,3-Trimethyl-Indole and 5-Carboxy-2,3,3-Trimetyl-Indole were synthesized according to the method by Peng et al [32] and our earlier publication [33]. Cobalt complexes like $[Co(bpy)_3(PF_6)_2]$ and $[Co(bpy)_3(PF_6)_3]$ used for cobalt-based redox electrolyte preparation have been synthesized in accordance with our earlier publication [34].

*Synthesis of 5-methoxy-2,3,3- trimethyl 3H-indole [**1**]*

In a 300 ml round bottom flask, 8.6 g (50 mmol) of 4-methoxy phenyl hydrazine hydrochloride, 10.9 g (125 mmol) of 3-methyl-2-Butanone and sodium acetate (4.0 g, 50 mmol) in 80 mL of Glacial acetic acid were taken and refluxed for 18 hours. Under reduced pressure, solvent was removed and compound obtained was dissolved in chloroform and washed with water. Compound was concentrated and finally purified by flash column chromatography using Ethyl acetate and Hexane (1:1) as eluting solvent to obtain in 94 % yield, the 8.9 g of titled compound as brown viscous liquid. HPLC purity (>98%), and MALDI-TOF mass (measured m/z: 248.0 $[M+2]^+$; calculated m/z: 246.19) confirms the synthesis of this intermediate.

*6.2.1.2 Synthesis of 5-Methoxy-2,3,3-Trimethyl-1-Dimethyl-Octyl-Indolium Iodide [**2**]*

In a condenser-fitted round bottom flask, 3.6 g (18.4 mmol) of compound (**1**) and 1.5 equivalents (7.4 gm; 27.6 mmol) of 3,7-Dimethyl-1-Octyl-Iodide were dissolved in 50 mL nitromethane and refluxed for 48 hours. After the reaction was completed as confirmed by TLC, the solvent was completely evaporated and the compound was washed with ample diethyl ether to obtain the titled

product as an orange viscous liquid with a yield of 67% and a >98 % HPLC purity [FAB-MS Calculated, 330.28 and measured, 331.57 $(M+1)^+$].

*6.2.1.3 Synthesis of 5-Methoxy-2,3,3-Trimethyl-N-Dimethyl-octyl-Semisquaraine ethyl-ester[**3**]and its hydrolyzed product [**4**]*

4.6 g (10 mmol) of 5-Methoxy-2,3,3-Trimethyl-N-Dimethyl-Octyl-Indolium Iodide, 3mL (20 mmol) of 3,4-diethoxy-3-cyclobutene-1,2-dione, 1 mL of triethylamine (Et_3N) and 50 mL of ethanol were taken in a round bottom flask, refluxed and the progress of the reaction was monitored by TLC and HPLC. Upon the completion of reaction, the solvent was evaporated under reduced pressure and crude product was subjected to flash column chromatography using hexane/ethyl acetate with a 50% yield and 99 % purity of the desired semisquaraine dye (**3**) [FAB-MS (calculated: 453.29) and measured (454.74)]. This semiquaraine dye (**3**) was subjected to the hydrolysis of ester using NaOH in ethanol under reflux, which was finished in 30 min. Ethanol was removed, compound was neutralized with HCl and extracted with ethyl acetate and finally evaporated to obtain hydrolyzed semisquaraine dye (**4**) as orange-yellow solid in quantitative yield. [FAB-MS (calculated: 425.25) and measured (426.40)].

*6.2.1.4 Synthesis of 5-Carboxy-2,3,3-Trimethyl-Indole [**5**]*

In 120 mL of glacial acetic acid, 7.5 g (49 mmol) of 4-Hydrazino benzoic acid was dissolved. Then 6.8 g (78 mmol) of 3-Methyl-2-butanone and 8.3 g of sodium acetate were added and reaction mixture was refluxed for 8 hours. Acetic acid volume was reduced by evaporating under reduced pressure to 25 % followed by adding 9:1 water/methanol mixture. The solution was left for crystallization and finally filtered in order to obtain the product as light brown solid in 54% yield and >99 % purity as confirmed by HPLC and FAB-MS [(calculated: 203.24) and measured (204.0)].

*6.2.1.5 Synthesis of 5-Carboxy-2,3,3-Trimethyl-1-Dimethyl-OctylIndolium Iodide [**6**]*

2.0 g (9.6 mmol) of 5-Carboxy-2,3,3-trimethyl indole and 3.7 g (13.8 mmol) of 3,7-dimethyl-1-octyl iodide were dissolved in 40 mL acetonitrile in a round bottom flask fitted with a condenser and refluxed while monitoring the progress of the reaction by TLC. After the reaction had been completed in 48 hours, solvent was removed under low pressure and excess amount of ether was added for

precipitation followed by filtration. Titled compound (**6**) was obtained in 60 % yield and 99 % purity as pinkish white solid. The intermediate synthesis is confirmed by FAB-MS (calculated: 345.26) and (measured: 345.72).

6.2.1.6 Synthesis of squaraine dye SQ-110

In a condenser-fitted with round bottom flask, 330 mg (0.7 mmol) of intermediate (**6**) and 300 mg (0.7 mmol) of the hydrolyzed semisquaraine dye (4) were dissolved in 50 ml of benzene-butanol (1:1) mixture, which was refluxed with Dean-Stark trap for 18 hours. After the condensation was completed, the solvent was evaporated and the crude dye was purified using chloroform/methanol as eluting solvent employing silica gel flash column chromatography to obtain a dark blue solid in 82% yield and >98 % purity as confirmed by HPLC. Finally, high resolution FAB-MS confirmed the identity of the synthesized dye (calculated m/z: 750.4972; measured: 751.5012 $[M+1]^+$) and ^{1}H NMR (500 MHz, d6-DMSO): d/ppm = 7.95 (d, H-30), 7.92 (d, H-4), 7.34 (dd, H-6), 7.28 (d, H-27), 7.23 (dd, H-29), 6.95 (dd, H-7), 5.87 (s, H-10), 5.72 (s, H-23), 4.03 (t, 2H, H-13), 4.15 (t, 2H, H-35), 1.03 (s, 6H, H-11 & H-12), 1.13 (s, 6H, H-33 & H-34), 0.87 (m, 15H, H-20, H-21, H-22, H-42 & H-43).

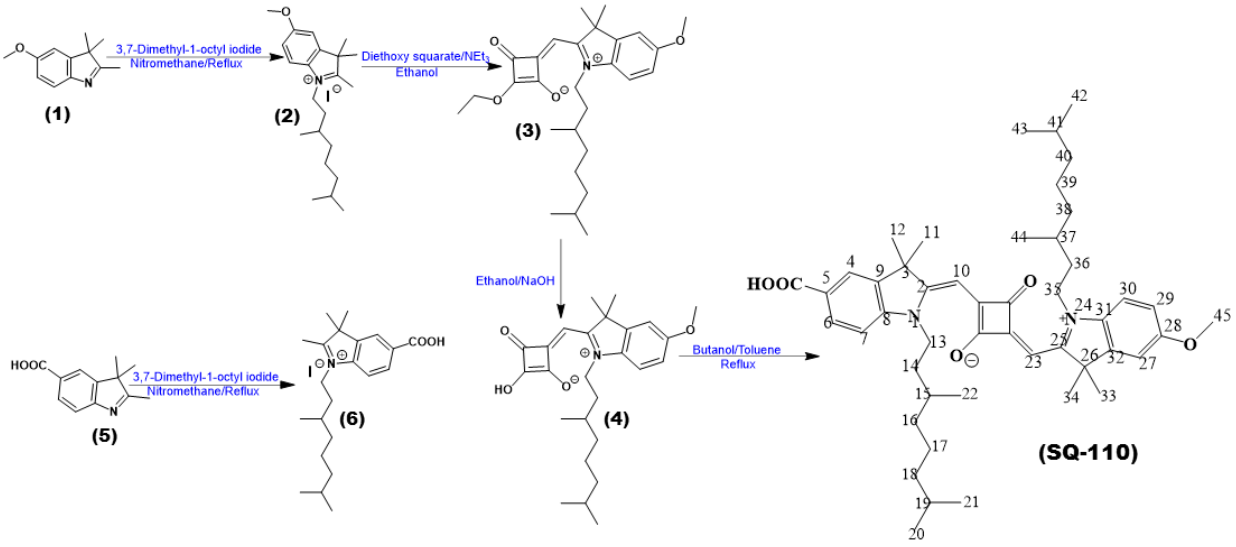

Figure 2. Depicts the schematic diagram for the synthesis of SQ 110.

6.2.1 Physical and Chemical Characterization of the dye

a. *Electronic Absorption Spectroscopy:* The dyes electronic absorption spectra is taken in both solution as well as on the solid state. 5 µM of the dye is subjected to UV-vis spectroscopy in ethanol solution to obtain the solution state spectra. For solid state absorption spectroscopy, 3 µm thick mesoporous TiO_2 coated glass was dipped in 100 µM of the ethanolic dye solution.

b. *Fluorescence Spectroscopy:* D35 and SQ 110 fluorescence emission spectrum with the same concentration as absorption spectroscopy in ethanol solution was measured using fluorescence spectrometer (JASCO FP-6600) to study its spectral overlap with the absorption spectrum of SQ-110. And fluorescence lifetimes for the dyes was taken in the solid state to monitor the dye interactions in close proximity. The dyes were allowed to adsorb about 4 µm thick on the thin film of ZrO_2. The lifetime was measured using a fluorescence lifetime measurement system (Quantarus Tau Model C-11370, Hamamatsu Photonics, Japan). Laser light source excited samples at 470 nm wavelength and fluoresecence decay for all the cases was measured at 680 nm.

c. *Calculation of Highest occupied molecular orbital (HOMO):* The HOMO energy level was estimated by photoelectron yield spectroscopy (PYS) (Bunko Keiki, model KV-205 HK, Japan). The solid dye powder was spread at the center on the FTO with carbon tape sufficient to reach the laser. The PYS was then conducted under high vacuum. The HOMO level value was derived from the yield curve plotted as an energy (eV) function. A tangent was drawn on the fitting curve, resulting in the energy level at the intersection point on the X axis. The lowest unoccupied molecular orbital (LUMO) energy was calculated by LUMO = HOMO + Eg relationship, where, Eg is the optical band gap. Eg has been estimated from the onset of solid state optical absorption.

d. *Electrochemical Impedance Spectroscopy:* The impedance of the DSSCs was measured using electrochemical impedance spectroscopy (EIS). A analysis was carried out using a frequency response analyzer (Solartron Analytical, 1255B), connected to a potentiostat (Solartron Analytical, 1287). A 10 mV AC perturbation of in the frequency range from 5×10^{-3} to 10^5 Hz was applied in similar ambient conditions to photovoltaic measurements in dark condition.

Fabrication of DSSCs

In this work, the conducting fluorine-doped tin-oxide glass (FTO) and mesoporous TiO_2 were treated with metal oxide for surface passivation. In the solution approach process, the compact oxide layer of TiO_2, MgO, Al_2O_3 and Nb_2O_5 etc. was formed from its respective precursor. The cut FTOs were sequentially washed for 15 min each under sonication with detergent, distilled water, acetone and isopropanol. In order to remove organic particles and dirt, the dried substrates were then treated with ozone plasma. Then the $TiCl_4$ surface treatment was executed by dipping the substrates at 70°C in 40 mM aqueous $TiCl_4$ solution for 30 min followed by sintering at 450°C for 30 min to form a very thin compact TiO_2 layer in few nanometers. [35]. The precursor like magnesium ethoxide and aluminium isopropoxide were used following the Kakiage et al protocol for the deposition of the compact layer of MgO and Al_2O_3 [36]. For the surface treatment with MgO, the substrates were dipped for 1 hour in the 50 mM solution of magnesium ethoxide in 2-propanol at 25°C, rinsed with distilled water and sintered at for 30 min at 500°C, while for the surface treatment with Al_2O_3, the substrates were dipped for 45 min in 25 mM of Aluminum isopropoxide in isopropanol at 25°C and then sintered under same condition. Similarly, surface treatment with Nb_2O_5 was executed for 30 minutes using 20 mM solution Niobium-butoxide in isopropanol at 25°C and then sintered.

DSSCs were fabricated using Ti-Nanoxide D/SP paste. It was coated to provide a thickness of about 6 µm by screen printing on the FTO glass plate followed by baking at 450^0C for 30 minutes. Mesoporous TiO_2 coated FTO substrates were then dipped in 0.2 mM ethanol solution of the respective dyes D-35, SQ-110 and their dye-cocktails at room temperature. The substrates were then allowed for 5 hours in case of the dye cocktails dye adsorption and 4 hours and 5 hours respectively with SQ-110 and D-35 dyes. Pt coated counter electrode was prepared by the thermopyrolysis of spin-coated solution of H_2PtCl_6 in isopropanol on FTO. The two electrodes were then affixed using a 25 µm hot melt polymer film as a spacer at 110^0C. Through the small void created while placing the spacers, electrolyte was injected finally sealed with a UV curable resin. Cobalt electrolyte was comprised of 0.22M $[Co(bpy)_3(PF6)_2]$, 0.033 M of $[Co(bpy)_3(PF6)_2]$, 0.2 M of tert.-butyl-pyridine and 0.1 M $LiClO_4$ in acetonitrile. A solar simulator equipped with a xenon lamp used as a source of simulated solar irradiation at 100 mW/cm^2, AM 1.5 G was used to measure photovoltaic performance. Using an amorphous Si photodetector, the light exposure power was calibrated. Photocurrent action spectra was measured using the action spectrum measuring system connected to the solar simulator with a constant photon flux of 1×10^{16}

photon/cm^2 in DC mode. The area of the cell was 0.25 cm^2, defined precisely using a black metal mask.

6.3 Results and Discussion

6.3.1. Optical Characterization

Sensitizing dyes D35 and SQ110 electronic absorption spectra were executed both in solution (ethanol) as well as on solid state where thin films of dyes adsorbed on 3 μm thick mesoporous TiO_2 are represented in the Fig. 3. It can be observed that D35 in ethanol solution exhibits optical absorption maximum (λ_{max}) at 444 nm with a molar extinction coefficient (ε) of 2.57×10^4 $dm^3mol^{-1}cm^{-1}$, contributed by π-π* transition from the dye`s Homo to LUMO. Interestingly, it can be seen that upon adsorption to TiO_2 surface, a good red shift occurred in λ_{max} by about 28 nm along with the spectral broadening, associated with the interaction of the acid group of the dye with the TiO_2 hydroxyl group leading to the formation of the ester linkage. This spectral broadening and red shift is attributed to the formation of aggregated dye molecules in the condensed state. Horiuchi et al in his report proved the formation of J aggregate using indolene class of dye D-205 on the mesoporous TiO_2 surface after adsorption [37]. Guo Chen et al report explains the good impact of J aggregate in squaraine dyes for higher Jsc and Voc in organic solar cells [38]. It can be observed that SQ-110 exhibits an intense and narrow absorption of light, mainly in the far-red wavelength (550-700) nm with absorption maxima and molar extinction coefficient (ε) of 650 nm and 2.16×10^5 $dm^3mol^{-1}cm^{-1}$ respectively, which is about one order of magnitude higher as compared to D-35. However, SQ-110 exhibits a vibronic shoulder around 600 nm, which is a distinctive characteristic of squaraine dyes. This vibronic shoulder is associated with molecular aggregation and get highly pronounced upon enhanced molecular aggregation. The blue shifted peak is due to the H-aggregation [39]. Observation of such a higher ε of SQ-110 is associated with the high electron density on the cyclobutene ring of the central squaric acid core when compared to D-35 [38]. The planarity of the molecular framework due to the extended π-conjugation promotes the transfer of delocalized intramolecular charge from the HOMO of donor moiety (indole ring) to the LUMO of the acceptor (squaric acid) resulting in to the high ε value [39-40].

It is observed that together with spectral broadening, the dye SQ-110 exhibits small bathochromically shifted λ_{max} at 655 nm. The planarity of the dye molecule facilitates the closer

approach of the dye molecules and leads to the formation of dye aggregates resulting in pronounced enhancement of vibronic shoulder to clearly visible peak around 610 nm upon dye adsorption on TiO_2 [41]. The behavior of spectral broadening in solid-state could be attributed to the deprotonation of the acidic anchoring group (–COOH) and its interaction with TiO_2 in the condensed state. Spectral broadening to a lower region of wavelength than monomeric absorption peak in solution and enhancement of vibronic shoulder intensity was attributed to the formation of H-aggregates in squaraine dyes [42, 43]. Thus, the ratio between H-aggregate band absorbance (around 610 nm) and the monomer band in solution (650 nm) can be used as indicator for the extent of H-aggregation [44]. In the work, demonstrated by Yum et al, it clearly states that the extent of squaraine dye H-aggregates on the mesoporous TiO_2 decreases as a function of added fraction of bulky CDCA in dye solution as co-adsorber which prevents the aggregation of dye. In the present case, as shown in the Fig. 3, SQ-110 displays a dye aggregation of 0.87 upon its adsorption to mesoporous TiO_2, which is slightly lower than Yum et al.`s 0.95 report. This could be attributed to the fact that the molecular structure of their squaraine dye possess one -methyl and one –octyl group as alkyl substituents while in SQ-110, there are two dimethyl-octyl branched and long alkyl chains hindering the self-aggregation of the dyes. A perusal of D-35 and SQ-110 absorption spectra, clearly confirms that they exhibit very good complementary electronic absorption, which turn out to be more pronounced in the solid-state. This suggests that dye cocktail of these two dyes is expected to provide much-improved light absorption in the entire region of visible wavelength when compared to the respective single dyes.

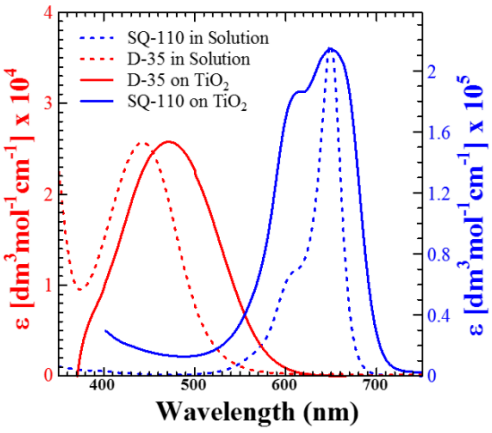

Figure 3. Electronic absorption spectra of D-35 and SQ-110 in solution and 3 µm thick transparent mesoporous TiO_2.

The Fig. 4 displays the electronic absorption spectra of D-35 and SQ-110 dye cocktail in various molar ratios in ethanol solution as well as on mesoporous TiO_2 film. The solution absorption spectra exhibit absorption in the range of 400 nm ~ 500 nm and 550 nm ~ 700 nm which is associated with the dyes D-35 and SQ-110, respectively. As expected, the increase in the ratio of D-35 leads to the corresponding decrease in the light absorption associated with SQ-110 and thus determines the need for higher D-35 fraction in the dye cocktail in consequence of its lower ε as shown in the Fig. 3. This also suggests the obvious need for D-35 and SQ-110 dye cocktails in 4:1 ratio to the appreciable wide photon-harvesting window which covers the entire region of visible wavelength. In the solution-state, absorption spectral feature of dye cocktail reflects the presence of both the dyes and is quantitatively governed by their ratio and relative ε values, which can be clearly seen in the Fig. 4. On the other hand, the more realistic representation of the situation occurring in the real DSSC is electronic absorption in the solid-state. This is controlled by the nature of dyes as previously reported by our group, their interaction with the TiO_2 surface and diffusion rate in the mesoporous TiO_2 are accountable [45, 46]. In the case of dye cocktails of two or more completely different dyes in particular, it becomes more important and clarifies the actual optimization and selection of optimum dye ratio in the cocktail.

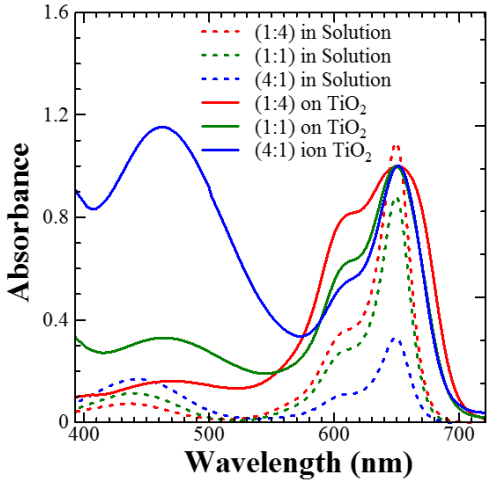

Figure 4. Electronic absorption spectra of different dye cocktail ratio of D-35 and SQ 110 in solution and 3 µm thick transparent mesoporous TiO_2.

To investigate differential spectral characteristics and optimize the ratio of individual dyes in the dye cocktail, other parameters such as concentration, temperature, thickness of the mesoporous TiO_2 layer and adsorption time of the dye were set to be 0.1 mM, 30°C, 3 µm and 30 min.,

respectively. Considering the absorption of dye cocktails at 460 nm and 650 nm corresponding to D-35 and SQ-110 respectively, we can predict the presence of respective dyes on the mesoporous TiO_2 (shown by solid lines). In this context, the normalized electronic spectra of solid-state absorption with respect to SQ-110 indicates the relative presence of respective dyes by comparing the relative absorbance at 460 nm and 650 nm associated with the D-35 and SQ-110, respectively taking in to consideration of their respective ε values. From the Fig. 4, it can be clearly seen that despite the presence of 20 % and 50 % of molar fractions of D-35 in (1:4) and (1:1) cocktail solutions, the presence of SQ-110 dye in 26 % and 64 %, respectively on the mesoporous TiO_2. On the other hand, in the dye cocktail ratio (4:1), there is appreciably good light absorption in the wavelength range of 400 nm-550 nm is associated with D-35 due it its highly enhanced extent (90 %) on the mesoporous TiO_2. About an order of magnitude lower ε than that of SQ-110, D-35 justifies the employment of this dye cocktail for facile photon harvesting by both dyes throughout the visible wavelength region. It is interesting and worth mentioning that the extent of H-aggregation of SQ-110 was estimated to be 0.81, 0.63 and 0.54 for the dye cocktails in ratio (1:4), (1:1) and (4:1) respectively, indicating a dual role of D-35 like co-adsorber and CDCA as dye de-aggregating agent in the dye cocktail for present investigation.

6.3.2 Energy Band diagram

Sensitizing dyes are one of the key essentials of the DSSC and their logical selection in terms of light absorption window and most importantly, energetics should be considered for the device operation. The dye`s LUMO energy level with respect to the conduction band (CB) of the mesoporous wide band gap semiconductor and its HOMO energy level with respect to the redox electrolyte should be carefully controlled for the facile injection of electron and regeneration of dye. To afford the necessary driving force for electron injection, the dye`s LUMO energy level should be sufficiently above the quasi Fermi level of TiO_2. Pandey et al., recently reported that a minimum energy barrier of 0.16 eV is necessary for the electron injection on utilizing different squaraine dyes from the excited dye molecules to the CB of TiO_2 [47]. The Fig. 5 exhibits the energy band diagram for various DSSCs components such as electrode, sensitizing dyes and electrolyte used for the present investigation. To construct the energy diagram, the report published by Gabrielsson et al., had provided with HOMO and LUMO energy levels of sensitizing dye D-35 [48]. Redox potential of cobalt electrolyte $Co(bpy)^{2+/3+}$ redox couple has been reported to be

0.57 V vs. NHE, which translates in to -5.00 eV with respect to the energy from vacuum level [49]. Considering the most negative quasi Fermi level corresponding to the flat band potential of TiO2 (0.7 V vs. SCE) the CB of TiO_2 was also considered and taken to be -4.00 eV [50].

The Fig. 5 shows that the LUMO level of squaraine dye SQ-110 is -3.22 eV with a driving force of 0.78 eV while it was even higher for D-35 at -2.99 eV with an energy difference of 1.01 eV from CB of TiO2. Such a high driving force ensures the facile electron injection from the photoexcited dye to the CB of TiO2. At the same time, the existence of energy cascade between sensitizing dyes and TiO2 CB provides an additional electron injection path from the excited state of D-35 to CB of TiO_2 through LUMO of SQ-110 stimulating the facile electron injection. On the other hand, there is a good congruence between the HOMO level of the dyes and the cobalt complex electrolyte redox potential, which designates the regeneration of oxidized dyes that competes the electron flow cycle while DSSC operates. It can be seen that SQ-110 carries an electron donating methoxy group together with the presence of two long and branched alkyl chains, leading to upward shift in the energy levels of this dye [51]. It is interesting to note that SQ-110 is being regenerated with the cobalt complex electrolyte used in this work, even with a very low driving force of 0.1 eV. Dye regeneration is justified by observing the good DSSC photovoltaic performances on using this dye alone as well as in the dye cocktails. Figure 6 exhibits the electronic absorption and fluorescence emission spectra of sensitizers in ethanol solution.

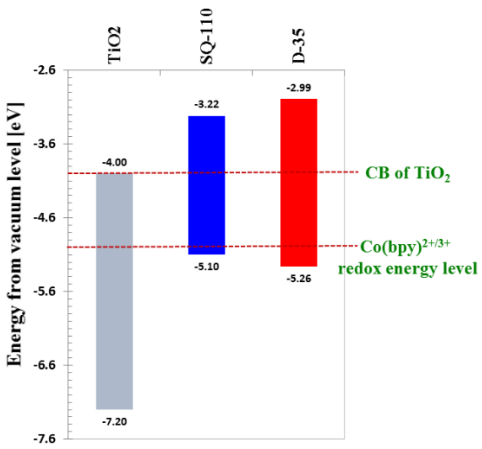

Figure 5. Energy band diagram of SQ-110 and D-35 against band energy of TiO_2 and the redox potential of Cobalt bipyridyl complex.

6.3.3 Energy Transfer and Time Resolved Fluorescence Studies

The band gap variation of the two dyes discussed in this chapter appealed us to study the energy transfer if possible in the two dyes. Approaches such as the use of fluorescence resonance energy transfer (FRET) for realization of FRET-enhanced DSSCs also gained momentum in the recent past [52, 53]. FRET has been reported to be a valuable tool for achieving a strong and wide photon harvesting of wavelengths leading to enhanced Jsc without having any adverse effects on the other key photovoltaic parameters like Voc and fill factor as advocated by Basham et al [54]. One of primary requirements for FRET to occur is to observe the significant overlap of the absorption spectrum of one sensitizer (acceptor) with emission spectrum of another sensitizer (acceptor). Since the band gap of D-35 is higher than SQ-110 as evident from the energy band diagram (Fig. 5), there might be a possibility of FRET between these two dyes, which may also be useful for FRET enhanced DSSCs especially fabricated with dye-cocktails in this work. Figure 6 (a) exhibits electronic absorption spectra of D-35 and SQ-110 and fluorescence emission spectrum of D-35 in ethanol solution. It can be perceived that D-35 displays a broad fluorescence emission from 550 nm-750 nm having emission maximum at 630 nm.

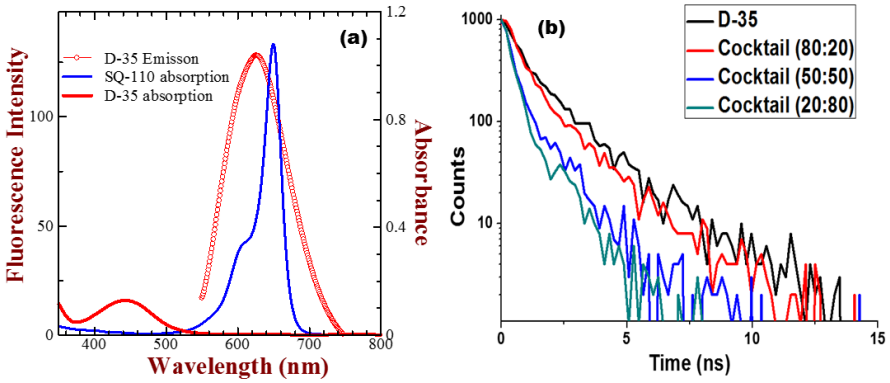

Figure 6: Includes the absorption spectra of SQ-110 and D-35 along with the emission spectra of D-35 (a) the lifetime plot of the various ratio of dye cocktails from TRPL (b)

Simultaneously, there is very good overlap between the emission spectrum of D-35 with the absorption spectrum of SQ-110 signifying the possibility of FRET by transfer of energy from the

excited state of D-35 to the SQ-110 provided that dyes should be in the close vicinity. Wide band gap ZrO2, had been used to provide close vicinity between the sensitizers and avoid the complexity due to electron injection. A very large band gap (5.0 eV) of ZrO_2 prevents the electron injection and enables us to probe the time resolved fluorescence decays while keeping the adsorbed dyes in the close proximity [55]. Dyes were adsorbed at room temperature for 1 hour from their respective 0.1 mM ethanol solutions (D-35and dye cocktails) on the mesoporous ZrO_2 (4 μm) to ensure adequate dye load. Time resolved fluorescence investigation were then executed with these dye adsorbed ZrO_2 film as shown in the Fig. 6(b) and the summary of the excited-state lifetime and its components obtained after 2nd order fitting of the decay curve are displayed in the table 1. A perusal of this figure and table 1 clearly indicates that fluorescence decay becomes faster after an increase in the mole fraction of average lifetime of SQ-110 which has been found to be decreased from 1.58 ns for D-35 only to 0.58 ns for dye cocktail having D-35 and SQ-110 in 1:4 ratio. Patwari et al., also reported a similar type of FRET observation with porphyrin and squaraine dyes dye cocktail system [56]. This could be explained considering the occurrence of FRET between the higher band gap dye D-35 and relatively narrow band gap dye SQ-110 which are working as donor and acceptor respectively. This lead to possibility of FRET enhanced photon to light conversion in the present dye cocktail system. For DSSCs fabricated using D-35 and SQ-110 dye cocktails, there is dual possibility of electron injection from excited dye molecules to TiO2 and energy transfer from the D-35 to SQ-110.

Table 1. Excited-state lifetime for the D-35(donor) adsorbed on ZrO_2 in the absence and presence the SQ-110 (acceptor) in different ratios.

Dye Cocktail (D-35:SQ-110)	$<\tau>$ (ns)	τ_1 (ns)	τ_2 (ns)
100:0	1.58	0.96	2.46
80:20	1.27	0.67	1.99
50:50	0.77	0.38	1.43
20:80	0.58	0.21	1.03

6.3.4 Photovoltaic Characterization

Various reports propose that the usage of cobalt electrolyte in DSSCs requires careful consideration regarding photoanode fabrication in terms of use of relatively thin mesoporous TiO_2 layer and surface passivation of both conducting substrate and mesoporous TiO2 as a result of

enhanced charge recombination [57]. A compact layer of wide band gap metal oxides delays the charge recombination between the TiO_2 injected electrons, oxidized dyes as well as electrolytic species. The surface treatment both on FTO and mesoporous TiO_2 is necessary to acquire the optimum DSSC performance has been widely accepted and verified by our group, based on single outer-sphere electron transfer of cobalt redox electrolytes [58]. In this chapter, three different most widely used metal oxides such as TiO_2, MgO and Al_2O_3 were used before dye adsorption by solution based approaches for the surface passivation of mesoporous TiO_2. As schematically shown in the Fig. 7, the mesoporous TiO_2 surface was passivated by single as well as multilayers of compact metal oxides to investigate the effect of surface passivation on the final device performance.

6.3.4.1 Surface passivation of mesoporous TiO_2 using different metal oxides

Different surface treatments for DSSCs have been employed for mesoporous TiO_2 with different metal oxides. For this purpose, DSSCs were fabricated using D-35 and SQ-110 (8:2) dye cocktail with sensitized photoanode based on superior spectral sensitivity as shown in the Fig. 4. FTO surface treatment was executed using aqueous $TiCl_4$ to form compact TiO_2 as a charge recombination blocking layer (CRBL) and retained the same in all of the cases.

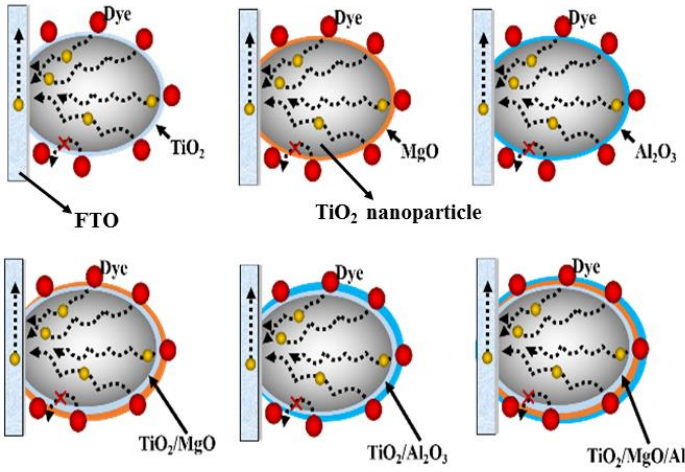

Figure 7. Schematic diagram of the various surface passivation layer discussed in this chapter.

In the Fig. 8 (a), photovoltaic characteristics of DSSCs fabricated using photoanodes, where mesoporous TiO_2 was passivated with compact layer of diverse metal oxides has been shown along with their photovoltaic parameters summarized in the table 2. With a power conversion efficiency

(PCE) of 4.8 % under simulated solar irradiation, surface passivation using $TiCl_4$ was employed to form compact TiO_2 which was par excellent amongst the different metal oxides used.

Table 2. Photovoltaic parameters for the DSSCs utilizing photoanodes fabricated using surface passivation of mesoporous TiO_2 by different type of compact metal oxides.

Surface treatment	Jsc (mA/cm^2)	Voc (V)	FF	Efficiency (%)
$TiCl_4$	10.36	0.67	0.68	4.78
MgO	8.90	0.72	0.68	4.45
Al_2O_3	4.65	0.66	0.49	1.52

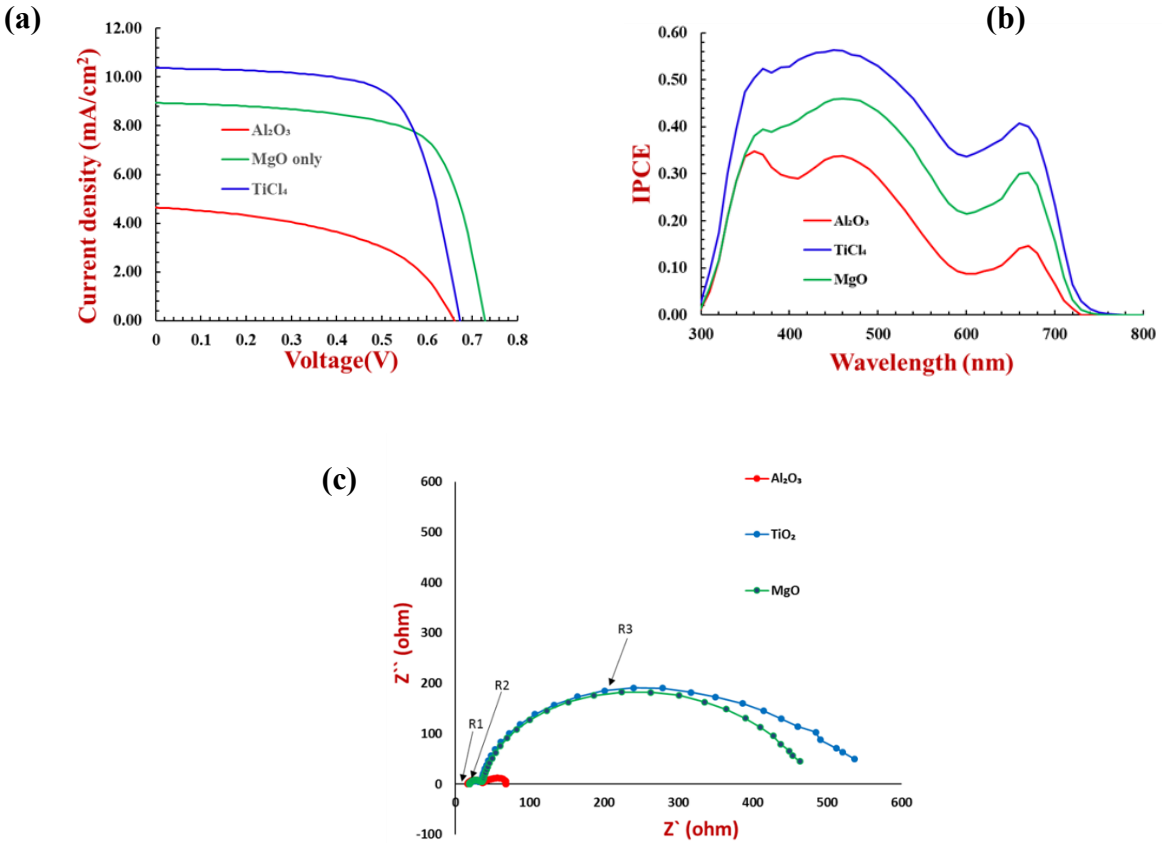

Figure 8: a) I-V plot b) Incident photocurrent action spectra and c) Nyquist plot of the DSSCs with various metal oxide mono surface passivation of mesoporous TiO_2.

Surface passivation using compact MgO although it works as better CRBL as observed by enhanced open circuit voltage (Voc) but hampered short-circuit current density (Jsc) ultimately leads to a decrease of 4.4 % overall PCE as shown in the table 2. In the current work, compact Al_2O_3 as CRBL was not found to be good owing to drastic decrease in Jsc and no benefit from Voc

enhancement. Thus, TiO_2 exhibits the optimum performance as a single compact oxide CRBL, and this could be attributed to the dual role of compact TiO_2. Firstly, there is an enhancement in Jsc, which is credited to the increased surface area in order to absorb more dye and secondly, the ultrathin TiO_2 layer functions as a CRBL towards the transfer of back electron [35]. Photocurrent action spectra which is otherwise known as incident photon variation to current conversion efficiency (IPCE) as a function of wavelength was also measured and displayed in the Fig. 8(b). Spectral response clearly reveals that the enhanced photosensitization by both dyes for the passivated photoanodes with compact TiO_2 and is consistent with the results of improved Jsc as shown in the Fig. 8(a). To further confirm the differential surface passivation by different layers of metal oxides, EIS was executed by applying a forward bias voltage near to open-circuit voltage in each case as shown in Fig. 8 (c).

The EIS pattern can be roughly divided into three regions, R1- resistance due to FTO/TiO_2 interface, R2- resistance associated with the counter electrode charge transfer and R3- resistance to recombination at the TiO_2/dye/electrolyte interface [59, 60]. There was almost no difference in the value of R1 for each device, which is evident in all cases due to the same photoanode according to the result obtained. Similarly, no significant difference was observed for R2, therefore, the major role was due to R3, which can be clearly answered by the difference in passivation by metal oxide layers. TiO_2 and MgO therefore, clearly exhibits better passivation then Al_2O_3, which was also reflected in I-V characteristics.

Considering the advantages and disadvantages of TiO_2 and MgO compact single layer surface passivation, it raised the curiosity to probe the influence of multiple layers of compact oxide surface passivation on the photovoltaic performance of DSSCs thus fabricated. In order to accomplish this, first $TiCl_4$ surface treatment was performed on both FTO and mesoporous TiO_2 followed by second surface passivation of the mesoporous TiO_2 by MgO and Al_2O_3 to make bilayer surface treated electrode using magnesium ethoxide and Aluminum isopropoxide, respectively. Another set of photoanodes were also fabricated using tri-layer surface passivation of the mesoporous TiO_2 where, TiO_2/MgO treated substrate was once more subjected to Al_2O_3 surface treatment, as shown schematically in the Fig. 7. These multilayer surface treated electrodes were finally sensitized with the dye cocktail ratio (4:1) of dyes D-35 and SQ-110 respectively for the preparation of respective photoanodes and DSSCs. After simulated solar irradiation, photovoltaic characteristics and

photocurrent action spectra of these DSSCs were recorded as showcased in the Fig. 9. Simultaneously, table 3 summarizes the photovoltaic parameters derived from the photovoltaic measurement. Figure 9(a) and table 3, clearly depicts that a bilayer surface treatment consisting of TiO_2/MgO on mesoporous TiO_2 outperforms when compared to bi-layer (TiO_2/Al_2O_3) and tri-layer (TiO_2/MgO/Al_2O_3) surface treatments. A pronounced Jsc enhancement of up to 12.50 mA/cm^2 in TiO_2/MgO treated photoanodes was witnessed from 10.36 mA/cm^2 and 8.90 mA/cm^2 for TiO_2 and MgO single surface treatments, respectively (Fig. 8, table 2). compared to other surface treatments , this increased Jsc was further supported by photocurrent action spectra as shown in the Fig. 9(b), for TiO_2/MgO bilayer surface devices, where photon-harvesting corresponding to both the sensitizer were increased. This reveals the superiority of these TiO_2/MgO bilayer surface treatments, which could be attributed to the facile electron tunneling charge injection rather than recombination [61].

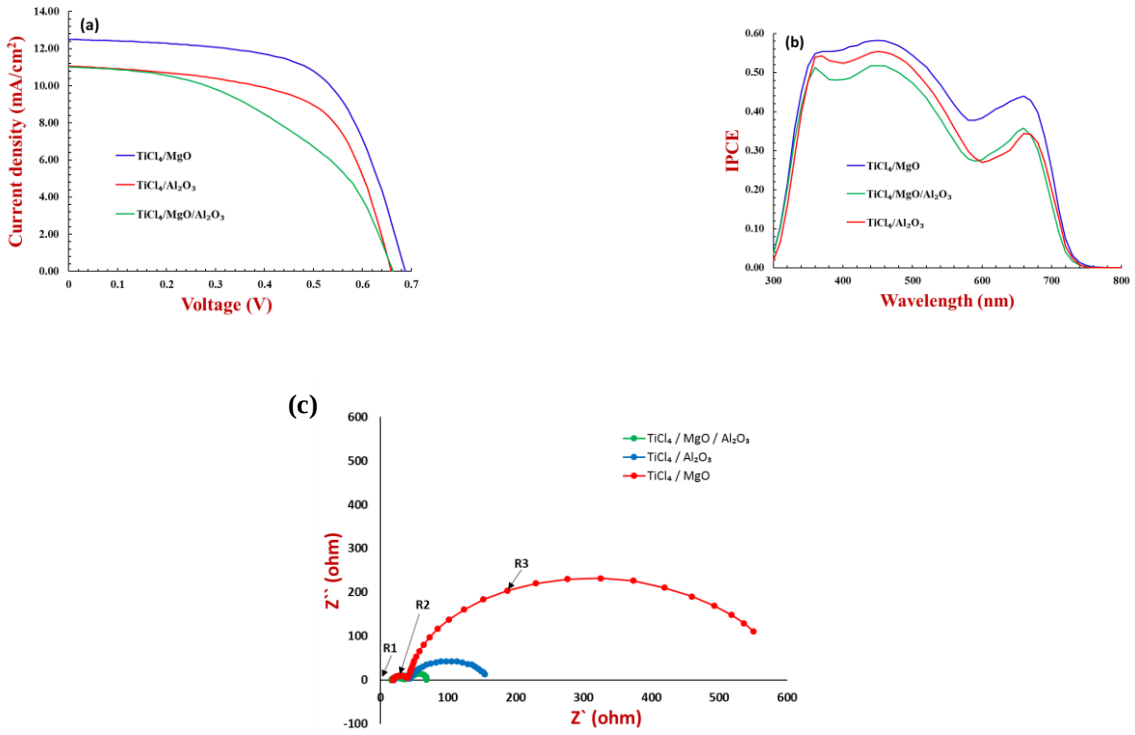

Figure 9: a) I-V plot b) Incident photocurrent action spectra and c) Nyquist plot of the DSSCs with various bilayer surface passivation of mesoporous TiO_2

On the contrary, for bilayer or tri-layer surface treatments, the treatment with aluminum isopropoxide to form compact Al_2O_3 on the mesoporous TiO_2 photoanode based DSSCs did not perform well. Poor performance of the TiO_2/MgO/Al_2O_3 tri-layer surface passivation could be

associated with the excessive thickness of the compact layer on the mesoporous TiO_2 with highly suppressed fill factor (FF) of 0.47 as displayed in the table 3. In addition, to further support the role of passivation and its consequence on the observed photovoltaic performance of the fabricated solar cells, EIS measurements were also carried out and results are exhibited in Fig. 9(c). A bilayer combination of TiO_2/MgO surface treatment was more effective passivating than TiO_2/Al_2O_3 bilayer. Furthermore, it was perceived that a drastic reduction in value of R3 occurred when a third layer of Al_2O_3 was deposited on top of TiO_2/MgO. This indicates that the alumina layer is not effective for surface passivation, rather works like as an insulator opposing the forward injection process leading to poor performance of solar cell as clearly reflected in the I-V characteristics.

Table 3. Photovoltaic parameters for the DSSCs utilizing photoanodes fabricated by surface passivation of mesoporous TiO_2 using multiple layer of different type of compact metal oxides. Data shown in the parentheses are average values and standard deviations in the photovoltaic parameters for four independent devices.

Surface treatments	Jsc (mA/cm^2)	Voc (V)	FF	Efficiency (%)
TiO_2/MgO	12.50	0.68	0.63	5.40
TiO_2/Al_2O_3	11.06	0.65	0.61	4.48
TiO_2/MgO/Al_2O_3	11.01	0.66	0.47	3.43

6.3.4.2 Effect of FTO surface passivation

In the previous section, the surface passivation of mesoporous TiO_2 layer was executed by various metal oxides keeping $TiCl_4$ treated FTO as most widely used conducting substrate. Encouraged by optimized surface passivation of mesoporous TiO_2 with compact TiO_2/MgO bilayers, a single and bilayer consisted compact TiO_2 and Nb_2O_5 surface passivation of conducting FTO substrate was also employed. To accomplish this, we employed four different variations which consists of single layer as well as bilayer surface treatment of FTO such as TiO_2, Nb_2O_5, TiO_2/Nb_2O_5 and Nb_2O_5/TiO_2 with aqueous $TiCl_4$, and Niobium butoxide in isopropanol. Nb_2O_5 has been reported to be an isolating barrier due to its very large band gap and functions as not only CRBL but also plays a significant role in the upward shift of TiO_2 conduction band edge [62]. Using an optimized TiO_2/MgO bilayer surface treatment of mesoporous TiO_2 subsequently dye adsorption with dye cocktail of D-35 and SQ-110 in 4:1 ratio, these surface treated FTO substrates were utilized for the photoanode fabrication. The thus, fabricated photovoltaic characteristics of DSSCs are shown in Fig. 10 along with their summarized photovoltaic parameters in table 4.

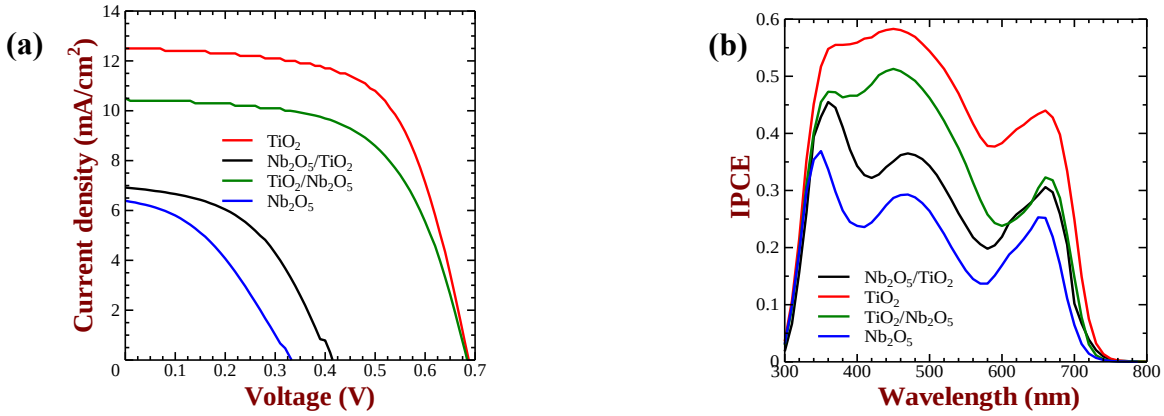

Figure 10: a) I-V plot b) Incident photocurrent action spectra of the DSSCs with various FTO surface passivation.

A perusal of this figure and table clearly confirms that single layer of compact TiO_2 on FTO delivered the best photovoltaic performance with a Jsc of 12.50 mA/cm^2, Voc of 0.68 V, FF of 0.63 leading to PCE of 5.40 %. On the other hand, FTO forming Nb_2O_5 direct surface treatment performed poorly, where all parameter of the device decreased drastically. Such a poor performance of DSSCs through FTO surface treatment with Nb_2O_5 indicates a very strong interaction between Niobium butoxide with FTO. This strong interaction between FTO and Nb_2O_5, probably led to the establishment of very thick insulating barrier. This was further verified by device performance recovery when Nb_2O_5 layer in the bilayer device was coated to compact TiO_2 layer on FTO. It probably seems that we had taken too high concentration of niobium butoxide solution (20 mM) based on procedure of MgO and Al_2O_3, which may not be similarly applicable for FTO surface treatments.

Table 4. Photovoltaic parameters for the DSSCs utilizing photoanodes fabricated by surface passivation by surface passivation of FTO using single and bilayers of compact metal oxides.

Surface treatments	Jsc(mA/cm^2)	Voc (V)	FF	Efficiency (%)
Nb_2O_5 only	6.38	0.33	0.38	0.81
Nb_2O_5/TiO_2	6.90	0.41	0.47	1.35
TiO_2 only	12.50	0.68	0.63	5.40
TiO_2/Nb_2O_5	10.44	0.68	0.60	4.29

6.3.4.3 Influence of dye cocktail ratio and top scattering layer

Results on surface passivation optimization of both FTO and mesoporous TiO_2 have indicated that single layer of compact TiO_2 and a bilayer of TiO_2/MgO surface treatments are optimum for the surface passivation of FTO and mesoporous TiO_2, respectively. As a final optimization, TiO_2 (PST-400) was further applied on TiO_2/MgO surface passivated mesoporous TiO_2 for the fabrication of photoanode with 3 μm scattering layer of large particle size (400 nm). DSSCs were then fabricated by sensitizing the mesoporous TiO_2 with dyes D-35, SQ-110 and their dye cocktails in diverse molar ratios such as (1:4), (1:1) and (4:1) together with $Co(bpy)^{2+/3+}$ redox electrolyte. The Fig. 11 displays, the photovoltaic characteristics of DSSCs thus prepared after simulated solar irradiation with their photovoltaic parameters summarized in the table 5.

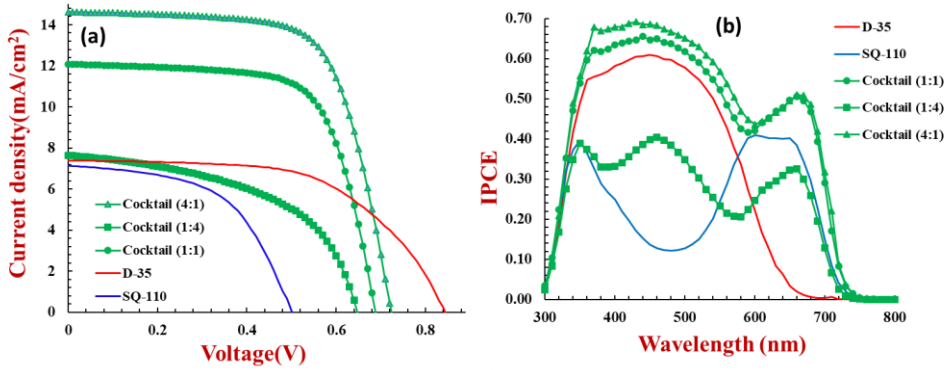

Figure 10: a) Current-voltage and b) incident photocurrent action spectra of the DSSCs with various dye cocktail ratio.

A perusal of photon harvesting by D-35 and SQ-110 individual dyes which are displayed in the Fig. 11(b) clearly supports that they complement each other and their dye cocktail results in wide wavelength range photon harvesting throughout the visible wavelength region, in accordance with solid-state electronic absorption spectra shown in the Fig. 4. D-35 has been widely reported as well as observed in this current work that it is a good sensitizer working well with cobalt complex electrolytes (Fig. 11b, table 5) but its narrow photon harvesting window needs its association with another far-red to NIR photon harvesting dye in order to have photon harvesting in the wide wavelength region. Despites an intense research on visible light harvesting dyes in combination with cobalt redox shuttle as an electrolyte, there are very few DSSCs reports based on NIR dyes in combination with cobalt complex electrolyte [63].

Table 5. Photovoltaic parameters for the for the DSSCs fabricated utilizing optimized surface passivated photoanodes sensitized with D-35, SQ-110 and their dye cocktails in different molar ratios. Data shown in the parentheses are average values and standard deviations in the photovoltaic parameters for four independent devices.

Sensitizing Dyes	Jsc (mA/cm^2)	Voc (V)	FF	Efficiency (%)
SQ 110	7.13	0.50	0.54	1.92
D-35	7.39	0.84	0.58	3.63
D-35:SQ 110 (1:4)	7.63	0.65	0.51	2.53
D-35:SQ 110 (1:1)	12.07	0.68	0.68	5.70
D-35:SQ 110 (4:1)	14.61	0.72	0.68	7.23

In fact, we have also challenged this issue previously, with the use of model squaraine dyes in combination with cobalt electrolyte but very poor efficiency (<0.2 %) specified the prerequisite for strict surface passivation along with appropriate molecular design of the sensitizers [64]. The data represented in Fig. 11(a) and table 5 conveys that our newly designed SQ-110 functions well with cobalt electrolyte having PCE of 1.92 % along with photon harvesting mainly in the far-red region. This could be accredited to the effective surface passivation of both FTO and TiO_2 together with the introduction of two branched long alkyl chain to assist with the additional TiO_2 surface passivation thus prohibiting the charge recombination between TiO_2 injected electrons and oxidized electrolyte [65].

It is remarkable to perceive from Fig. 11(a, b) and table 5 that the individual dyes complement each other in the dye cocktail sensitized photoanodes where, lower Voc of SQ-110 in the presence of D-35 is enhanced. At the same time, due to presence of SQ-110 photon harvesting in the far-red region which was absent in D-35 is significantly improved. Enormous differences in the molar extinction co-efficient of constituent dyes D-35 and SQ-110 as showcased in the figures (3, 4) evidently directs the necessity for their optimum ratio in the dye cocktail to maximize their advantages. A dye cocktail solution of D-35 and SQ-110 in (1:4) molar ratio although it exhibits photon harvesting in both the wavelength region visible (due to D-35) and far-red (due to SQ-110) but overall PCE was only 2.53 %, although higher than SQ-110 (1.92 %) and lower than D-35 (3.63 %). This could be accredited to the

comparatively smaller extent (26 %) of D-35 molecules that hamper the photon harvesting in lower wavelength region, which is clear from the solid-state absorption spectra portrayed in the Fig. 4. In the section 3.1 it was discussed that increasing the mole fraction of D-35 in the dye cocktails ratio with (1:1) and (4:1) resulted in significant increase of up to 64% in its fraction and 90 % on the mesoporous TiO_2, respectively. Simultaneously, increasing the ratio of D-35 not only resulted in facile photon harvesting in the 300–550 nm but also led to a pronounced suppression of SQ-110 H-aggregation from 0.81 and o.54 with the dye cocktail in ratio (4:1) and (1:4) correspondingly. This prominent suppression of SQ-110 dye aggregation by D-35 along with its higher extent presence (90 %) in the dye cocktail led to the best 7.23 % photovoltaic performance under simulated solar irradiation. This enhanced DSSC performance using the (4:1) D-35 and SQ-110 dye cocktail is associated with both the enhanced Jsc as well as Voc (table 5) and photon harvesting in entire visible wavelength region associated with the respective dyes (Fig. 11b).

Here one can argue that why in the dye cocktails in particular with the ratio (1:1) and (4:1) photon harvesting is higher than respective individual dyes as depicted by photocurrent action spectra in the Fig. 11(b). This could be attributed to suppression of SQ-110 dye aggregation by D-35 and promotion of J-aggregation on the mesoporous TiO_2 in D-35 by SQ-110. Although the aggregation behavior of D-35 on the TiO_2 surface is still being debated but based on experimental and theoretical quantum chemical calculations, it has been demonstrated that J-aggregate formation by D-35 and small butoxy substituent is not sufficient to prevent the aggregation of dye even using D-35 and CDCA in 1:50 ratio [66, 67]. J-aggregate formation is expected to broaden the spectral response and might be responsible for the enhanced Jsc. In the current case, dye cocktails, SQ-110 appears to work as J-aggregate promoter like CDCA resulting in increased photon harvesting associated with D-35. On the other hand, D-35 has a double role as a complementary light harvesting co-sensitizer as well as SQ-110 dye H-aggregate preventer leading to enhanced photon harvesting in the far-red region compared to the single dye. Another reason could be associated with the enhanced fluorescence energy transfer from D-35 to SQ-110 as discussed earlier in the section 3.4. In addition to increasing light harvesting window, the presence of both dyes favours the incidence of FRET from D-35 to SQ-110 leading to substantial photocurrent increase. In fact, the report by Patwari et al, also states that enhancement primarily in Jsc for the DSSCs fabricated using porphyrin and squaraine dye cocktails without affecting the Voc which was explained taking in to consideration that FRET promoted

enhanced photon harvesting [56]. Ogura et al and Lin et al, also reported prominent photon harvesting by dye cocktails when compared to their respective individual dye counterparts [68, 69].

6.4 Conclusion

A novel far-red sensitive unsymmetrical squaraine dye (SQ-110) with direct-carboxy functionalized indole ring and branched long alkyl substituent was successfully synthesized from their respective intermediates, characterized and used as sensitizer towards application in the DSSC using cobalt complex redox electrolyte. A commercial dye D-35 having complementary light absorption with SQ-110 was employed to sensitize the mesoporous TiO_2 with the dye-cocktails in different molar ratios resulting in not only improved photon harvesting but also improved wide-wavelength photon harvesting from visible to far-red region of the spectrum compared to individual constituent dyes. Considering the prominence of surface passivation for charge recombination suppression particularly in the DSSCs based on cobalt electrolytes, both FTO as well as mesoporous TiO_2 surface passivation has been systematically performed and their implication on the photovoltaic performance have been inspected in detail. It has been demonstrated that in order to meet the requirement of optimum DSSC performance, a compact TiO_2 on FTO and a bilayer TiO_2/MgO surface passivation was necessary. A DSSC fabricated with dye cocktail of D-35 and SQ-110 in (4:1) ratio as sensitizer in combination with $Co(bpy)^{2+/3+}$ redox electrolyte displayed a Jsc of 14.61 mA/cm^2, Voc of 0.72 V and FF of 0.68 resulting in PCE of 7.23 %, much higher than the individual component dyes. Mutual control of dye aggregation, complementary photon harvesting and FRET interactions are key factors responsible for synergistically enhanced photon harvesting in the wide wavelength region are found in present dye-cocktail DSSCs. Interestingly, successful dye regeneration of SQ-110 even with a very low driving force of 0.10 eV specifies the possibility of further molecular design of novel sensitizers with photon harvesting in the NIR wavelength region.

References

1. Demirbas, A., Potential Applications of Renewable Energy Sources, Biomass Combustion Problems in Boiler Power Systems and Combustion Related Environmental Issues. *Progress in Energy and Combustion Science* **2005**, *31*, 171-192.
2. Strümpel, C.; McCann, M.; Beaucarne, G.; Arkhipov, V.; Slaoui, A.; Švrček, V.; del Cañizo, C.; Tobias, I., Modifying the Solar Spectrum to Enhance Silicon Solar Cell

Efficiency—an Overview of Available Materials. *Solar Energy Materials and Solar Cells* **2007**, *91*, 238-249.
3. Miles, R. W.; Zoppi, G.; Forbes, I., Inorganic Photovoltaic Cells. *Materials Today* **2007**, *10*, 20-27.
4. Britt, J.; Ferekides, C., Thin ‐ Film Cds/Cdte Solar Cell with 15.8% Efficiency. *Applied Physics Letters* **1993**, *62*, 2851-2852.
5. Tiwari, A. N.; Romeo, A.; Baetzner, D.; Zogg, H., Flexible Cdte Solar Cells on Polymer Films. *Progress in Photovoltaics: Research and Applications* **2001**, *9*, 211-215.
6. Park, S. H.; Roy, A.; Beaupré, S.; Cho, S.; Coates, N.; Moon, J. S.; Moses, D.; Leclerc, M.; Lee, K.; Heeger, A. J., Bulk Heterojunction Solar Cells with Internal Quantum Efficiency Approaching 100%. *Nature Photonics* **2009**, *3*, 297.
7. Yin, W.-J.; Shi, T.; Yan, Y., Unique Properties of Halide Perovskites as Possible Origins of the Superior Solar Cell Performance. *Advanced Materials* **2014**, *26*, 4653-4658.
8. McConnell, I.; Li, G.; Brudvig, G. W., Energy Conversion in Natural and Artificial Photosynthesis. *Chemistry & Biology* **2010**, *17*, 434-447.
9. O'Regan, B.; Grätzel, M., A Low-Cost, High-Efficiency Solar Cell Based on Dye-Sensitized Colloidal Tio2 Films. *Nature* **1991**, *353*, 737.
10. Zhang, B.; Yuan, H.; Zhang, X.; Huang, D.; Li, S.; Wang, M.; Shen, Y., Investigation of Regeneration Kinetics in Quantum-Dots-Sensitized Solar Cells with Scanning Electrochemical Microscopy. *ACS Applied Materials & Interfaces* **2014**, *6*, 20913-20918.
11. Hamann, T. W.; Jensen, R. A.; Martinson, A. B. F.; Van Ryswyk, H.; Hupp, J. T., Advancing Beyond Current Generation Dye-Sensitized Solar Cells. *Energy & Environmental Science* **2008**, *1*, 66-78.
12. Wang, Y.; Runnerstrom, E. L.; Milliron, D. J., Switchable Materials for Smart Windows. *Annual Review of Chemical and Biomolecular Engineering* **2016**, *7*, 283-304.
13. Pastore, M.; De Angelis, F., Intermolecular Interactions in Dye-Sensitized Solar Cells: A Computational Modeling Perspective. *The Journal of Physical Chemistry Letters* **2013**, *4*, 956-974.
14. Gao, P.; Tsao, H. N.; Grätzel, M.; Nazeeruddin, M. K., Fine-Tuning the Electronic Structure of Organic Dyes for Dye-Sensitized Solar Cells. *Organic Letters* **2012**, *14*, 4330-4333.
15. Cui, Y.; Wu, Y.; Lu, X.; Zhang, X.; Zhou, G.; Miapeh, F. B.; Zhu, W.; Wang, Z.-S., Incorporating Benzotriazole Moiety to Construct D–a−Π–a Organic Sensitizers for Solar Cells: Significant Enhancement of Open-Circuit Photovoltage with Long Alkyl Group. *Chemistry of Materials* **2011**, *23*, 4394-4401.
16. Wu, Y.; Zhu, W., Organic Sensitizers from D–Π–a to D–a–Π–A: Effect of the Internal Electron-Withdrawing Units on Molecular Absorption, Energy Levels and Photovoltaic Performances. *Chemical Society Reviews* **2013**, *42*, 2039-2058.
17. Chang, D. W.; Lee, H. J.; Kim, J. H.; Park, S. Y.; Park, S.-M.; Dai, L.; Baek, J.-B., Novel Quinoxaline-Based Organic Sensitizers for Dye-Sensitized Solar Cells. *Organic Letters* **2011**, *13*, 3880-3883.
18. Jørgensen, M.; Norrman, K.; Gevorgyan, S. A.; Tromholt, T.; Andreasen, B.; Krebs, F. C., Stability of Polymer Solar Cells. *Advanced Materials* **2011**, *24*, 580-612.
19. Kimura, M.; Nomoto, H.; Masaki, N.; Mori, S., Dye Molecules for Simple Co-Sensitization Process: Fabrication of Mixed-Dye-Sensitized Solar Cells. *Angewandte Chemie* **2012**, *124*, 4447-4450.

20. Cid, J.-J.; Yum, J.-H.; Jang, S.-R.; Nazeeruddin, M. K.; Martínez-Ferrero, E.; Palomares, E.; Ko, J.; Grätzel, M.; Torres, T., Molecular Cosensitization for Efficient Panchromatic Dye-Sensitized Solar Cells. *Angewandte Chemie* **2007**, *119*, 8510-8514.
21. Choi, H.; Kim, S.; Kang, S. O.; Ko, J.; Kang, M.-S.; Clifford, J. N.; Forneli, A.; Palomares, E.; Nazeeruddin, M. K.; Grätzel, M., Stepwise Cosensitization of Nanocrystalline Tio2 Films Utilizing Al2o3 Layers in Dye-Sensitized Solar Cells. *Angewandte Chemie* **2008**, *120*, 8383-8387.
22. Zhou, D.; Yu, Q.; Cai, N.; Bai, Y.; Wang, Y.; Wang, P., Efficient Organic Dye-Sensitized Thin-Film Solar Cells Based on the Tris(1,10-Phenanthroline)Cobalt(Ii/Iii) Redox Shuttle. *Energy & Environmental Science* **2011**, *4*, 2030-2034.
23. Nelson, J. J.; Amick, T. J.; Elliott, C. M., Mass Transport of Polypyridyl Cobalt Complexes in Dye-Sensitized Solar Cells with Mesoporous Tio2 Photoanodes. *The Journal of Physical Chemistry C* **2008**, *112*, 18255-18263.
24. Carli, S.; Casarin, L.; Caramori, S.; Boaretto, R.; Busatto, E.; Argazzi, R.; Bignozzi, C. A., A Viable Surface Passivation Approach to Improve Efficiency in Cobalt Based Dye Sensitized Solar Cells. *Polyhedron* **2014**, *82*, 173-180.
25. Palomares, E.; Clifford, J. N.; Haque, S. A.; Lutz, T.; Durrant, J. R., Control of Charge Recombination Dynamics in Dye Sensitized Solar Cells by the Use of Conformally Deposited Metal Oxide Blocking Layers. *Journal of the American Chemical Society* **2003**, *125*, 475-482.
26. Merazga, A.; Al-Subai, F.; Albaradi, A. M.; Badawi, A.; Jaber, A. Y.; Alghamdi, A. A. B., Effect of Sol–Gel Mgo Spin-Coating on the Performance of Tio2-Based Dye-Sensitized Solar Cells. *Materials Science in Semiconductor Processing* **2016**, *41*, 114-120.
27. Sreejith, S.; Carol, P.; Chithra, P.; Ajayaghosh, A., Squaraine Dyes: A Mine of Molecular Materials. *Journal of Materials Chemistry* **2008**, *18*, 264-274.
28. de Miguel, G.; Ziółek, M.; Zitnan, M.; Organero, J. A.; Pandey, S. S.; Hayase, S.; Douhal, A., Photophysics of H- and J-Aggregates of Indole-Based Squaraines in Solid State. *The Journal of Physical Chemistry C* **2012**, *116*, 9379-9389.
29. Wu, K.-L.; Huckaba, A. J.; Clifford, J. N.; Yang, Y.-W.; Yella, A.; Palomares, E.; Grätzel, M.; Chi, Y.; Nazeeruddin, M. K., Molecularly Engineered Ru(Ii) Sensitizers Compatible with Cobalt(Ii/Iii) Redox Mediators for Dye-Sensitized Solar Cells. *Inorganic Chemistry* **2016**, *55*, 7388-7395.
30. Feldt, S. M.; Gibson, E. A.; Gabrielsson, E.; Sun, L.; Boschloo, G.; Hagfeldt, A., Design of Organic Dyes and Cobalt Polypyridine Redox Mediators for High-Efficiency Dye-Sensitized Solar Cells. *Journal of the American Chemical Society* **2010**, *132*, 16714-16724.
31. Hao, Y., et al., Novel Blue Organic Dye for Dye-Sensitized Solar Cells Achieving High Efficiency in Cobalt-Based Electrolytes and by Co-Sensitization. *ACS Applied Materials & Interfaces* **2016**, *8*, 32797-32804.
32. Li, H.; Pang, M.; Wu, B.; Meng, J., Synthesis, Crystal Structure and Photochromism of a Novel Spiro[Indoline–Naphthaline]Oxazine Derivative. *Journal of Molecular Structure* **2015**, *1087*, 73-79.
33. Inoue, T.; Pandey, S. S.; Fujikawa, N.; Yamaguchi, Y.; Hayase, S., Synthesis and Characterization of Squaric Acid Based Nir Dyes for Their Application Towards Dye-Sensitized Solar Cells. *Journal of Photochemistry and Photobiology A: Chemistry* **2010**, *213*, 23-29.

34. Marchena, M. J.; de Miguel, G.; Cohen, B.; Organero, J. A.; Pandey, S.; Hayase, S.; Douhal, A., Real-Time Photodynamics of Squaraine-Based Dye-Sensitized Solar Cells with Iodide and Cobalt Electrolytes. *The Journal of Physical Chemistry C* **2013**, *117*, 11906-11919.
35. Sommeling, P. M.; O'Regan, B. C.; Haswell, R. R.; Smit, H. J. P.; Bakker, N. J.; Smits, J. J. T.; Kroon, J. M.; van Roosmalen, J. A. M., Influence of a Ticl4 Post-Treatment on Nanocrystalline Tio2 Films in Dye-Sensitized Solar Cells. *The Journal of Physical Chemistry B* **2006**, *110*, 19191-19197.
36. Kakiage, K.; Osada, H.; Aoyama, Y.; Yano, T.; Oya, K.; Iwamoto, S.; Fujisawa, J.-i.; Hanaya, M., Achievement of over 1.4 V Photovoltage in a Dye-Sensitized Solar Cell by the Application of a Silyl-Anchor Coumarin Dye. *Scientific Reports* **2016**, *6*, 35888.
37. Horiuchi, T.; Miura, H.; Sumioka, K.; Uchida, S., High Efficiency of Dye-Sensitized Solar Cells Based on Metal-Free Indoline Dyes. *Journal of the American Chemical Society* **2004**, *126*, 12218-12219.
38. Chen, G.; Sasabe, H.; Igarashi, T.; Hong, Z.; Kido, J., Squaraine Dyes for Organic Photovoltaic Cells. *Journal of Materials Chemistry A* **2015**, *3*, 14517-14534.
39. Ajayaghosh, A., Chemistry of Squaraine-Derived Materials: Near-Ir Dyes, Low Band Gap Systems, and Cation Sensors. *Accounts of Chemical Research* **2005**, *38*, 449-459.
40. Soman, S.; Rahim, M. A.; Lingamoorthy, S.; Suresh, C. H.; Das, S., Strategies for Optimizing the Performance of Carbazole Thiophene Appended Unsymmetrical Squaraine Dyes for Dye-Sensitized Solar Cells. *Physical Chemistry Chemical Physics* **2015**, *17*, 23095-23103.
41. Eisfeld, A.; Briggs, J. S., The J- and H-Bands of Organic Dye Aggregates. *Chemical Physics* **2006**, *324*, 376-384.
42. Yum, J.-H.; Walter, P.; Huber, S.; Rentsch, D.; Geiger, T.; Nüesch, F.; De Angelis, F.; Grätzel, M.; Nazeeruddin, M. K., Efficient Far Red Sensitization of Nanocrystalline Tio2 Films by an Unsymmetrical Squaraine Dye. *Journal of the American Chemical Society* **2007**, *129*, 10320-10321.
43. Unger, E. L.; Morandeira, A.; Persson, M.; Zietz, B.; Ripaud, E.; Leriche, P.; Roncali, J.; Hagfeldt, A.; Boschloo, G., Contribution from a Hole-Conducting Dye to the Photocurrent in Solid-State Dye-Sensitized Solar Cells. *Physical Chemistry Chemical Physics* **2011**, *13*, 20172-20177.
44. Yum, J. H.; Moon, S. J.; Humphry-Baker, R.; Walter, P.; Geiger, T.; Nüesch, F.; Grätzel, M.; Nazeeruddin, M. d. K., Effect of Coadsorbent on the Photovoltaic Performance of Squaraine Sensitized Nanocrystalline Solar Cells. *Nanotechnology* **2008**, *19*, 424005.
45. Kawano, M.; Nishiyama, T.; Ogomi, Y.; Pandey, S. S.; Ma, T.; Hayase, S., Relationship between Diffusion of Co3+/Co2+ Redox Species in Nanopores of Porous Titania Stained with Dye Molecules, Dye Molecular Structures, and Photovoltaic Performances. *RSC Advances* **2015**, *5*, 83725-83731.
46. Ogomi, Y.; Pandey, S. S.; Kimura, S.; Hayase, S., Probing Mechanism of Dye Double Layer Formation from Dye-Cocktail Solution for Dye-Sensitized Solar Cells. *Thin Solid Films* **2010**, *519*, 1087-1092.
47. Pandey, S. S.; Morimoto, T.; Fujikawa, N.; Hayase, S., Combined Theoretical and Experimental Approaches for Development of Squaraine Dyes with Small Energy Barrier for Electron Injection. *Solar Energy Materials and Solar Cells* **2017**, *159*, 625-632.

48. Gabrielsson, E.; Ellis, H.; Feldt, S.; Tian, H.; Boschloo, G.; Hagfeldt, A.; Sun, L., Convergent/Divergent Synthesis of a Linker-Varied Series of Dyes for Dye-Sensitized Solar Cells Based on the D35 Donor. *Advanced Energy Materials* **2013**, *3*, 1647-1656.
49. Wang, M.; Grätzel, C.; Zakeeruddin, S. M.; Grätzel, M., Recent Developments in Redox Electrolytes for Dye-Sensitized Solar Cells. *Energy & Environmental Science* **2012**, *5*, 9394-9405.
50. Ogomi, Y.; Kato, T.; Hayase, S., Dye Sensitized Solar Cells Consisting of Ionic Liquid and Solidification. *Journal of Photopolymer Science and Technology* **2006**, *19*, 403-408.
51. Pandey, S. S.; Inoue, T.; Fujikawa, N.; Yamaguchi, Y.; Hayase, S., Substituent Effect in Direct Ring Functionalized Squaraine Dyes on near Infra-Red Sensitization of Nanocrystalline Tio2 for Molecular Photovoltaics. *Journal of Photochemistry and Photobiology A: Chemistry* **2010**, *214*, 269-275.
52. Han, L.; Islam, A.; Chen, H.; Malapaka, C.; Chiranjeevi, B.; Zhang, S.; Yang, X.; Yanagida, M., High-Efficiency Dye-Sensitized Solar Cell with a Novel Co-Adsorbent. *Energy & Environmental Science* **2012**, *5*, 6057-6060.
53. Shiu, J.-W.; Chang, Y.-C.; Chan, C.-Y.; Wu, H.-P.; Hsu, H.-Y.; Wang, C.-L.; Lin, C.-Y.; Diau, E. W.-G., Panchromatic Co-Sensitization of Porphyrin-Sensitized Solar Cells to Harvest near-Infrared Light Beyond 900 Nm. *Journal of Materials Chemistry A* **2015**, *3*, 1417-1420.
54. Basham, J. I.; Mor, G. K.; Grimes, C. A., Förster Resonance Energy Transfer in Dye-Sensitized Solar Cells. *ACS Nano* **2010**, *4*, 1253-1258.
55. Emeline, A. V.; Kuzmin, G. N.; Purevdorj, D.; Ryabchuk, V. K.; Serpone, N., Spectral Dependencies of the Quantum Yield of Photochemical Processes on the Surface of Wide Band Gap Solids. 3. Gas/Solid Systems. *The Journal of Physical Chemistry B* **2000**, *104*, 2989-2999.
56. Patwari, J.; Sardar, S.; Liu, B.; Lemmens, P.; Pal, S. K. Three-in-One Approach Towards Efficient Organic Dye-Sensitized Solar Cells: Aggregation Suppression, Panchromatic Absorption and Resonance Energy Transfer *Beilstein J Nanotechnol* **2017**, DOI: 10.3762/bjnano.8.171.
57. Wang, M.; Grätzel, C.; Zakeeruddin, S. M.; Grätzel, M., Recent Developments in Redox Electrolytes for Dye-Sensitized Solar Cells. *Energy & Environmental Science* **2012**, *5*, 9394-9405.
58.
59. Hoshikawa, T.; Yamada, M.; Kikuchi, R.; Eguchi, K., Impedance Analysis of Internal Resistance Affecting the Photoelectrochemical Performance of Dye-Sensitized Solar Cells. *Journal of The Electrochemical Society* **2005**, *152*, E68-E73.
60. Kapil, G.; Ohara, J.; Ogomi, Y.; Pandey, S. S.; Ma, T.; Hayase, S., Fabrication and Characterization of Coil Type Transparent Conductive Oxide-Less Cylindrical Dye-Sensitized Solar Cells. *RSC Advances* **2014**, *4*, 22959-22963.
61. Koops, S. E.; O'Regan, B. C.; Barnes, P. R. F.; Durrant, J. R., Parameters Influencing the Efficiency of Electron Injection in Dye-Sensitized Solar Cells. *Journal of the American Chemical Society* **2009**, *131*, 4808-4818.
62. Barea, E.; Xu, X.; González-Pedro, V.; Ripollés-Sanchis, T.; Fabregat-Santiago, F.; Bisquert, J., Origin of Efficiency Enhancement in Nb2o5 Coated Titanium Dioxide Nanorod Based Dye Sensitized Solar Cells. *Energy & Environmental Science* **2011**, *4*, 3414-3419.

63. Yum, J.-H.; Holcombe, T. W.; Kim, Y.; Rakstys, K.; Moehl, T.; Teuscher, J.; Delcamp, J. H.; Nazeeruddin, M. K.; Grätzel, M., Blue-Coloured Highly Efficient Dye-Sensitized Solar Cells by Implementing the Diketopyrrolopyrrole Chromophore. *Scientific Reports* **2013**, *3*, 2446.
64. Marchena, M. J.; de Miguel, G.; Cohen, B.; Organero, J. A.; Pandey, S.; Hayase, S.; Douhal, A., Real-Time Photodynamics of Squaraine-Based Dye-Sensitized Solar Cells with Iodide and Cobalt Electrolytes. *The Journal of Physical Chemistry C* **2013**, *117*, 11906-11919.
65. Kroeze, J. E.; Hirata, N.; Koops, S.; Nazeeruddin, M. K.; Schmidt-Mende, L.; Grätzel, M.; Durrant, J. R., Alkyl Chain Barriers for Kinetic Optimization in Dye-Sensitized Solar Cells. *Journal of the American Chemical Society* **2006**, *128*, 16376-16383.
66. Dryza, V.; Bieske, E. J., Does the Triphenylamine-Based D35 Dye Sensitizer Form Aggregates on Metal-Oxide Surfaces? *Journal of Photochemistry and Photobiology A: Chemistry* **2015**, *302*, 35-41.
67. Dryza, V.; Bieske, E. J., Suppressing Förster Resonance Energy Transfer between Organic Dyes on a Cosensitized Metal Oxide Surface. *The Journal of Physical Chemistry C* **2014**, *118*, 19646-19654.
68. Ogura, R. Y.; Nakane, S.; Morooka, M.; Orihashi, M.; Suzuki, Y.; Noda, K., High-Performance Dye-Sensitized Solar Cell with a Multiple Dye System. *Applied Physics Letters* **2009**, *94*, 073308.
69. Lin, R. Y.-Y., et al., Dihydrophenanthrene-Based Metal-Free Dyes for Highly Efficient Cosensitized Solar Cells. *Organic Letters* **2012**, *14*, 3612-3615.

CHAPTER SEVEN

7. 1 General conclusions

Research work carried out enabled me to conclude about the need for minimum energy barrier of about 0.12 eV for dye regeneration for this class of far red squaraine dyes utilizing most commonly employed iodine based redox electrolyte. This indicates the way for the NIR dye design, which is one of the major tasks in the area of DSSCs.

A series of direct –COOH bearing asymmetric far red squaraine dyes were synthesized for the application of DSSCs in conjunction with the cobalt bipyridyl redox mediator. It was interestingly found that the far red dyes were compatible with the employed redox shuttle for dye generation and as well as for electron injection onto the mesoporous TiO_2 which are the essential requirements for functioning of DSSC. As employing NIR dyes with cobalt electrolyte may not always work due to energetics mismatch, however, we were able to employ them in conjunction with good output. Apparently even with the sharp and intense photon harvesting, employment of squaraine dyes with the cobalt electrolyte were able to reach an efficiency of 1.98%. Apart from the function of the main squaraine moiety for better efficiency, the introduction of longer alkyl chain onto it was found to be productive in controlling the back electron transfer. It was observed that the dye with longer alkyl chains screened the direct contact of cobalt electrolyte with the TiO_2 surface. Hence, along with the good photon harvesting efficiency, the inclusion of the longer alkyl chains was found be necessary for cobalt electrolyte.

To achieve the aim for panchromatic photon harvesting, the commercial visible dye D-35 was found to give a good complementary photon harvesting with our newly synthesized squaraine dye SQ-110. These two dyes employed in a cocktail of (4:1) ratio was found to be optimum to meet the demand. The value of the optimum ratio could be explained in terms of their relative molar extinction coefficient. SQ-110 has its molar extinction coefficient 10 times greater than visible dye D-35. Hence higher concentration of D-35 was required to have sufficient photon absorption. It was also observed that the ratio (4:1) of D-35 and SQ-110 had a comparable light absorption. Therefore it depicts that our SQ-110 is excellent not only in light absorption but also in the photon harvesting. Portray of the IPCE of the two dyes in cocktail revealed the wide wavelength photon harvest from 300-750 nm. This opens up the room for further extension of light harvesting window in NIR wavelength region by logical molecular design. The energetics of the two dyes employed

also favored each other in electron transfer as well as energy transfer as proven by fluorescence resonance energy transfer. This has not only enhanced the electron injection as shown by the enhanced current density but also the overall performance of the device (5.5%), which was rather poor using constituent single dyes D-35 (3.63 %) and SQ-110 (1.92 %). This efficiency was further improved to 7.23% by optimized surface passivation. The surface passivation of mesoporous TiO_2 with compact TiO_2 followed by wide band gap magnesia was found to be effective for this.

7.2 Future prospects

Research works of this thesis could be extended to further improve the efficiency in the near future. The far red dyes synthesized with the minimum driving force of 0.12 eV and good efficiency of 4.25 % is expected to broaden the hope for the novel NIR dye design. The idea is to incorporate a chromophore onto the squaraine structure to red shift the absorption and harvest the longer wavelength photons for more current density.

In order to have a wide wavelength light absorption, more π conjugation contributed by a good electron donating group could also be introduced on the edge of the one of the indole groups. On the other hand, again the cocktail ratio of the longer wavelength squaraine dye and a visible dye could be used to achieve the wide wavelength photon harvesting. In order to attain longer wavelength photon harvesting beyond 800 nm by extending the π-conjugation may lead to its incompatibility for electron injection owing its relatively lower band gap. In such case, mesoporous semiconductors like SnO_2 could be used instead of TiO_2 to maintain better driving force. However such device would furnish lesser open circuit voltage. To circumvent this problem, deeper redox potential bearing redox shuttle could be used.

Very recent past has witnessed the use of copper complex based electrolytes having deeper redox potential and attainment of higher Voc has already been demonstrated using visible sensitizers. Interestingly, direct contact DSSCs using this electrolyte may further open up the realization of high efficiency solid-state DSSCs. In this context, using these state-of-art technologies and combining them with newly designed NIR dyes is expected to open up the door for high efficiency and stable DSSCs.

ACHIEVEMENTS

JOURNAL PAPERS:

1. **Anusha Pradhan,*** Takuya Morimoto, Maryala Saikiran, Gaurav Kapil, Shuzi Hayase and Shyam S. Pandey*: ``***Investigation of the minimum driving force for dye regeneration utilizing model squaraine dyes for dye-sensitized solar cells``,*** J. Mater. Chem. A, 2017,**5**, 22672-22682 . (IF: 9.93)
2. **Anusha Pradhan**, Maryala Saikiran, Gaurav Kapil, Shyam Sudhir Pandey and Shuzi Hayase: ``***Parametric Optimization of Dye-Sensitized Solar Cells Using Far red Sensitizing Dye with Cobalt Electrolyte``,*** Journal of Physics: Conference Series, **924** 012001.
3. **Anusha Pradhan*,** Maryala Sai Kiran, Gaurav Kapil, Shuzi Hayase, and Shyam S. Pandey*: ``***Synthesis and Photophysical Characterization of Unsymmetrical Squaraine Dyes for Dye-Sensitized Solar Cells Utilizing Cobalt Electrolytes***``, ACS Appl. Energy Mater., **2018**, *1* (9), pp 4545–4553.
4. **Anusha Pradhan***, Maryala Sai Kiran, Gaurav Kapil, Shuzi Hayase and Shyam Sudhir Pandey*: ``***Wide Wavelength Photon Harvesting: Implication of dye cocktail and surface Passivation``,*** Sol. Energy Mater Sol. Cells., (Revised manuscript submitted).

CONFERENCES PRESENTATIONS

1) **Anusha Pradhan**, Maryala Sai Kiran, Gaurav Kapil, Shyam S. Pandey and Shuzi Hayase: "***Dye-Sensitized Solar Cells utilizing Far-red Sensitive Dyes in Combination with Cobalt Complex based Redox Electrolyte"***: The 12th International Conference on Nanomolecular Electronics (ICNME-2016), Kobe International Conference Center, Kobe, Japan.

2) **Anusha Pradhan,** Maryala Saikiran, Gaurav Kapil, Shyam S. Pandey and Shuzi Hayase: "***Parametric Optimization for Dye-Sensitized Solar Cells using Far-Red Sensitizing Dyes with Cobalt Electrolyte";*** Kyutech-UPM International Symposium (SAES-2016), Kyushu Institute of Technology, Tobata Campus, Japan.

3) **Anusha Pradhan,** Maryala Saikiran, Gaurav Kapil, Shyam S. Pandey and Shuzi Hayase: "***Effect of Compact Oxide Layer Surface Passivation for Dye-Sensitized Solar Cells Utilizing Cobalt Complex based Redox Electrolyte";*** *International Conference on Materials for Advanced Technology (* ICMAT-2017), Singapore.

4) **Anusha Pradhan,** Maryala Saikiran, Gaurav Kapil, Shyam S. Pandey and Shuzi Hayase: "***Dye-Sensitized Solar Cells utilizing Far-Red Sensitive Dye-Cocktail with Cobalt Electrolyte: Importance of Compact Oxide Surface Treatment";*** Japan Society for Applied Physics autumn meeting (2017), Fukuoka, Japan.

5) **Anusha Pradhan,** Maryala Saikiran, Gaurav Kapil, Shyam S. Pandey and Shuzi Hayase: "***Novel NIR dyes in Combination with Cobalt Redox Shuttle for High Efficiency Dye Sensitized Solar Cells"*** Kyushu branch chemical society meeting (2017), Kokura, Japan.

6) **Anusha Pradhan,** Maryala Saikiran, Gaurav Kapil, Shyam S. Pandey and Shuzi Hayase: "***Synthesis and characterization of positively charged NIR dyes for Cobalt electrolyte based dye-sensitized solar cells"*** Asia-Pacific Hybrid and Organic Photovoltaic International conference (APHOPV-2018), Kokura, Japan.

7) **Anusha Pradhan,** Maryala Saikiran, Gaurav Kapil, Shyam S. Pandey and Shuzi Hayase:
8) ***"Synthesis and Photophysical Characterization of Positively Charged NIR Dyes for Dye-Sensitized Solar cells";*** Japan Chemical Society, spring meeting (2018), Chiba, Japan.

9) **Anusha Pradhan,** Maryala Saikiran, Gaurav Kapil, Shyam S. Pandey and Shuzi Hayase: "***Combining NIR dyes and Cobalt Electrolyte for High Efficiency Dye Sensitized Solar Cells";*** International Conference on Science and Technology of Synthetic Metals (ICSM-2018), Busan, South Korea.

10**)** **Anusha Pradhan,** Ajendra Kumar Vats Shyam Sudhir Pandey: "***Design and Development of Novel Blue Colored sensitizers for Efficient Cobalt Redox Shuttle Based Dye Sensitized Solar Cells";*** Material Research Society- Japan, Kokura, Japan 18 Dec 2018

11) Shyam S. Pandey, **Anusha Pradhan**, Takuya Morimoto, Maryala Saikiran and Shuzi Hayase: ***Theoretical Molecular Design of Novel Near Infra-red Sensitizers for Dye-Sensitized Solar Cells using Gaussian Program Package***; 3rd International Conference on Computational Methods in Engineering and Health Sciences (ICCMEH2016), December 17-18, 2016, Kyushu Institute of Technology, Tobata, Kitakyushu, Japan 17 Dec 2016.

10) Shyam S Pandey*, Takuya Morimoto, **Anusha Pradhan**, Maryala Sai Kiran, Shuzi Hayase: ***Molecular Design of far-red Sensitive Squaraine Dyes in-order to Probe the Minimum Energy Barrier for Dye-Regeneration***; 26th Annual Meeting of Materials Research Society Japan, December 19-22, Yokohama Port Opening Plaza, Yokohama, Japan 19 Dec 2016.

11) Shyam S. Pandey**,** **Anusha Pradhan**, Md. Zaman Molla and Shuzi Hayase: ***Amicable Solutions for the Charge Recombination by Controlling the Ion Transport in Cobalt Electrolyte based Dye-Sensitized Solar Cells****;* 27th Annual Meeting of Materials Research Society, Japan, Yokohama Port Opening Plaza, December 5-7, 2017.

12) Shyam S. Pandey, **Anusha Pradhan** and Shuzi Hayase*; **Prospects and Challenges with the Development of Near Infrared Dyes for Dye-Sensitized Solar Cells**:* 5th International Conference on Advanced Nanomaterials and Nanotechnology (ICANN-2017), IIT-Guwahati, Assam, India, December 18-21, 2017.

13) Shyam S. Pandey, **Anusha Pradhan**, Maryala Saikiran and Shuzi Hayase: ***Prospects and Challenges with Dye-Sensitized Solar Cells utilizing Far-red Sensitive Dyes and Cobalt***

Complex Redox Electrolyte*;* 2nd Asia-Pacific Hybrid Organic Photovoltaic Conference (AP-HOPV 2018), Kitakyushu, Japan Jan. 28-30, 2018.

14) Ajendra Kumar Vats, **Anusha Pradhan**, and Shyam S. Pandey: ***Prediction of Nature of Anchoring Groups on Electron Density Distribution in NIR Dyes by Quantum Chemical Calculations***; 55th Kyushu Branch Chemical Society, Meeting, Kokura International Conference Center, Kokura, Kitakyushu, Japan 30 Jun 2018.